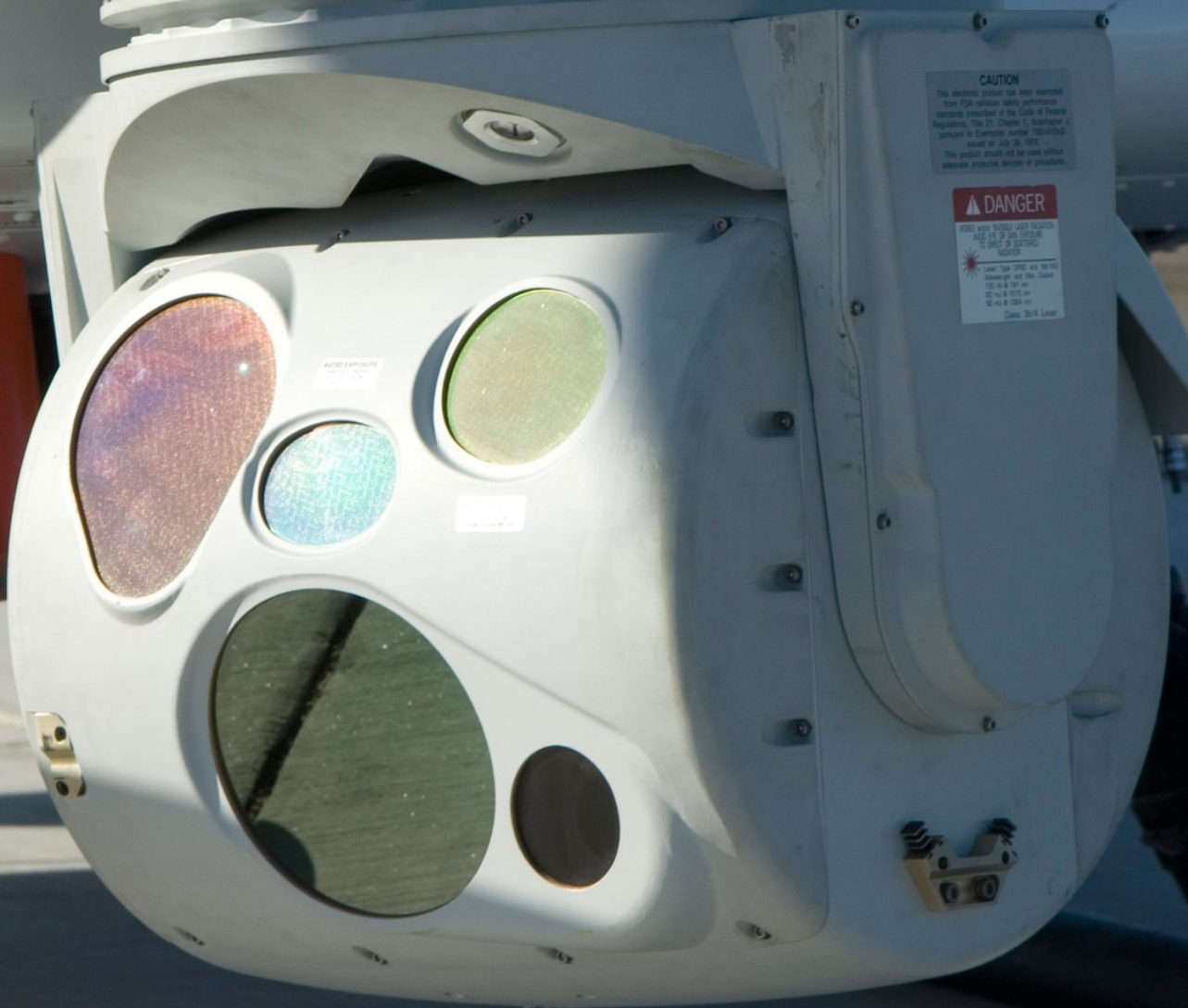


Airborne Minesweeper

Final Report

AE3200 Design Synthesis
Group 09

Delft University of Technology



This page is intentionally left blank

Airborne Minesweeper

Final Report

by

Group 09

Student Name	Student Number
Amund Kiste	5001706
Ekaterina Skorobogatova	5269539
Guido van der Veen	5533996
Jonathan Poot	5528798
Marcin Poplawski	5452333
Nour Al-Bayaty de Ridder	5090148
Simina Dragotă	5290872
Sophie Loogman	5315417
Tuomas Simula	5457386
Vlad-Mihai Iliescu	5231493

Instructor: M. Brown
Coaches: E. van den Bos and M. Lourenço Baptista
Teaching Assistant: M. Piperigou Grammatika
Project Duration: April, 2024 - June, 2024
Faculty: Faculty of Aerospace Engineering, Delft

Cover: ASTAMIDS mounted on Fire Scout, Northrop Grumman
Style: TU Delft Report Style, with modifications by Daan Zwaneveld

Nomenclature

Abbreviations

Abbreviation	Definition
ADS-B	Automatic Dependent Surveillance-Broadcast
ASL	Above Sea Level
BSFC	Brake-specific Fuel Consumption
BVLOS	Beyond Visual Line-of-Sight
CAN	Control Area Network
CG	Center of Gravity
DSE	Design Synthesis Exercise
DT	Destructive Testing
EMS	Emergency Management System
EPM	Electrical Power Management
ESC	Electronic speed controller
FOD	Foreign Object Debris
GNSS-RTK	Global Navigation Satellite System - Real-Time Kinematics
GPS	Global Positioning System
I2C	Inter-Integrated Circuit
IMU	Inertial Measurement Unit
ISA	International Standard Atmosphere
ITC	Intended To Comply
LiDAR	Light Detection And Ranging
LOS	Line Of Sight
LRU	Line Replaceable Unit
MAC	Mean Aerodynamic Chord
MIMO	Multiple-Input Multiple-Output
MTBF	Mean Time Between Failures
MTOW	Maximum Take-Off Weight
N/A	Not Available/Applicable
NDT	Non-Destructive Testing
NGO	Non-Governmental Organisation
OBC	On-Board Computer
OEW	Operating Empty Weight
OOS	Out Of Scope
PL	Payload
PMU	Power Management Unit
PTSD	Post Traumatic Stress Disorder
PWM	Pulse-Width Modulation
RAMS	Reliability, Availability, Maintainability and Safety
RADAR	Radio Detection And Ranging
RID	Remote Identification
TO	Take-off
TOP	Take-Off Parameter
TTL	Transistor-Transistor Logic
UART	Universal Asynchronous Receive Transmit
UAV	Unmanned Aerial Vehicle
UN	United Nations
UXO	Unexploded ordnance
VLM	Vortex Lattice Method
VTOL	Vertical Take-off and Landing

Symbols

Symbol	Definition	Unit
A	Aspect ratio	-
A	Area	[m ²]
A_{box}	Enclosed area of the wing box	[m ²]
A_{fus}	Fuselage Frontal Area	[m ²]
A_{LG}	Landing Gear Frontal Area	[m ²]
A_{nac}	[m ²]	
Nacelle		
Frontal		
Area		
AR	Aspect ratio	-
AR_P	Propeller aspect ratio	-
B_p	Number of blades per propeller	-
b	Wing span	[m]
b	Panel width	[m]
b_f	Fuselage width	[m]
c	Chord	[m]
\bar{c}	Mean aerodynamic chord	[m]
C	Buckling coefficient	-
C_D	Drag coefficient	-
C_{D_0}	Zero Lift Drag	-
$C_{D_{misc}}$	Miscellaneous Drag Coefficient	-
$C_{D_0_{fus}}$	Fuselage zero lift Drag Coefficient	-
$C_{D_0_{LG}}$	Landing gear zero lift Drag Coefficient	-
$C_{D_0_{nac}}$	Nacelle zero lift Drag Coefficient	-
$C_{D_0_{horiz}}$	Horizontal Tail zero lift Drag Coefficient	-
$C_{D_0_{vert}}$	Vertical tail zero lift Drag Coefficient	-
C_f	Plane skin friction coefficient	-
C_L	Wing lift coefficient	-
C_{LP}	Propeller blade lift coefficient	-
C_M	Moment coefficient	-
C_{mac}	Moment coefficient around ac	-
C_N	Normal force coefficient	-
C_s	Shear buckling coefficient	-
c_{sp}	Specific fuel consumption	[N J ⁻¹]
D	Drag	[N]
D	Diameter	[m]
D_{fus}	Fuselage Diameter	[m]
D_{nac}	Nacelle Diameter	[m]
E	Endurance	[h]
E	Young's modulus	[Pa]
e	Oswald efficiency factor	-
e	eccentricity	[m]
F_{brake}	Force provided by the brakes	[N]
F_{fs}	Fuel multiplication factor	-
$F_{install}$	Installation factor	-
F_{Matl}	Correction factor for material	-
F_{MG}	Correction factor of main gear	-
F_{nac}	Nacelle multiplication factor	-
F_{NG}	Correction factor of nose gear	-
F_{Press}	Correction factor due to pressurization	-
F_{tfo}	Trapped oil and fuel mass fraction	-
$F_{touchdown}$	Load sustained at moment of touchdown	[N]
F_{LG}	Landing gear mass fraction	-

Symbol	Definition	Unit	Symbol	Definition	Unit
F_{VT}	Correction factor for vertical tail	-	Q	Brake torque	[N m]
FF	Form Factor	-	Q	First moment of area	[m ³]
FF_{fus}	Fuselage form factor	-	q	Dynamic pressure	[N m ⁻²]
FF_{horiz}	Horizontal tail form factor	-	q_{vfs}	Shear flow front spar	[N m ⁻¹]
FF_{nac}	Nacelle form factor	-	q_{vrs}	Shear flow front spar	[N m ⁻¹]
FF_{vert}	Vertical tail form factor	-	q_t	Shear flow due to torque	[N m ⁻¹]
FF_{fus}	Fuselage form factor	-	R	Range	[m]
f	Length to diameter ration	-	Re	Reynolds number	-
f_{Avion}	Avionics mass fraction	-	RoC	Rate of climb	[m s ⁻¹]
g	Gravitational acceleration	[m s ⁻²]	S	Surface area	[m ²]
h	Altitude	[m]	S	Landing gear stroke	[m]
h	Height	[m]	S_{Emp}	Empennage surface area	[ft ²]
h_f	Fuselage height	[m]	S_{horiz}	Horizontal wing are	[m ²]
h_{fs}	Height front spar	[m]	S_{ref}	Reference wing are	[m ²]
h_{rs}	Height rear spar	[m]	S_{up}	Length upper panel	[m]
I	Area moment of inertia	[m ⁴]	S_{low}	Length lower panel	[m]
IF	Interference factor	-	S_{vert}	Vertical wing are	[m ²]
IF_{fus}	Fuselage interference factor	-	S_w	Wing surface area	[m ²]
IF_{horiz}	Horizontal tail interference factor	-	S_{wet}	Wetted area	[m ²]
IF_{nac}	Nacelle interference factor	-	S_{wetfus}	Fuselage wetted area	[m ²]
IF_{vert}	Vertical tail interference factor	-	$S_{wethoriz}$	Horizontal wing wetted area	[m ²]
IF_{fus}	Fuselage interference factor	-	$S_{wetvert}$	Vertical wing wetted area	[m ²]
K_g	Gust elevation factor	-	$S_{wetwing}$	Wing wetted area	[m ²]
K_{nP}	Propeller power correction factor	-	T	Thrust	[N]
K_{Prop}	Propeller multiplication factor	-	T	Torque	[N m]
L	Lift	[N]	t	Thickness	[m]
L_1	Nosecone Length	[m]	t_{max}	Maximum thickness	[m]
L_2	Middle Fuselage Length	[m]	t_{up}	Thickness upper panel	[m]
L_3	Tail-cone Length	[m]	t_{low}	Thickness lower panel	[m]
L_{Boom}	Boom length	[ft]	t/c	Thickness to chord ratio	-
L_{nac}	Nacelle length	[m]	U	Wind speed	[m s ⁻¹]
L_{Struct}	Fuselage length	[ft]	V	Velocity	[m s ⁻¹]
L_{Tot}	Total structural length	[ft]	V	Shear force	[N]
l	Length	[m]	V_{av}	Average velocity along blade span	[m s ⁻¹]
M	Aeroplane Mass	[kg]	V_C	Cruise velocity	[m s ⁻¹]
M_{ac}	Moment around aerodynamic center	[N m]	V_{dive}	Dive speed	[m s ⁻¹]
MF_{Paint}	Paint mass fraction	-	$V_{eq,Max}$	Maximum equivalent velocity	[kts]
N	Number of wheels	-	v	Velocity	[m s ⁻¹]
N_{Blades}	Number of blades	-	v_{max}	maximum deflection	[m]
N_{Props}	Number of propellers	-	w_e	Effective sheet width	[m]
N_Z	Ultimate load factor	g	W	Weight	[N]
n	Load Factor	-	W_{Avion}	Avionics mass	[kg]
n	Coefficient for crippling	-	W_{Booms}	Boom mass	[lbs]
P	Power	[W]	W_{Cant}	Cantilever mass	[lbs]
P_{CR}	Critical buckling load	[N]	$W_{Carried}$	Mass carried by the fuselage	[lbs]
P_{flight}	Power required for staying airborne	[W]	W_{Elec}	Electrical system mass	[lbs]
$P_{generator}$	Power produced by the generator	[W]	W_{Emp}	Empennage mass	[lbs]
P_L	Applied load	[N]	$W_{A_{Emp}}$	Aerial mass of the empennage	[lbs ft ⁻²]
P_{Max}	Maximum engine power	[hp]	W_{Engine}	Engine mass	[lbs]
P_{max}	Maximum engine power	[W]	$W_{Eng,Installed}$	Installed engine mass	[lb]
P_{maxSL}	Maximum engine power at sea-level	[W]	W_F	Fuel mass	[kg]
$P_{PL,Max}$	Maximum payload power	[W]	W_{Fuel}	Fuel mass	[lbs]
P_r	Required power	[W]	$W_{FuelSys}$	Weight of fuel systems	[N]
P/W_{Ref}	Reference engine power to weight	[hp/lb]	$W_{FuelSys}$	Mass of fuel systems	[lbs]
			W_{Fuse}	Mass of the fuselage	[lbs]
			W_{LG}	Landing gear mass	[lbs]
			W_{nac}	Nacelle mass	[lbs]
			W_{Paint}	Paint mass	[kg]
			W_{PL}	Payload mass	[kg]
			W_{Prop}	Propellor mass	[lbs]
			W_{tfo}	Trapped oil and fuel mass	[kg]
			W_{TO}	Take-off mass	[kg]

Symbol	Definition	Unit	Symbol	Definition	Unit
W_{wing}	Mass of the wing	[kg]	C_{Y_p}	Sideforce-due-to-sideslip derivative	[$^{\circ-1}$]
x	Distance	[m]	C_{l_p}	Rolling-moment-due-to-roll-rate derivative	[$^{\circ-1}$]
x_{ac}	Aerodynamic center	[m]	C_{n_p}	Yawing-moment-due-to-roll-rate derivative	[$^{\circ-1}$]
y	Distance	[m]	C_{D_q}	Drag-due-to-pitch-rate derivative	[$^{\circ-1}$]
\bar{y}	Centroid location	[m]	C_{L_q}	Lift-due-to-pitch-rate derivative	[$^{\circ-1}$]
y_0	Distance to the neutral axis	[m]	C_{m_q}	Pitching-moment-due-to-pitch-rate derivative	[$^{\circ-1}$]
$y_{low_{max}}$	Maximum distance to lower panel	[m]	C_{Y_r}	Sideforce-due-to-sideslip derivative	[$^{\circ-1}$]
$y_{up_{max}}$	Maximum distance to upper panel	[m]	C_{l_r}	Rolling-moment-due-to-roll-rate derivative	[$^{\circ-1}$]
Symbol	Definition	Unit	Symbol	Definition	Unit
α	Angle of attack	[rad]	C_{n_r}	Sideforce-due-to-sideslip derivative	[$^{\circ-1}$]
α	Coefficient for crippling	-	$C_{D_{i_{hs}}}$	Drag-due-to-stabilizer-incidence derivative	[$^{\circ-1}$]
α_t	Angle of twist	[$^{\circ}$]	$C_{L_{i_{hs}}}$	Lift-due-to-stabilizer-incidence derivative	[$^{\circ-1}$]
β	Prandtl/Glauert factor	-	$C_{m_{i_{hs}}}$	Pitching-moment-due-to-stabilizer-incidence derivative	[$^{\circ-1}$]
Γ	Dihedral angle	[$^{\circ}$]	$C_{D_{ivs}}$	Drag-due-to-stabilizer-incidence derivative	[$^{\circ-1}$]
ϵ	Downwash angle	[rad]	$C_{L_{ivs}}$	Lift-due-to-stabilizer-incidence derivative	[$^{\circ-1}$]
η	Efficiency	-	$C_{m_{ivs}}$	Pitching-moment-due-to-stabilizer-incidence derivative	[$^{\circ-1}$]
η_p	Propeller efficiency	-	$C_{D_{\delta_e}}$	Drag-due-to-elevator derivative	[$^{\circ-1}$]
η_t	effective distance correction	-	$C_{L_{\delta_e}}$	Lift-due-to-elevator derivative	[$^{\circ-1}$]
θ	Angle	[$^{\circ}$]	$C_{m_{\delta_e}}$	Pitching-moment-due-to-elevator derivative	[$^{\circ-1}$]
Λ	Sweep	[$^{\circ}$]	$C_{Y_{\delta_r}}$	Sideforce-due-to-rudder derivative	[$^{\circ-1}$]
λ	Taper Ratio	-	$C_{l_{\delta_r}}$	Rolling-moment-due-to-rudder derivative	[$^{\circ-1}$]
μ	Viscosity	[N s m $^{-2}$]	$C_{n_{\delta_r}}$	Yawing-moment-due-to-rudder derivative	[$^{\circ-1}$]
μ	Friction coefficient	-	$C_{Y_{\delta_a}}$	Sideforce-due-to-aileron derivative	[$^{\circ-1}$]
μ_g	Aeroplane Mass Ratio	-	$C_{l_{\delta_a}}$	Rolling-moment-due-to-aileron derivative	[$^{\circ-1}$]
ν	Airfoil efficiency	-	$C_{n_{\delta_a}}$	Yawing-moment-due-to-aileron derivative	[$^{\circ-1}$]
ν	Poisson's ratio	-			
ρ	Density	[kg m $^{-3}$]			
ρ_0	Air Density at Sea-Level	[kg m $^{-3}$]			
σ	Density ratio	-			
σ_{cr}	Critical stress	[Pa]			
σ_{cc}	Crippling stress	[Pa]			
$\sigma_{low_{max}}$	Maximum stress lower panel	[Pa]			
$\sigma_{up_{max}}$	Maximum stress top panel	[Pa]			
τ	Shear stress	[Pa]			
τ_{cr}	Critical shear stress	[Pa]			
τ_{max}	Maximum shear stress	[Pa]			
$C_{Y_{\beta}}$	Sideforce-due-to-sideslip derivative	[$^{\circ-1}$]			
$C_{l_{\beta}}$	Rolling-moment-due-to-sideslip derivative	[$^{\circ-1}$]			
$C_{n_{\beta}}$	Yawing-moment-due-to-sideslip derivative	[$^{\circ-1}$]			
$C_{n_{T_{\beta}}}$	Yawing-moment-due-to-thrust-in-sideslip derivative	[$^{\circ-1}$]			

Executive Summary

The clearance of landmines is an important humanitarian problem to solve. It has been determined that an unmanned aerial vehicle (UAV) can offer significant benefits in the detection of landmines and minefields. In this report, a first iteration of the detailed design of a minefield detecting UAV, and detailed design choices are presented.

Design Concept

Before going into the detailed design of the UAV, a concept and configuration have been chosen. Four different concepts were considered, namely: lighter than air visualized in Figure 1a, rotorcraft shown in Figure 1b, hybrid VTOL in Figure 1d, and fixed-wing in Figure 1c. A fixed-wing UAV was deemed most suitable to assist in mine clearance and thus is the concept selected.



(a) Lighter-than-air



(b) Rotorcraft



(c) Fixed wing



(d) Hybrid VTOL

Figure 1: The feasible concepts selected for the trade-off

After selecting a concept, a configuration of systems was chosen to best suit the requirements. The resulting systems are: An internal combustion engine will be used for the propulsion system. A conventional wing and aft tail configuration will be designed. Horizontal take-off and landing from an unmaintained road will be designed for. The propulsion system will be mounted atop the UAV in a pusher configuration. A taildragger landing gear will be designed. Finally, for the tail, an H-Tail configuration is chosen.

Class II Estimations

As a first step in achieving a more detailed design, more accurate and detailed estimations are made of various important parameters of the UAV for further design.

First, a new estimate of the mass of the UAV is made. This time the mass of individual systems, such as the wings and the propulsion system, is determined. This results in a more detailed mass breakdown of all major components of the UAV. The results are a new take-off mass of 55.3 kg for which all subsystems will be sized as well as a mass breakdown of each subsystem. The mass of each subsystem acts as an upper limit for their respective design teams as well to ensure a proper design.

With more detailed information about the dimensions of the UAV available, a better estimate for the drag can also be made. This is done by estimating the drag of each component and subsequently adding these contributions up to reach the total UAV drag. This results in a new total zero-lift drag of 0.079.

Wing Planform Design

For the wing planform, some structural considerations are important. To simplify the wing structure and facilitate disassembly a quasi-elliptical wing planform was selected. This planform consists of a straight section of 0.7 m followed by a tapered section of 1.44 m adding up to a wing span of 4.28 m. The aircraft loading is also revisited and results in a wing surface area of 1.5 m^2 . With the taper ratio of 0.4 chosen this results in a root chord of 0.438 m and a tip chord of 0.175 m.

Engine Sizing

For the sizing of the engine, the take-off requirements are most limiting. It is determined that to take-off within the required 500 m at 4000 m altitude the engine should provide at least 6 kW of power at sea level. A suitable engine to satisfy these requirements is the 'Genpod 120 LRU' which is used in the design. For the fuel tank and fuel lines, it is determined that 10 L of fuel should be carried. For this a kevlar fuel tank with 10 L capacity is selected.

Control Surfaces

For the sizing of the control surfaces all stability coefficients are determined and later verified via simulations. The control derivatives are also determined and control surfaces are sized to assure controllability and stability. Furthermore, care is taken to ensure stable eigenmotions are achieved. It is ensured that all stability derivatives have the correct sign to ensure directional stability.

Structural Characteristics

The two main structural components of the UAV, wing and fuselage, are designed in detail. Not only does this serve as an initial structural design but also gives a mass estimate of higher accuracy for these parts of the UAV.

The load-carrying structure inside the wing is designed to sustain all aerodynamic loads under a maximum load factor of 3.8 g, for this critical structural part aluminum (7075-T6) will be used. First, an initial sizing is performed using a simplified wing box structure. This is then refined further to incorporate the effect of stringers and their dimensions as well as the spar caps. This detailed analysis resulted in a wing box structure with dimensions as shown in Figure 2. This also results in a mass estimate of 4.506 kg for the wing box structure. Well within the mass estimate of the wing however it should be noted this does not yet include the mass of the skin and any wing ribs. In Figure 3 the integration of the wing box inside the wing can also be seen.

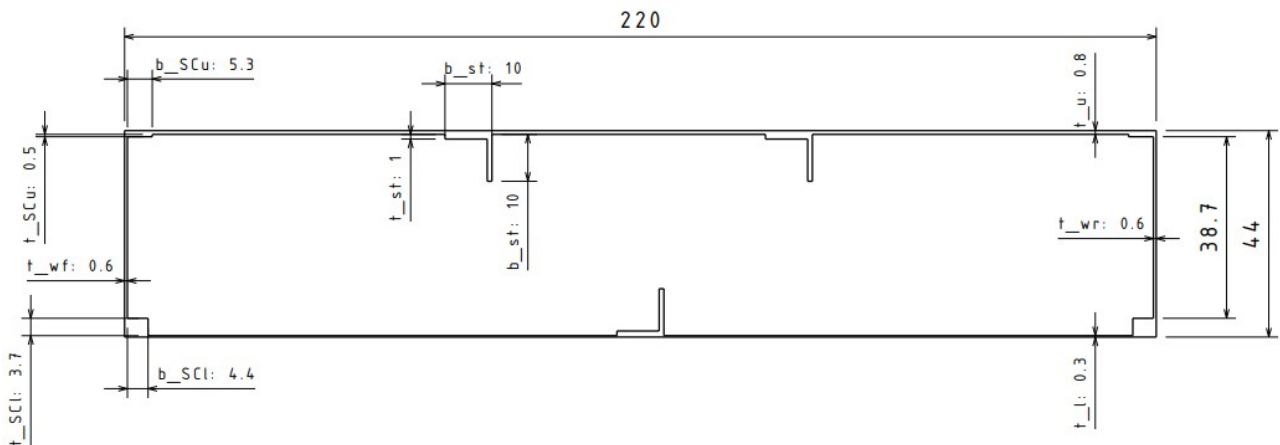


Figure 2: Wingbox Drawing with dimensions in mm

The load-carrying structure of the fuselage is to sustain all loads induced by the parts attached to it. This consists of the engine, wing, payload, and landing gear but also contains its own aerodynamic drag forces. The structure is modeled as a truss structure as shown in Figure 4. This results in the dimensions shown in Table 1.

Landing Gear

The detailed design of the landing gear is split into two parts. First, the main landing gear and secondly the tail gear is designed. The landing gear shall not only be able to support the weight of the UAV, it shall also provide sufficient grip for braking purposes on uneven terrain to satisfy the requirements.

The main landing gear carries the majority of the load and should be sized appropriately. For this ample safety factors are included such that particularly hard landings are also sustained. An off-the-shelf wheel and tire that satisfies these requirements is selected. The 'Electron Retracts 150 mm wheel' is to be used and the brake system corresponding to this product will also be used as it provides the necessary brake force. An ABS system is used as well to ensure optimal braking

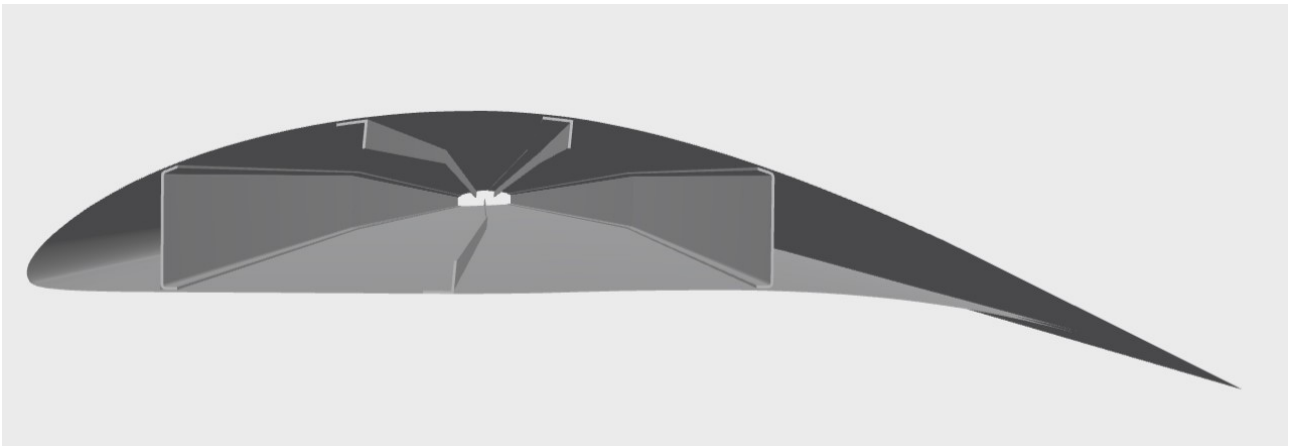


Figure 3: Wingbox implemented in the wing

Table 1: Dimensions of the load supporting trusses within the fuselage structure

output	Dimension [mm]
Bulkhead truss thickness	9.9 mm
Bulkhead truss width	28.5 mm
Horizontal truss thickness	1.8 mm
Horizontal truss width	17.9 mm
Weight bulkhead truss	0.357 kg
Weight horizontal truss	0.052 kg
Total weight bulkheads (8)	2.857
Total weight horizontal trusses (12)	0.622 kg

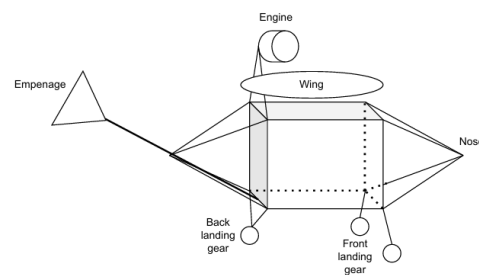


Figure 4: Truss structure of the fuselage

performance. The strut connecting the wheels to the fuselage is made of aluminum (7075-T6) and is sized to sustain all loads during landing. The mass of the wheels and brakes is known from the manufacturer and totals to 1.644 kg and the strut as designed has a mass of 104 g.

For the tail gear, the design is less complicated. There are no brakes attached to the tail gear and it only carries 20% of the weight. The strut of the tail gear is made of aluminum (7075-T6) and is sized to sustain these loads. Furthermore, to improve stability a caster of 6° is used for the tail gear strut. The mass of the strut as designed is only 18 g.

The placement of the main and tail gear is determined based on the clearance required both longitudinally and laterally. Tipover is also considered which is especially important given that a taildragger configuration is prone to tip over forwards. To satisfy these requirements the landing gear is placed 19 cm ahead of the center of gravity with a wheel track of 58.3 cm. The tail gear is placed as far aft as possible.

Avionics

For the avionics, a large selection of off-the-shelf components is selected to reduce development costs. Components are selected for the autopilot, navigation subsystem, obstacle avoidance system, auxiliary electronics, and communications. Systems for the ground station are also selected and a layout is designed. In Table 2 the selected components are listed and Figure 5 shows a visualization of the layout of the avionics systems.

Flight Performance

With the first iteration of detailed design performed the performance of the UAV is assessed. The performance in relevant scenarios such as take-off and landing, climb, and cruise is assessed. Fuel consumption is also assessed.

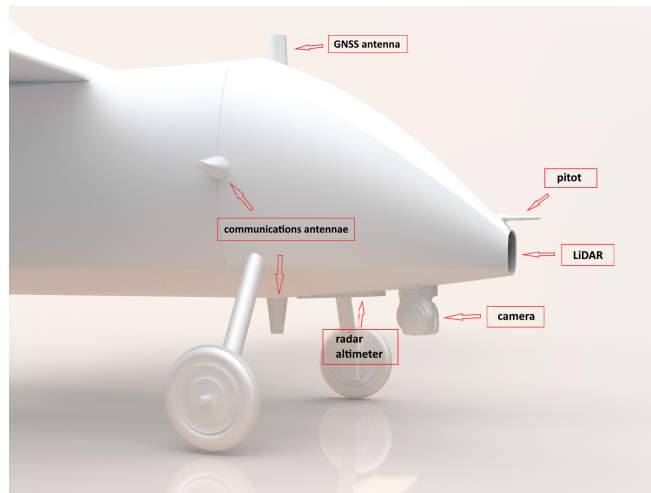
First, take-off is assessed. This results in a confirmation that the UAV can take-off within 500 m at 4000 m altitude given the engine selected.

Next, Climb performance is analyzed. To satisfy the required climb rate 1447.4 W of power is required at sea level. The selected engine can provide 7 kW thus climb performance is easily reached.

The performance of the UAV during its mission is also analyzed. Here the focus is placed on endurance and the required fuel mass is determined based on the parameters of the detailed design. It is determined that a fuel mass of 6.91 kg is necessary to reach the 4-hour endurance. This is lower than estimated in the Class II weight estimate and thus shows

Table 2: Overview of Chosen Avionics Components

Component	Chosen product
Autopilot	CubeOrange+
GNSS receiver	VectorNav VN-200CR
GNSS antenna	Tallysman HC771
Radar altimeter	Nanoradar NRA24
LiDAR	Livox Avia
Companion computer	Raspberry Pi 5
Camera	Trillium HD25-LV
Radio	UAVOS pMDDLRadio
Antenna	ICEFIN24NMOHF
Pitot-static tube	LUN 1154
Pressure sensor	MS4525DO
RID	Holybro RemoteID
ADS-B	uAvionix ping2020i

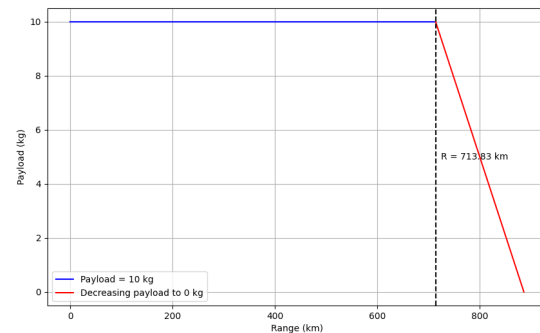
**Figure 5:** Placement of external avionics.

adequate performance of the UAV.

A payload range diagram is constructed to analyze the increased range of the UAV if the payload is removed. It is now clear that more fuel cannot be added however range can still be increased by removing payload weight as illustrated in Figure 6.

Budgets

With the information gathered from the detailed design budgets are reevaluated. The current most accurate mass estimate yields a take-off mass of 50.86 kg when incorporating the masses of designed components. The power budget is also detailed further incorporating the actual power consumption of the avionics yielding a power budget of 277 W for all systems except the payload yielding a total power budget of 777 W. For drag a total budget is determined to be 0.079.

**Figure 6:** Payload-range diagram

Systems Analysis

All relevant systems are again analyzed and their functional breakdown is specified further given the design choices made. The risk assessment is also updated to incorporate the detailed design choices made and their effect on risks. Aspects regarding logistics and operations are also detailed further based on the detailed design.

Based on the current vehicle, it is not possible to give much better estimates for reliability, availability, manufacturability, and safety (RAMS) than before. Thus using preliminary estimates, a mission failure rate of 0.0015 per flight hour is expected, resulting in a mean time between failures (MTBF) of 667 hours. Man hours of maintenance per flight hours will be equal to roughly 0.75. It is now known based on the selected engine that the engine requires a full overhaul every 300 flight hours. Furthermore, the spark plugs and air filters should be checked every 50 hours and replaced every 100 hours. The expected basic failure rate is roughly 0.0151 per flight hour, resulting in a MTBF of 66 hours. The basic failure rate includes minor errors and failures that require maintenance but do not cause mission failure. The risk to other people is expected to be small, due to landmines being found mostly in sparsely populated areas. At a later stage, the safety assessment needs to be evaluated and updated.

Verification and Validation

Throughout the design process, special care is taken to verify used models and validate their results. The steps and procedures to perform this verification as identified beforehand are followed. Assumptions made in these models are verified as well.

Given the detailed design and its characteristics, the requirements that were determined before will be verified as well. Requirements will be checked one by one and any requirements that are no longer relevant to the design due to choices made are stricken. Requirements that have not been met are listed as well. The One requirement that is not met is:

STK-0.3.2-CND-MIS-TOF-1 as the UAV can only achieve this take-off requirement at an altitude of 4000 m. Given the environmental conditions in the regions of interest, this requirement has thus been reduced to the 4000 m altitude. FUN-NAV-4.N.3.b.i is also not met as the navigation system can not determine the altitude within 10 m accuracy.

In addition to verifying requirements, a sensitivity analysis is performed to assess the sensitivity of the design. This shows that the design is most sensitive to weight increases, especially concerning the take-off performance. The sensitivity of the design concerning other requirements such as endurance is far smaller thus special care is taken when take-off is concerned.

Production Plan

While the design is not yet finalized, it is useful to already consider manufacturing. For that, four main phases have been identified, which are:

1. Manufacturing structural elements: Build the elements that make up the overall shape of the aircraft, such as the wings and fuselage.
2. Assemble primary structure: Connect the main structural elements and install components that are hard to reach afterward.
3. Install subsystems: Install all smaller subsystems that have not been installed before.
4. Ship product to the customer: Disassemble the product if necessary and package and ship it to the customer.

Given the material choices made during the design, some suitable manufacturing techniques are presented as well as the parts required to assemble intermediate structures such as the wing box. A flow diagram has been created to work out these phases in more detail. Thus, the work will start by assembling the main structural elements, after which the smaller subsystems are installed. As the payload and engine are the most expensive parts, they will be installed last. Finally, the product is prepared for shipping.

Sustainable Development Strategy

Several strategies have been employed to ensure the sustainability of the UAV over its lifecycle. The project promotes social sustainability by addressing an important humanitarian issue. To mitigate the environmental impact of the UAV, a life-cycle analysis has been carried out. Based on the analysis, several strategies have been found that can be employed to reduce that impact, such as using a modular design or focusing on local production as well as utilizing sustainable materials for noncritical parts.

Concluding Remarks

Based on this, one can be relatively certain that the design in its current state satisfies all requirements. Further development is required to ensure all subsystems are designed to sufficient detail and an actual product can be produced.

Contents

	Nomenclature	i		
	Executive Summary	iv		
1	Introduction	1		
2	Design Concept	2		
2.1	Concept Trade-Off	2		
2.2	System Trade-Offs	3		
3	Class II Estimations	6		
3.1	Class II Weight	6		
3.2	Class II Drag	8		
3.2.1	Component Build Up	8		
3.2.2	Excessive Fuselage Drag	9		
3.2.3	Zero Lift Drag Estimates	10		
4	Wing Planform Design	11		
4.1	Options	11		
4.2	Aircraft loading diagram	12		
4.3	Wing Details	13		
4.4	Design of quasi elliptical wing	13		
5	Engine Sizing	15		
5.1	Subsystem Requirements	15		
5.2	Power required	15		
5.3	Engine Sizing and Selection	15		
5.4	Propeller Sizing	15		
5.5	Fuel Tank Sizing	16		
5.6	Verification and validation	16		
5.6.1	Total mass budget	16		
5.6.2	Unit tests	16		
5.6.3	Subsystem verification	16		
6	Control Surfaces	17		
6.1	Subsystem Requirements	17		
6.2	Tail Positioning	17		
6.2.1	Scissor Plot	18		
6.2.2	Moment-Lift Curve	18		
6.3	Tail Sizing	19		
6.3.1	Horizontal Stabilizer	20		
6.3.2	Vertical Stabilizer	20		
6.3.3	Moment Equilibrium	20		
6.4	Control Surfaces Sizing	20		
6.4.1	Elevator	21		
6.4.2	Rudder	21		
6.4.3	Aileron	22		
6.5	Derivatives	22		
6.5.1	Stability and Control	22		
6.5.2	Hinge moment	23		
6.6	Static stability	24		
6.6.1	Static longitudinal stability	24		
6.6.2	Static Lateral-Directional Stability	25		
6.7	Dynamic stability	25		
6.7.1	Dynamic longitudinal stability	26		
6.7.2	Dynamic Lateral-Directional Stability	27		
6.8	Verification And Validation	29		
7	Structural Characteristics	31		
7.1	Subsystem requirements	31		
7.2	Material considerations	31		
7.3	Wing design	31		
7.3.1	Wing elements	32		
7.3.2	Internal loads	32		
7.3.3	First-order wing box design	33		
7.3.4	Detailed wing box design	34		
7.4	Fuselage design	40		
7.5	Verification and Validation	42		
7.5.1	Unit tests	42		
7.5.2	Subsystem verification	43		
8	Landing Gear	44		
8.1	Subsystem Requirements	44		
8.2	Main gear wheel sizing	44		
8.3	Wheel brake sizing	45		
8.4	Gear position	45		
8.4.1	Longitudinal clearance	45		
8.4.2	Lateral clearance	46		
8.5	Strut sizing	47		
8.5.1	Main gear strut	47		
8.5.2	Tail gear strut	48		
8.5.3	Total mass budget	49		
8.6	Verification and Validation	49		
8.6.1	Unit tests	49		
8.6.2	Subsystem verification	49		
9	Avionics	50		
9.1	System & Subsystem Requirements	50		
9.2	Autopilot	52		
9.3	Navigation	53		
9.4	Obstacle avoidance	54		
9.5	Auxiliary Electronics	54		
9.6	Communications	55		
9.7	Ground Control Station	56		
9.8	Layout and Electrical Design	56		
9.8.1	Physical Layout	57		
9.8.2	Electrical and Software Interface	58		
9.8.3	Battery Sizing	60		
9.8.4	Wiring and Circuitry	61		
9.9	Flight Software	61		
9.10	Verification and Validation	63		
10	Aerodynamic Performance	65		
10.1	XFLR5 modeling	65		
10.1.1	Advantages and disadvantages of XFLR5	65		
10.1.2	Disadvantages of XFLR5	65		
10.1.3	Modeling method chosen	65		
10.2	Stall angle determination	66		
10.3	Results of stability modeling	66		
10.4	Optimisation for cruise	67		
10.5	Verification Validation of XFLR5	68		
10.5.1	Lift and Drag	68		
10.5.2	Moment	69		
10.5.3	Tail incidence angle	69		
10.6	Ultimate load	69		
11	Flight performance	71		
11.1	Flight performance requirements	71		
11.2	Take-off and landing	71		
11.3	Climb	72		
11.4	Mission profile	72		
11.5	Fuel fractions	73		
11.6	Payload-range diagrams	74		
11.7	Noise	74		
11.8	Verification and validation	75		
11.8.1	Unit tests	75		
11.8.2	Subsystem verification	75		
12	Budgets	77		
12.1	Power budget	77		
12.2	Drag budget	77		
12.3	Data handling budget	77		
12.4	Mass Budget	77		
12.5	Cost budget	78		

12.6	Market analysis	80	14.4.4	STK-0.3.2-CND-MIS-TOF-1: Take-off limit	106
12.6.1	Stakeholders	80	14.4.5	STK-0.2.6-MIS-PLD-5: Payload power	107
12.6.2	Economic Impact of Mines	81	14.4.6	STK-1.2-MIS-RNG-1: Distance to suspected minefield	107
12.6.3	Cost of Demining	81	14.4.7	Future possibilities	108
12.6.4	Countries Affected	82			
12.6.5	Organizations	82	15	Production Plan	109
12.6.6	Customer Needs	83	15.1	Manufacturing structural parts	109
12.7	Return on Investment	83	15.1.1	Aluminum deformation	109
13	Systems Analysis	84	15.1.2	Shaping structure	109
13.1	Functional Analysis	84	15.2	Assembling primary structure	110
13.1.1	Functional Breakdown	84	15.3	Installing subsystems	110
13.1.2	Systems	84	15.4	Shipping	110
13.1.3	System Functional Breakdown	84	16	Sustainable Development Strategy	112
13.1.4	Project Risk Assessment	85	16.1	Social Sustainability	112
13.1.5	System Functional Hazard Assessment	87	16.2	Life-Cycle Analysis	113
13.2	Logistics and Operations	94	16.2.1	Development	113
13.3	Reliability, Availability, Maintainability and Safety	95	16.2.2	Use	114
13.3.1	Reliability	95	16.2.3	Recovery	115
13.3.2	Availability	95	16.2.4	Sourcing	116
13.3.3	Maintainability	96	16.2.5	Manufacturing	116
13.3.4	Safety	96	16.2.6	Distribution	116
14	Verification and Validation	97	16.3	Environmental Impact Mitigation Strategies	116
14.1	Model validation	97	17	Future Design and Development	117
14.2	Product verification	97	18	Organization & Planning	119
14.2.1	Compliance Matrices	97	18.1	Work Flow Diagram	119
14.2.2	Stricken Requirements	103	18.2	Work Breakdown Diagram	119
14.2.3	Requirements not met	103	18.3	Gantt Chart	119
14.3	Product Validation	104	18.4	Organogram	119
14.4	Sensitivity Analysis	104	19	Conclusion	125
14.4.1	STK-0.2.1-MIS-PLD-1: Payload mass	104	References	126	
14.4.2	STK-0.3.1-MIS-ENV-1: Endurance	105	A	Drawings and Layout	130
14.4.3	FUN-SUS-4.S.1.3.a: Maximum loading	106			

Introduction

After conflict, long after the tanks have left the battlefield, people continue to suffer due to the effects of the battle. Decades after a war, civilians still get injured by residual unexploded ordinance and, crucially, landmines [1]. In 2022, 1661 people were killed by landmines, with an additional 3015 injured, with civilians making up 85% of these casualties and children making up nearly half of the civilian casualties [2]. However, removing landmines is currently a very slow process, with an estimated 1100 years required to clear all the mines currently present [1]. Thus, faster and safer methods, such as using an unmanned aerial vehicle (UAV), can bring significant benefits.

Before demining takes place, first a non-technical survey is conducted. In this survey, using analysis of records and interviews with the local population, it is determined which areas require extra intervention [3]. Here, the UAV can offer serious benefits by giving a quick overview of areas that warrant further investigation. Thus, this project deals with the development of such a UAV, to aid with the detection of minefields in contaminated areas. Previously, the preliminary design of the UAV has been completed, resulting in the decision that a fixed-wing UAV in a conventional configuration with engine mounted on top will be designed.

In this report, a detailed design of the UAV is presented. After presenting an overview of the various design concepts selected in the previous report in chapter 2, a class II estimation is used to improve the estimate on the mass and drag of the UAV in chapter 3. Next, design of the major systems of the UAV begins, including choosing some systems and subsystems from commercially available ones. In chapter 4, the wing planform is designed in more detail than the previously selected preliminary characteristics. Requirements for the engine, in particular the power required, are calculated in chapter 5. Subsequently, the various subsystems of the propulsion system are sized and a suitable engine is picked from commercially available ones. In chapter 6, the stabilizers and control surfaces of the UAV are sized, and the stability is analyzed. In chapter 7, loads are estimated for the main structures of the UAV and some preliminary structural design is done. Additionally, a suitable material is selected for the wing and fuselage structure. Next, the landing gear is designed in chapter 8. The wheel itself is sized, its position is calculated and the strut connecting the wheels to the body are designed. Finally, the last major system of the UAV is designed in chapter 9: Suitable components are selected for autopilot, navigation, and communications, and preliminary physical, electrical, and software interfacing is planned.

Once the various systems of the UAV are planned, some additional analysis of the aircraft as a whole is carried out based on the newly known details of the system sizing. In chapter 10, the aerodynamic performance of the UAV is analyzed, followed by an analysis of the flight performance in chapter 11. Mass, cost, power, drag, and data handling budgets are established in chapter 12. A systems analysis is performed in chapter 13, including a functional analysis, logistics planning, and an analysis of the reliability, availability, maintainability, and safety of the UAV. In chapter 14, the verification and validation efforts are detailed. A production plan of the UAV is presented in chapter 15, and sustainability is considered in chapter 16. Future design plans are laid out in chapter 17, the organization of the entire project is revised in chapter 18, and finally the currently reported design phase is concluded in chapter 19. Technical drawings of the UAV are presented in Appendix A.

Design Concept

In this report, a conventional fixed-wing UAV is designed. To show how this concept was chosen, a review of the concept and system trade-offs from the midterm report [4] is given, as these are the decisions that resulted in the concept and systems currently being designed. In section 2.1, the main trade-off, its options and its results are detailed. In section 2.2, the preliminary design choices done for the different systems of the UAV are presented to set the stage for the detailed design of the systems presented later in this report.

2.1. Concept Trade-Off

By constructing a design option tree as shown in Figure 2.1, in the preliminary design phase various initial concept ideas were limited down to four concepts that were deemed most feasible: lighter-than-air, rotorcraft, fixed wing, and hybrid VTOL.

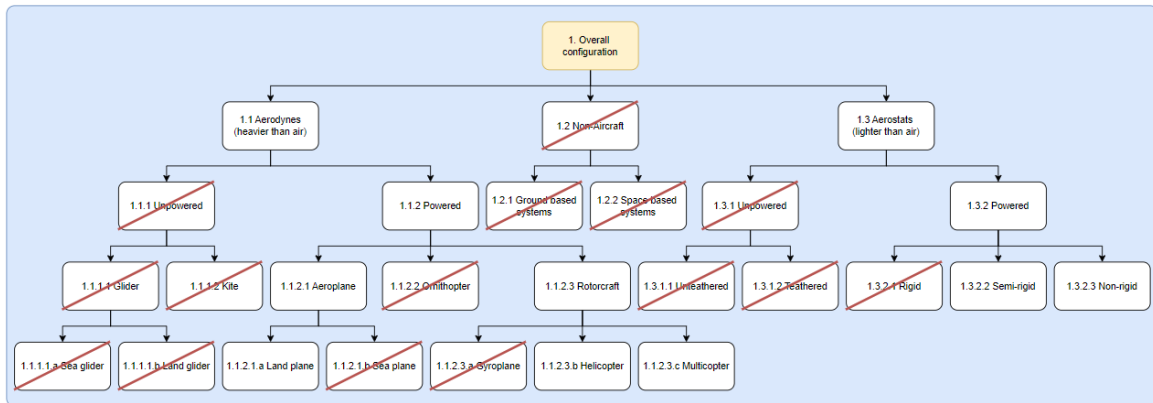


Figure 2.1: Design option tree



(a) Lighter-than-air



(b) Rotorcraft



(c) Fixed wing



(d) Hybrid VTOL

Figure 2.2: The feasible concepts selected for the trade-off

An example of each concept is shown in Figure 2.2. Lighter-than-air aircraft produce lift through the use of buoyant gasses such as helium, hydrogen or hot air. Lighter-than-air concepts can be further divided into rigid, non-rigid and semi-rigid airships and balloons; mainly non-rigid airships were considered for the trade-off. Next, rotorcraft are aircraft that produce lift by rapidly rotating aerodynamic surfaces. The category involves single-rotor aircraft or helicopters, and

multi-rotor concepts such as quadcopters. Single-rotor configurations are considered due to their improved endurance and range. Conventional or fixed-wing aircraft are aircraft that produce lift using a fixed aerodynamic surface, namely a wing. Finally, hybrid VTOL is a broad category containing aircraft that take-off and land vertically, but generate lift by fixed aerodynamic surfaces in cruise flight. A typical VTOL configuration would be a combination of a rotorcraft and a fixed-wing configuration, using the vertical propellers to provide lift during take-off and landing, and the wing during cruise.

In the midterm report, the four selected concepts were compared in a trade-off study to determine the optimal concept. Six criteria were considered in the trade-off: mass of the system, reliability, efficiency, maintenance costs, operations (namely airfield performance), and development risk. The results of the trade-off are shown in Table 2.1, including the final scores of the concepts. Based on the trade-off, the conventional fixed-wing configuration won with a score of 4.15, and this is the configuration that is designed in more detail in this report.

Table 2.1: Trade-off scores

Concept	Weight (0.15)	Reliability (0.15)	Efficiency (0.25)	Maintenance (0.15)	Operations (0.20)	Development (0.10)	Final score
Lighter-than-air	2 12.5%	4	5 - 61	4	3	3	3.65
Rotorcraft	3 18.53%	2	1 - 5	2	4	4	2.3
Fixed-wing	4 21.47%	5	5 - 45	3	3	5	4.15
Hybrid VTOL	3 16.84%	3	4 - 39	2	5	4	3.6

2.2. System Trade-Offs

Besides the overall configuration, concepts for the main systems of the UAV were also selected through a series of trade-offs. The results of these trade-offs are presented in this section, as a review of the results of the midterm report. The selected concepts for each system are designed in more detail in later chapters of this report.

First, the propulsion system was chosen from four choices, of which two were electric propulsion systems and two internal combustion engines. The options considered were hydrogen-electric propulsion, battery-electric propulsion, and piston and Wankel engines. The criteria used were power-to-weight ratio, energy density of the fuel, logistics (namely availability of fuel), emissions, maintainability, and reliability. The scoring of the trade off, including the final scores, is shown in Table 2.2. The Wankel engine won the trade-off with a score of 3.55, with the piston engine coming second at a score of 3.35. As the two engine types are very similar and the variation in their scores is not very large, the choice between the two was left open. Eventually in section 5.3, a piston engine is chosen as the actual concept to be used, as a commercially available Wankel engine meeting the requirements could not be found.

Table 2.2: Trade-off scores propulsion

Concept	Power-to-weight (0.25)	Energy density (0.30)	Logistics (0.20)	Emissions (0.05)	Maintainability (0.10)	Reliability (0.10)	Final score
Hydrogen-electric	1	5	1	4	2	3	2.65
Battery-electric	5	1	2	5	5	5	3.2
Piston engine	3	3	5	2	3	3	3.35
Wankel engine	4	3	5	1	2	4	3.55

For the wing configuration, six different concepts were considered. In the conventional configuration, the main wing is attached to the body while the horizontal and vertical stabilizers form the tail assembly aft of the main wing. In the canard configuration, the horizontal stabilizers are located ahead of the main wing, near the nose of the aircraft. A tandem wing configuration consists of two similarly sized main wings, that act as both lifting and control surfaces. The blended wing body configuration is similar to the conventional one, but the wing is attached to the body smoothly to increase the aerodynamic properties. A flying wing has the payload integrated as part of the wing structure, lacking a distinct body, and finally the joined wing is a variation of the tandem configuration where the two wings are connected at their tips.

The wing configurations were traded off based on the following criteria: ease of disassembly, transportation volume, ease of payload integration, development risk, the estimated lift-to-drag ratio of the configuration, stability and controllability, and finally the mass of the configuration. The results of the trade-off are shown in Table 2.3, with the conventional concept winning the trade-off with a score of 4.15. Some wing characteristics, including the airfoil selection, were already designed in the midterm report, while more detailed wing design is presented in chapter 4 of this report.

Table 2.3: Trade-off criteria and corresponding scoring for wing configuration

Concept	Disassembly (0.10)		Transportation volume (0.05) Payload integration (0.15)		Development risk (0.20)		Lift-to-drag (0.25)		Controllability & Stability (0.15)		Mass (0.10)	Final score
Conventional	5	4	5	5	3	3	5	2	2	3	4.15	
Canard	5	4	5	4	3	3	4	2	2	3	3.80	
Tandem	4	5	5	4	3	3	4	3	3	3	3.85	
Blended wing	2	2	3	2	4	4	3	3	3	3	2.90	
Flying wing	1	3	1	3	5	5	1	4	4	4	2.80	
Joined wing	3	3	5	1	5	5	4	5	5	5	3.75	

For take-off and landing, various concepts were also traded off. Besides horizontal and vertical take-off under the power of the UAV itself, assisted take-off with either a rail or tow launcher was considered. The scoring was based on operational constraints (namely the required runway length), operational complexity, system complexity, reliability, and cost. The scoring of the trade-off is shown in Table 2.4; the conventional horizontal take-off won the trade-off due to its simplicity and reliability.

More options were considered for landing methods: stopping the UAV using a catch wire, wheel brakes, reverse thrust, passive braking, aerodynamic braking, or a parachute were all considered, as well as landing using vertical propulsion. The criteria used were the same as the ones for the take-off: operational constraints, operational complexity, system complexity, reliability, and cost. Based on the trade-off, passive braking wins, with wheel brakes coming close second. As the difference is not large, the two options are left open and in section 8.3 of this report, active brakes are eventually integrated into the landing gears.

As for both take-off and landing, a conventional horizontal solution was chosen, design of additional systems for assisted take-off or landing is not necessary. Therefore the take-off and landing systems themselves don't require further detailed design. Instead, take-off and landing performance is considered in the design of various systems, in particular the wing in chapter 4, propulsion system in chapter 5 and the landing gears in chapter 8. Additionally, take-off and landing performance are an important part of the flight performance design in chapter 11.

Table 2.4: Trade-off scores take-off

Concept	Operational constraints (0.10)		Operational complexity (0.30)		System complexity (0.25)		Reliability (0.20)		Cost (0.15)		Final score
Rail launcher	5	3	2	2	3	3	4	4	3	3.1	
Tow launcher	3	2	4	4	5	5	2	2	2	3.2	
Horizontal take-off	3	4	4	4	5	5	4	4	4	4.1	
Vertical take-off	5	5	2	2	3	3	2	2	2	3.4	

Table 2.5: Trade-off scores landing

Concept	Operational constraints (0.10)		Operational complexity (0.30)		System complexity (0.25)		Reliability (0.20)		Cost (0.15)		Final score
Catch wire	5	2	1	1	3	3	3	3	3	2.4	
Wheel brakes	3	5	3	3	5	5	4	4	4	4.15	
Reverse thrust	3	4	2	2	5	5	2	2	2	3.3	
Passive braking	1	5	4	4	5	5	5	5	5	4.35	
Aerodynamic braking	3	4	3	3	5	5	4	4	4	3.85	
Vertical propulsion	5	3	2	2	3	3	1	1	1	2.65	
Parachute	5	3	1	1	3	3	3	3	3	2.7	

For landing gear, only two concepts were compared: a taildragger or tricycle landing gear. The difference between the two concepts is in the positioning of the landing gear: the taildragger has a pair of landing gears in front and a singular one in the back, while for the tricycle this is reversed. The options were traded off based on stability, performance on uneven terrain, drag, and runway length required for take-off and landing, as shown in Table 2.6. Based on the trade-off, the taildragger concept is better for the UAV being designed. The design of the landing gear is detailed in chapter 8.

Table 2.6: Trade-off scores landing gear

Concept	Stability (0.30)	Terrain performance (0.35)	Drag (0.10)	Take-off & landing run (0.25)	Final score
Taildragger	4	5	4	3	4.1
Tricycle	5	2	2	5	3.65

Four options were considered for the location of the propulsion system. In the tractor configuration, the engine is located in the nose of the UAV. The wing-mounted configuration involves two engines mounted on or under the wings, while the twin-boom pusher has the engine mounted behind the body, pushing the UAV forwards. Finally, the top-mounted configuration has the engine mounted on top of the body.

The criteria used were mass, ground clearance, susceptibility to foreign object debris, aerodynamic performance, and ease of integration. As shown in Table 2.7, the top-mounted configuration won the trade-off with a score of 3.9, as being mounted above the body brings advantages for take-off and landing from uneven roads. The structure connecting the engine to the fuselage is considered in section 7.4.

Table 2.7: Trade-off scores propulsion location

Concept	Mass (0.15)	Ground clearance (0.25)	Foreign object debris (0.25)	Aerodynamics (0.10)	Integration (0.25)	Final score
Tractor	5	2	3	4	4	3.65
Wing-mounted	1	3	2	5	3	2.65
Twin-boom pusher	2	1	1	2	2	1.5
Top-mounted	3	5	5	2	3	3.9

Finally, the tail configuration was traded off. Concepts considered were the H-tail, V-tail, T-tail and the conventional tail configuration. For the H-, V-, and T-tails, the shape of each configuration is well visualized by the shape of the letters representing them, while the conventional tail is similar to an upside-down T, as seen on most conventional fixed-wing aircraft. The scores used to choose the tail configuration were mass of the configuration, control and stability, development risk, and ease of integration. As shown in Table 2.8, the H-tail won the trade-off with a score of 4.2. In chapter 6, the design of the tail is carried out in more detail.

Table 2.8: Trade-off Scores Tail configuration

Concept	Mass(0.20)	Control and stability (0.30)	Development risk (0.10)	Integration (0.40)	Final score
H-tail	3	4	4	5	4.2
V-tail	5	2	3	5	3.9
T-tail	4	4	5	1	2.9
Conventional tail	4	5	5	2	3.6

Class II Estimations

Now that more detailed information is known about the general dimensions of the UAV an improved estimate of the weight can be determined in section 3.1 as well as for the drag in section 3.2.

3.1. Class II Weight

Based on a literature study, methods for structural weight estimations for similarly sized UAV designs are found to be lacking. As such, methods defined for medium altitude long endurance UAVs are to be used, based on [5, CHA. 6.3]. These are larger than the minesweeper UAV, but present similar configurations. Most importantly the absence of crew is considered in these equations which is the main differing factor compared to classical manned aircraft in the weight estimation.

As a start, the mass of the wing is determined using Equation 3.1 [5, p. 206]. Where N_Z is the ultimate load factor in g (The maximum load factor multiplied by a safety factor of 1.5), where the maximum load factor is taken as 3.8 as determined in [4]. W_{TO} is the take-off mass in kg, AR is the aspect ratio, S_w the surface area of the wing in m^2 , λ the taper ratio, and t/c the thickness to chord ratio.

$$W_{wing} = 0.0038 \cdot (N_Z \cdot W_{TO})^{1.06} \cdot AR^{0.38} \cdot S_w^{0.25} \cdot (1 + \lambda)^{0.21} \cdot (t/c)_{root}^{-0.14} \quad (3.1)$$

Subsequently, the mass of the fuselage is estimated using Equation 3.2 [5, p. 208]. Where F_{MG} , F_{NG} , F_{Press} , F_{VT} , F_{Matl} are parameter defined as in Figure 3.1. Here the main gear was incorporated into the fuselage and the nose gear was not given that the UAV will be a taildragger. The fuselage will not be pressurized and there will be no vertical tail on the fuselage. Finally, the Material factor was set at 1 for now. L_{Struct} is the length of the fuselage structure in feet, $W_{Carried}$ is the mass carried by the fuselage structure in pounds this includes the payload and the fuel, N_Z is again the ultimate load factor, $V_{eq,Max}$ the maximum equivalent velocity in knots.

Term	Definition	Value
F_{MG}	Main gear on the fuselage factor	1 if no main gear is on fuselage 1.07 if main gear is on fuselage
F_{NG}	Nose gear on the fuselage factor	1 if no nose gear is on fuselage 1.04 if nose gear is on fuselage
F_{Press}	Pressurized fuselage factor	1 if unpressurized 1.08 if pressurized
F_{VT}	Vertical tail on the fuselage factor	1 if vertical tail weight not included 1.1 if vertical tail weight included
F_{Matl}	Materials factor	1 if carbon fiber 2 if fiberglass 1 if metal 2.187 if wood 2 if unknown

Figure 3.1: Fuselage weight estimation parameters [5, p. 208]

$$W_{Fuse} = 0.5257 \cdot F_{MG} \cdot F_{NG} \cdot F_{Press} \cdot F_{VT} \cdot F_{Matl} \times L_{Struct}^{0.3796} \cdot (W_{Carried} \cdot N_Z)^{0.4863} \cdot (1.3 \cdot V_{eq,Max} / 100)^2 \quad (3.2)$$

For the empennage mass Equation 3.3 [5, p. 207] was used. Here WA_{Emp} is the aerial weight of the empennage in pounds per square feet which should be approximately 1 according to [5, p. 207], S_{Emp} the empennage planform area in square feet which results from section 6.3.

$$W_{EMP} = WA_{Emp} \cdot S_{Emp} \quad (3.3)$$

With the empennage mass, the mass of the boom connection between the fuselage and the tail can be estimated using Equation 3.4 [5, p. 208]. Where L_{Boom} is the length of the boom in feet as determined in section 6.2 and W_{Cant} the mass of the empennage following from Equation 3.3 in pounds.

$$W_{Booms} = 0.14 \cdot L_{Boom} \cdot W_{Cant} \quad (3.4)$$

Next, the landing gear mass was estimated using Equation 3.5 [5, p. 210]. Here F_{LG} is the landing gear mass fraction proposed to be 0.4 as a start by [5, p. 210] and W_{TO} is the take-off mass in pounds.

$$W_{LG} = F_{LG} \cdot W_{TO} \quad (3.5)$$

For a first estimate of the engine mass Equation 3.6 from [5, p. 212] is used. Where P_{Max} is the maximum required power in horsepower, P/W_{Ref} is a reference power-to-weight ratio of a relevant engine and is set at 1 hp/lb as suggested by [5, p. 297].

$$W_{Engine} = P_{Max} \cdot P/W_{Ref} \quad (3.6)$$

With an estimate for the engine mass, an estimate can be made for the engine mass including its mounting and integration using Equation 3.7 [5, p. 212]. This includes the engine mounting frame, mufflers, vibration isolators, and cooling system. With $F_{Install}$ the installation factor which is set at 1.2 [5, p. 212].

$$W_{Eng,Installed} = F_{Install} \cdot W_{Engine} \quad (3.7)$$

For the nacelle structure that accompanies the propulsion system the mass can also be estimated using Equation 3.8 [5, p. 209]. Here F_{nac} nacelle multiplication factor which is set at a value of 0.27 as recommended by [5, p. 210] for UAVs. $E1$ is set as 1 as per [5, p. 210] and P_{MAX} is the maximum power the propulsion system generates in horsepower.

$$W_{nac} = F_{nac} \cdot P_{Max}^{E1} \quad (3.8)$$

For the propellers that will be attached to the engine, the mass can be estimated using Equation 3.9 [5, p. 213]. Where K_{Prop} is a multiplication factor set at 15 as recommended by [5, p. 213] for engines with less than 50 shaft horsepower. N_{Proprs} is the number of propellers which is equal to the number of engines so 1. N_{Blades} are the number of blades per propeller initially set at 3. D is the propeller diameter in feet and P_{Max} the maximum power coming from the engine in horsepower

$$W_{Prop} = K_{Prop} \cdot N_{Proprs} \cdot N_{Blades}^{0.391} \cdot \left(\frac{D \cdot P_{Max}}{1000 \cdot N_{Proprs}} \right)^{0.782} \quad (3.9)$$

The fuel system mass can be estimated using Equation 3.10 [5, p. 213]. This includes fuel tanks, pumps, fuel lines, valves, and venting, among other components for traditional fuel types [5, p. 213]. Here F_{fs} is the fuel multiplication factor set at 0.075 as [5, p. 214] suggests. W_{Fuel} is the fuel weight in pounds and $E1$ is set at 1 as stated by [5, p. 214].

$$W_{FuelSys} = F_{fs} \cdot W_{Fuel}^{E1} \quad (3.10)$$

For the avionics, [5, p. 216] suggest to use Equation 3.11. This includes avionics, instrumentation, communication, and wiring. Where the avionics is composed of among others the autopilot, the processor, and the inertial navigation system. for f_{Avion} a value between 0.06 and 0.16 is suggested as many of the components incorporated in this avionics weight are accounted for by themselves (such as the autopilot, processor, and the wiring) a value of 0.06 is selected. W_{TO} is again the take-off mass.

$$W_{Avion} = f_{Avion} \cdot W_{TO} \quad (3.11)$$

For smaller components such as the autopilot and the GPS, weight fractions make little sense. As such a set weight was estimated for these components. Which is listed in Table 3.1. For the electrical system mass, which includes all the wiring, converters, and power distribution units Equation 3.12 [5, p. 221] was used. Here $P_{PL,Max}$ is the maximum payload power in watts, W_{Avion} is the total avionics mass which includes the individual systems such as the autopilot but not the avionics mass from Equation 3.11 as the wiring was incorporated in that estimation. L_{Tot} is the total length of the structure in feet, thus fuselage and boom combined, and b is the wingspan in feet.

$$W_{Elec} = 0.003 \cdot (P_{PL,Max} + 15 \cdot W_{Avion})^{0.8} \cdot (L_{Tot} + b)^{0.7} \quad (3.12)$$

For the paint weight Equation 3.13 [5, p. 225] was used. With MF_{Paint} is the paint mass fraction set at 0.003 as suggested by Roskam [6].

$$W_{Paint} = MF_{Paint} \cdot W_{TO} \quad (3.13)$$

The mass of the trapped fuels and oils can be determined using Equation 3.14 [5, p. 226]. Where F_{ifo} is the multiplication factor set at 0.01 as suggested by [5, p. 226].

$$W_{ifo} = F_{ifo} \cdot W_{Fuel} \quad (3.14)$$

All of the initial inputs used for these formulas are listed in Table 3.1 and all the outputs generated are listed in Table 3.2. It should be noted that Equation 3.6 and Equation 3.7 were not used in the calculation. Instead, an engine was selected that satisfies the critical power requirements during take-off and its weight along with the mounting weight was implemented as well as its power output. P_{MAX} of this engine can be seen in Table 3.1 and the installed engine weight in Table 3.2. This significantly improves the accuracy of the class II estimate as one of the parts is now no longer an estimate but has a definitive mass. Summing all of the masses results in a new improved estimate for the empty operating weight (OEW) which is now estimated to be 37.71 kg. The take-off mass can then be determined using Equation 3.15 where the fraction $\frac{W_F}{W_{TO}}$ is the fuel fraction determined in the midterm report [4] using the Breguet range equation.

$$W_{TO} = \frac{W_{PL} + OEW}{1 - \left(\frac{W_F}{W_{TO}} \right)} \quad (3.15)$$

Subsequently, The fuel mass can be determined by using Equation 3.16.

$$W_{fuel} = W_{TO} - OEW - W_{PL} \quad (3.16)$$

These calculations were then iterated until the take-off mass changes with less than 0.1% the values that result from that are listed in Table 3.2. As part of this iteration loop the wing surface area is also constantly updated based on the wing loading value found in the midterm report [4] and the wingspan is changed accordingly as well. As such the resulting mass is as accurate as can be as all changes except for changes in the empennage size are accounted for.

These calculations will have to be performed multiple times as this new take-off weight might result in changes required for the empennage design for example. As such these values are far from final and are merely meant as an initial step. When more accurate weight estimations become available such as with the engine mass these will be implemented instead of the estimation formulas presented before. As such the avionics mass estimate will be completely replaced by the actual weights of the avionics components. This way the weight estimation becomes increasingly more accurate. The final mass breakdown after this process is applied is given in chapter 12.

Table 3.1: Inputs for Class II weight estimation

Name	Symbol	Value	Unit
Ultimate load factor	N_Z	5.7	-
Take-off Weight	W_{TO}	39.84676	[kg]
Aspect ratio	AR	12	-
Wing surface area	S_w	1.08	[m ²]
Taper ratio	λ	0.4	-
Thickness to chord ratio	t/c	0.15	-
Fuselage structure length	L_{Struct}	1.3	[m]
Mass carried by the fuselage	$W_{Carried}$	15.47	[kg]
maximum equivalent velocity	$V_{eq,Max}$	50	[m s ⁻¹]
aerial weight of the empennage	$W_{A_{Emp}}$	1	[lb/ft ²]
empennage planform area	S_{Emp}	0.36	[m ²]
length of the boom	L_{Boom}	1.1	[m]
Cantilever mass	W_{Cant}	2.25	[kg]
landing gear mass fraction	F_{LG}	0.04	-
maximum required power	P_{Max}	7	[kW]
power-to-weight ratio of engine	P/W_{Ref}	1	[hp/lb]
installation factor	$F_{Install}$	1.2	-
nacelle multiplication factor	F_{nac}	0.27	-
Propellor multiplication factor	K_{Prop}	15	-
number of propellers	N_{Props}	1	-
number of blades	N_{Blades}	3	-
Propellor Diameter	D	0.7	[m]
fuel multiplication factor	F_{fs}	0.075	-
Fuel mass	W_{Fuel}	5.47	[kg]
Avionics mass fraction	f_{Avion}	0.06	-
Autopilot mass	$W_{autopilot}$	0.07	[kg]
Air data sensors mass	$W_{airdata}$	0.5	[lb]
GPS mass	W_{GPS}	0.5	[lb]
INS mass	W_{INS}	0.5	[lb]
Payload power	$P_{PL,Max}$	500	[W]
Total structural length	L_{Tot}	2.4	[m]
Wingspan	b	3.6	[m]
paint mass fraction	MF_{Paint}	0.003	-
Trapped Fuel & Oil mass fraction	F_{ifo}	0.01	-

Table 3.2: Outputs for Class II weight estimation

Name	Symbol	Value	Unit
Wing mass	W_{wing}	6.74	[kg]
Fuselage mass	W_{Fuse}	9.66	[kg]
Empennage mass	W_{EMP}	2.25	[kg]
Boom mass	W_{Booms}	0.51	[kg]
Landing gear mass	W_{LG}	2.21	[kg]
Installed engine mass	$W_{Eng,Installed}$	8.33	[kg]
Nacelle mass	W_{nac}	1.15	[kg]
Propellor mass	W_{Prop}	0.23	[kg]
Fuel System mass	$W_{FuelSys}$	0.57	[kg]
Avionics mass	W_{Avion}	3.32	[kg]
Electrical system mass	W_{Elec}	1.76	[kg]
Paint mass	W_{Paint}	0.17	[kg]
Trapped fuel and oil mass	W_{ifo}	0.08	[kg]
Operational empty mass	OEW	37.71	[kg]
Fuel mass	W_{fuel}	7.60	[kg]
Maximum take-off weight	W_{TO}	55.31	[kg]
Wing surface area	S_w	1.507	[m]
Wingspan	b	4.25	[m]

3.2. Class II Drag

With more definition of the UAV dimensions, it is possible to come up with more accurate drag estimations. To this end, [7, Sec. 12.5] provides methods to be used, specifically the drag build up method. Additionally, [8] is used to validate the results, on an order of magnitude scale.

3.2.1. Component Build Up

Component build up method is a method consisting of adding all individual aircraft components to come up with the total aircraft drag. It is detailed in Equation 3.17, where each aircraft component is characterised by three parameters:

- **Plate skin friction coefficient** (C_f): This represents the drag that is produced by a flat plate, laid out in the air stream [9, pp.25-26].
- **Form Factor** (FF): This parameter aims to account for the difference in shape between each component and the flat plate [7, Sec. 12.5].
- **Interference factor** (IF) accounts for the mutual interaction of components, leading to non-ideal airflow conditions [7, Sec. 12.5].
- **Wetted area** S_{wet} is the total component area immersed in the flow [7, Sec. 12.5].

Additionally, miscellaneous drag is added, for example due to excrescence [7, Sec. 12.5].

$$C_{D_0} = \frac{1}{S_{ref}} \sum_c C_{f_c} \cdot FF_c \cdot IF_c \cdot S_{wet_c} + \sum C_{D_{misc}} \quad (3.17)$$

Parasitic drag is based on flat plate skin friction, for both turbulent (Equation 3.20), and laminar (Equation 3.19) flow. The Reynold's number, which characterises the airflow properties, is noted as Re (Equation 3.18) and differs for each component due to their differing lengths. It is assumed, that the wings observe 35% laminar airflow, and the fuselage 10%, with all the rest of the airflow being turbulent [7, Sec. 12.5]. Thus, the skin friction for each component is the weighted sum of turbulent and laminar skin friction coefficient.

$$Re = \frac{\rho v l}{\mu} \quad (3.18) \quad C_f = \frac{1.328}{\sqrt{Re}} \quad (3.19) \quad C_f = \frac{0.455}{(\log_{10} Re)^{2.58} (1 + 0.144 M^2)^{0.65}} \quad (3.20)$$

Form factor is calculated using statistical relationships. For the wing tail surfaces, it is calculated according to Equation 3.21, where $(x/c)_m$ is the chord-wise location of the maximum airfoil thickness, and $\frac{t}{c}$ is the thickness to chord ratio of the airfoil. For the fuselage, Equation 3.22 is used to obtain the form factor [7, Sec. 12.5]. This method overestimates drag, especially compared to numerical results for similar aircraft [8], but is used until a more refined estimate can be created. The issues dealing with excessive fuselage drag are further discussed in subsection 3.2.2. In equations (Equation 3.22, Equation 3.23, Equation 3.21) f represents the ratio of length to diameter ($f = l/d$).

$$FF = \left[1 + \frac{0.6}{(x/c)_m} + 100 \left(\frac{t}{c} \right)^4 \right] \quad (3.21) \quad FF = \left(1 + \frac{60}{f^3} + \frac{f}{400} \right) \quad (3.22) \quad FF = 1 + (0.35/f) \quad (3.23)$$

Interference factor for each of the components is calculated through multiplication of interference factors for all components it interferes with, i.e. the interference factor for the fuselage is $1.65 = 1.0 \cdot 1.5 \cdot 1.1$, where 1.0 is the interference factor due to the fuselage itself, 1.5 due to interference with the nacelle, and 1.1 due to interference with the wing. The empennage is deemed not to interfere with the fuselage for the purpose of this interference factor, as it is distanced by a boom. All the individual interference factors are taken from [7, Sec. 12.5], and the component interference factors can be found in Table 3.4.

Wetted area represents the entire surface that is subjected to the airflow, and it does not account for components "hidden" by others, e.g. the nacelle and fuselage wetted areas partly overlap. The fuselage wetted area, due to its shape, is calculated according to Equation 3.24; the wings, and the tail surfaces according to Equation 3.25, where S_{ref} is the wing surface area. For the rest of the components, the wetted area is represented by the total surface area. The wetted and frontal areas of all components is compiled in Table 3.3.

$$S_{wet_{fus}} = \frac{\pi D}{4} \left(\frac{1}{3L_1^2} \left[\left(4L_1^2 + \frac{D^2}{4} \right)^{1.5} - \frac{D^3}{8} \right] - D + 4L^2 + 2\sqrt{L_3^2 + \frac{D^2}{4}} \right) \quad (3.24) \quad S_{wet_{wing}} = 1.07 \cdot 2 \cdot S_{ref} \quad (3.25)$$

Miscellaneous drag components are accounted for by the landing gear drag components, which is calculated according to Equation 3.26 [7, Sec. 12.5]. Additionally, excrescence and leakage account for an addition of 5% to the sum of all other drag components.

$$C_{D_{LG}} = \frac{1.4 A_{LG}}{S_{ref}} \quad (3.26)$$

3.2.2. Excessive Fuselage Drag

As previously explained, [7, Sec. 12.5] gives excessive estimates regarding drag due to the fuselage, especially regarding base drag, or fuselage upsweep drag when compared to numerical estimates for aircraft similar to the minesweeper UAV [8]. Additionally, [7] is intended for designing aircraft at much higher speeds, 0.6 Mach, where the UAV flies at 0.071 Mach.

Based on [7, Sec. 12.5], the zero lift drag can also be estimated using Equation 3.27, where C_{f_e} represents the statistical skin friction coefficient, which for small aircraft is given as 0.0065. As such, the zero lift drag is quickly estimated to be ~ 0.032 , which is significantly lower than that estimated using component build up. Much of the excessive increase in drag would be produced by the upsweep/ base drag ($C_{D_{0_{upsweep}}} \simeq 0.1$), which is caused by a pressure loss at the tail of the aircraft. Due to the slow speeds and Reynold's numbers the aircraft is expected to fly at, such pressure losses are not expected. As such, that component of the drag build up method is to be ignored.

$$C_{D_0} = C_{f_e} \frac{S_{wet}}{S_{ref}} \quad (3.27)$$

Table 3.3: Dimensions Used for Parasitic Drag Estimation

Name	Symbol	Value	Unit	Origin
Wing Surface Area	S_{ref}	1.086	m ²	Wing Loading Diagram
Horizontal Surface Area	S_{horiz}	0.3	m ²	Control & Stability
Vertical Surface Area	S_{vert}	0.072	m ²	Control & Stability
Wing Wetted Area	$S_{wetwing}$	2.323	m ²	Equation 3.25
Fuselage Wetted Area	S_{wetfus}	1.576	m ²	Equation 3.24
Horizontal Tail Wetted Area	$S_{wethoriz}$	0.630	m ²	Equation 3.25
Vertical Tail Wetted Area	$S_{wetvert}$	0.151	m ²	Equation 3.25
Fuselage Diameter	D_{fus}	0.5	m	Payload Diagonal Dimension
Nosecone Length	L_1	0.4	m	First Estimate for Aerodynamic Shape
Central Fuselage Length	L_2	0.6	m	Payload Length + Contingency
Tailcone Length	L_3	0.4	m	First Estimate for Aerodynamic Shape
Fuselage Area	A_{fus}	0.196	m ²	Circle with Payload Diameter
Landing Gear Frontal Area	A_{LG}	0.012	m ²	Estimate
Nacelle Length	L_{nac}	0.4	m	Engine Length
Nacelle Diameter	D_{nac}	0.36	m	Engine Diameter
Engine Nacelle Frontal Area	A_{nac}	0.102	m ²	Circle with Engine Diameter

Table 3.4: Form and Interference Factors

Name	Symbol	Value
Fuselage Form Factor	FF_{fus}	1.123
Wing Form Factor	FF_{wing}	1.080
Nacelle Form Factor	FF_{nac}	1.315
Horizontal Tail Form Factor	FF_{horiz}	1.080
Vertical Tail Form Factor	FF_{vert}	1.080
Wing Interference Factor	IF_{wing}	1.1
Horizontal Tail Interference Factor	IF_{horiz}	1.08
Vertical Tail Interference	IF_{vert}	1.08
Fuselage Interference Factor	IF_{fus}	1.65
Nacelle Interference Factor	IF_{nac}	1.5

This issue needs to be further investigated, but for the time being, the more conservative (higher) zero lift drag is to be used. This is expected to be an overestimation of the drag coefficient of the UAV, since it is extremely high when compared to that for similar configurations of UAV [8], and even higher than that for a double elliptical airship [10].

3.2.3. Zero Lift Drag Estimates

Ignoring the drag due to upsweep/ base drag, the drag estimates can be found in Table 3.5. The largest source of drag remains the fuselage, which produces $C_{D0} = 0.02383$. Additionally, excrescence adds 10% to the sum of all other drag components. The total C_{D0} is thus 0.05731, which is higher than for similar aircraft [8], but in the same factor of magnitude range.

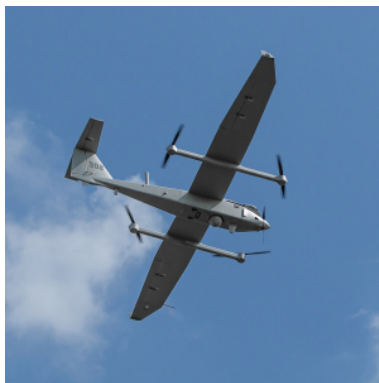
Table 3.5: Zero Lift Drag Estimates

Name	Symbol	Value
Drag due to Wing	$C_{D0_{wing}}$	0.01004
Drag due to Vertical Tail	$C_{D0_{vert}}$	0.000934
Drag due to Horizontal Tail	$C_{D0_{horiz}}$	0.001926
Drag due to Fuselage	$C_{D0_{fus}}$	0.02383
Drag due to Nacelle	$C_{D0_{nac}}$	0.00421
Drag due to Landing Gear	$C_{D0_{LG}}$	0.0111
Sum of Above	$C_{D0_{sum}}$	0.0521
Drag due to Excrescence	$C_{D0_{excrescence}}$	0.00521
Total Zero Lift Drag	C_{D0}	0.05731

Wing Planform Design

4.1. Options

As a result of the preliminary aerodynamic design, two main options of the wing planform with almost the same efficiency have been proposed. The first option is the tapered wing with a taper ratio (λ) of 0.4, the latter option is a quasi-elliptical shape, which is an elliptical shape approximated with linear segments. Both options are illustrated in Figure 4.1 with the quasi-elliptical shape visualized in Figure 4.1a and the tapered wing in Figure 4.1b. A truly elliptical wing is not considered an advantageous solution due to its complex geometry as well as the fact that it generally does not outperform a straight wing when a fuselage is mounted to the wing [11]. Furthermore, when twist is applied to the wing, an elliptical lift distribution can also be obtained with a straight wing [11].



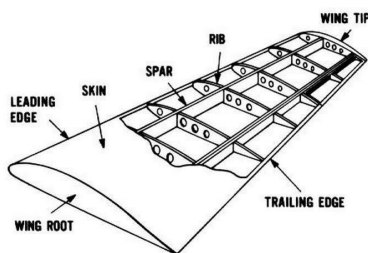
(a) Quasi-elliptical wing [12]



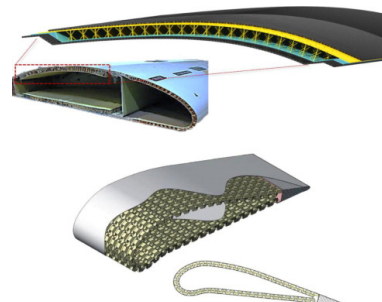
(b) Tapered wing [13]

Figure 4.1: Proposed wing shapes

Several structural options are available. For one, a single spar can be used as a stiffening element. However, as stated before, this spar would then need to have a continuously changing cross-section when a straight taper is considered, or for the most part one continuous section when the Quasi-elliptical solution is concerned which only would have to change towards the wing tip. A second option would be a sandwich lay-up, where the wing skin is a load-carrying sandwich structure. This solution does not have the drawback of a continuously changing cross-section for the stiffening elements compared to the beams. However, it does introduce the complexity of composite sandwich structures. Both considerations are visualized in Figure 4.2. With the spar structure shown in Figure 4.2a and the sandwich in Figure 4.2b.



(a) Wing Structure with a spar [14]



(b) Wing Sandwich Structure [15]

Figure 4.2: Proposed Wing structure

To compare the different options, the proposed wing shapes are separated into four different ones: a quasi-elliptical wing with a conventional wing structure, a tapered wing with a conventional wing structure, a quasi-elliptical wing with a composite sandwich structure, and a tapered wing with a composite sandwich structure. These four options for the wing planform are compared with each other concerning the way they would perform. In general, composites are less recyclable [16] just as they are less repairable due to their non-homogeneous nature. Composite materials are also less easy to use for manufacturing. Disassembly, which is desired for the aircraft to fit in a Toyota car used for transport, is harder because some form of additional strengthening is needed for the parts of disassembly. Altogether, the usage of composites is not ideal. When metal is used, it is easier to locally enforce parts of the wing with ribs, which is beneficial for the disassembly

capabilities of the wing. It is also easier to recycle conventional, metal-based material because of the homogeneity of the material. The advantage of using composite material is that it is slightly more cost-effective than metal [17]. This is however not that big of an advantage and it thus seems generally better to go with a metal wing structure. The wing planform is determined, based on the same criteria. A tapered wing is less easy to manufacture than a quasi-elliptical wing due to the change in cross-sectional area, which means the size of ribs has to change throughout the wing structure. This is not the case for the quasi-elliptical wing since the tips would not be load-carrying elements.

4.2. Aircraft loading diagram

As a start to the design of the wing planform, a decision on the wing position between a high, mid, and low wing was made. It was decided that a high wing would be most suitable for the design, as then the payload can be placed in the fuselage underneath. This allows a clear line of sight down. Furthermore, a high-wing configuration improves lateral stability [6]. However, the implications on the landing gear need to be investigated.

As good endurance is of great importance for operation of the UAV, an initial aspect ratio of 12 is selected before iteration. This ensures high lift and low induced drag [6], which enables higher endurance and thus better performance.

Subsequently, a sweep angle and thickness ratio are selected. As the UAV is supposed to operate at moderate speeds (15-40 m s⁻¹), the subsonic operation does not have to be accounted for, so wing sweep is not required [6]. Furthermore, for an unswept wing, a taper ratio that is between 0.4 and 0.5 results in an almost elliptical lift distribution [18]. As this is the most efficient for induced drag, a taper ratio of 0.4 was selected. A near-elliptical wing distribution can also be achieved by a quasi-elliptical wing. The final choice will be determined by structural reasons.

Next, a dihedral angle and angle of twist are selected. Given that it is an unswept high wing, positive dihedral is not necessary [18]. Therefore, the dihedral angle is set at 0° for now. For the angle of twist, -2° was selected, as a little bit of twist is generally preferred as it delays tip stall and subsequently improves stability [6]. In the current design phase, this can not be assessed in detail yet, so it remains a placeholder until a more accurate value can be determined.

For the thickness-to-chord ratio t/c , the choice is made to aim for the highest lift coefficient possible, as this results in the lowest required wing area [18] and thus saves weight. Thus, an initial t/c ratio of 14% is selected [18]. This does increase the drag generated compared to thinner airfoils, however, the gain in lift is considered more important. The exact t/c ratio will later be established by the selection of a specific airfoil.

With some of the basic parameters defined, a first-order analysis of the wing loading can be performed. For this, the procedure presented in AE1222-II [18] is followed to construct a wing-loading to power-loading diagram. This serves as a starting point for selecting the required wing area and engine power. For now, it is based on first-order estimates for $C_{L_{max}}$ (1.8), C_{D0} (0.03) as well as the propulsive efficiency η_p (0.8), which are estimated based on available data from Roskam [6]. A range of values was considered for C_L , from 1 to 1.8, to ensure the design point is still feasible if C_L differs from the estimate. The Oswald efficiency factor is estimated using Equation 4.1 for the selected aspect ratio and sweep [19].

$$e = \frac{2}{2 - A + \sqrt{4 + A^2 \cdot (1 + \tan \Lambda_{0.5c})^2}} \quad (4.1)$$

Sizing is then performed for the constraining scenarios the UAV will encounter based on the requirements. First, sizing is performed for the stall speed, which shall be at least 20 m s⁻¹. This is done for a range of C_L values from 1 to 1.8. Furthermore, stall is considered at sea level as well as for 2000 meters above sea level using Equation 4.2, where V_s is the stall speed, ρ the air density and $C_{L_{max}}$ the maximum lift coefficient. The limiting wing loading is hence found.

A similar methodology was applied for take-off and landing, where the requirements state that the UAV shall take off and land within 500 m distance at a density altitude of 5000 m. For take-off, the method presented in [7] is used to determine the take-off parameter, which is then used to determine the required wing loading using Equation 4.3 [18].

$$\frac{W}{S} = \frac{1}{2} \rho V_s^2 C_{L_{max}} \quad (4.2) \quad \text{TOP}_{\text{prop}} = \left(\frac{W}{S}\right)_{\text{TO}} \cdot \left(\frac{W}{P}\right)_{\text{TO}} \cdot \frac{1}{C_{LT}} \cdot \frac{1}{\sigma} \quad (4.3)$$

For landing Equation 4.4 [18] is used, where S_{land} is the landing distance of 500 m. Next, sizing is performed for the climb rate. This is required to be 100 feet/minute due to regulations [20]. For this, Equation 4.5 [18] is used.

$$\left(\frac{W}{S}\right)_{\text{TO}} = \frac{C_{L_{max}} \cdot \rho \cdot \frac{S_{\text{land}}}{0.5847}}{2} \quad (4.4) \quad \frac{W}{P} = \frac{\eta_p}{c + \frac{\sqrt{\frac{W}{S}} \cdot \sqrt{\frac{2}{\rho}}}{1.345 \cdot \frac{(Ae)^{3/4}}{C_{D0}^{1/4}}}} \quad (4.5)$$

Finally, for cruise sizing Equation 4.6 [18] is used to determine the design limits considering the requirements for cruise speed and altitude. Here, the aspect ratios A selected are 9, 12 and 15 to compare the effect of different aspect ratios.

Even though an aspect ratio of 12 is selected as an initial design choice, different aspect ratios are considered in the wing loading diagram to ensure compliance with the requirements if changes are made.

$$\frac{W}{P_{TO}} = \frac{0.9}{0.8} \eta_p \left(\frac{\rho}{\rho_0} \right)^{3/4} \left[\frac{C_{D_0} \frac{1}{2} \rho V^3}{(0.8W/S)} + \left(0.8 \frac{W}{S} \right) \frac{1}{\pi A e \frac{1}{2} \rho V} \right]^{-1} \quad (4.6)$$

This results in the wing loading diagram provided in Figure 4.3, which shows the most constraining limits on the design. The feasible design region is visualized in green. In general, a design point should be selected to the top right of the feasible design region, as it minimizes the wing surface area required and thus reduces the required structural weight, as well as minimizes the engine power and thus optimizes the engine choice. The wing surface area is a continuous variable, which can be chosen freely to optimize the design. The engine power, however, is a discrete variable, since an existing engine satisfying the power needed is chosen. Taking that into consideration, as well as the fact that increasing wing loading does not significantly decrease power loading, the design point indicated by the black diamond is opted for.

The design point selected results in a value for $W/S = 360$ and $W/P = 0.16$. As visualized, it lies on the intersection of take-off and stall, both at $C_L = 1.8$, meaning that special care will be taken when considering these conditions. Furthermore, from the perspective of the aircraft loading diagram, $C_{L_{max}}$ and stall performance will be dictating criteria in the airfoil selection trade-off. The selection of an airfoil should consider the estimated values of C_L presented before, and changes should be made to the wing loading diagram if the selected C_L is not achievable.

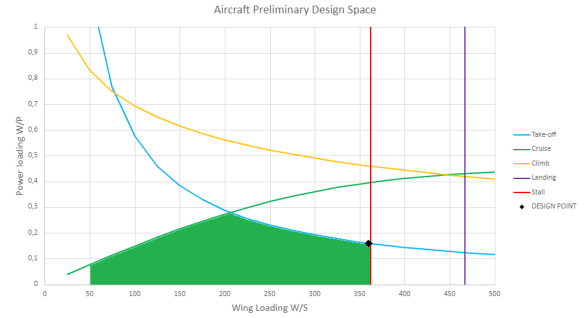


Figure 4.3: Wing loading diagram

4.3. Wing Details

With the wing loading diagram completed, several parameters describing the geometry of the wing can be determined. Their values are listed in Table 4.1.

Table 4.1: Wing planform parameters, blue signifies the design wing loading, while yellow changeable parameters

Name	Symbol	Value	Unit	Name	Symbol	Value	Unit
Wing area	S	1.5	[m ²]	y position of mac	y_{MAC}	0.77	[m]
Aspect ratio	A	12	[-]	x position of leading edge mac	x_{LEMAC}	0.03	[m]
Oswald efficiency	e	0.92	[-]	Quarter chord sweep angle	$\Lambda_{c/4}$	0.00	[rad]
Wingspan	b	4.28	[m]	Leading edge sweep angle	Λ_{LE}	0.0357	[rad]
Taper ratio	λ	0.4	[-]	Sweep angle ($c/2$)	$\Lambda_{c/2}$	-0.0357	[rad]
Root chord	c_r	0.438	[m]	beta	β	0.995	[-]
Tip chord	c_t	0.175	[m]	efficiency	ν	0.950	[-]
Mean aerodynamic cord length (mac)	\bar{c}	0.367	[m]	Twist angle	α_t	-2	[deg]
Thickness to chord ratio	t/c	15.0	[%]	Dihedral angle	Γ	0	[deg]

4.4. Design of quasi elliptical wing

The quasi-elliptical wing will be designed by first designing an elliptical wing and then drawing the quasi-elliptical wing inside the main wing. This method leads to the area of the fitted quasi-elliptical wing being smaller than the elliptical wing it is fitted inside. It is hence important to parameterize the elliptical wing such that it can be easily adjusted.

The elliptical wing is characterized by the chord distributed as the width of an ellipse along its semi-major axis. For structural purposes, it was decided that the ellipse would be modified such that its semi-major axis will actually shift to a quarter of its semi-minor axis, instead of halfway. This is based on the location of the aerodynamic center of the wing located at the quarter-chord. This allows us to assume that the main forces on the wing act at a quarter point.

Next, the quasi-elliptical wing needs to fit into the elliptical wing. Based on the dimensions of the Toyota cruiser the disassembly cut of the wing needs to be made at 0.7 m from the root chord, as the central section of the fuselage needs to fit the roof rack. [21] The width of an elliptical wing at 0.7m determines the root chord length. The middle section of the fuselage is, therefore, rectangular. The location of the tip is decided such that the tip chord length is 40% of the root chord, the span is therefore controlled by the tip chord location. the section where the taper ratio changes is arbitrary, and is chosen by balancing approximation of the elliptical wing and the loads distributed in the structure.

The input parameters to optimize the wing surface are the semi-major axis, semi-minor axis, and the 'scale factor' k of the ellipse.

$$\frac{x^2}{a^2} + \frac{y^2}{b^2} = k \quad (4.7)$$

The input parameters are manually optimized, to achieve the desired aspect ratio of 12 and the desired surface area of 1.5 m². This results with the following wing platform parameters, with the quarter chord line being straight throughout

the wing. As the ailerons need quite a large section of the wing to be most efficient, it was decided to only split the wing in two sections with the parameters of those sections given in Table 4.2.

Table 4.2: Wing planform

section	location along the span	Chord length
1	0	0.438
2	0.7	0.438
3	2.14	0.175

Based on the above parameters the mean aerodynamic chord (MAC) can be calculated, based on Equation 4.8 [22].

$$MAC = \frac{2}{S} \left[\int_0^{b/2} c^2 dy \right] = 0.367m \quad (4.8)$$

Engine Sizing

In the previous report, it was determined that an internal combustion engine is used for propulsion, mostly due to its lower energy mass. Therefore, in this chapter, the engine and fuel storage are designed in further detail.

5.1. Subsystem Requirements

For this subsystem, the following requirements apply:

Table 5.1: Requirements for powerplant

ID	Requirement
SYS-ENG-01	4.2kW of Power shall be available for take-off at a density altitude of 4000m.
SYS-ENG-02	Sufficient electrical power shall be produced during cruise to power the subsystems.
SYS-ENG-03	Electrical power shall be available throughout a mission at altitude.

SYS-ENG-01 comes from chapter 11.

5.2. Power required

As seen in chapter 11, the total power required to be able to take-off in all the required conditions, is 4.2 kW of available power. However, this does not include the multiple inefficiencies that the propulsion system encounters, namely the effect of a reduced density, from flying at altitude, on the engine's power production.

The power to power the other sub-systems must be included in the power requirement as well, as the engine shall have to transfer part of its generated power to provide for these systems, using an alternator. Finally, Sadraey mentions how a piston engine's performance is reduced by the altitude at which it operates [23]. Due to the likeness of a rotary engine to a piston engine, in comparison to a turboprop, this equation can be used, even though the choice of whether to use a piston or rotary engine is yet to be made. The reduction in power coming from the lower density at altitude is portrayed in the following equation:

$$P_{max} = P_{max_{SL}} \left(\frac{\rho}{\rho_0} \right)^m \quad (5.1)$$

In Equation 5.1, m is set at 0.9 for piston engines [23]. At the take-off condition where maximum power is required, namely at 4000 m pressure altitude, the density is reduced to 0.81913. This reduces the power available, in comparison to the sea level power to 70 percent. This provides the total power required by the engine to be 6 kW.

5.3. Engine Sizing and Selection

For the actual engine, several additional components are necessary, such as fuel pumps and filters. However, a package deal can save a large amount of work. For the required 4.2 kW at 4000 m, the Genpod 120 LRU is an appealing option [24]. At 4000 m, it still produces 60% of the nominal power, while having a nominal sea-level sustained power of 7.0 kW. Not only that, but it also comes with a generator. This generator can generate up to 500 W, which enables the engine to power the payload completely. The whole package comes in at a total mass of 5.44 kg and has a break-specific fuel consumption (BSFC) of 590 g kW⁻¹ h.

5.4. Propeller Sizing

Before doing propeller sizing, it is necessary to select the number of blades. For a propeller engine, the diameter is given by [23, p. 458]

$$D_p = K_{np} \cdot \sqrt{\frac{2 \cdot P \cdot \eta_p \cdot AR_p}{\rho \cdot V_{av}^2 \cdot C_{LP} \cdot V_C}} \quad (5.2)$$

with the following values: with K_{np} a correction factor for having more blades, being 1 for a two-blade propeller and 0.93 for a three-blade [23, p. 458]. Thus, more blades gives a smaller propeller, but not much. However, as the engine comes with a recommended three-blade propeller with a diameter of 61 cm [24], that propeller is used in this design. Nevertheless, to allow for some growth in propeller size, in the positioning of the engine in the CAD-model a diameter of 70 cm is used.

5.5. Fuel Tank Sizing

Before doing any complicated performance analysis, it is necessary to get a quick estimate of the required fuel mass. For this analysis, the following assumptions are used:

- The extra energy expended due to take-off, landing and climb is neglected
- The aircraft flies the full duration of the flight at the estimated MTOW of 55.3 kg
- For the entire duration of the flight, the aircraft generates 500 W of electrical power
- The flight has a total duration of six hours to cover loiter, cruise and take-off
- The propeller and the generator have the same efficiency of 0.8 [25] for converting the shaft energy to useful energy

Based on these assumptions, the required power follows as

$$P_r = P_{flight} + P_{generator} = \frac{C_D}{C_L} \cdot W \cdot V_e + 500 = \frac{1}{10} \cdot 55.3 \cdot 9.81 \cdot 21.6 + 500 = 1672W, \quad (5.3)$$

which leads to the total energy used by multiplying with six hours, giving a total energy expenditure of 10.03 kWh. Given the propeller efficiency of 0.8 [25] and the BSFC of 590 g kW⁻¹ h [24], this corresponds to a fuel mass of 7.4 kg. Then, the density of gasoline of 0.748 kg L⁻¹ [26] at 15 °C yields a volume of 9.9 L. A tank that fulfils this requirement with some margin is the 10 L fuel tank produced by Mugin [27]. Coming in at 489 g, it is light and large enough to do the job. Therefore, this fuel tank is used for the design. As in chapter 3, the weight of all fuel systems is estimated by

$$W_{FuelSys} = F_{fs} \cdot W_{Fuel}^{E1} \quad (5.4)$$

which yields a fuel system mass of 507 g. Subtracting the fuel tank mass from this value gives a total budget for fuel lines of 18 g. At a later stage, this number may need some revision. However, it is only for the fuel lines, as all other components are already included in the engine package [24].

5.6. Verification and validation

5.6.1. Total mass budget

Table 5.2: Overview of Chosen Engine Components

Component	Chosen product	Mass	Cost
Engine unit	Genpod 120 LRU	5440 g	\$25 870
Fuel tank	Mugin 10L kevlar fuel tank	489 g	\$590
Fuel lines	TBD	18 g	\$-
Total		5947 g	\$26 359

5.6.2. Unit tests

The requirements have been analysed using uncomplicated methods, hence the unit tests are not complicated either. The unit tests were performed by calculating the values once more. SYS-ENG-01 was verified using Equation 5.1 and choosing an engine that supplied sufficient power to meet this requirement. SYS-ENG-02 was verified by calculating the power requirement in chapter 11. SYS-ENG-03 was verified by inspection, as the engine chosen in section 5.3 meets this.

5.6.3. Subsystem verification

After all calculations are done, it is necessary to check that the designed landing gear meets the requirements set-up in section 5.1. This will be done through one of the four methods (analysis, demonstration, inspection or testing, as elaborated upon in chapter 14. In Table 5.3, the compliance matrix of the structural requirements is visualised.

Table 5.3: Requirements for propulsion system

ID	Check	Reasoning	Requirement
Fuselage (FUS)			
SYS-ENG-01	✓	Analysis: Computation of shaft power and efficiencies	4.2kW of power shall be available for take-off at a density altitude of 4000m.
SYS-ENG-02	✓	Analysis: Simulation of all power required for electrical subsystems.	Sufficient electrical power shall be produced during cruise to power the subsystems.
SYS-ENG-03	✓	Analysis: Simulation with summation of all power requirements throughout mission	Electrical power for the payload shall be available throughout a mission at altitude.

Control Surfaces

This chapter will delve into the control surfaces present in the aircraft. First, in section 6.1 subsystem requirements are stated to give an idea of what aspects of control surfaces sizing the chapter will focus on. Then, in section 6.2 the preliminary tail positioning takes place utilising scissor plot and moment-lift curve. Knowing the position of the tail, the size is determined in section 6.3, simultaneously assessing the moment equilibrium for chosen parameters. Following that, control surfaces - elevator, rudders and ailerons - are sized in section 6.4. To verify the design of control surfaces, stability and control derivatives are presented in section 6.5. This allows for an insight into longitudinal and lateral stability conducted in section 6.6, focusing on elevator deflection, elevator control force, sideslip derivatives and rudder pedal force. Similarly, dynamic longitudinal and lateral stability is analysed in section 6.7, consisting of analysing eigenmotions (short-period, phugoid, aperiodic roll, Dutch roll, spiral) and angular rates (roll, pitch, yaw rates). The chapter commences with the discussion on verification of acquired results and assessing the compliance of the requirements with results presented in this section.

6.1. Subsystem Requirements

The subsystem requirements presented in Table 6.1 flow from the overall requirements list compiled for the baseline report. Additional requirements are derived based on more insight into the control and stability topic, and acquaintance with Roskam [6].

Table 6.1: Requirements for Control Surfaces

ID	Requirement
Mission requirements	
STK-0.3.9-MIS-ENV-4	The UAV shall be able to take off and land with a cross wind of 9 m s^{-1} .
STK-0.3.9-MIS-ENV-5	The UAV shall be able to take off and land with a tail wind of 2 m s^{-1} .
STK-0.3.9-MIS-ENV-6-OPT	The UAV shall be able to take off and land with a head wind of 15 m s^{-1} .
Stability & Control	
FUN-CS-1	The UAV shall exhibit a moment equilibrium at the trimmed flight.
FUN-CS-2	Elevator sizing shall allow for the placement of the horizontal tail spar.
FUN-CS-3	Rudder sizing shall allow for the placement of the vertical tail spar.
FUN-CS-4	Aileron sizing shall allow for the placement of the rear wing spar.
FUN-CS-5	All stability derivatives shall have a correct sign.
FUN-CS-6	All control derivatives shall have a correct sign.
FUN-NAV-4.N.iv	The UAV shall be laterally stable.
FUN-NAV-4.N.v	The UAV shall be longitudinally stable.
FUN-NAV-4.N.vi	The UAV shall be directionally stable.
FUN-NAV-4.N.v.1	The PULL shall be required to obtain and maintain speeds below the trim speed.
FUN-NAV-4.N.v.2	The PUSH shall be required to obtain and maintain speeds above the trim speed.
FUN-NAV-4.N.v.3	The speed shall return to within 10 % of the trim speed if the control is released from the push or pull.
FUN-NAV-4.N.v.4	The stick-force speed gradient shall be recorded for further processing by the autopilot.
FUN-NAV-4.N.iv.1	The UAV shall return to the original condition when put in a sideslip.
FUN-NAV-4.N.iv.2	The rudder pedal force required to put the airplane in sideslip condition shall be such that the pedal-force-gradient does not reverse its sign.
FUN-NAV-4.N.iv.3	The UAV shall raise the right wing when put in a sideslip.
FUN-NAV-4.N.v.5	The UAV shall be stable in short-period eigenmotion.
FUN-NAV-4.N.v.6	The UAV shall be stable in phugoid eigenmotion.
FUN-NAV-4.N.iv.4	The UAV shall be stable in aperiodic roll eigenmotion.
FUN-NAV-4.N.iv.5	The UAV shall be stable in Dutch roll eigenmotion.
FUN-NAV-4.N.iv.6	The UAV shall have a time-to-double the amplitude higher than 12 seconds.
FUN-NAV-4.N.6.a.ii	The UAV shall be able to pitch TBD deg/s.
FUN-NAV-4.N.6.b.ii	The UAV shall be able to yaw TBD deg/s.
FUN-NAV-4.N.6.c.ii	The UAV shall be able to roll 60 deg in 4 seconds.

6.2. Tail Positioning

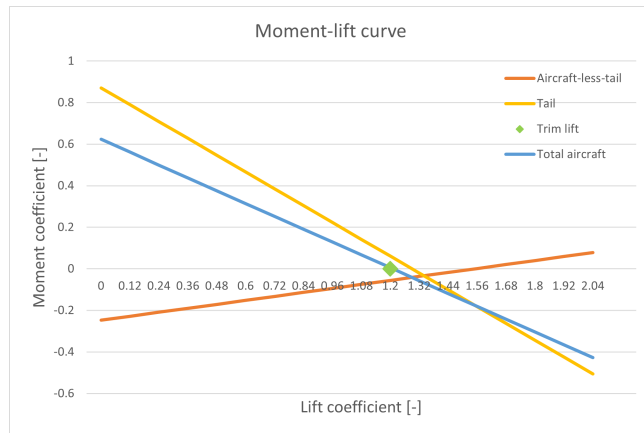
The first step of the tail design involves the positioning of the tail within the aircraft. For this purpose, assumptions on fuselage, engine and airfoil are made, which combined with wing planform parameters allow for preliminary estimate of main wing and tail parameters. Two tools used for this procedure are the so-called "scissor plot" and the moment-lift curve.

$$C_{m_{A-h}} = C_{m_{ac}} + C_L(\bar{x}_{cg} - \bar{x}_{ac}) \quad (6.3) \quad C_m = C_{m_0} + \frac{dC_m}{dC_L} C_L \quad (6.4) \quad C_{m_h} = C_m - C_{m_{A-h}} \quad (6.5)$$

Table 6.3: Moment-lift curve parameters

Input parameters					Output parameters				
Name	Symbol	Value	Unit	Source	Name	Symbol	Value	Unit	Source
Horizontal tail-wing area ratio	S_h/S	0.3	—	Scissor plot	Zero lift correction factor for twist	α_{0_1}	-0.425	—	Torenbeek eq. E-17
figure parameters	$\frac{2\pi A}{c_{l_\alpha}}$	12	—	Torenbeek fig. E-5	Wing-fuselage optimal lift coefficient	$C_{L_{wf}}^*$	1.26	—	Torenbeek eq. E-47
parameter C1	C_1	0.535	—	Torenbeek fig. E-5	Wing root-fuselage incidence	i_w	7	deg	Torenbeek eq. E-46
parameter C2	C_2	0.07	—	Torenbeek fig. E-5	Wing-fuselage lift coefficient	$C_{L_{wf}}$	1.20	—	Torenbeek eq. E-29
parameter C3	C_3	0.39	—	Torenbeek fig. E-5	Trimmed aircraft lift	$C_{L_{trim}}$	1.26	—	Torenbeek eq. E-45
parameter C4	C_4	0.62	—	Torenbeek fig. E-5	Tail-fuselage incidence	i_{hf}	3.2	deg	Torenbeek eq. E-54
Normalised distance between cg and ac	$\bar{x}_{cg} - \bar{x}_{ac}$	0.16	—	Calculating	Induced tail incidence	i_h	-0.171	rad	Torenbeek eq. E-55
Normalised neutral point, stick-free	\bar{x}_n	0.86511	—	Torenbeek eq. 9-5	Moment coefficient gradient	$\frac{dC_m}{dC_L}$	-0.515	—	Torenbeek eq. E-57
Fuselage angle of attack	α_f	0	—	Torenbeek p. 481	Zero moment coefficient	C_{m_0}	0.6231	—	Torenbeek eq. E-58
Twist angle	ϵ_t	-2	deg	Wing loading					
Airfoil zero lift angle	$(\alpha_{l_0})_r$	-9	deg	XFLR5					
Wing zero lift angle	$(\alpha_{l_0})_r$	-8.1	deg	Torenbeek eq. E-19					

The orange curve represent the hypothetical aircraft without tail, which allows for extracting C_{m_0} at $C_L = 0$. The positive slope indicates, that the aircraft alone is not stable, as the aircraft does not restore to its initial state following a disturbance. This also shows in the scissor plot, for which the absolute minimum of the horizontal-tail-to-wing surface area ratio is approximately 0.06, meaning the tail has to be present. The yellow curve then represents the tail contribution, which has a high negative slope, indicating its ability to stabilize the aircraft. Summing those two curves results in the curve for the total aircraft. As can be seen, the blue curve has a negative slope, meaning the aircraft will be stable with the chosen tail parameters. Additionally, an intersection of this curve with the x-axis defines the trim lift coefficient. This is an important parameter, as it allows for the calculation of the trim speed, the speed at which the aircraft will cruise with minimal (auto)pilot input. Knowing the trim speed allows for further narrowing of the design space, as most of the time the aircraft will be flying at this speed. This paves the way for tail sizing and control surfaces sizing.

**Figure 6.2:** Moment-lift curve

Finally, two important angles are the result of the analysis - the wing-fuselage incidence angle of 7 degrees and the tail-fuselage incidence angle of 3.2 degrees. Although the tail incidence value seems plausible, the wing incidence angle appears to be excessive. Fortunately, however, it has been ensured, that the airfoil with high lift coefficient is chosen, thus reducing the wing incidence angle should only compromise the endurance, and not critically affect the capability of the aircraft to take off or manoeuvre. These values have been a starting point for the aerodynamic analysis in XFLR5 conducted in chapter 10, which commenced with the optimal wing incidence angle of 2° and optimal horizontal tail incidence of 2°. Due to more realistic values from software, these values have been chosen for further sizing procedures.

It is worth noting, that Table 6.2 and Table 6.3 presented in this section contain all necessary input and output parameters to recreate the design with methods summarised by Torenbeek [28]. Parameters in the next sections have been similarly documented, which eased the search for parameters and accelerated the verification process. However, due to the page limit, and growing complexity of calculations, including full tables is not only impossible, but also redundant. Interested readers are referred to chapter 9 of Torenbeek for section 6.3, chapter 10 of Roskam part VI for sections 6.4-6.5 and chapter 3 of Roskam part VII for sections 6.6-6.7.

6.3. Tail Sizing

Having obtained the horizontal-tail-to-wing surface area S_h/S , it is necessary to consider the detailed planforms of the H-tail. For both the horizontal and vertical tail, NACA0012 airfoil is used, since the airfoils for horizontal and vertical tailplanes are usually symmetrical, with thickness-to-chord ratio of 12% and increased nose radius to allow for large range of angles of attack [28].

6.3.1. Horizontal Stabilizer

The horizontal stabilizer is a fundamental aerodynamic surface located at the tail of an aircraft. Its primary function is to provide stability and control in the pitch axis, helping to maintain a balanced and level flight attitude. Its relevant parameters are shown in Table 6.4. For the aspect ratio A_h , a value from statistical estimate from Torenbeek is taken [28]. Moreover, due to the H-tail design, the observed aspect ratio increases by 1.5 [29], which is used for tail lift coefficient gradient calculation. This has been iterated with the scissor plot to confirm the tail lift gradient.

6.3.2. Vertical Stabilizer

Vertical stabilizer is a control surface responsible for lateral stabilising of the aircraft. In an H-tail configuration selected for this aircraft, the vertical stabilizer is split into two smaller vertical fins located at the ends of the horizontal stabilizer, creating the distinctive H-shape. To obtain vertical tail surface area, S_v , a procedure outlined by Torenbeek is used [28, Sec. 9.6]. A critical requirement in designing this aircraft part is the directional stability, quantified with parameter C_{n_β} . Fuselage, propeller and wing contribute to this parameter, which is then used to obtain vertical tail volume from a statistical relationship for propeller aircraft, equal to 0.08. Assuming the chords of vertical and horizontal tails are at the same distance from the mean aerodynamic center ($l_v = l_h$), an area of each vertical tail is obtained. Further assuming, that the tip chord of the horizontal tail is the same as the root chord of the vertical tail, gives the vertical tail span. The taper ratio of 0.8 is chosen due to a good balance between aerodynamic performance of the vertical stabilizer and control performance of the rudder. Finally, A_v is determined, which aligns with the literature values of small-sized propeller aircraft [6].

Table 6.4: Horizontal tail parameters

Name	Symbol	Value	Unit
Position of vertical tail	l_s	1.75	m
Surface area	S_h	0.45	m^2
Aspect ratio	A_h	4.00	—
Span	b_h	1.34	m
Taper ratio	λ_h	1	—
Chord	c_h	0.33	m
Quarter-chord sweep	$\Lambda_{h_{c/4}}$	0	m
Incidence angle	i_h	2	deg

Table 6.5: Vertical tail

Name	Symbol	Value	Unit
Position of horizontal tail	l_s	1.75	m
Surface area	S_v	0.145	m^2
Aspect ratio	A_v	2.49	—
Span	b_v	0.482	m
Taper ratio	λ_v	0.8	—
Root chord	c_{v_r}	0.34	m
Mean aerodynamic chord	\bar{c}_v	0.34	m
Quarter-chord sweep	$\Lambda_{h_{c/4}}$	0	—

6.3.3. Moment Equilibrium

Following the choice of main tail parameters, it is worth assessing the moment equilibrium of the aircraft. Forces acting on the aircraft are weight W , wing lift L_{A-h} and tail lift L_h , as shown in Figure 6.3. For moment analysis the most important point is the aerodynamic center, around which the moment does not change with the angle of attack. The resulting moment difference has to be compensated by the wing moment M_{ac} to ensure moment equilibrium. All values present in Equation 6.7 have already been calculated, however, they need to be verified to result in an equilibrium.

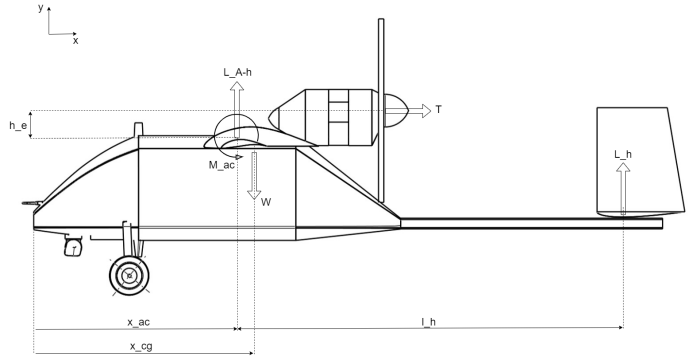


Figure 6.3: Moment equilibrium in-flight

$$\sum M_{ac} = 0 : \quad M_{ac} - W \cdot (x_{ac} - x_{cg}) + l_h \cdot L_h - h_e T = 0 \quad (6.6)$$

$$C_{m_{ac}} \frac{1}{2} \rho V^2 S \bar{c} + W \cdot (x_{ac} - x_{cg}) - l_h \cdot C_{L_h} \frac{1}{2} \rho V^2 \left(\frac{V_h}{V} \right)^2 S \frac{S_h}{S} - h_e \frac{P}{V} = 0 \quad (6.7)$$

In this case C_{L_h} is not taken at its maximum value, but at the lift coefficient of 0.2 at 3 degrees, representing the loiter flight. It is further considered, that the propeller thrust during loiter is 1.2kN, and it acts 0.2m from the aerodynamic center. For these parameters, the moment equilibrium is achieved at 21 m/s - above the stall speed but below the trimmed lift coefficient condition. To compensate for this, the elevator should be deflected during flight to appropriately increase or decrease the lift of the tail. This will allow for changing the speed with minimal generated moment, and thus increased stability. Hence, it is concluded, that the aircraft has an achievable moment equilibrium at trim speed.

6.4. Control Surfaces Sizing

With stabilizer sizing completed, it is important to size the control surfaces as well. The three types of control surfaces present on this UAV are elevator, rudders and ailerons, shown in Figure 6.4. The sizing has again been performed according to [6, VI, Ch. 9].

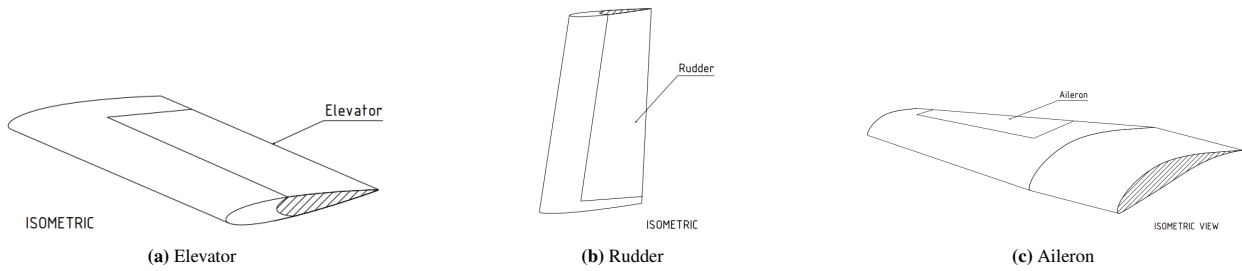


Figure 6.4: Control surfaces of the Minesweeper

6.4.1. Elevator

The elevator is a critical control surface located on the horizontal stabilizer at the tail of an aircraft, as shown in Figure 6.4a. Its primary function is to control the aircraft pitch, which is the movement around the lateral axis. By deflecting upward or downward, the elevator changes the angle of attack of the aircraft wings, causing the nose to pitch up or down. This controls the aircraft climb or descent and helps maintain level flight. Effective use of the elevator is essential for takeoff, landing, and overall stability during flight.

Table 6.6: Elevator sizing

Name	Symbol	Value	Unit
Surface area	S_e	0.225	m^2
Taper ratio	λ_e	1	—
Span	b_e	1.207	m
Chord	c_e	0.186	m
Maximum spar position		$0.41\bar{c}_h$	—
Chosen spar position		$0.40\bar{c}_h$	—

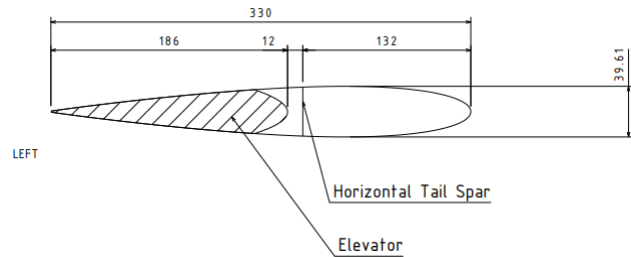


Figure 6.5: Elevator CATIA drawing

Elevator-to-horizontal-tail area ratio was chosen as the recommended $S_e/S_h = 0.5$ ratio [6, II, p. 191]. The same taper as for the horizontal stabilizer was applied to facilitate transfer of the load from the control surface to the tail spar. Finally, elevator span was taken to be 0.90 horizontal tail span, to allow for the mounting of the vertical tails on both ends of the horizontal stabilizer. With these parameters, spar positioning was performed, visualised in Figure 6.5.

6.4.2. Rudder

The rudder is a crucial control surface on an aircraft, located on the vertical stabilizer, as shown in Figure 6.4b. By deflecting to the left or right, the rudder generates a lateral force that pushes the tail in the opposite direction, causing the nose of the aircraft to yaw in the direction of the rudder deflection. This helps in directional control, especially during takeoff, landing, and in response to crosswinds. From the perspective of H-tail design, the rudder parameters are split between the two surfaces, and the Table 6.7 presents the parameters for one of these surfaces.

Table 6.7: Rudder sizing

Name	Symbol	Value	Unit
Surface area	S_r	0.087	m^2
Taper ratio	λ_r	0.8	—
Span	b_r	0.458	m
Root chord	c_{r_r}	0.20	m
Mean aerodynamic chord	\bar{c}_r	0.18	m
Maximum spar position		$0.22\bar{c}_v$	—
Chosen spar position		$0.20\bar{c}_v$	—

For rudder sizing, a rudder-to-vertical-tail area ratio is $S_r/S_v = 0.6$, which follows from the observation that UAVs possess larger rudders than home-built airplanes, for which the ratio oscillates around 0.4. The span of the rudder is taken to be 0.95 of the vertical tail span, to allow attachment to the horizontal tail. Other parameters are chosen to align with the vertical stabilizer, and allow for the placement of a spar. The drawing of the rudder positioned on the vertical tail is depicted in Figure 6.6.

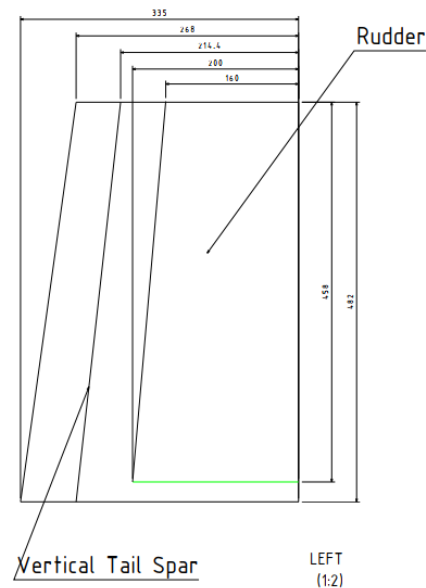


Figure 6.6: Rudder CATIA drawing

6.4.3. Aileron

Ailerons are essential control surfaces located on the trailing edges of each wing, near the wing tips, visualised in Figure 6.4c. They function to control the aircraft's roll, which is the movement around the longitudinal axis. By deflecting in opposite directions one aileron moving up while the other moves down they create differential lift on the wings. This causes one wing to rise and the other to lower, allowing the aircraft to bank left or right. This rolling motion is crucial for turning the aircraft and maintaining balance during flight.

For aileron sizing, the procedure outlined by Roskam in part II is used. Using statistical relationships for home-built aircraft, aileron area, its start and end locations and taper ratio is obtained. The aileron should be positioned aft of

the main wing rear spar, to preserve the structural integrity and load-carrying capabilities. From Table 6.8 it can be seen, that the maximum rear spar position allowing for the aileron integration is 0.61 times the local wing chord c . Hence, the rear span location of $0.60c$ is chosen and visualised in Figure 6.7. This will be further considered in the creation of structure in chapter 7.

Table 6.8: Aileron sizing

Name	Symbol	Value	Unit
Surface area	S_a	0.07	m^2
Start span location	$b_{a_{in}}$	1.210	m
End span location	$b_{a_{out}}$	1.910	m
Taper ratio	λ_a	0.64	-
Span	b_a	0.70	m
Root chord	c_{a_r}	0.118	m
Tip chord	c_{a_t}	0.075	m
Mean aerodynamic chord	\bar{c}_a	0.098	m
Wing chord at aileron root chord position	$c_{w_{a_r}}$	0.344	m
Aileron tip chord	c_{a_t}	0.075	m
Wing chord at aileron tip chord position	$c_{w_{a_t}}$	0.214	m
Maximum rear spar position		0.61c	-
Chosen rear spar position		0.60c	-

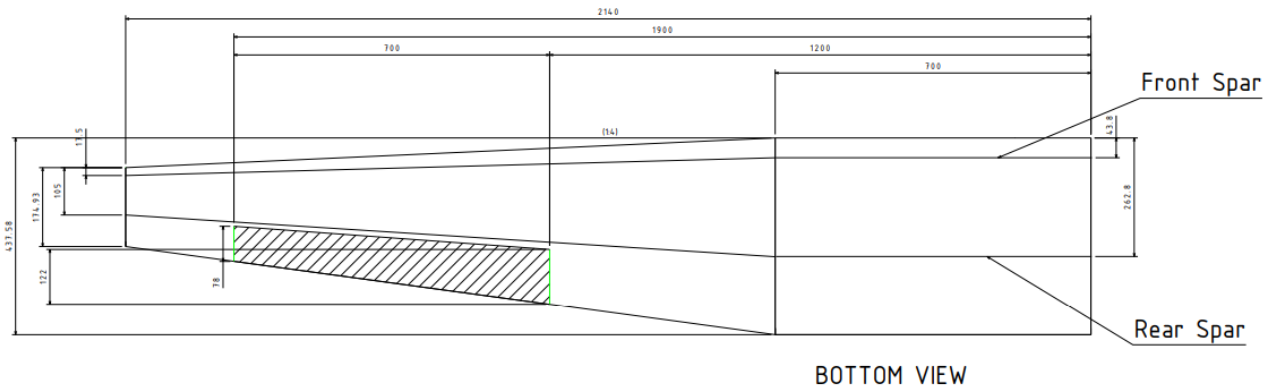


Figure 6.7: Aileron CATIA drawing

6.5. Derivatives

Stability derivatives quantify the aircraft's tendency to return to its initial state after experiencing an external disturbance, such as a wind gust. These parameters are crucial for assessing whether the aircraft can be flown safely without the risk of force build-up and subsequent divergence from stable flight. By measuring the sensitivity of aerodynamic forces and moments to changes in flight variables such as angle of attack or sideslip angle, stability derivatives provide insight into the aircraft's dynamic stability characteristics. Control derivatives quantify the aircraft's responsiveness to control inputs from the pilot or autopilot, such as control surface deflections. These parameters are vital for designing control software and fine-tuning controllers to ensure precise and effective manoeuvring. While designing the autopilot is beyond the scope of this project, the results indicate that the aircraft exhibits promising controllability characteristics, suggesting that developing an effective autopilot system is feasible.

6.5.1. Stability and Control

In determining stability and control derivatives it is important to ensure, that they have a correct sign, which represents a correct reaction of the system to a particular disturbance. The full list of stability and control derivatives is presented in Table 6.9 and Table 6.10 respectively. The values are further compared with literature and XFLR5 results in Table 6.11.

Table 6.9: Stability derivatives

Name	Symbol	Number	Unit
Sideslip			
Sideforce	$C_{Y\beta}$	-0.49336	per deg
Rolling moment	$C_{l\beta}$	-0.00472	per deg
Yawing moment	$C_{n\beta}$	0.15346	per deg
Yawing moment due to thrust	$C_{nT\beta}$	0.00243	per deg
Roll rate			
Sideforce	C_{Yp}	-0.05182	per deg
Rolling moment	C_{lp}	-0.54002	per deg
Yawing moment	C_{np}	-0.25923	per deg
Pitch rate			
Drag	C_{Dq}	0	per deg
Lift	C_{Lq}	11.27486	per deg
Pitching moment	C_{mq}	-8.90024	per deg
Yaw rate			
Sideforce	C_{Yr}	0.34434	per deg
Rolling moment	C_{lr}	0.45057	per deg
Yawing moment	C_{nr}	-0.32879	per deg

Table 6.10: Control derivatives

Name	Symbol	Number	Unit
Horizontal stabilizer incidence			
Drag	$C_{D_{i_{hs}}}$	0.16079	per deg
Lift	$C_{L_{i_{hs}}}$	1.47718	per deg
Pitching moment	$C_{m_{i_{hs}}}$	0.36929	per deg
Vertical stabilizer incidence			
Drag	$C_{D_{i_{vs}}}$	0.08348	per deg
Lift	$C_{L_{i_{vs}}}$	0.76691	per deg
Pitching moment	$C_{m_{i_{vs}}}$	0.19173	per deg
Elevator			
Drag	$C_{D_{\delta_e}}$	0.02059	per deg
Lift	$C_{L_{\delta_e}}$	0.18913	per deg
Pitching moment	$C_{m_{\delta_e}}$	0.04728	per deg
Rudder			
Sideforce	$C_{Y_{\delta_r}}$	0.26975	per deg
Rolling moment	$C_{l_{\delta_r}}$	0.00499	per deg
Yawing moment	$C_{n_{\delta_r}}$	-0.06015	per deg
Aileron			
Sideforce	$C_{Y_{\delta_a}}$	0	per deg
Rolling moment	$C_{l_{\delta_a}}$	-1.83363	per deg
Yawing moment	$C_{n_{\delta_a}}$	0.34656	per deg

To verify the correct signs of the derivatives, XFLR5 software was used to verify the results. As shown in Table 6.11, most stability derivatives align in order of magnitude and sign with XFLR5 prediction. Furthermore, all derivatives have the correct expected sign, comparing with lecture notes and Cessna Citation 2 data sheet from [30]. This allows for extraction of other longitudinal derivatives, which were not found using Roskam methodology, but were provided by XFLR5. The complete list of new derivatives determined from XFLR5 is shown in Table 6.12.

Table 6.11: Verification of stability derivatives

Name	Symbol	Roskam	XFLR5	Correct sign	Unit
Sideslip					
Sideforce	$C_{Y\beta}$	-0.49336	-0.46382	✓	per deg
Rolling moment	$C_{l\beta}$	-0.00472	-0.0030654	✓	per deg
Yawing moment	$C_{n\beta}$	0.15346	0.17911	✓	per deg
Yawing moment due to thrust	$C_{nT\beta}$	0.00243	NA	✓	per deg
Roll rate					
Sideforce	C_{Yp}	-0.05182	-0.0922954	✓	per deg
Rolling moment	C_{lp}	-0.54002	-0.5793	✓	per deg
Yawing moment	C_{np}	-0.25923	-0.015281	✓	per deg
Pitch rate					
Drag	C_{Dq}	0	NA	✓	per deg
Lift	C_{Lq}	11.27486	16.03	✓	per deg
Pitching moment	C_{mq}	-8.90024	-51.05	✓	per deg
Yaw rate					
Sideforce	C_{Yr}	0.34434	0.41045	✓	per deg
Rolling moment	C_{lr}	0.45057	0.17196	✓	per deg
Yawing moment	C_{nr}	-0.32879	-0.1301	✓	per deg

Table 6.12: Longitudinal derivatives from XFLR5

Symbol	XFLR5	Correct sign	Unit
C_{X_u}	-0.77157	✓	per deg
C_{Z_u}	-0.00428	✓	per deg
C_{m_u}	0.02533	✓	per deg

6.5.2. Hinge moment

For all control surfaces, hinge moment coefficient $c_{h\delta}$ is also determined. This allows for calculating the hinge moment, for the elevator described by Equation 6.5.2. For the rudder and the aileron, similar calculation is performed, with results summarised in Table 6.13.

Table 6.13: Hinge moment

Name	Symbol	Elevator	Rudder	Aileron	Unit
Hinge moment derivative	$c_{h\delta}$	-0.298	-0.379	-0.088	-
Control moment at trim speed	M_{trim}	-3.62	-1.74	-0.17	Nm

$$M_e = c_{h\delta_e} \frac{1}{2} \rho V^2 \left(\frac{V_h}{V} \right)^2 S_e \bar{c}_e \quad (6.8)$$

Based upon the required control moments as shown in Table 6.13, servo sizing is performed. Given that the control surfaces do not need to deflect more than approximately $\pm 30^\circ$, it is possible to use gearing to utilize smaller, more lightweight servos while maintaining sufficient control moments. Based on a servo with a maximum traverse of $\pm 90^\circ$, a gearing ratio of 3 can be utilized, for a minimum torque of 1.133 N m. This sets the Volz DA 15-N-HT-30 as a reasonable servo for the elevator and rudders, providing 1.5 N m direct, or up to 4.5 N m when geared for a weight of only 66 g per servo [31]. While this servo is technically oversized for the ailerons, it is also used here in order to reduce complexity. By using this servo for ailerons instead of a smaller alternative, parts are more interchangeable and less spares must be carried. Thus, five DA 15-N-HT-30 servos are utilized for a total weight of 330 g.

These servos are placed in the wing-box of each wing, with the servo horn sticking out, as shown in Figure 6.8a. The

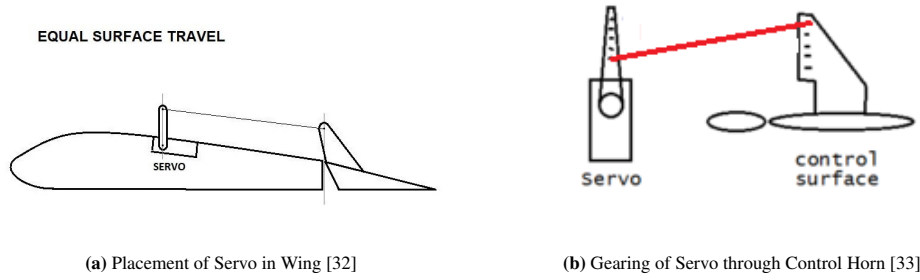


Figure 6.8: Placement of Servos

locations of these servos should receive local reinforcement due to the break in the skin. In order to achieve the desired gearing for sufficient control, the length of the control horns are used as shown in Figure 6.8b. By using a control horn for the servo that is three times shorter than that of the control surface, a gearing ratio of 3 is achieved.

6.6. Static stability

Static stability in aircraft refers to their inherent tendency to return to their original flight condition following a disturbance. It is a crucial aspect of flight dynamics, ensuring controlled and predictable flight behavior. Static stability can be categorized into longitudinal and lateral stability. Longitudinal stability concerns the aircraft stability in the pitch axis, dictating how it behaves after disturbances that cause nose-up or nose-down movements. This type of stability is influenced by the position of the center of gravity relative to the aerodynamic center and the design of the horizontal stabilizer. On the other hand, lateral stability pertains to stability around the roll axis, affecting how the aircraft responds to roll disturbances. Key factors contributing to lateral stability include the dihedral angle of the wings, wing sweep, and the placement of the vertical stabilizer. Both longitudinal and lateral stability are essential for maintaining a steady and controllable flight, and are discussed in the following subsections.

6.6.1. Static longitudinal stability

The primary control surface capable of providing longitudinal stability is the elevator. By investigating its necessary deflection and control force to actuate it at various speeds allows for finding the most critical condition, and size the control surface further.

Elevator Deflection

Elevator deflection is quantified by Equation 6.6.1.

$$\delta_e = -\frac{1}{C_{m\delta_e}} \left(C_{m_0} + \frac{W}{\frac{1}{2}\rho V^2 S} \frac{x_{cg} - x_{n_{fixed}}}{\bar{c}} \right) \quad (6.9)$$

It can be seen that at the trim speed the elevator deflection is zero, which is desired due to no actuation required at the target cruise flight. Considering other velocities, elevator deflection has to be downward for speeds below the trim speed and upward for speeds above the trim speed. This slope of the deflection-velocity curve is desired, as it increases the lift at speeds below the trim speed, allowing for easier take-off, and decreases the lift above the trim speed, bringing the aircraft back to equilibrium state. The critical elevator deflection is 8° downwards for V_{stall} . This elevator deflection does not result in elevator trailing edge touching the ground, which verifies the allowable pitch angle, detailed for tail-landing-gear combination in section 8.4.

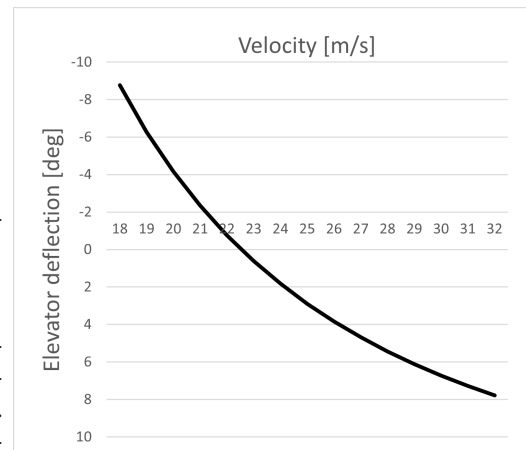


Figure 6.9: Elevator deflection $(\partial\delta_e/\partial V)_{trim} = 1.13$

Elevator Control Force

Another important parameter for the control surfaces is the control force required to actuate it. The main output parameters are the control force at trim speed, and the variance of the control force with speed. The input parameters related to the geometry of the control surface, and are compiled according to [34, Cha. 6], [28, Sec. 9], and from the geometry of the rest of the aircraft.

$$F_S = \eta_h G S_e \bar{c}_e (W/S) \frac{C_{h\delta_e}}{C_{m\delta_e}} (SM_{free}) \left(\left(1 - \frac{V}{V_{trim}} \right)^2 \right) \quad (6.10)$$

As shown, the elevator control force increases, requiring zero force at trim speed. This is desirable, as below the trim speed a "push" is needed, while above the trim speed a "pull" on the stick is required. Additionally, due to the monotonic behavior of the curve, releasing the stick will cause the aircraft to return to its trimmed speed, and the relatively low gradient will likely keep it within 10% of the trim speed. Regulations stipulate that the control force slope must be at least 0.147 kgs/m, and the values for this aircraft's elevator is 3.23, satisfying the requirement.

Although this regulation is intended to allow the pilot to feel the control force change, the pilot-less design means that the control force slope will be processed for further control with the autopilot. Consequently, all static longitudinal stability requirements are satisfied.

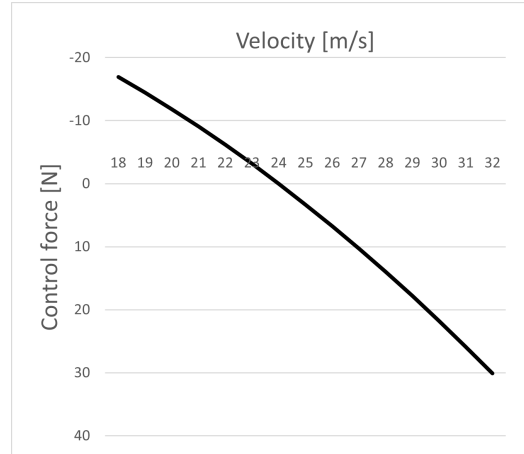


Figure 6.10: Elevator control force
 $(\partial F_e / \partial V)_{trim} = 3.23$

6.6.2. Static Lateral-Directional Stability

Stability derivatives

Two most important stability derivatives for lateral-directional stability are $C_{l\beta}$ and $C_{n\beta}$. The parameter $C_{l\beta}$, called weathervane stability, quantifies the rolling moment as a result of increase in sideslip angle [29]. Its desired sign is **negative**, since then the aircraft counteracts the positive rolling moment and returns to its equilibrium state without a need for pilot's influence. Another parameter is a weathercock stability $C_{n\beta}$. It quantifies the yaw of the aircraft resulting from side wind, and the desired **positive** sign signifies that the aircraft will turn to the direction the air velocity was coming from, eliminating the sideslip. The correct signs of these two derivatives ensure the static lateral-directional stability

Rudder pedal force

Similarly to the elevator control force, it is possible to assess rudder performance by plotting rudder pedal force as a function of angle of sideslip β .

$$F_r = \eta_r G S_r \bar{c}_r (W/S) \frac{C_{h\delta_r}}{C_{n\delta_r}} (SM_{free}) \left(\left(1 - \frac{V}{V_{stall}} \right)^2 \right) \quad (6.11)$$

In this case, velocity V is not the free-stream velocity, but the increased stall velocity due to side wind $\sqrt{V_{stall}^2 + v_{wind}^2}$, since at the stall the side winds are most critical. As shown in Figure 6.11, the pedal-force-gradient does not reverse its sign when crossing zero sideslip angle. From requirements, the maximum encountered side wind is 9 m s^{-1} , which combined with $V_{stall} = 20 \text{ m s}^{-1}$ results in 24° of sideslip angle. To counteract this momentarily gust, the rudder should deflect more than 25° .

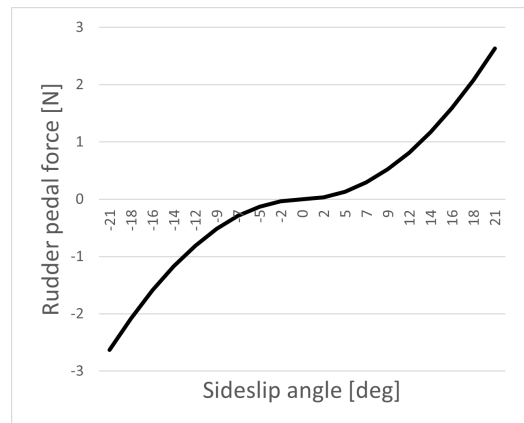


Figure 6.11: Rudder pedal force

6.7. Dynamic stability

Dynamic stability refers to aircraft's ability to not only return to their original flight condition after a disturbance, but also to do so at a smooth and progressively diminishing rate over time. This aspect of stability is crucial for ensuring comfortable and safe flight by preventing oscillations from growing uncontrollably. Dynamic stability, like static stability, can be categorized into longitudinal and lateral stability. Longitudinal dynamic stability addresses the aircraft's response over time to pitch disturbances, involving oscillatory motions known as phugoid and short-period oscillations. These motions are influenced by factors such as damping characteristics and the aerodynamic properties of the aircraft. Lateral dynamic

stability, on the other hand, concerns the aircraft's behavior in response to roll and yaw disturbances. It encompasses the Dutch roll and spiral modes, which are governed by the aircraft's yaw and roll damping properties, as well as the interaction between the vertical and horizontal stabilizers. Both longitudinal and lateral dynamic stability are essential for maintaining a smooth flight path, and are discussed in this section.

6.7.1. Dynamic longitudinal stability

The eigenmotions were analysed based on the methods proposed in [30], which proposes analysis based on eigenvalues obtained from symmetric and asymmetric equations of motion.

- **Frequency** refers to the number of oscillations that an eigenmotion undergoes per unit of time. Equation 6.12
- **Damping ratio** is a dimensionless measure of how oscillations in a system decay after a disturbance Equation 6.13
- **Period** is the time taken in second for one complete cycle of oscillation Equation 6.14.
- **Half-time** refers to the time for the amplitude of the oscillation to reduce to half of its initial value. Equation 6.15

$$\omega_0 = \sqrt{\text{Re}[\lambda]^2 + \text{Im}[\lambda]^2} \quad (6.12) \quad \zeta = \frac{-\text{Re}[\lambda]}{\omega_0} \quad (6.13) \quad P = \frac{2\pi}{\omega_0 \cdot \sqrt{1 - \zeta^2}} \quad (6.14) \quad T_{\frac{1}{2}} = \frac{\ln(0.5)}{\text{Re}[\lambda]} \quad (6.15)$$

The symmetric equations of motion are shown in Equation 6.16. Moreover, the unitless symmetric parameters are presented in Table 6.14.

$$\begin{bmatrix} C_{X_u} - 2\mu_c D_c & C_{X_\alpha} & C_{Z_0} & C_{X_q} \\ C_{Z_u} & C_{Z_\alpha} + (C_{Z_{\dot{\alpha}}} - 2\mu_c) D_c & -C_{X_0} & C_{Z_q} + 2\mu_c \\ 0 & 0 & -D_c & 1 \\ C_{m_u} & C_{m_\alpha} + C_{m_{\dot{\alpha}}} D_c & 0 & C_{m_q} - 2\mu_c K_{yy}^2 D_c \end{bmatrix} \begin{bmatrix} \hat{u} \\ \alpha \\ \theta \\ \frac{q\bar{c}}{V} \end{bmatrix} = \begin{bmatrix} -C_{X_\delta} \\ -C_{Z_\delta} \\ 0 \\ -C_{m_\delta} \end{bmatrix} \delta_e \quad (6.16)$$

Table 6.14: Unitless symmetric parameters

Unitless mass	μ_c	99.66
Unitless mass moment of inertia along X-axis	K_Y^2	1.07

Short period

The short period is a symmetric eigenmotion response to a momentarily vertical disturbance, such as an elevator deflection control input. The most important motion variables are angle of attack and pitch attitude angle. The expected period is less than 5 seconds, the undamped natural frequency is low, while the damping ratio is low [6, VII, p. 77].

It is assumed, that throughout this motion the flight is level and steady, there is an equilibrium of forces in the body axis direction, and the pitch rate is zero. This reduces the symmetric equations of motion to Equation 6.17, allowing for finding the eigenvalues:

$$\begin{bmatrix} C_{Z_\alpha} + (C_{Z_{\dot{\alpha}}} - 2\mu_c) D_c & C_{Z_q} + 2\mu_c \\ C_{m_\alpha} + C_{m_{\dot{\alpha}}} D_c & C_{m_q} - 2\mu_c K_Y^2 D_c \end{bmatrix} \begin{bmatrix} \alpha \\ \frac{q\bar{c}}{V} \end{bmatrix} = \mathbf{0} \quad (6.17)$$

Phugoid

The phugoid is an eigenmotion, which is a continuation of short period motion with oscillations over a long period. The most important motion variables are speed and pitch attitude angle. The expected period is more than 5 seconds, the undamped natural frequency is high, while the damping ratio is moderately high [6, VII, p. 77].

It is assumed, that throughout the phugoid motion the accelerations, pitch rate and angle of attack variations are negligible due to long period and prolonged oscillation around equilibrium point. In this case, the symmetric equations of motion from Equation 6.16 reduce to the following:

$$\begin{bmatrix} C_{X_u} - 2\mu_c D_c & C_{X_\alpha} & C_{Z_0} & 0 \\ C_{Z_u} & C_{Z_\alpha} & 0 & 2\mu_c \\ 0 & 0 & -D_c & 1 \\ C_{m_u} & C_{m_\alpha} & 0 & C_{m_q} \end{bmatrix} \begin{bmatrix} \hat{u} \\ \alpha \\ \theta \\ \frac{q\bar{c}}{V} \end{bmatrix} = \mathbf{0} \quad (6.18)$$

Eigenmotions results

The final results of eigenmotion analysis can be found in Table 6.15.

Table 6.15: Symmetric eigenmotions

Name	Symbol	Short-period	Phugoid	Unit
Real part of eigenvalue	$\text{Re}(\lambda)$	-0.03426	-0.00191	-
Imaginary part of eigenvalue	$\text{Im}(\lambda)$	0.04511	0.00463	
Period	P	2.13	20.77	s
Half-time	$T_{\frac{1}{2}}$	0.31	5.55	s
Natural frequency	ω_n	2.95	0.30	rad/s
Damping ratio	ζ	0.60	0.38	

Both symmetric eigenmotions are positively dampened, due to the negative real part of the eigenvalue. The period of the short-period motion is smaller than 5 seconds, while the period of phugoid motion larger than 5 seconds. Both of these values satisfy the longitudinal stability criteria, thus the aircraft is deemed to be stable in symmetric eigenmotions.

Pitch Rate

The knowledge of eigenvalues allows for solving the simplified equations of motion for a combination of angle of attack, pitch angle and yaw rate, which allows for extracting the pitch rate. Assuming equilibrium of forces in the body axis, much like in the phugoid eigenmotion, yields the derivative of angle of attack with respect to pitch rate in Equation 6.19. Similarly, an equation for pitch rate q is obtained in Equation 6.20.

$$\frac{d\alpha}{d\frac{q\bar{c}}{V}} = -\frac{C_{m_q}}{C_{m_\alpha}} \quad (6.19) \quad \frac{q\bar{c}}{V} = -\frac{C_{m_\alpha}}{C_{m_q}} \alpha \quad (6.20)$$

For instance, at trim speed, the pitch rate is -4 deg/s per 1 deg of angle of attack, counteracting the increase in the angle of attack. This value is an estimate of performance but reflects the approximate behaviour of the aircraft. Due to no legal requirements on achievable pitch rate, this procedure is just outlined to allow the determination of pitch rate at various flight conditions.

6.7.2. Dynamic Lateral-Directional Stability

Due to the diverging nature of the Dutch roll mode, the half-time is redefined to doubling time, as in Equation 6.21. To quantify the period in the absence of imaginary part of the eigenvalue, a so-called time constant is defined for aperiodic roll and spiral Equation 6.22:

$$T_2 = \frac{\ln(2)}{\text{Re}[\lambda]} \quad (6.21) \quad \tau = -\frac{1}{\lambda} \quad (6.22)$$

$$\begin{bmatrix} C_{Y_\beta} + (C_{Y_{\dot{\beta}}} - 2\mu_b)D_b & C_L & C_{Y_p} & C_{Y_r} - 4\mu_b \\ 0 & -\frac{1}{2}D_b & 1 & 0 \\ C_{\ell_\beta} & 0 & C_{\ell_p} - 4\mu_b K_X^2 D_b & C_{\ell_r} + 4\mu_b K_{XZ} D_b \\ C_{n_\beta} + C_{n_{\dot{\beta}}} D_b & 0 & C_{n_p} + 4\mu_b K_{XZ} D_b & C_{n_r} - 4\mu_b K_Z^2 D_b \end{bmatrix} \begin{bmatrix} \beta \\ \phi \\ \frac{pb}{2V} \\ \frac{rb}{2V} \end{bmatrix} = \begin{bmatrix} -C_{Y_{\delta_a}} & -C_{Y_{\delta_r}} \\ 0 & 0 \\ -C_{\ell_{\delta_a}} & -C_{\ell_{\delta_r}} \\ -C_{n_{\delta_a}} & -C_{n_{\delta_r}} \end{bmatrix} \begin{bmatrix} \delta_a \\ \delta_r \end{bmatrix} \quad (6.23)$$

Table 6.16: Unitless asymmetric parameters

Unitless mass	μ_b	8.916
Unitless mass moment of inertia along X-axis	K_X^2	0.00225
Unitless mass moment of inertia along Z-axis	K_Z^2	0.00736
Unitless mass moment of inertia along XZ-axis	K_{XZ}	0.001

Aperiodic Roll

The aperiodic roll is an asymmetric eigenmotion characterized by a non-oscillatory, exponential decay response to a roll disturbance. It is initiated primarily by the ailerons, which deflection results in a differential lift over the wing, causing the aircraft to roll about its longitudinal axis. The most important motion variable is the bank angle, and the time constant is small [6, VII, p. 88].

This eigenmotion can be simplified by assuming no yawing moment, and no lateral forces. In such a case, the asymmetric equations of motion simplify greatly to Equation 6.24.

$$(C_{\ell_p} - 4\mu_b K_X^2 D_b) \frac{pb}{2V} = 0 \quad (6.24)$$

Dutch Roll

Dutch roll motion is an asymmetric eigenmotion induced by a rudder deflection. The important property of the eigenmotion is that the initiated roll rate, over time, induces a yaw rate and vice versa. The most important motion variables are sideslip and bank angles. The expected period is short, the undamped natural frequency is moderately high, while the damping ratio is low [6, VII, p. 88].

The Dutch roll equations of motions have been derived in Equation 6.25 discarding the rolling component and assuming dynamic derivatives to be zero.

$$\begin{bmatrix} C_{Y\beta} - 2\mu_b\lambda_b & -4\mu_b \\ C_{n\beta} & C_{n_r} - 4\mu_b K_Z^2 \lambda_b \end{bmatrix} \begin{bmatrix} \beta \\ \frac{rb}{2V} \end{bmatrix} = \mathbf{0} \quad (6.25)$$

Spiral

Finally, the spiral is a very slow asymmetric mode, characterised by sideslip, yaw and roll. The most important motion variables are the heading and bank angles. The time constant is large, and the eigenmotion is accepted to be unstable [6, VII, p. 88].

For the equations of motion it has been assumed, that all linear and angular accelerations are negligible, simplifying the asymmetric equations of motion to Equation 6.26.

$$\begin{bmatrix} C_{Y\beta} & C_L & 0 & -4\mu_b \\ 0 & -\frac{1}{2}D_b & 1 & 0 \\ C_{l\beta} & 0 & C_{l_p} & C_{l_r} \\ C_{n\beta} & 0 & C_{n_p} & C_{n_r} \end{bmatrix} \begin{bmatrix} \beta \\ \phi \\ \frac{pb}{2V} \\ \frac{rb}{2V} \end{bmatrix} = \mathbf{0} \quad (6.26)$$

Eigenmotions results

Obtaining eigenvalues of the lateral eigenmotions allows for determining other parameters, shown in Table 6.17. The qualitative descriptors of parameter magnitudes such as "small", "high", "moderately high" were compared between aircraft eigenmotions and with literature [30].

Table 6.17: Asymmetric eigenmotions

Name	Symbol	Dutch roll	Aperiodic Roll	Spiral	Unit
Real part of eigenvalue	$\text{Re}(\lambda)$	-0.04614	-1.95202	0.05813	
Imaginary part of eigenvalue	$\text{Im}(\lambda)$	0.86837	-	-	
Period	P	7.24	-	-	s
Half-time	$T_{\frac{1}{2}}$	15.02	-	-	s
Doubling time	T_2	-	-	13.8	s
Time-constant	τ	-	0.51	-	s
Natural frequency	ω_n	0.87	-	-	rad/s
Damping ratio	ζ	0.05	-	-	

For aperiodic roll, the time constant is small, as recommended by regulations [6]. For Dutch roll, the period is within expected duration, the natural frequency is high, and the damping ratio is small. Finally, for the spiral, the time to double the amplitude is over 12 seconds, proving the slow progression of this eigenmotion.

Lateral Stability Diagram

Both weathervane and weathercock stability are important parameters, which allow for designing the aircraft against two unstable eigenmotions - Dutch roll and spiral. The stability of these eigenmotions can be assessed with a lateral stability diagram, visualised in Figure 6.12.

The parameter E is determined from the characteristic polynomial of asymmetric equations of motion matrix Equation 6.27.

$$A\lambda_c^4 + B\lambda_c^3 + C\lambda_c^2 + D\lambda_c + E = 0 \quad (6.27)$$

The parameter R can be determined from the Routh-Hurwitz Stability Criterion, shown in Equation 6.28.

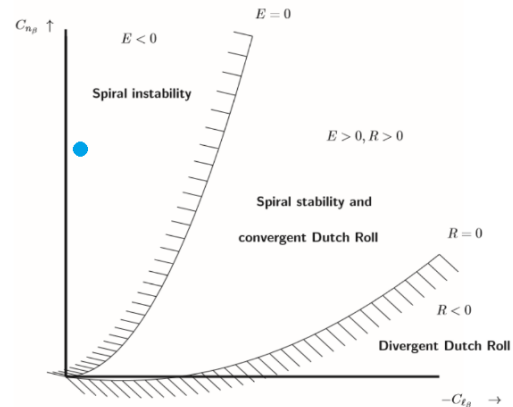


Figure 6.12: Lateral stability diagram

$$R = BCD - AD^2 - B^2E > 0 \quad (6.28)$$

From analysis $E = -0.0855$ and $R = 6.15$. On the lateral stability diagram, these parameters of the aircraft are approximated by the blue dot. This verifies, that the aircraft is stable in Dutch roll, but unstable in spiral.

Roll Rate

Assuming zero roll acceleration, the roll rate is found by Equation 6.29 [6, VII, p57], and all relevant parameters are summarised in Table 6.18. Roll time constant is below 1.0, as required. The obtained roll rate well satisfies the requirement of roll rate of at least 60 deg in 4 seconds.

Table 6.18: Roll rate

Roll time constant	τ_r	0.5
Dimensional roll damping derivative	L_p	-11
Dimensional roll control power derivative	$L_{\delta_{cpt}}$	92
Lateral cockpit control deflection	δ_{cpt}	5 deg
Roll rate	$\dot{\phi}$	41 deg/s

$$\dot{\phi} = \frac{-L_p}{L_{\delta_{cpt}} \delta_{cpt}} \quad (6.29)$$

Yaw Rate

Yaw rate is an important property in the turning flight, where the equations of motion from Equation 6.30. apply [30].

$$\begin{bmatrix} C_L & C_{Y\beta} & -4\mu_b & 0 & 0 \\ 0 & C_{l\beta} & C_{l_r} & C_{l_{\delta_a}} & 0 \\ 0 & C_{n\beta} & C_{n_r} & 0 & C_{n_{\delta_r}} \end{bmatrix} \begin{bmatrix} \varphi \\ \beta \\ \frac{rb}{2V} \\ \delta_a \\ \delta_r \end{bmatrix} = \mathbf{0} \quad (6.30)$$

Contrary to the roll rate, it is not trivial to estimate the yaw rate without further assumptions on flight conditions. A reasonable situation of a coordinated turn may be considered, for which the angle of sideslip β is zero, thus minimising drag and maximising comfort of the operator [30]. In this case, the derivatives with respect to the yaw rate can be found by Equation 6.31, Equation 6.32 and Equation 6.33 [30]. This way, the required deflection of the control surfaces in coordinated turn can be calculated, and the resulting yaw rate determined by Equation 6.34, Equation 6.35 and Equation 6.36. Due to no yaw rate legal requirement, these equations are provided for completeness.

$$\frac{d\varphi}{d\frac{rb}{2V}} = \frac{4\mu_b}{C_L} \quad (6.31) \quad \frac{d\delta_a}{d\frac{rb}{2V}} = -\frac{C_{l_r}}{C_{l_{\delta_a}}} \quad (6.32) \quad \frac{d\delta_r}{d\frac{rb}{2V}} = -\frac{C_{n_r}}{C_{n_{\delta_a}}} \quad (6.33)$$

$$\frac{rb}{2V} = \frac{C_L}{4\mu_b} \varphi \quad (6.34) \quad \frac{rb}{2V} = -\frac{C_{l_{\delta_a}}}{C_{l_r}} \delta_a \quad (6.35) \quad \frac{rb}{2V} = -\frac{C_{n_{\delta_a}}}{C_{n_r}} \delta_r \quad (6.36)$$

6.8. Verification And Validation

To verify this chapter, a thorough investigation in the available literature has been conducted. Sources such as DATCOM and Torenbeek has been initially consulted, the former one containing too detailed and complex derivations, while the latter missing critical steps for control surfaces sizing. As a result, Roskam part VI has been used for calculating parameters in sections 6.2-6.5, while Roskam part VII for parameters in sections 6.6-6.7. This methodology ensured consistency of derivations and facilitated reading of a well-respected source.

Calculations for all parts have been conducted in Excel, mainly due to the possibility of referencing multiple values and ease of documentation. Every parameter has been verified by ensuring that each subsubsubscript is correctly labelled ($C_{L_{h\alpha}} \neq C_{L_{\alpha h}}$ as sometimes confused in literature), checking final results of partial calculations with literature, and eventually performing the calculations again in case of major differences.

To monitor the accuracy of the results, frequent consultations with the tutor have taken place to verify the work and determine if the design is converging in the right direction. Finally, proofreading of the chapter facilitated the comprehensiveness of the chapter and provided critical feedback.

For the purpose of control and stability, XFLR5 software has been used for verification of parameters. Due to the time-limitation, software such as OpenVSP for precise stability simulations has not been utilised. However, experience with XFLR5 from the aerodynamic design part allowed for the verification of control derivatives.

Table 6.19: Requirements for control surfaces

ID	Check	Reasoning	Requirement
Mission (MIS)			
STK-0.3.9-MIS-ENV-4	✓	Analysis: Rudder deflection of at least 25deg needed	The UAV shall be able to take off and land with a cross wind of 9 m s^{-1} .
STK-0.3.9-MIS-ENV-5	✓	Analysis: Operational speeds 20-40 m s^{-1}	The UAV shall be able to take off and land with a tail wind of 2 m s^{-1} .
STK-0.3.9-MIS-ENV-6-OPT	✓	Analysis: Operational speeds 20-40 m s^{-1}	The UAV shall be able to take off and land with a head wind of 15 m s^{-1} .
Control & Stability (CS)			
FUN-CS-1	✓	Analysis: Moment equilibrium obtained in subsection 6.3.3	The UAV shall exhibit a moment equilibrium at the trimmed flight.
FUN-CS-2	✓	Analysis: Elevator sizing obtained in subsection 6.4.1	Elevator sizing shall allow for the placement of the horizontal tail spar.
FUN-CS-3	✓	Analysis: Rudder sizing obtained in subsection 6.4.2	Rudder sizing shall allow for the placement of the vertical tail spar.
FUN-CS-4	✓	Analysis: Aileron sizing obtained in subsection 6.4.3	Aileron sizing shall allow for the placement of the rear wing spar.
FUN-CS-5	✓	Analysis: Stability derivatives obtained in Table 6.9	All stability derivatives shall have a correct sign.
FUN-CS-6	✓	Analysis: Control derivatives obtained in Table 6.10	All control derivatives shall have a correct sign.
FUN-NAV-4.N.iv	✓	Analysis: All child requirements met	The UAV shall be laterally stable.
FUN-NAV-4.N.v	✓	Analysis: All child requirements met	The UAV shall be longitudinally stable.
FUN-NAV-4.N.vi	✓	Analysis: All child requirements met	The UAV shall be directionally stable.
FUN-NAV-4.N.v.1	✓	Analysis: Elevator Control Force from subsection 6.6.1	The PULL input shall be required to obtain and maintain speeds below the trim speed.
FUN-NAV-4.N.v.2	✓	Analysis: Elevator Control Force subsection 6.6.1	The PUSH input shall be required to obtain and maintain speeds above the trim speed.
FUN-NAV-4.N.v.3	✓	Analysis: Elevator Control Force subsection 6.6.1	The speed shall return to within 10 % of the trim speed if the control is released from the push or pull.
FUN-NAV-4.N.v.4	✓	Analysis: Elevator Control Force subsection 6.6.1	The stick-force speed gradient shall be recorded for further processing by the autopilot.
FUN-NAV-4.N.iv.1	✓	Analysis: Stability Derivatives subsection 6.6.2	The UAV shall return to the original condition when put in a sideslip.
FUN-NAV-4.N.iv.2	✓	Analysis: Rudder Pedal Force subsection 6.6.2	The rudder pedal force required to put the airplane in sideslip condition shall be such that the pedal-force-gradient does not reverse its sign.
FUN-NAV-4.N.iv.3	✓	Analysis: Stability Derivatives subsection 6.6.2	The UAV shall raise the right wing when put in a sideslip.
FUN-NAV-4.N.v.5	✓	Analysis: Short-period subsection 6.7.1	The UAV shall be stable in short-period eigenmotion.
FUN-NAV-4.N.v.6	✓	Analysis: Phugoid subsection 6.7.1	The UAV shall be stable in phugoid eigenmotion.
FUN-NAV-4.N.iv.4	✓	Analysis: Aperiodic Roll subsection 6.7.2	The UAV shall be stable in aperiodic roll eigenmotion.
FUN-NAV-4.N.iv.5	✓	Analysis: Dutch Roll subsection 6.7.2	The UAV shall be stable in Dutch roll eigenmotion.
FUN-NAV-4.N.iv.6	✓	Analysis: Spiral subsection 6.7.2	The UAV shall have a time-to-double the amplitude higher than 12 seconds for spiral eigenmotion.
FUN-NAV-4.N.6.a.ii	Stricken	Pitch rate derivative has been determined as a function of angle of attack subsection 6.7.1	The UAV shall be able to pitch TBD deg/s.
FUN-NAV-4.N.6.b.ii	Stricken	Yaw rate derivatives has been determined as function of angle of roll, elevator deflection and rudder deflection subsection 6.7.2	The UAV shall be able to yaw TBD deg/s.
FUN-NAV-4.N.6.c.ii	✓	Analysis: Roll rate subsection 6.7.2	The UAV shall be able to roll 60 deg in 4 seconds.

Structural Characteristics

The UAV consists of several structural elements that carry the applied loads during flight. This chapter will cover the detailed design of the two key structural components, namely the wing and the fuselage. This is done by first mentioning the subsystem requirements in section 7.1, followed by elaborating on the material to be used in the main load-carrying structures in section 7.2. Subsequently, the design of the wing and the fuselage will be elaborated upon in section 7.3 and section 7.4, respectively. Finally, the verification and validation process of the methods used in the design of the structures will be discussed in section 7.5.

7.1. Subsystem requirements

Table 7.1: Requirements for structural system

ID	Requirement
Wing (WIN)	
SYS-STR-WIN-01	The wing shall maintain structural rigidity.
SYS-STR-WIN-02	The wing shall withstand a bending load induced by the aerodynamics of at most 1470 N m at the root.
SYS-STR-WIN-03	The wing shall withstand a shear load induced by the aerodynamics of at most 1546 N at the root.
SYS-STR-WIN-05	The wing shall withstand all aerodynamically induced loads till 3.8 g with a safety factor of 1.5 during operation.
Fuselage (FUS)	
SYS-STR-FUS-01	The fuselage of the UAV shall maintain structural rigidity.
SYS-STR-FUS-02	The fuselage shall withstand an engine induced trust load of 90 N loads during cruise operation.
SYS-STR-FUS-03	The fuselage shall withstand all lift loads till 3.8 g with a safety factor of 1.5 during operation up.
SYS-STR-FUS-04	The fuselage shall withstand all wing induced drag loads during operation.
SYS-STR-FUS-05	The fuselage shall withstand its own aerodynamic drag loads during operation.
SYS-STR-FUS-06	The fuselage shall withstand all weight loads induced by the landing gear during operation.
SYS-STR-FUS-07	The fuselage shall withstand all weight loads induced by the engine during operation.
SYS-STR-FUS-08	The fuselage shall withstand all weight loads induced by the avionics during operation.
SYS-STR-FUS-09	The fuselage shall support the weight of the payload during operation.
FUN-STR-4.S.1.3	The UAV shall withstand ultimate loads of up to 3.8 g. with a safety factor of 1.5

7.2. Material considerations

Before the UAV can be built, it is useful to select a material for the main structural elements. This decision concerns solely the structural elements that need to carry the loads applied, such that other materials for non-load-carrying elements are still under consideration. The design of the secondary structure is left for future development. As a result, the following material options have been considered:

- E-glass fibers-epoxy
- Carbon fiber-reinforced polymer
- Polyvinyl chloride
- Aluminum (7075-T6)
- Titanium (Ti-6Al-4V)
- Wood

For the initial design of the wing box which is to be performed, it is important to choose a material whose properties line up with the requirements. As the wing box is a critical load-carrying part, stiffness of the material is of great importance as well as a high yield stress. Furthermore, the weight of the structure should be minimized to achieve the most efficient design. In addition, the manufacturability and sustainability of the material should be kept in mind. For these reasons, Aluminum (7075-T6) will be used as the material for the initial wing box and fuselage sizing. It is both stiff and lightweight while being easier to manufacture and more sustainable than titanium. As the wing box is a critical part, more complex composite materials such as carbon fiber are avoided. This way the structure can be more easily analyzed as aluminum is a homogeneous material.

7.3. Wing design

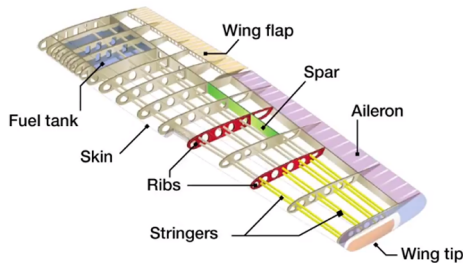
The wing is probably the most important aerodynamic surface on the aircraft as such its structural elements should be designed with care. The structural elements inside the wing should carry all aerodynamic loads that act on the wing.

Furthermore, it should do so without deforming significantly as the aerodynamic shape should be sustained. In order to achieve a structural design that not only is capable of carrying all loads but also is lightweight multiple steps are taken. Firstly, the main wing elements and wing components definitions will be presented in subsection 7.3.1. Further, the internal loads on the wing box, as well as the loading diagrams will be discussed in subsection 7.3.2. Lastly, the two approaches taken for sizing the wing box will be elaborated upon, starting with a first-order sizing presented in subsection 7.3.3 and followed by a detailed design of the wing box in subsection 7.3.4.

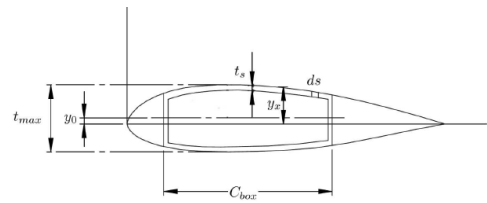
7.3.1. Wing elements

According to [35], the wing structure can be split into primary and secondary elements. The primary structure refers to the load-carrying elements which make up the wing box. These include the skin panels, spars, and ribs, as well as non-optimum weights which take into account the effects of cut-outs, joints, and attachments. The contribution of fixed leading and trailing edges, as well as wing control surfaces (aileron, slats, flaps, etc.) and all other miscellaneous items such as actuators, are included in the secondary group. While the skin of the panels, spar webs and caps of the wing box can be approximated by conducting a first-order stationary structural sizing, the rest of the weight contributions can be determined using empirical equations. An illustration of the wing elements as well as the wing box structure can be seen in Figure 7.1a and Figure 7.1b, respectively.

The rest of this section will mainly focus on sizing the wing box, while other elements that make up the wing are left for further evaluation in future design phases that go into more detail. The sizing of the wing box has been performed through two methods, where the first step is to get an idea of the material distributions along the wing box and the second procedure focuses on sizing all elements the wing box consists of.



(a) Wing elements



(b) Simplified wing box structure

7.3.2. Internal loads

During flight, the wing produces the required lift due to the pressure differences along its surface. Additionally, when the UAV is stationary or it taxis the wing should be able to sustain its own weight. Thus, due to the external forces that act on the wing, the structure will experience internal loads that vary along the wing span. These include internal shear forces and bending moments which have to be carried by the wing box and influence its design. Therefore, before starting the design of the wing box the internal loads are determined.

As mentioned in section 4.4 the wing will consist of a straight part of 0.7 m starting from the root and a tapered part that runs for another 1.44 m until the wing tip. For this a first-order conservative estimation of the lift distribution over the wing span has been considered. Figure 7.2 shows an illustration of the lift distribution over one wing where it can be seen that the first part of the wing experiences a constant lift distribution, after which it starts to decrease such that the wing tip only produces half the lift at the root. The distribution on one wing sums up to half of the maximum lift force the wings have to produce which is equal to the maximum take-off mass of 55.3 kg (class-II mass estimation) multiplied by the maximum loading factor of 3.8 g and a safety factor of 1.5.

Considering the approximated lift distribution the internal shear force and internal bending moment diagrams have

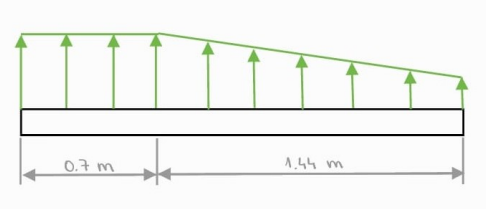


Figure 7.2: Lift distribution

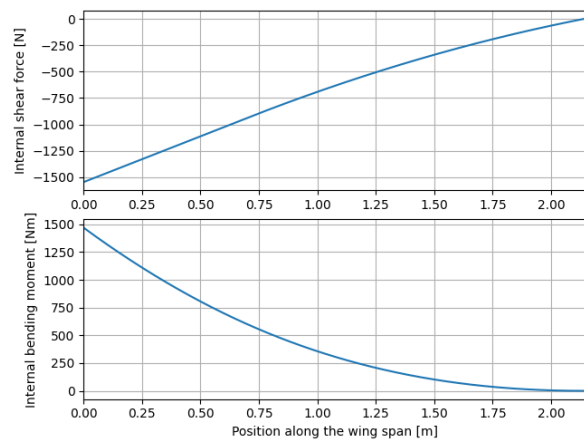


Figure 7.3: Internal loads in wing structure

been constructed considering the wing is a beam clamped at the root. In Figure 7.3, it is evident that both the shear load and bending moment reach their maximum values at the root, then gradually decrease along the span, ultimately reaching zero at the wing tip. Thus, for the purpose of wing box design the maximum shear force in magnitude of 1546.1 N and the maximum internal bending moment of 1469.8 N m have been considered.

In addition to internal shear and bending loads, the wing is also subjected to a torque which depends on the position of the shear center of the wing cross-section. The shear center is defined as the point at which a load applied introduces no torsion in the structure. Thus, a force applied parallel to the surface anywhere else but the shear center produces a torque on the structure. To estimate the magnitude of the torque the wing box structure will be subjected to, the position of the shear center is approximated to coincide with the centroid of the cross-section. According to [36], for closed sections the shear center is close to the centroid. Thus, for an initial analysis this is a good approximation, but for further, more detailed calculations it's recommended that the position of the shear center is computed more accurately.

Considering that the lift force acts in the aerodynamic center of the wing, the torque can be determined by summing up the contribution of the lift force and the moment around the aerodynamic center to determine the moment around the shear center as can be seen in Equation 7.1. Here L is the lift force, x_{ac} and x_{sc} stand for the location of the aerodynamic center and shear center, respectively, and M_{ac} is the moment around the aerodynamic center. The aerodynamic center is considered to be located at quarter chord point on the wing profile. The moment around the aerodynamic center is determined using the Equation 7.2, where ρ is the air density, V_{div} stands for the dive speed, S is the surface area of the wing, \bar{c} is the mean aerodynamic chord and $C_{m_{ac}}$ is the moment coefficient around the aerodynamic center. All parameters are determined either considering the requirements or estimations from other subsystems. The torque to be sustained by the wing box varies for all wing box configurations, given that the centroid of the cross-section differs every time. Therefore, the torque to be sustained is determined for every configuration and it's not a fixed value that needs to be sustained by the wing box.

$$T = M_{ac} + L \cdot (x_{ac} - x_{sc}) \quad (7.1) \quad M_{ac} = \frac{1}{2} \rho V_{div}^2 S \bar{c} C_{m_{ac}} \quad (7.2)$$

7.3.3. First-order wing box design

To perform a first-order structural sizing of the wing box structure, a simplified geometry has been used by modeling elements of the wing box as equivalent panels [35]. The idealization of the wing box is made according to several assumptions that have to be taken into consideration when determining the accuracy of the method employed. Thus, the wing skin, the stringers, as well as the lower and upper spar caps have been modeled by a lower and upper panel, while the spar webs are modeled as two vertical panels, one front and one rear. The upper and lower panels are considered to only carry bending moments, while the spar webs sustain shear loads. An illustration of the simplified wing box structure can be seen in Figure 7.1b. The minimum thickness of the panels and spar webs can be determined by performing an analysis of the elements using the maximum allowable load experienced by the wing structure during flight.

In the case of the upper and lower panels, the maximum allowable bending moment has been computed by considering the maximum internal bending moment experienced at the root of the wing determined in subsection 7.3.2. Thus, the thicknesses of the upper and lower panels have been calculated using Equation 7.3 and Equation 7.4, where M is the maximum applied bending moment and $\sigma_{up_{max}}$ and $\sigma_{low_{max}}$ are the maximum allowable stress of the upper and lower panels, respectively. These are the compressive yield strength of the material used for the wing box in the case of the upper panel and the tensile yield strength of the material for the lower panel. $\eta_t t_{max}$ represents the effective distance between the equivalent upper and lower panels. The equivalent panels are represented by an upper and a lower flat panel placed at an effective distance $\eta_t t_{max}$ from each other, with the same lengths S_{up} and S_{low} as the curved panels. The fraction η_t is calculated as can be seen in Equation 7.5 in such a way that the applied bending moment on the curved and flat panels is the same [35]. By performing this simplification the upper and lower panels experience a uniform stress distribution.

$$t_{up} = \frac{M}{\eta_t t_{max} \sigma_{up_{max}} S_{up}} \quad (7.3) \quad t_{low} = \frac{M}{\eta_t t_{max} \sigma_{low_{max}} S_{low}} \quad (7.4)$$

$$\eta_t = \frac{1}{t_{max}} \left(\frac{1}{S_{up} y_{up_{max}}} \sum (y_{up} - y_0)^2 ds_{up} + \frac{1}{S_{low} y_{low_{max}}} \sum (y_{low} - y_0)^2 ds_{low} \right) \quad (7.5)$$

The vertical parts shown in Figure 7.1a are called spar webs. The wing box has a front spar located near the leading edge of the airfoil and a rear spar located near the trailing edge. In the model used in [35], the spar webs are designed to withstand shear stresses, which are calculated through the shear flow due to the vertical forces applied on the wing box and the shear flow due to torsional moment. A method by Howe [37] is used that calculates the shear flow due to the vertical force applied through Equation 7.6 and Equation 7.7. In these equations, the fs subscript represents the front spar, and the rs subscript represents the rear spar. To determine the height of the front and rear spar, the idealization of the airfoil (FX72MS150B) was used which resulted in a height of 44.44 mm (front spar) and 43.66 mm (rear spar). With these heights the shear flow due to the shear force can be determined in each web.

$$q_{v_{fs}} = \frac{h_{fs}}{h_{fs}^2 + h_{rs}^2} \cdot V \quad (7.6)$$

$$q_{v_{rs}} = \frac{h_{rs}}{h_{fs}^2 + h_{rs}^2} \cdot V \quad (7.7)$$

In addition to the vertical shear force, there is also a torsional load that induces shear flow. This happens according to Equation 7.8. The enclosed area denoted by A_{box} is calculated using the idealization of the airfoil. Subsequently, these two shear flows are added together to get the most limiting loading scenario for which the thickness of the webs is determined as can be seen in Equation 7.9.

$$q_t = \frac{T}{2A_{box}} \quad (7.8)$$

$$t = \frac{(q_t + q_v)}{\tau} \quad (7.9)$$

Lastly, with the acquired thickness of the front and rear spar webs, their area needs to be checked for potential shear buckling. Shear buckling occurs when thin plates are supporting loads normal to their surface in addition to membrane forces that lie in the plane of the plate. Compressive in-plane stresses cause the plate to buckle at stresses much lower than its shear stress limit [38]. The structure is now unstable and it is unsure it can successfully support the loads it is subjected to. Via Equation 7.10, Equation 7.11 and Equation 7.12 [39] the critical shear load for buckling is calculated which is lower than the maximum shear strength of aluminum (7075-t6). this means the spars will fail due to shear buckling before they fail due to shear flow. Because all the shear flow has to be carried during flight, the thickness of the front as well as the rear spar is increased to the thickness at which shear buckling is no longer a problem, since the critical load is equal to the maximum shear strength. The thickness found for each panel in this initial analysis is listed in Table 7.2.

$$\tau_{cr} = C_s \frac{\pi^2 E}{12(1-\nu)^2} \left(\frac{t}{b}\right)^2 \quad (7.10)$$

$$C_s = 5.34 + \frac{4}{r^2} \quad (7.11)$$

$$r = \frac{a}{b} \quad (7.12)$$

Table 7.2: Dimensions of the wing box initial

Panel dimensions	
t_u	5.2 mm
t_l	1.1 mm
Spar dimensions	
t_{Wf}	0.2 mm
t_{Wr}	0.2 mm

7.3.4. Detailed wing box design

To get a more detailed result for the wing box structure which includes the spar with spar caps as well as stringers attached to the skin, a different model is set up. In this approach, the wing box is modeled as an upper and lower skin panel with different thicknesses, stringers with fixed dimensions and a set number attached to each skin panel, and a front and rear spar with their respective upper and lower spar caps. The front and rear spar webs have different thicknesses and the spar caps also differ in size based on their vertical position. An illustration of the idealized structure can be seen in Figure 7.4.

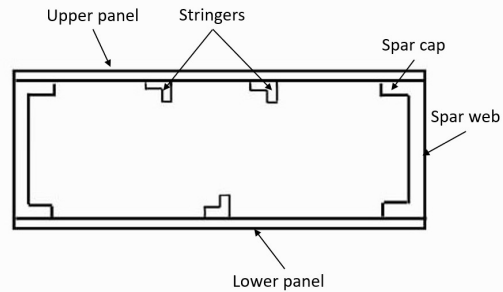


Figure 7.4: Idealized wingbox structure

In order to find the optimal combination of parameters such that the wing box can sustain all loads applied and the mass of the structure is minimized, a genetic algorithm is applied. This algorithm initializes a population with random values for each parameter chosen from a range set by the design team. Subsequently, each solution is assessed to check whether it can sustain all applied loads and does not fail, here all failure scenarios are accounted for such as yield and buckling of different parts. Solutions that fail in any of the criteria are considered invalid and given a fitness score of 0 as a result. The solutions that do not fail are given a fitness score based on their cross-sectional area, where a smaller area resulted in a higher score as this would minimize the mass of the structure. The best-performing solutions then pass on their genes (parameters) and the algorithm iterates this procedure for a set amount of generation in order to converge to a solution. The result of this algorithm is a dimensioned idealized wing box structure capable of sustaining all applied loads and having a minimal required mass. Therefore, the process of arriving to the final results will be further elaborated in this section, starting with explanations about the geometrical calculations of the cross-section and continuing with detailing all the applied stresses on the structure and critical conditions.

Geometrical characteristics

Prior to determining the applied stresses, geometrical characteristics of the cross-section such as centroid, moment of inertia and first moment of area have to be calculated. In the idealization employed here, the wing box is a rectangle such that the front and rear spar have the same height. This height is defined as the average of the actual height of the

front and rear spar as determined from the airfoil profile. This assumption of a rectangular wing box was made as the height difference between the front and rear spar was minimal ($\approx 1mm$) and it significantly simplifies calculations of for example the moment of inertia. Similarly, the length of the upper and lower panel is determined by the average of the upper and lower airfoil profile length.

First, the centroid of the structure is calculated. Especially the location of the centroid along the y-axis, where the origin is defined to be the bottom left corner of the wing box, is of interest as this has a significant impact on the moment of inertia and thus the bending stresses. The centroid is calculated by first determining the centroid of all individual parts, namely the upper and lower panels, the stringers, the spar webs and spar caps. Using the individual centroids and their respective area, the centroid of the entire wing box can be calculated using Equation 7.13[40], where A_i is the area of an individual segment and y_i is the distance of that individual element's centroid to the origin. The same procedure can of course be applied for the x coordinate as can be seen in Equation 7.14, thus resulting in the x and y coordinates of the wing box cross-section centroid.

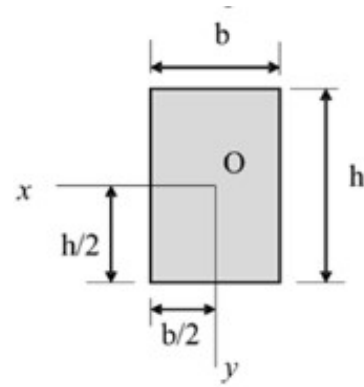


Figure 7.5: Moment of Inertia of a rectangle [40]

$$\bar{y} = \frac{\sum A_i y_i}{\sum A_i} \quad (7.13)$$

$$\bar{x} = \frac{\sum A_i x_i}{\sum A_i} \quad (7.14)$$

Next, the moment of inertia easily follows from the centroid. First, the moment of inertia of each individual element is computed again. As all elements consist of rectangular sections Equation 7.15 [40] can be used to find the moment of inertia of each element, where b and h are defined in Figure 7.5 [40].

$$I_x = \frac{bh^3}{12} \quad (7.15)$$

$$I_x = \bar{I}_{x'} + Ad_y^2 \quad (7.16)$$

The moment of inertia of the complete wing box around the x-axis is subsequently computed using the parallel axis theorem as defined in Equation 7.16 [40], where $\bar{I}_{x'}$ is the moment of inertia of the element, A is its area and d_y^2 the distance of its centroid to the centroid of the wing box as determined in Equation 7.13. In addition to the moment of inertia, the first moment of area is also determined using Equation 7.17 [41], where A is the area, and y the distance of the elements centroid to the centroid of the wing box.

$$Q_x = \int y dA \quad (7.17)$$

The final geometrical parameter that should be determined is the cross-sectional area. This will be used to assess the fitness score of a solution and is simply a sum of the area of all elements.

Applied stresses

Now that all geometrical parameters are addressed, the applied stress due to bending can be calculated using Equation 7.18 [36], where M is the maximum applied moment, \bar{y} is the distance of the relevant element to the centroid, and I_{xx} is the moment of inertia of the wing box. The maximum moment is taken here, as defined in subsection 7.3.2, to design the wing box for the most limiting load.

$$\sigma_{max} = \frac{M\bar{y}}{I_{xx}} \quad (7.18)$$

The applied stress due to bending is then computed for both the upper and lower panels, as well as for the spar caps and stringers. This bending stress is assumed to be carried by the skin, stringers, and spar caps, while the spar webs only carry shear stresses. Thus, the next step is assessing these applied shear stresses to the spar web. There are two main contributions to the shear stress in the spar webs, namely shear due to the torque applied to the wing box and shear stress due to the shear force. The maximum shear force applied at the root of the wing and the torque discussed in subsection 7.3.2 have been used for sizing the spar webs.

The shear flow that the torque generates is defined in Equation 7.19 [35], where A refers to the area enclosed by the wing box. Furthermore, the shear flow due to the shear force is determined using Equation 7.20 [35], which is an adaptation

of Equation 7.6, however now incorporating the fact that both spars have the same height. Here V is again the maximum internal shear force and h_{web} is the height of the spar web.

$$q_{torque} = \frac{T}{2A} \quad (7.19) \quad q_{force} = \frac{V}{2h_{web}} \quad (7.20)$$

These two shear flows are then added together as this is the worst scenario where both shear flows act in the same direction and thus the web should be sized for this case. The stress in the webs is then determined using Equation 7.21, where t_w is the thickness of the respective web for which stress is determined.

$$\tau = \frac{(q_{torque} + q_{force})}{t_w} \quad (7.21)$$

Critical stresses

Depending on the element of the wing box, its position and the loads it is subjected to, multiple critical situations are assessed for each component and the most limiting case is compared to the applied stress on the respective element. For the upper panel skin for example one limiting condition is the compressive yield stress of the material and another is the critical buckling stress of the panel. The most limiting of the two is used for the sizing and the same analogy is applied for all other elements with their respective limiting scenarios.

First, the critical cases for the spar webs are assessed. It is assumed the spar web only carries shear loads. Thus, there are two failure criteria, one is the shear yield stress of the material and the other is the shear buckling of the spar web. Whichever value is lower out of the shear yield stress and the critical buckling stress is used as a limit for the applied shear stress in the webs and is thus driving the design. For the shear yield stress, the value can be found to be 331 MPa for aluminum 7075-T6 [42]. A safety factor of 1.5 is applied to ensure the design does not reach this yield point. The critical stress at which shear buckling occurs can be determined using Equation 7.22 [39]. Here C_s is the buckling coefficient determined to be 5.35 according to [39] for the most critical case (longest web with the least supports). E is the materials elastic modulus of 71.7 GPa [42] for aluminum 7075-T6, ν refers to the Poisson's ratio of 0.33, t is the thickness of the spar web in question and b the height of the web.

$$\tau_{cr} = C_s \frac{\pi^2 E}{12(1-\nu)^2} \left(\frac{t}{b}\right)^2 \quad (7.22)$$

Next, the critical scenario for the spar caps is analyzed. The spar caps can fail in a multitude of ways. First, it could fail at its compressive yield stress of 530 MPa for aluminum 7075-T6 [42], where once again a safety factor of 1.5 is applied. Secondly, the spar as a whole could buckle as a column. The critical stress at which this occurs is determined using Equation 7.23 [36], where l_e and r stand for the effective length of the column and radius of gyration, respectively. The effective length is defined as KL , where K is a buckling coefficient set to 0.65 as a conservative estimate based on [36] and L is the actual length of the spar cap. The radius of gyration is defined by Equation 7.24 where I_x is the moment of inertia around the x-axis of the spar cap and A refers to the cross-sectional area of the spar cap.

$$\sigma_{cr} = \frac{\pi^2 E}{\left(\frac{l_e}{r}\right)^2} \quad (7.23) \quad r = \sqrt{\frac{I_x}{A}} \quad (7.24)$$

Additionally, the spar cap can also buckle as a thin plate. The critical stress at which this occurs is given by Equation 7.25 [43]. Here C is a buckling coefficient set at 0.425 as conservatively one edge is considered free and the others simply supported [36]. t is the plate thickness of the spar cap and b is the width of the spar cap. Of these critical stresses again the lowest one is considered as the limiting factor for the spar cap design.

$$\sigma_{cr} = C \frac{\pi^2 E}{12(1-\nu^2)} \left(\frac{t}{b}\right)^2 \quad (7.25)$$

Going forward, the panel and the stringers are considered. For this, the design can either be limited by the compressive yield stress for the upper panel or the buckling of the panel. The compressive yield stress is the same as before and given by [42]. The procedure presented in [43] is used for the buckling. Here first the crippling stress of the stringer is determined after which an effective panel width is computed to determine the buckling stress of the skin. The critical stress of the panel (skin and stringers) is then computed as the limiting stress. The crippling stress of the stringers is computed following Equation 7.26 [43], where σ_y is the compressive yield stress, t the thickness of the stringer, b the width of one plate making up the stringer, while α and n are coefficients set at 0.8 and 0.6, respectively [43]. The buckling coefficient C is again set at 0.425 as a conservative estimate based on [43] and [36].

$$\frac{\sigma_{cc}^{(i)}}{\sigma_y} = \alpha \left[\frac{C}{\sigma_y} \frac{\pi^2 E}{12(1-\nu^2)} \left(\frac{t}{b}\right)^2 \right]^{1-n} \quad (7.26)$$

This equation is applied to all elements making up the stringer and the crippling stress of the entire stringer is determined using Equation 7.27 [43], where A_i is the area of each element making up the stringer and $\sigma_{cc}^{(i)}$ the crippling stress of each element.

$$\sigma_{cc} = \frac{\sum \sigma_{cc}^{(i)} A_i}{\sum A_i} \quad (7.27)$$

With the crippling stress of the stringers known, the effective width of the sheet can be determined. This is the width of the sheet that is susceptible to buckling and corrects for the fact that parts of the skin are significantly stiffer due to the stringers being mounted there. This effective sheet width is calculated using Equation 7.28 [43]. Here C is the buckling coefficient and is given a value of 4 based on [36] and [43] and t is the thickness of the skin panel under consideration.

$$2w_e = t \sqrt{\frac{C\pi^2}{12(1-\nu^2)}} \sqrt{\frac{E}{(\sigma_{cc})_{\text{stiffener}}}} \quad (7.28)$$

With the effective skin width determined, the critical buckling stress of the upper skin panel can be determined using Equation 7.29 [43]. Here t is the thickness of the skin panel and b is the stringer pitch.

$$\sigma_{cr} = C \frac{\pi^2 E}{12(1-\nu^2)} \left(\frac{t}{b-2w_e} \right)^2 \quad (7.29)$$

The critical stress for the stiffened panel can now be determined using Equation 7.27. Now using the area of the stringers, their crippling stress and the area of the skin panel and its buckling stress determined in Equation 7.29. Again the lowest value of these critical stresses is the most limiting condition the design should satisfy.

Finally, the lower skin panel is sized for two loading cases. The lower part of the wing box is mainly subjected to tension loads during flight, but during taxi it also sustains lower in magnitude compression loads because the wing needs to support its own weight. Therefore, to be able to sustain this load one stringer will be used for the lower panel too, and the critical situation is the minimum stress between the tensile yield stress of the material and the compressive load. Thus, a similar procedure as for the upper panel has been used to determine the critical stress under compression loads, which has been compared to the material yield tensile stress of 434 MPa for aluminum 7075-T6 [42].

With all of the critical stresses and the applied stresses defined a multitude of possible combinations of parameters can be assessed to determine whether they satisfy the limiting conditions. The genetic algorithm was built to do just this. A large selection of possible combinations of parameters was assessed and checked for each condition. Only the possible solutions that satisfy all requirements were allowed to receive a fitness score based on their total cross-sectional area. The best performing were allowed to pass on their genes (parameters) and this was iterated on many times to find a converged solution.

Final results and discussion

With the procedure described in subsection 7.3.4 the wing box is sized. The final dimensions of the load-carrying wing box as determined following the procedure are given in Table 7.3. The exact definition of the dimensions can be seen in Figure 7.6, where all dimensions are specified in mm and the full drawing is shown in Figure A.11. The integration of the wing box inside of the wing is also shown in Figure 7.7 where the front spar starts at 10% of the chord and the rear spar is located at 60% of the chord. Here the upper skin panel was made curved to follow the contour of the wing. For future more detailed design, the same procedure can also be applied to the tapered section of the wing. Keeping in mind that the loads should be slightly smaller for that section and that the cross section decreases in size. However, this is outside of the current scope and is left as a point for further development.

After getting the final dimensions of the wing box, a visual inspection of the applied and critical stresses in each part of the wing box has ensured that all elements can actually sustain all loads and that no further optimization is possible. The applied and critical stresses are shown in Table 7.4 for all components. One key observation is the significant difference of 90.21 MPa between the applied and critical stresses on the lower panel during buckling. This led us to consider the possibility of not needing a stringer on the lower panel. To determine this, we checked the critical buckling stress on the lower panel, which turned out to be 0.49 MPa. This indicates that without a stringer, the lower panel cannot sustain the applied stress of 17.44 MPa. To support the applied load, the panel's thickness would need to be increased 5 times larger, significantly raising its mass. Consequently, we decided to keep the stringer. The same analysis was conducted for the upper panel to determine how much its thickness would need to increase to sustain the load if one stringer were removed. The results showed that the upper panel's thickness would need to increase by 1.5 times, leading to a total mass increase of about 20%.

After obtaining the final results, it was observed that the thicknesses of the lower and upper spar caps differed significantly from the thickness of the spar web. This variation would complicate the manufacturing process, as changing the thickness dimensions along the cross-section is challenging. Consequently, the dimensions were manually adjusted to achieve uniform thickness throughout the spar.

Matching the spar web thickness with the lower spar cap presented issues in other loading scenarios, such as the applied stress on the lower panel, necessitating a compromise. The web thicknesses were increased to 1 mm, and the same thickness was applied to the spar caps. Additionally, to withstand the tension load, the thickness of the lower panel and the width of the lower spar cap were increased. The width of the upper spar cap was reduced as much as possible while still meeting the loading requirements of the upper panel.

All modifications resulted in an increase in the wing's mass. However, this increase is necessary to reduce the complexity of the manufacturing process. The final dimensions of the wing box after the modifications are presented in Table 7.3.

Table 7.3: Dimensions of the wing box

Symbol	Initial dimensions	Updated dimensions
Panels		
t_u	0.8 mm	0.8 mm
t_l	0.3 mm	0.4 mm
Spars		
t_{Wf}	0.6 mm	1 mm
t_{Wr}	0.6 mm	1 mm
t_{SCu}	0.5 mm	1 mm
t_{SCL}	3.7 mm	1 mm
b_{SCu}	5.9 mm	5 mm
b_{SCL}	5 mm	8 mm
Stringers		
t_{St}	1 mm	1 mm
b_{St}	10 mm	10 mm
$n_{StringerUp}$	2	2
$n_{StringerLow}$	1	1

Table 7.4: Applied and critical stresses on the wing box elements

Wing box component	Failure mode	Applied Stress [MPa]	Critical stress [MPa]	Percentage
Lower panel	Buckling	17.44	107.65	16.2 %
Lower panel	Tension	289.04	289.33	99.8 %
Upper panel	Buckling	149.92	178.74	83.8 %
Upper spar caps	Buckling	141.95	289.33	49 %
Lower spar caps	Tension	286.05	289.33	98.8 %
Spar webs	Shear	53.94	84.89	63.5 %

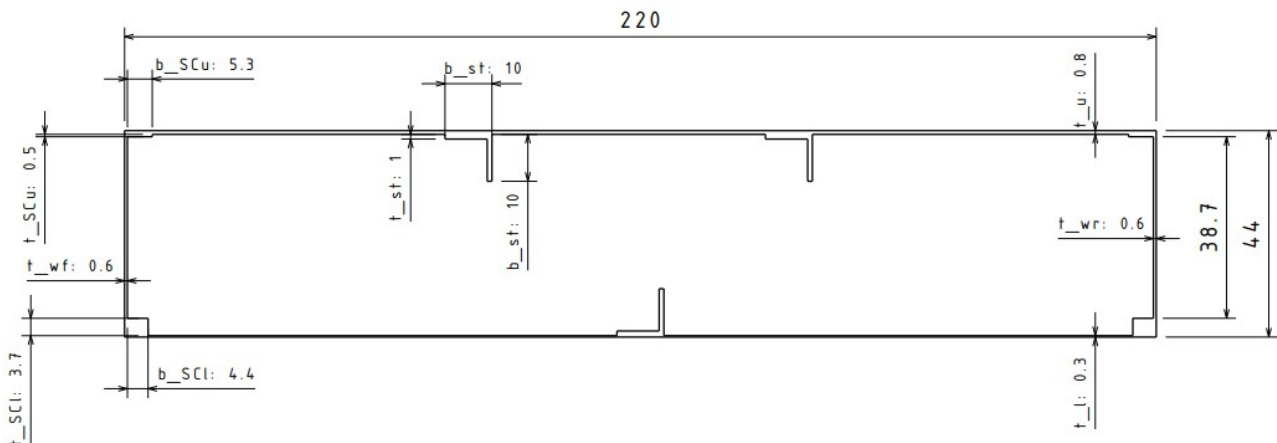


Figure 7.6: Wingbox Drawing

Wing box mass

With the dimension of the wing box determined in subsection 7.3.4 an improved estimate for the wing weight can be obtained. To achieve this the cross-sectional area of the wing box structure is calculated as is implemented in the model explained before. Using the cross-sectional area and the wing span, the volume taken up by the wing box is determined and, subsequently, the mass is computed by multiplying it to the density of the material of 2710 kg/m^3 for aluminum [42]. For this, it is assumed that the wing box has a constant cross-section throughout the wing. This is not the case in the full design as part of the wing is tapered as discussed in chapter 4. Thus, this estimate serves as a higher limit of the structural weight of the wing as it overestimates the size of the wing box and, as a result, the weight too. Performing the

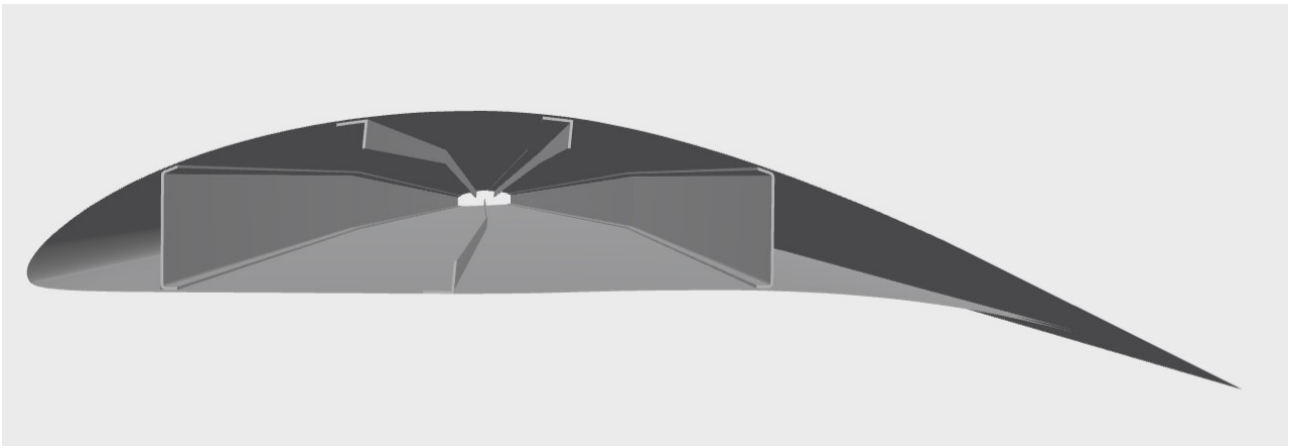


Figure 7.7: Wingbox integrated in the wing

calculation described here results in a wing box mass of 4.51 kg using the initial dimensions of the wing box. After the modifications the wing box mass has been increased to 4.97 kg. This result was verified by constructing the wing box with its parameters as defined in Table 7.3 in 3DEXPERIENCE and having it calculate the weight as well. This resulted in a mass of 4.967 kg thus verifying the model performs correctly. Given that this mass does not include the skin of the leading and trailing edges as well as any ribs added to maintain the shape of the wing it is not the total mass of the wing. For the total wing mass the estimate from section 3.1 still seems a reasonable estimate when these additional masses are accounted for.

Limitation of genetic algorithm

The detailed wing box sizing has been performed using a genetic algorithm to optimize the dimensions for minimal mass. However, several limitations of the optimization algorithm have been discovered during its implementation. Consequently, the obtained results need to be properly validated to ensure that the sizing of individual elements of the wing box is both practical for real-world application and logically consistent.

A key observation is that when trying to optimize a high number of parameters, the results tend to be highly variable. Running the algorithm multiple times yields substantially different results, as visualized in Figure 7.8, where the algorithm was run 20 times to optimize 8 parameters. It was noted that some parameters, such as the width of the spar caps, vary significantly, while others, like the thickness of the front and rear spars, remain mostly constant. This variation leads to different minimal masses each time the algorithm is run, which raises questions about the credibility of the results.

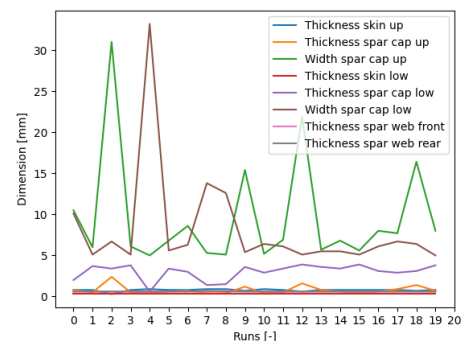


Figure 7.8: Variability of first iteration results

The variability in the results is expected due to the inherent randomness in key areas of the genetic algorithm's implementation, such as the initialization of potential solutions and the selection of parent solutions for reproduction. The algorithm incorporates a random factor alongside the fitness factor, leading to slightly different outcomes each time it is run. To reduce this randomness and increase the credibility of the results, fewer parameters should be optimized. It has been observed that optimizing fewer parameters results in more consistent outcomes over several runs. Therefore, the following approach was taken to determine the final dimensions of the wing box elements.

Initially, all 8 parameters were optimized over 20 runs of the algorithm as can be seen in Figure 7.8. The mean value and standard deviation of all parameters were computed over these 20 runs. Parameters with low standard deviations, indicating consistent results, were fixed to their mean values. These fixed parameters included the thicknesses of the front and rear spar webs and the upper and lower panels. The algorithm was then run again to optimize the remaining 4 parameters, with the previously fixed parameters held constant as can be seen in Figure 7.9a. The same procedure was applied, and the thickness of the upper spar cap was fixed based on its consistency. Finally, the algorithm was used to optimize the remaining 3 parameters, which resulted in mostly consistent results over several runs as can be seen in Figure 7.9b. By following this iterative approach, the variability in the results was reduced, leading to more reliable and credible dimensions for the wing box elements. This led to the final results of the wing box sizing summarized in Table 7.3.

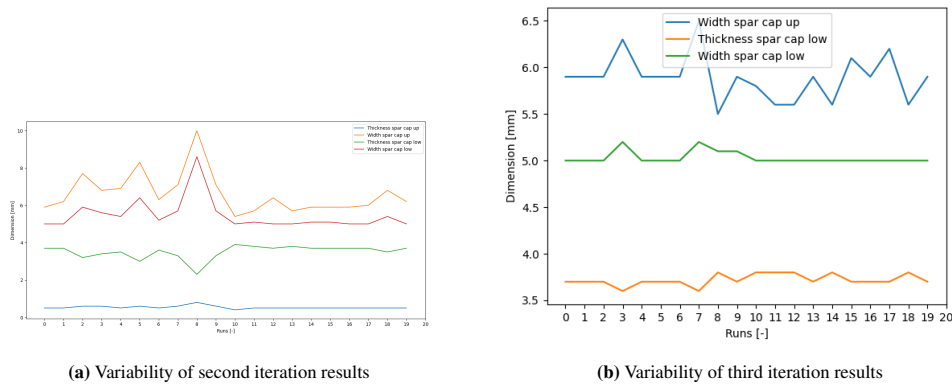


Figure 7.9: Variability of results

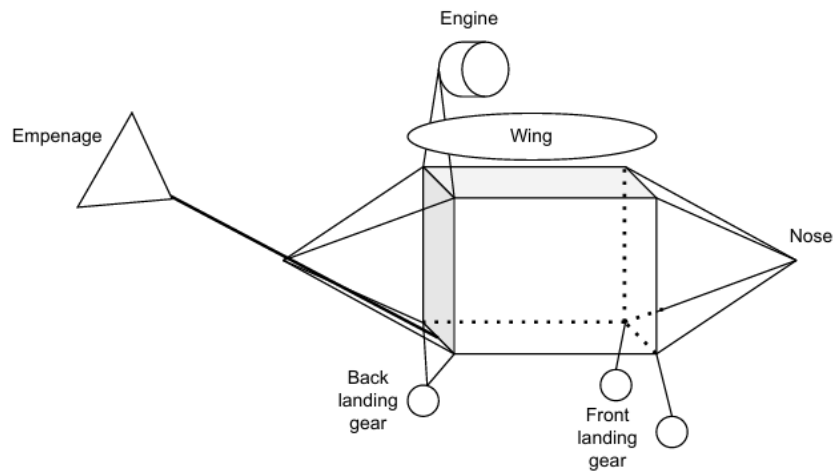


Figure 7.10: Truss structure of the fuselage

7.4. Fuselage design

After the wingbox is designed, the next step on the structural department is to set-up a structure for the fuselage. In this process it is important to firstly, set-up the structure and the loads applied to it, so that it can then be further analyzed and dimensionalize according to the applied loads. In Figure 7.10 an image of the chosen fuselage structure can be seen. The choice for a simple truss structure was made, because of the simple load case the aircraft is experiencing. Two cross-sectional, rectangular bulkheads are seen of which the upper corners are the attachment points for the wing. The upper corners of the back bulkhead also support the attachment of the engine to the fuselage. The landing gear is placed under the front bulkhead (two separate wheels) and the back bulkhead (one wheel with two attachment points in the corners because of load distribution).

Per load carrying member of the fuselage, they are subject to different load cases. The five load cases possible are tension, compression, shear, torsion and bending. All of these load cases have different failure modes that are to be considered. Before an analysis of different members of the fuselage is provided, all failure modes and their corresponding formulas are provided. Shear force was considered but as it was proficiently small, it was assumed to be negligible. The four different load stresses calculated in the equations are compression Equation 7.30, stress due to tension (Equation 7.33), bending stress (Equation 7.35) and shear due to torsion (Equation 7.38) respectively. For each of these stresses, the required information can be calculated using the other formulas. Because of low loads, and high aluminum strength, column buckling is likely to occur if the truss is only sized for strength. Equation 7.31 is thus used to prevent this limit from being overflowed.

$$\sigma_{compr} = \frac{F}{A} \quad (7.30) \quad P_{cr} = \frac{\pi^2 EI}{(KL)^2} \quad (7.31) \quad I_{xx} = \frac{tb^3}{12} \quad (7.32)$$

$$\sigma_{tensile} = \frac{F}{A} \quad (7.33) \quad \Delta L = \frac{FL}{AE} \quad (7.34)$$

$$\sigma_{bending} = \frac{My}{I_{xx}} \quad (7.35) \quad M = L \cdot F \quad (7.36) \quad M = \frac{L \cdot F}{4} \quad (7.37)$$

$$\tau_{max} = \frac{3T}{At} \quad (7.38) \quad T = F_{applied} \cdot t + \frac{q}{2A} \quad (7.39)$$

Because the fuselage structure is designed by using a simple truss structure, a general set of assumptions set up by [44] are taken as leading. These assumptions are required to analyze the fuselage as a truss structure. The assumption that the truss structure is only loaded at the joints specifically, but all assumptions in general shall be revisited in a later design iteration. General assumption of a truss structure [44]:

- Truss members are connected at their ends only.
- Truss are connected together by friction-less pins.
- The truss structure is loaded only at the joints.
- The weights of the members may be neglected.
- Members deformation under loads are negligible and of insignificant magnitude to cause appreciable changes in the geometry of the structure.

Besides the assumptions made about the fuselage being a truss structure, there are additional assumptions made during the sizing of the fuselage. They are shown below, including the validation of the assumptions.

Assumptions:

- The spars will have different failure modes when they have thin plate characteristics. The thickness cannot be lower than 10% of the width. When the thickness is lower than this percentage, the truss will behave like a thin plate and general truss assumptions are no longer valid. [45]
- ~~The vertical beams that carry the most load are located in the middle of the fuselage. The other eight spars perform well when they have the same dimensions.~~ This assumption was made but during the design process it was found that the weight of the avionics in the nose, was not negligible in the sizing process. As part of the iterative design process it was thus removed from the assumption list.
- The performance of a beam in any loading conditions, is not affected by other loading conditions the beam is experiencing. This assumption flows down from the general truss structure assumptions that state the deformation of members is negligible.
- The slight curve in the beams that are part of the bulkhead, does not affect the performance of the beam and it behaves like a straight beam. A consequence of this assumption is also a rectangular shape for the bulkheads.[46]
- The additional length if the beams that are curved, is compensated for by using the maximum height and width dimensions of the bulkhead at all times. The change in load carrying abilities due to the curve is hereby compensated.
- When using the dimensions of the fuselage in calculations, the thickness of the surrounding beams is assumed to be negligible.
- The lift force (and thus the drag) is distributed equally over the attachment points of the wing and the fuselage.

Now that the assumptions used and the load analysis are known, the different load cases will be analyzed. The first step in this process was to take the bulkheads, which are the load carrying members if the cross-section of the fuselage, to a free body diagram and analyze the loads applied to it. This cross-section with corresponding load case can be seen in Figure 7.11. In this figure, the back and the front bulkhead are shown in two different conditions. Firstly, the flight conditions during cruise are shown (left). During cruise the wing generates a lift force which is distributed over the four attachment points between the wing and the fuselage. Similarly, the drag force is distributed over the same four points and directed into the page since the fuselage is looked at from the front. When the aircraft is flying, the engine is propelling, causing a forward force on the structure which is transferred to the bulkheads by two beam. During cruise, this engine power will not be maximum, but to ensure all loads can be carried by the structure, this maximum condition of 90 N (which can be seen in Table 7.5) is taken as a basis for cruise.

The outcome of these load calculations let to a minimum thickness and width for the spars. A python function was written for that that minimized the area, while maintaining the truss characteristics thus being at least 10% thick compared to wide. Because the length of the truss was set, a minimum area due to thickness and width let to a minimum weight of the truss, that could still carry respective load. When all four failure modes are analysed for each of the eight bulkhead structures, it can be found that the torsional load due to the empennage attachment in the bottom truss of the back bulkhead is the one that results in both the highest required thickness and width for the truss. Because of manufacturing purposes, it was chosen to use this area combination for all trusses in the bulkhead structure. This results in a conservative design of the fuselage of which the summed weight of the bulkhead trusses can be seen in 'Table 7.6. The same was then done for the connecting trusses, which are 4 trusses for the back section, 4 for the middle section and 4 for the front section. For these

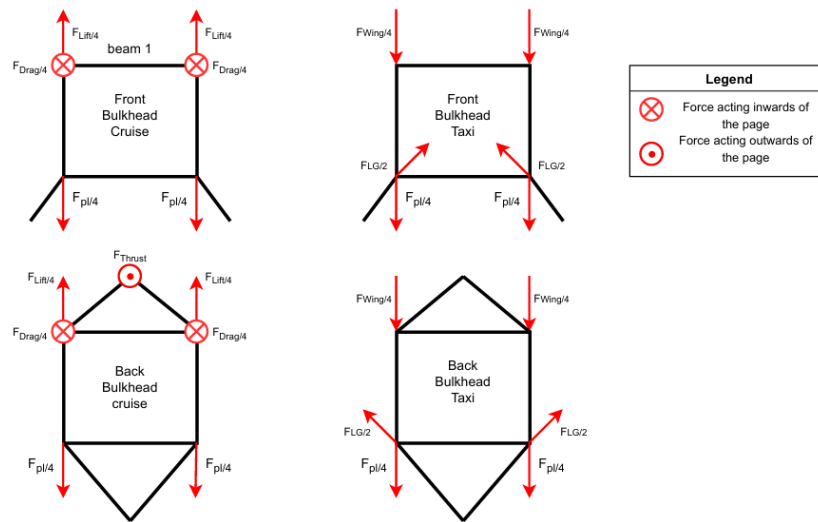


Figure 7.11: Loading conditions of the fuselage during cruise flight and taxi.

sections, the driving load was bending of the back trusses due to the empennage loads. Again, for manufacturing purposes, and also for stability, all twelve trusses will be of the same thickness. Altogether, this leads to resulting dimensions and weight for the connecting trusses can be seen in Table 7.6.

Input	Value
F_T	90 N
l1	0.4 m
l2	0.6 m
l3	0.4 m
clearance engine (c11)	0.05 m
engine diameter (d1)	0.68 m
LG front clearance (lg1)	0.4
LG front stick out (lg2)	0.09
LG back clearance (lg3)	
LG front θ	
LG back θ	
width _{max}	0.45 m
width _{min}	0.4 m
height _{max}	0.4 m
height _{min}	0.3 m

Table 7.5: Input values for fuselage calculations

7.5. Verification and Validation

Now that all calculations of the structural characteristics are set-up, the verification and validation of the design is conducted. For the structural characteristics, this consists of several steps. Firstly, unit tests on the functions written in the Python code are conducted. These unit tests are conducted partially by 3DEXPERIENCE, which is a model that is verified in the respective session as well. Then, the subsystem requirements introduced in Table 7.1 are verified in Table 7.7 where their verification method is explained and it is validated that those subsystem requirements are met, which concludes the verification and validation for the structural characteristics.

7.5.1. Unit tests

The unit tests that are performed can be split up in code verification and weight verification. For the code verification, manual calculations and extreme value tests are performed. For the weight verification, the structural parts are generated in 3DEXPERIENCE, so that their corresponding weight is verified. This is also part of the code verification.

The manual tests that are performed are done per function written in the code. An example of this was calculating the moment of inertia by hand, and then comparing it to the outcome of the function in Python by printing the returned value. This was done for all functions. The extreme value tests are conducted by putting extremely large- or small force values, small material strength and stiffness values, and big and small lengths into the functions and see what their effect is in the

Output	Dimension	Driving load
Bulkhead truss thickness	9.9 mm	Torsion due to empennage
Bulkhead truss width	28.5 mm	Torsion due to empennage load
Horizontal truss thickness	1.8 mm	Bending due to empennage
Horizontal truss width	17.9 mm	Bending due to empennage
Weight bulkhead truss	0.357 kg	-
Weight horizontal truss	0.052 kg	-
Total weight bulkheads (8)	2.857 kg	-
Total weight horizontal trusses (12)	0.622 kg	-

Table 7.6: Dimensions of the load supporting trusts within the fuselage structure

outcome of the structural sizing. For example, one extreme value test of the fuselage included a trust power of 1000 N instead of 90 N. This resulted in an unreasonably large thickness and width of the respective truss as was expected. These extreme value verifications result in the assurance that the formulas perform their task well, by putting in unrealistic conditions.

The weight verification is a unit test that compares the output of the entire structural subsystem (which is the structural weight), to the weight of the structure if it is modeled in 3DEXPERIENCE. 3DEXPERIENCE generates the structure as if it is real and measures its weight after which it is compared to the output weight of the Python code. By comparing the output weight to its weight in 3DEXPERIENCE, the subsystem as a whole and its total set of calculations are verified.

7.5.2. Subsystem verification

After all calculations are done, it is checked that the designed structure meets the requirements set-up in section 7.1. This can be done through one of the four methods, namely analysis, demonstration, inspection or testing, which are elaborated on in chapter 14. In Table 7.7, the compliance matrix of the structural requirements can be seen.

Table 7.7: Requirements for structural system and its subsystems

ID	Check	Reasoning	Requirement
Wing (WIN)			
SYS-STR-WIN-01	✓	Analysis: Simulation with all applied loads	The wing shall maintain structural rigidity.
SYS-STR-WIN-02	✓	Analysis: Simulation with the applied load	The wing shall withstand a bending load induced by the aerodynamics of at most 1470 N m at the root.
SYS-STR-WIN-03	✓	Analysis: Simulation with the applied load	The wing shall withstand a shear load induced by the aerodynamics of at most 1546 N at the root.
SYS-STR-WIN-04	✓	Analysis: Simulation with the applied load	The wing shall withstand a torque load induced by the aerodynamics of 230 N m.
SYS-STR-WIN-05	✓	Analysis: Simulation with all applied loads	The wing shall withstand all aerodynamically induced loads till 3.8 g with a safety factor of 1.5 during operation.
Fuselage (FUS)			
SYS-STR-FUS-01	✓	Analysis: Simulation with all applied loads	The fuselage of the UAV shall maintain structural rigidity.
SYS-STR-FUS-02	✓	Analysis: Simulation with applied load	The fuselage shall withstand an engine induced trust load of 90 N loads during cruise operation.
SYS-STR-FUS-03	✓	Analysis: Simulation with applied load	The fuselage shall withstand all lift loads till 3.8 g with a safety factor of 1.5 during operation up.
SYS-STR-FUS-04	✓	Analysis: Simulation with applied load	The fuselage shall withstand all wing induced drag loads during operation.
SYS-STR-FUS-05	✓	Analysis: Simulation with applied load	The fuselage shall withstand its own aerodynamic drag loads during operation.
SYS-STR-FUS-06	✓	Analysis: Simulation with applied load	The fuselage shall withstand 2.5 g loads induced by the landing gear during operation.
SYS-STR-FUS-07	✓	Analysis: Simulation with applied load	The fuselage shall withstand all weight loads induced by the engine during operation.
SYS-STR-FUS-08	✓	Analysis: Simulation with applied load	The fuselage shall withstand all weight loads induced by the avionics during operation.
SYS-STR-FUS-09	✓	Analysis: Simulation with applied load	The fuselage shall support the weight of the payload during operation.

Landing Gear

In the previous report, it was determined that a taildragger configuration is used for this UAV [4], mostly due to its lower drag and better terrain performance. Therefore, in this chapter, the landing gear is designed in further detail.

8.1. Subsystem Requirements

To this subsystem the following requirements apply:

Table 8.1: Requirements for landing gear

ID	Requirement
SYS-LAN-01	The landing gear shall provide a braking coefficient of 0.315.
SYS-LAN-02	The landing gear shall weigh no more than 2 kg.
SYS-LAN-03	The landing gear shall provide the braking coefficient on an unprepared runway.
SYS-LAN-04	The landing gear shall withstand all forces applied during take-off and landing.

8.2. Main gear wheel sizing

Designing landing gear for aircraft that do not operate from high-quality asphalt or concrete is difficult, due to an absence of design methods for landing gear that must operate on unprepared runways [7, p. 237]. Hence, in order to design or select wheels for the aircraft, special attention must be taken to account for the factors that cause landings to be rougher on unprepared runways than on tarmac. For instance, there is a certain crush load that must be considered, for this reason much stronger tires are required for this UAV [47, p. 128]. According to Currey, the worst case landing situation must be considered when sizing the tires of the aircraft [47, p.128]. Currey, uses an analogy to explain the different safety factors that must be applied to the maximum static load in order to size the tires: An aircraft landing on an aircraft carrier experiences a large impact load, so large that the tires experience their bottoming load (2.5 times the static load), so the tires deform up to the wheel rims [47, p.128]. Now imagine the aircraft touches down on the carrier at the very moment that its gear crosses an arresting wire. This is the crush load that must be accounted for and Currey simplifies it by a further multiplication of 3 times the static load [47, p.128]. This situation translates perfectly for the UAV being designed for an already rough landing situation, for example in the case of strong winds, where the UAV's gear touches down on the unprepared runway on a hard, jagged surface such as a rock.

According to Roskam, sizing for the wheels and tires should be done according to the static load present on the tire, simply put: when the aircraft stands still and is fully loaded, what is the weight on each tire [6]? This value is used to find the required strength of tires. Roskam mentions that the landing gear should be sized for 1.25 times the aircraft's maximum take-off weight, in order to account for future changes to the aircraft's weight [6]. So for this UAV this would be $55 \text{ kg} \cdot 1.25 = 68.75 \text{ kg}$. Typically a taildragger aircraft will want to touch-down simultaneously on all of its landing gear, this is done as this allows the aircraft to land at its $C_{L_{max}}$, allowing for the aircraft to fly at the slowest forward velocity possible during landing [48]. However, the worst possible landing situation will be assumed, hence the the full static load will be place on the UAV's main gear. Hence per main landing gear wheel, 34.375 kg of mass is carried statically. Converting this to a load factor, multiplying it by the acceleration of gravity, provides a weight of approximately 337 N. This value, multiplied by the safety factors for the bottoming load and the crush load, 2.5 and 3 respectively [47, p.128], provides a maximum loading requirement of 2528 N per wheel.

A tire that nicely matches these requirements is the Tost Mini 150 L wheel [49]. Using the lightweight variant of the wheel gives a wheel mass of 230 g, a tire mass of 135 g and a tube mass of 43 g [50] gives a total assembly mass of 408 g per side (not counting the brake or strut). This wheel has a maximum static load of 1.0 kN and a limit load of 2.8 kN, so it conservatively fulfils the requirements. Another option is Electron Retracts' 150 mm wheel, which is sized the same, and is designed for a maximum aircraft weight of 100 kg [51]. This wheel has also been designed for use on "the most demanding runways" and has a mass of 810 g per wheel [51]. In order to match the wheels with a brake system, this latter wheel will be chosen for testing the landing gear. These two options are given, as their performance can be evaluated during later testing.

The tail wheel is generally 25-33% of the main wheels' size for taildraggers [7, p. 233], so for now a diameter of 50 mm is used. Based on this diameter, several wheels are available, most of which were originally designed for model aircraft. These wheels are also extremely cheap, on the order of magnitude of less than 5 euros per wheel [52], so two of these wheels are used as tail landing wheels. Given the low price compared to the total cost of the aircraft, the ultimate loads can be determined using destructive testing at little cost. In addition, if necessary, these wheels can even be considered expendable and replaced every few flights.

8.3. Wheel brake sizing

For sizing the wheel brakes, it is necessary to know the moment provided by the brakes and the type of brakes. For the kind of brakes, several options are available, but the most important ones are hydraulic and electric brakes. The moment provided by the brakes is given by [53, p. 317]:

$$Q = F_{brake} \cdot R \quad (8.1)$$

Given the mass of 55 kg, the friction coefficient of 0.315 (including ABS), as derived in section 11.2 and the safety factor of 25%, the maximum expected brake force per wheel is

$$F = \frac{W \cdot \mu \cdot 1.25}{2} = \frac{9.81 \cdot 55 \cdot 0.35 \cdot 1.25}{2} = 106 \text{ N} \quad (8.2)$$

which gives a brake torque (with a main wheel diameter of 150 mm) of 7.97 N m.

In order to achieve this, the Electron Retracts brake system will be used. This is an electromagnetic brake system. In addition, the ABS system will be used in order to ensure that the brakes do not lock, this also been assumed in the flight performance section section 11.2, as this trades a small percentage of the theoretical maximum possible braking coefficient for an improved stopping performance and ensures that the autonomously controlled UAV, can safely steer and come to a stop during taxi and landing.

In the unlikely case that the Electron Retracts system does not meet requirements, a hydraulic system can be used. For example, Tost Flugzeuggerätebau produces disks for the wheels and hydraulic master actuators with a rated torque of 15 N m. However, this option is not preferred, as it adds another layer of complexity and still requires electric actuators to push the hydraulics.

8.4. Gear position

For considering longitudinal and lateral positioning of main and rear gear, various requirements have to be considered for a taildragger. Also, the assessment of the gear and tail interaction need to take place, to ensure the operations on ground. The location and size of the landing gear shall allow any combination of pitch and roll angle that might occur during normal operations [29].

8.4.1. Longitudinal clearance

Longitudinal clearance criterion is considered for the longitudinal position of the main landing gear with respect to the center of gravity b_m .

Determining the size and longitudinal location of the landing gear requires multiple steps. Conventionally, it starts with the longitudinal position of the landing gear. However, this UAV uses a tail-dragger configuration in order to deal with the rough, unprepared runways where the UAV is designed to operate. This brings different restrictions to design of the landing gear. For this reason, for this tail-dragging UAV, the position and length of the landing gear are found simultaneously using the design angle for the take-off rotation of the UAV and the tip-over angles of the aircraft.

In order to determine the angle for the take-off rotation (θ_r), it was determined to use 7.5° , as this is the stall angle as shown in chapter 10. As seen in Figure 8.1, θ_r determines that the contact point of the main gear with the ground must be sufficiently below the UAV in order for the aircraft not to strike its tail on the ground when rotating (pitching up) during take-off and separate off the ground. The tip-over angles are necessary for ensuring that the UAV is not rotated forward when landing, digging the nose into the ground, as force is applied in the longitudinal direction upon the main landing gear. The angles are found from the extrema of the c.g. (most forward and most aft locations). For the minima, an angle of 15° is used, while an angle of 25° is used for the maxima [54]. While for the control surfaces a range of center of gravity is allowed of between -0.05 and 0.75 times the mean aerodynamic chord, to reduce the size and mass of the landing gear this is reduced to between 0 and 0.35 times the MAC. The 0.35 times MAC is the MAC expected during cruise. The height of the centre of gravity was initially assumed to be at 0.25 m, which was used further during sizing. This is very close to the actual position of 0.27 m.

The intersection of the lines drawn according to two tip-over angles together yields a point where the main gear's wheel touches the ground, the so-called contact point. From this point, a line is drawn at a counter-clockwise angle equal to θ_r from the horizontal, to find the take-off rotation limit. Along this line, the contact point of the tail-wheel is placed. This positioning gives the view presented in Figure 8.2.

In general for ground operation, the gear responsible for steering should carry between 8% and 15% of the total aircraft weight [29]. This is however only the case for tricycle design aircraft, as for these aircraft the the nose gear is used for steering. In the case of some UAVs, differential braking will be used to steer the aircraft, this ensures that steering is possible even when higher percentages of the aircraft weight is placed on the auxiliary landing gear. This is the case for this UAV. As shown later, approximately 20% of the aircraft weight is carried by the tail landing gear. This has significant consequences. Firstly, doing so reduces the weight on the main gear, reducing the normal force on this gear,

which reduces the amount of brakeforce that can be applied during landing or an aborted take-off, slightly increasing the aircraft's distance to stop. Approximately by 30 m, which still allows the aircraft to operate at all design flight conditions. On the other hand, the increase in weight on the tail's gear has a very positive effect, as the tail can be shorter (hence lighter), and thus the choice was made to include this in the design. Considering the UAV is designed for very rough runways, the forces applied by the runway will be significantly higher than for smooth runways. This means that there is an increased chance for the UAV to tip over forwards, or for a ground loop to take place. The extra weight on the UAV's tail increases the moment required to tip the aircraft over its front wheels during a take-off or landing run, making the aircraft safer to operate during these operations.

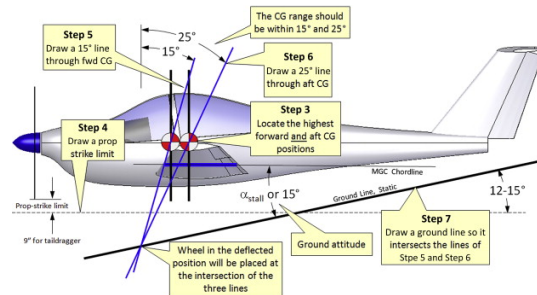


Figure 8.1: Longitudinal position of wheels [55, p. 570]

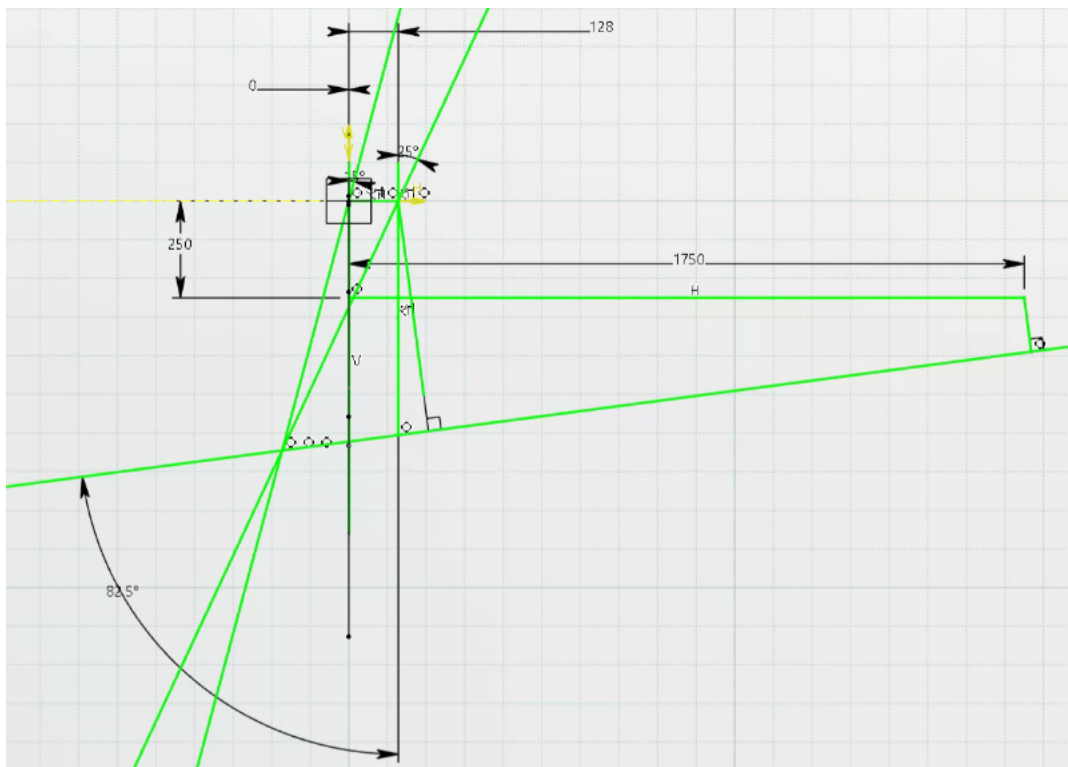


Figure 8.2: Lateral Position of the Wheels

8.4.2. Lateral clearance

The gear arrangement shall guarantee that the center of gravity is located sufficiently low inside the gears' triangle to ensure stability during sharp turns [29]. For taildraggers, a good rule of thumb is that the lateral position follows by taking a minimum angle of 25° , as shown in Figure 8.3 [55, p. 570]. This also designs for the situation where tail-draggers ground loop, so the UAV is designed with this safety factor in mind. This gives a total strut length of 36 cm, at an angle of 27.1° .

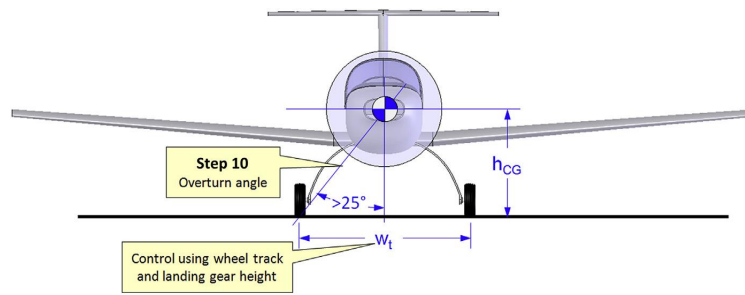


Figure 8.3: Turnover angle definition [55, p. 571]

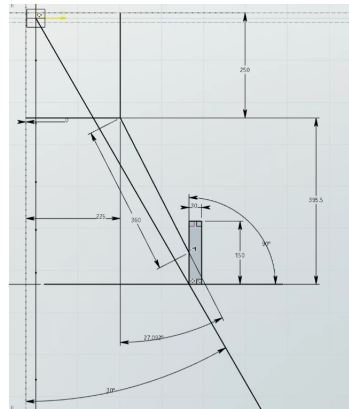


Figure 8.4: Actual landing gear position

8.5. Strut sizing

8.5.1. Main gear strut

For the strut, it is necessary to satisfy several requirements at the same time. The most relevant for this load case is the desired deflection at touchdown. At touchdown, the aircraft experiences the maximum load, of up to 2.5 times the maximum take-off weight, although it also needs to carry a crush load factor of three. Thus, the front gear needs to be sized for a touchdown force of:

$$F_{touchdown} = 9.81 \cdot W \cdot 2.5 \cdot 3 = 4.05kN \quad (8.3)$$

As in chapter 7, a safety factor of 50% is applied to the load. In addition, the gear is sized for an increase in weight of up to 25%, as with the wheels. Thus, each wheel needs to carry a force of 1.266 kN.

Before moving on to the solution, it is necessary to state which assumptions were made. For this strut, the following assumptions were used:

- The crush load of going over an obstacle is fully carried by the tires.
- The tires do not deflect at all, instead all deflection is carried by the strut.
- The deflection due to axial loads in the strut is negligible compared to tangential loads.
- The aircraft has a glide slope of 3°.
- Any hollow structure has to have a thickness of at least 1 mm for manufacturing reasons.

Now that the assumptions are stated, it is time to look at the actual load cases. The first of these is the deflection load case. For a good absorption of the energy, the deflection should be neither too large, nor too small. The stroke length is thus given by [7, p. 243]

$$S = \frac{V_{vert}^2}{2 \cdot g \cdot \eta_{gear} \cdot N_{gear}} \quad (8.4)$$

with η_{gear} a parameter describing the efficiency of absorbing kinetic energy (0.5 for a leaf spring) and N_{gear} the load factor. The gear is sized for a load factor of 2.5, as the deflection is not dependent on the actual load [7, p. 243]. The actual stroke is given by [7]

$$S = F_x \cdot (\sin(\theta))^2 \cdot \frac{l^3}{3 \cdot E \cdot I} \quad (8.5)$$

with θ the angle that the strut makes with the ground, which was determined to be 27.1°. The length l is equal to 360 mm. Using the same aluminium as before gives an E of 71.7 GPa. Thus, the area moment of inertia I needs to be optimized to

give as close to the desired stroke as possible. However, a more pressing issue is the point of bending. The stress induced by bending due to a load at an angle is given by [36, p. 457]

$$\sigma = \frac{M \cdot y}{I}. \quad (8.6)$$

For ease of manufacturing, the same aluminium is used as the one used for the primary structure. For its good torsional resistance and ample supply, a hollow circular rod is used. Now, it is possible to calculate the thickness, assuming a solid rod. Using aluminium gives a yield stress of 530 MPa [42]. This gives a strut diameter of 32 mm, which gives a strut mass of 782 g per strut and a deflection at maximum load of 8.3 mm. This is clearly not enough to transfer the full impact at landing, so it is necessary to select springs and dampers at a later stage to make the landing softer.

8.5.2. Tail gear strut

In order to improve the UAV's handling on the ground, castering will be used on the tail gear. This has multiple influences upon the aircraft's handling. Amongst those are that it improves stability of the aircraft on the ground, and is more effective on uneven surfaces [54, p.553]. Most importantly however, is that by using a certain amount of castering, and including a mechanical trail, will ensure that the tail gear will not shimmy, hereby no shimmy damping needs to be included, in the form of a damper or second tire, the latter of which would produce a significant extra amount of drag, both on the ground and aerodynamic drag [54, p.553].

The method used to establish the sizing of the landing gear is as follows. Firstly, to ensure that no tail striking will occur during operations, and because as mentioned in subsection 8.4.1, the rear landing gear carries approximately 20% of the load (derived from the angular restrictions as explained in the same subsection), the rear landing gear needs to be placed as far aft along the fuselage as possible. This is hence done and the contact point of the tail gear's wheel with the ground must be exactly 140 mm below the rearmost part of the aircraft fuselage.

Secondly, the geometry of the landing gear must be established. The following is considered: the caster and the mechanical trail. In order for both static and dynamic stability, the caster of the main strut must be between four and six degrees [54, p.553]. A caster of 6° is chosen so that the tail wheel trails behind the fuselage as much as possible, reducing the possibility for tail strikes, especially since the elevators are located near the bottom of the tail boom. In order to ensure that shimmy is accounted for in the design without using multiple wheels or shimmy dampers, the mechanical trail must be between 1 to 1.2 radii of the tail gear's wheel [54, p.553]. Establishing the angle between the wheel and main strut was done by hand, and an angle of 50.3° was chosen for the wheel strut, allowing bending of this strut, which provides an elastic deformation, absorbing landing impact force, reducing the load experienced by the fuselage during high impact landings. This then defines the shape of the fuselage.

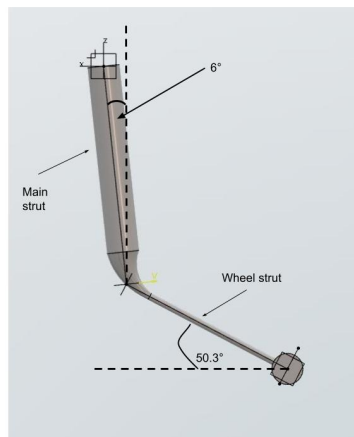


Figure 8.5: Castering and mechanical trail of tail gear - Not to scale

The established geometry is analysed for its suspected failure methods. For the tail gear's wheel strut, Raymer's method for a leaf spring gear is used as this method fits the geometry and purpose of this part of the landing gear best [7]. For this, Equation 8.5 is used. A deflection of 70 mm is used, in order to deflect equally with the main landing gear. This provides a cylindrical beam thickness of 2.34 mm.

The other section of the tail gear's strut is sized differently. Here, a buckling method is used. It is important to mention that the leaf spring section provides an internal moment to the other section. This means that simple euler buckling cannot be used to size this section, as this assumes a load is placed directly onto the beam with no offset to its centroid. A combined loading method of analysing buckling is used in order to accurately size the strut; namely, the secant formula [56]:

$$v_{max} = e \cdot \left(\sec\left(\sqrt{\frac{P_L \cdot l}{E \cdot I \cdot 2}}\right) - 1 \right) \quad (8.7)$$

Allowing a deflection of the main strut of 5 mm, sizes for a cylindrical beam with radius 5.144 mm.

8.5.3. Total mass budget

From this, the total mass budget for the landing gear is given as

Table 8.2: Overview of Chosen Landing Gear Components

Component	Chosen product	Mass	Cost
Main wheels with brakes	Electron retracts Set Wheels & Brakes Ø150 mm (Pair)	1620 g	€749
Braking controller	E_Brakes	24 g	€54
Main gear strut	Own design	1562 g	€-
Tail gear	Own design	18 g	€-
Total		3224 g	~€803

As the total mass is significantly more than originally estimated, further iteration is necessary. For example, perhaps a rod structure can be made lighter than the current beam structure. In addition, the mass budget does not yet include the springs or dampers.

8.6. Verification and Validation

8.6.1. Unit tests

Unit testing the method for reaching the subsystem requirements is a necessary step in order to ensure that the requirements have been met. The first three requirements, SYS-LAN-01 to SYS-LAN-03 are all quickly verified. SYS-LAN-01 requirement is verified using simulations of stopping as elaborated upon in section 11.2. SYS-LAN-02 is a summation of the landing gear masses, this is done using the strut masses as provided in 3DEXPERIENCE and with masses of landing gear wheels as provided by manufacturers, Electron Retracts and Tost. SYS-LAN-03 is verified using data from sources, as described in section 11.2. SYS-LAN-04 on the other hand is necessary to perform manual unit tests for. This is done by manually checking the functions performed in the code that calculate the required thickness of the main gear struts. For the tail gear strut and for all the tires and wheels, manual calculations are done in order to verify them.

8.6.2. Subsystem verification

After all calculations are done, it is checked that the designed landing gear meets the requirements set-up in section 8.1. This is done through one of the four methods (analysis, demonstration, inspection or testing, as explained in chapter 14. In Table 8.3, the compliance matrix of the structural requirements can be seen.

Table 8.3: Requirements for landing gear system and its subsystems

ID	Check	Reasoning	Requirement
Fuselage (FUS)			
SYS-LAN-01	✓	Analysis: Simulation with all applied loads	The landing gear shall provide a braking coefficient of 0.315.
SYS-LAN-02	✓	Analysis: Catia summation of component weights.	The landing gear shall weigh no more than 2 kg.
SYS-LAN-03	✓	Analysis: Simulation with applied loads	The landing gear shall provide the braking coefficient on an unprepared runway.
SYS-LAN-04	✓	Analysis: Simulation with applied loads	The landing gear shall withstand all forces applied during take-off and landing.

Avionics

Avionics (aviation electronics) is a broad term describing the various electronic components of an aircraft. In the current design phase, the avionics system is defined to contain the autopilot, navigation, object detection, auxiliary, and communication subsystems, in addition to the ground control station. To reduce development costs, off-the-shelf components are used whenever possible. Requirements for the avionics system are presented in section 9.1. Next, the autopilot is designed in section 9.2 and the navigation subsystem in section 9.3. Then, section 9.4 designs the obstacle avoidance system and section 9.5 provides the auxiliary electronics. Communications is then planned in section 9.6 and the ground control station is given in section 9.7. Following the selection of components, section 9.8 designs the physical layout and interfaces between component. Following this design, the software is handled in section 9.9. Finally, section 9.10 verifies the fulfilment of the system requirements.

9.1. System & Subsystem Requirements

Before an avionics and navigation package can be designed, it is first important to define the requirements that the system should follow. The requirements for the avionics and navigation packages are given in Table 9.1 with rationale in Table 9.2. Avionics subsystems are separated into the autopilot (AUT), navigation (NAV), obstacle-detection (OBS), auxiliary electronics (AUX), and communications (COM). Requirements are based primarily on flow-down from mission and functional requirements which specify the desired working of the avionics system.

Table 9.1: Requirements for avionics system and its subsystems

ID	Requirement
SYS-AVN-01	Avionics system shall draw no more than 200 W of power.
SYS-AVN-02	Avionics system shall weigh no more than 2 kg.
SYS-AVN-03	Avionics system shall cost no more than €20 000.
SYS-AVN-04	Total volume of avionics, excluding communications, shall be no larger than $0.4 \times 0.3 \times 0.4$ m.
SYS-AVN-05	Active sensors shall be eye & human safe.
SYS-AVN-06	Avionics shall be operable in 4 mm h^{-1} rain.
SYS-AVN-07	Avionics shall implement redundancy on critical components.
SYS-AVN-08	Avionics shall use open-source software.
SYS-AVN-AUT-01	Autopilot shall have self-takeoff & landing capabilities.
SYS-AVN-AUT-02	Autopilot shall detect runway markers.
SYS-AVN-AUT-03	Autopilot shall support backup landing locations.
SYS-AVN-AUT-04	Autopilot shall support in-flight way-point updates.
SYS-AVN-AUT-05	Autopilot shall support manual operator override.
SYS-AVN-AUT-06	Autopilot shall support at least 6 actuators.
SYS-AVN-AUT-07	Autopilot shall avoid detected obstacles.
SYS-AVN-NAV-01	Navigation subsystem shall determine velocity with accuracy of at least 0.1 m s^{-1} .
SYS-AVN-NAV-02	Navigation subsystem shall determine attitude with accuracy of at least 0.1° .
SYS-AVN-NAV-03	Navigation subsystem shall determine attitude rates with accuracy of at least 0.1° s^{-1} .
SYS-AVN-NAV-04	Navigation subsystem shall determine density altitude with an accuracy of 10 m.
SYS-AVN-NAV-05	Navigation subsystem shall determine ground altitude up to 160 m with an accuracy of 0.05 m.
SYS-AVN-NAV-06	Navigation subsystem shall determine position with accuracy of at least 1 m.
SYS-AVN-NAV-07	Navigation subsystem shall integrate GPS.
SYS-AVN-OBS-01	Obstacles shall be detected at ranges of at least 200 m.
SYS-AVN-OBS-02	Obstacles shall be detected in vertical sector $+20^\circ/-40^\circ$ and horizontally $\pm 35^\circ$.
SYS-AVN-OBS-03	Obstacles larger than 0.25 m^2 shall be detected at a range of 100 m.
SYS-AVN-AUX-01	Avionics shall include a companion computer.
SYS-AVN-AUX-02	There shall be a camera available to the operator.
SYS-AVN-COM-01	An Automatic Dependent SurveillanceBroadcast (ADS-B) transponder shall be integrated.
SYS-AVN-COM-02	Communication range shall be at least 30 km line-of-sight.
SYS-AVN-COM-03	Communication shall occur on worldwide license-free bands.

Table 9.2: Rationale for avionics requirements

ID	Rationale
SYS-AVN-01	Maximum electric power available to the system was estimated based on knowledge of similar systems and engineering judgement.
SYS-AVN-02	Maximum mass was estimated based on knowledge of similar systems and engineering judgement.
SYS-AVN-03	Maximum cost was estimated based on knowledge of similar systems and engineering judgement.
SYS-AVN-04	Avionics bay is limited in size by the size of the fuselage forwards of the payload.
SYS-AVN-05	The use of LiDAR in the navigation subsystem poses a possible risk of eye damage to operators of the UAV and the general public, which has to be addressed.
SYS-AVN-06	Navigation back to a safe landing site should be possible in limited visibility conditions such as rain. Flow-down from STK-0.3.9-MIS-ENV-7.
SYS-AVN-07	Redundancy is required to ensure that the UAV can return to a safe landing site in the event of failure of a critical component. Flow-down from STK-0.4.5-MIS-CTR-7.
SYS-AVN-08	Open source software allows the expansion of software features such that necessary adjustments can be integrated to full achieve the mission. Open-source also drives down costs of software [57].
SYS-AVN-AUT-01	Autonomous take-off and landing capabilities enable carrying out the entire mission autonomously under nominal conditions, reducing operator workload and thus operational costs. Flow-down from FUN-LND-4.4.1.
SYS-AVN-AUT-02	Runway markers are used to aid the autopilot align with the runway during landing. Flow-down from FUN-LND-4.4.1.b.
SYS-AVN-AUT-03	Alternative safe landing sites should be located and added to the autopilot database to be used in the case of emergency landing.
SYS-AVN-AUT-04	The autopilot carries out a predetermined mission autonomously under nominal conditions. If needed, the flight path can be changed during the mission by updating the waypoints. Flow-down from STK-0.3.5-MIS-CTR-2.
SYS-AVN-AUT-05	The option for manual piloting is required in case of any issues with the autopilot.
SYS-AVN-AUT-06	Actuators are required to control the control surfaces of the UAV; the avionics should have sufficient output ports and processing power to control 6 actuators.
SYS-AVN-AUT-07	Avoiding detected obstacles is integral for safety of the UAV and the general public. Flow-down from STK-0.4.1-MIS-CTR-3 and FUN-NAV-4.N.4.
SYS-AVN-NAV-01	Detecting the velocity with sufficient accuracy is integral for accurate navigation. Flow-down from FUN-NAV-4.N.3.a.
SYS-AVN-NAV-02	Detecting the attitude with sufficient accuracy is integral for accurate navigation. Flow-down from FUN-NAV-4.N.3.c.
SYS-AVN-NAV-03	Detecting the attitude rate with sufficient accuracy is integral for accurate navigation. Flow-down from FUN-NAV-4.N.3.c.
SYS-AVN-NAV-04	Flow-down from FUN-NAV-4.N.3.b.i.
SYS-AVN-NAV-05	Detecting the ground altitude is important for operations at a low altitude. At ground altitudes lower than 160 m, the ground altitude should be measured accurately in addition to the pressure altitude. Flow-down from FUN-NAV-4.N.3.b.ii.
SYS-AVN-NAV-06	Accurate positioning of the UAV is integral for accurate navigation. Flow-down from FUN-NAV-4.N.1., FUN-COM-4.N.7.b
SYS-AVN-NAV-07	It is decided that GPS is required for accurate positioning.
SYS-AVN-OBS-01	Obstacles shall be detected at sufficient range to execute an evasive maneuver. Flow-down from FUN-NAV-4.N.2.
SYS-AVN-OBS-02	A wide field of view is required to enable avoidance of moving objects, such as birds or other aircraft.
SYS-AVN-OBS-03	Detection of obstacles depends on both distance and size. A minimum size that should be detected at the distance of 200 m has been set. Flow-down from FUN-NAV-4.N.2.i.
SYS-AVN-AUX-01	Companion computer is necessary to process results from payload and to handle cameras and other advanced sensors.
SYS-AVN-AUX-02	A forward-facing camera can be used for visual navigation by the operator, especially in case of failure of another navigation sensor(s). The camera may also be integrated as an additional sensor for the autopilot.
SYS-AVN-COM-01	An ADS-B transponder is required by many aviation authorities. It is integral in avoiding other aircraft in the airspace. Flow-down from req STK-0.4.2-MIS-CTR-4 and STK-6.5-MIS-COM-4.
SYS-AVN-COM-02	Flow-down from FUN-COM-4.3.6, STK-0.1.1-MIS-COM-1, STK-1.2-MIS-RNG-1.
SYS-AVN-COM-03	Communications system needs to be usable anywhere in the world without having to go through communication authorities wherever it is flown.

9.2. Autopilot

The first subsystem in the avionics system is the autopilot. This subsystem is responsible for controlling the UAV and carrying out the mission. Six major options were identified for the autopilot by Unmanned Systems Technology [58]. While other options exist, it is infeasible to investigate every autopilot on the internet, and thus the ones recommended by Unmanned Systems Technology are deemed as sufficient. A short summary of the primary findings for each of the autopilots available is given below:

- **UAVOS AP 10.2:** The first autopilot investigated is the UAVOS AP 10.2 [59]. According to UAVOS [59], the AP 10.2 is an autopilot for systems weighing between 15 and 100 kg. This system shows support for a wide variety of interfaces and includes the ground control unit as part of the system [59]. However, the documentation available on the website is very lacking and it is unknown if it supports open source software. Thus, this unit is not considered for the autopilot system.
- **uAvionix George G3:** The George G3 autopilot by uAvionix is an autopilot designed for group 3 UAVs (UAV with MTOW between 25-600 kg) [60]. It is built on the open-source CubePilot Cube Orange architecture and thus supports open-source autopilot software in the form of Ardupilot or PX4 [60]. It is also stated to be certifiable and tested to aviation standards with support for a wide set of first and third-party modules for access to controlled airspace [60]. Lastly, the documentation is extensive including a complete installation manual for incorporating the George G3 into a design [60].
- **CubePilot Cube Orange+:** The CubePilot Cube Orange+ is the latest iteration of the CubePilot Cube architecture [61]. Unlike the Cube Orange integrated in the George G3 [60], the Cube Orange+ is updated with a more powerful dual-core processor [61]. Additionally, a secondary fail-safe co-processor is placed on the board for redundancy [61]. It also features redundancy in the integrated inertial measurement units and power delivery to ensure the safety of the system [61]. With support for custom carrier boards and a wide set of interfaces, the Cube Orange+ is easily extensible and allows for excellent custom solutions [61].
- **Embention Veronte Autopilot 1x:** Embention's Veronte Autopilot 1x is an advanced autopilot with a large amount of integrated features [62]. With internal Inertial Measurement Units (IMUs), magnetometers, barometers, a pitot tube, and a Global Navigation Satellite System - Real Time Kinematics (GNSS-RTK) system, the 1x integrates many of the most critical features without the necessity for additional hardware [62]. However, this autopilot incorporates a proprietary software suite that is not open source and thus it will not be utilized for the UAV.
- **MicroPilot MP2128:** An extremely lightweight autopilot at only 28 g, the MicroPilot MP2128^{g2} is integrated with many features [63]. With the inclusion of Global Positioning System (GPS), IMUs, barometers, and a pitot tube, the MP2128 has a lot of strength out of the box [63]. However, the processing power of the system is quite limited and this processor does not fully support Control Area Network (CAN) [63]. Further, the use of a proprietary software suite means that this autopilot will not be utilized.
- **Auterion Skynode X:** The final autopilot considered is the Auterion Skynode X [64]. While this autopilot is quite powerful, documentation is not readily available. It is more than likely that assistance from Auterion is required to incorporate the autopilot into the design and thus this is excluded as an option.

As identified in the summary above, only the George G3 and Cube Orange+ are identified as viable autopilots due to requirement SYS-AVN-08. As the George G3 is built on the same architecture as the Cube Orange+ but with a more restricted hardware, it is deemed best to use the more recent Cube Orange+. Thus, a Cube Orange+ is used as the primary autopilot for the UAV, with properties shown in Table 9.3.

Table 9.3: Cube Orange+ Specifications [61]

Main Processor	STM32H757
Co-processor	STM32F100
Redundancy	Triple redundant power Triple redundant IMU
Supported firmware	ArduPilot, PX4, and Hionos DO-178C
Mass	73 g
Size	38.4x38.4x22 mm
Temperature range	-10-55 °C
Interfaces	CAN, I2C, UART, SPI, PWM, USB
Cost	€400 per unit

Based on the selected autopilot, three options are available for the autopilot software as shown in Table 9.3. Of these, only ArduPilot and PX4 are open-source and thus only these are considered. As they are fundamentally very similar, the option to choose one over the other generally comes down to a combination of personal preference and licensing.

PX4 is licensed under Berkeley Software Distribution (BSD), which allows the free use and modification of the software without the need to share the code. On the other hand, ArduPilot is licensed under the GNU General Public License, and as thus any improvements in the code-base must also be contributed to the general public. As this project aims to be sustainable and humanitarian, the code should be freely available anyhow, and improvements in the code-base should be integrated into the main branch. Thus, the license of either software does not make a significant contribution to this project.

In the end, PX4 is known to be slightly more powerful and support more accurate control of UAVs. Thus, while PX4 and ArduPilot are extremely similar, an autopilot architecture based on PX4 is to be used.

9.3. Navigation

The navigation subsystem combines data from various sensors to obtain knowledge of the position, attitude, and velocity of the UAV at the required accuracy. The various sensors used for navigation can be classified as electronic and inertial navigation systems [65, Ch. 8]. Electronic navigation systems use a signal such as radio or communication with a satellite to determine the position relative to external references. Inertial navigation systems use measurements of the motion of the UAV to extrapolate navigational data from an earlier known state. Inertial sensors can never be used in isolation, but instead there always needs to be a way to calibrate the position and heading measurements to correct the drift of the inertial sensors [65, Ch. 8]. Therefore, for redundancy, an autonomous UAV should combine the output of a few different sensors. Sensors commonly used for navigation are presented in Table 9.4, with their benefits and disadvantages explained. It is decided to integrate all sensors shown to the navigation subsystem. The autopilot unit chosen already contains three accelerometers and gyroscopes, a magnetometer and two barometers, so these sensors do not need to be selected separately. Additionally, the camera will be integrated mainly for the purpose of giving the operator a visual reference in the case of manual override. The camera can be used to aid autonomous navigation if deemed useful and not too complex to implement, however it is not strictly necessary for navigation and therefore will not be considered in this section.

Table 9.4: Different navigation systems compared [65, Ch. 8]

Sensor	Use	Disadvantages
GNSS	Provides position, velocity and altitude knowledge, errors do not accumulate.	Requires unobstructed contact with multiple satellites.
Accelerometer	Measures acceleration of UAV, which can be integrated to get velocity	Errors accumulate, quickly resulting in large inaccuracies.
Gyroscope	Measures angular accelerations, used to determine attitude.	Errors accumulate, quickly resulting in large inaccuracies.
Pressure altimeter	Measures pressure altitude of UAV.	Pressure altitude does not correspond to actual altitude, as the pressure depends on atmospheric conditions in addition to altitude.
Radar altimeter	Measures ground altitude of UAV.	Only usable when relatively near ground.
Pitot tube	Measures airspeed.	Airspeed does not correspond to ground speed, as it depends on wind and atmospheric density.
Optical (camera)	Comparing images to a map can be used to determine position.	Requires high processing power, complex to implement autonomously.

For the global satellite navigation systems (GNSS) receiver, a module with position accuracy of 1 m or less and velocity accuracy of 0.1 m or less is sought to meet the requirements SYS-AVN-NAV-05 and SYS-AVN-NAV-01. An average off-the-shelf GNSS module can meet these requirements, so it is decided that GNSS enhancements such as RTK are not required. While RTK can increase the accuracy of GNSS positioning by two orders of magnitude [66], it requires a ground station with a very accurately known position, which increases operational cost and complexity. Additionally, the range of a RTK groundstation is limited to a few kilometers [67], which is less than the required range of the UAV. A GNSS receiver that meets the requirements is the Vectornav VN-200 Rugged, a GNSS-aided inertial navigation system that combines GNSS with an inertial measurement unit to provide accurate position, velocity and heading data [68]. The module is lightweight at only 16 g and a power draw of 0.5 W, however it does not include an antenna which has to be integrated separately. Vectornav recommends some suitable patch and helical antennas to go with the VN-200; for a UAV, helical antennas are more suitable [69], and thus the Tallysman HC771 single-band helical antenna is chosen [70]. It is important to remember that the stated accuracy of a GNSS module assumes ideal conditions, and can vary depending on the conditions and environment the UAV is flying in. Additionally, there can be moments where GNSS position data is not available due to loss of connection. Therefore, the GNSS position and velocity data is augmented with measurements from an IMU.

A radar altimeter is useful for low-altitude operations, as it is the only altitude sensor that measures the ground altitude as opposed to the absolute altitude. While GNSS and barometers can provide altitude data, their measurements don't give information about distance to the ground, unless precise position of the UAV and an accurate contour map of the area are known. The radar altimeter should be able to measure the ground altitude with an accuracy of 0.05 m up to the altitude of 160 m, as specified in SYS-AVN-NAV-05. The Nanoradar NRA24 is found to meet the requirements with its measurement range of 200 m and accuracy of 0.02 m [71], [72]. It also has relatively low mass and low power consumption at 95 g and

1.8 W respectively [71]. The radar altimeter should be placed on the bottom surface of the UAV to provide view of the ground.

To measure airspeed, a pitot-static tube is required. The most important function of a pitot-static tube is to ensure that the speed of the UAV doesn't decrease below the stall speed [73]. Small and lightweight pitot-static tubes commonly used on small UAV are susceptible to errors due to rain [74]. As the UAV is required to operate in light rain, a pitot-static system with heating and a drainage system to mitigate the effect of water entering the probe is used. The LUN 1154 produced by MIKROTECHNA PRAHA a.s. seems promising, as it is lightweight at a weight of 30 g, while still including a drainage system and a 6 W heater [75]. For locating the sensors, the placing of the pitot-static tube is most critical, as it needs to be in undisturbed airflow to produce accurate measurements. The best location for the pitot-static tube is at the frontmost point in the nose of the UAV, extended far enough that the effect of the body on the airflow doesn't affect the measurements [76]. The pitot-static tube has to be connected to a sensor that measures the pressure differential, from which airspeed can be calculated. The MS4525DO comes in various configurations, including differential pressure measurement ranging from 1 to 150 psi (6.9 kPa to 1.0 MPa) [77]. The highest expected pressure differential is found at the highest speed and density according to Equation 9.1 [78, p. 191].

$$\Delta p = p_0 - p = \frac{1}{2} \rho V^2 \quad (9.1)$$

At the velocity of 40 m s^{-1} and nominal sea level density of 1.225 kg m^{-3} [79], the resulting pressure differential is 980 Pa, so the MS4525DO configuration with a 1 psi measurement range is suitable for airspeed measurement. With 14 bit output the sensor has 16384 discrete values it can reach in its measurement range, meaning a resolution of 0.42 Pa or 0.83 m s^{-1} in the air density of 1.225 kg m^{-3} .

9.4. Obstacle avoidance

In order to fly in airspace that may be occupied by other aircraft and to fly near the ground, obstacle avoidance techniques must be integrated into the avionics. The goal of the obstacle avoidance subsystem is to identify and avoid obstacles and hazards in a safe, reliable, and timely manner.

According to [80] and [81], obstacle detection at the range required by SYS-AVN-OBS-01 of 200 m can be done through the use of Light Detection And Ranging (LiDAR), radar, or infrared and thermal cameras. Utilizing the sensor attribute comparison presented in [80, Table 1], it can be observed that relative to radar systems, LiDAR is generally smaller and requires less power. The drawbacks of LiDAR sensors are identified as more limited range and greater sensitivity to weather conditions [80, Table 1]. Thermal and IR cameras are also identified as an option, but their higher dependency on weather, lower accuracy and greater processing requirements do not place them as a better alternative than LiDAR [80, Table 1]. While LiDAR may be known to degrade in inclement weather [80, Table 1], this is not a significant factor for the sensor selection for collision avoidance in the UAV. According to requirement STK-0.3.9-MIS-ENV-7, the UAV should handle only 4 mm h^{-1} of rain, which is below where [82] identifies there as being any significant reduction in performance. Thus, it is decided that a LiDAR sensor is to be used for detecting obstacles.

Investigating LiDAR systems based on the requirements given in Table 9.1, only the Livox Avia [83], shown in Figure 9.1, was identified as meeting all requirements. With a maximum detection range of 450 m and a 70.4° by 77.2° FOV, the Avia is capable of detecting hazards effectively and in a timely manner [83]. The Avia sensor weights 498 g in addition to an 88 g converter, for a total system weight of 586 g [83]. This system should be connected to the companion computer for processing using Ethernet [83]. Software for the companion computer can be built using the Livox-SDK¹ and detected obstacles and threats should be forwarded to the flight computer.

This system is also used for the detection of markers, in order to ensure a smooth landing. Using LiDAR targets as specified in [84], the position and direction of the runway is determined, aiding accuracy.



Figure 9.1: Livox Avia [83]

9.5. Auxiliary Electronics

In addition to the sensors and systems used for the autopilot, a companion computer should also be integrated into the design to process the LiDAR scans, handle the camera system, and to detect errors and emergencies.

There are some features that the selected companion computer must have to be used effectively in the UAV. The computer

¹<https://github.com/Livox-SDK/Livox-SDK>

should have Ethernet to be able to connect to the Livox Avia, and should run on an operating system supported by Livox-SDK. For this reason, a single board computer (SBC) running Ubuntu on x86 or ARM should be used.

Based upon the necessary features given above, the Raspberry Pi 5 is selected as the companion computer. The Pi 5 is a cheap and lightweight SBC with up to 8GB of ram and a large community of support. While the weight of the module is not in the technical manual, it can be assumed to be no more than the package weight given in the store at 67 g [85].

The use of a Raspberry Pi 5 provides a large set of useful features. With 40 pins of GPIO including hardware SPI, I2C, and serial together with USB connectivity, the companion computer can listen to flight computer communications and detect the presence of errors or emergencies and respond accordingly [85]. Further, the inclusion of a GPU and 8GB of memory means that it is possible to implement complex algorithms as necessary to detect and classify obstacles using the LiDAR sensor [85].

Based upon SYS-AVN-AUX-02, a camera shall also be integrated into the system. For this purpose, it is preferable to use a camera mounted on a gimbal such that the camera operator is able to look around and is able to observe the area being scanned. For this purpose the Trillium HD25-LV is chosen, shown in Figure 9.2 [86]. With a 720p camera in the visual spectrum and 640x512 LWIR camera, the HD25-LV is a useful tool for the operator that can both be used when manually piloting the UAV and for making additional visual observations when necessary [86]. The inclusion of an infrared camera also ensures the system can be used to navigate the UAV at night. In addition to the 350 g camera, a 25 g power converter is also used to ensure a consistent supply of (24.0 ± 0.5) V [86]. Given the price of the HD-25LV is not publicly available, an order-of-magnitude estimate of €10000 is used based on a slightly heavier similar system with slightly more capabilities, namely the Gremsy VIO G1 [87].

This camera supports both serial and Ethernet for communication with the companion computer, and can also be partially controlled by the autopilot [86]. While the camera has a peak power of 75 W, the bench-top power average is only 10 W [86]. In order to view and control the camera, a minimum bandwidth of 200kbps is required [86].



Figure 9.2: HD25-LV [86]

9.6. Communications

In order to control the drone and camera from the ground station, a data-link is required. In addition to supporting 200kbps of data for the camera, the data-link should also be able to support telemetry and control signals for the flight computer. Using a safety factor of 2 on the camera bitrate to compensate for potential data-bursts and additional telemetry and control, a minimum desired bitrate of 0.4Mbps is established. As the system should operate on license-free radio-bands, the most common available bands are 915 MHz, 2.45 GHz and 5.8 GHz [88]. However, as 915 MHz is not license-free worldwide, this band is not to be used [88]. 2.45 GHz is also preferable over 5.8 GHz as there is less free-space loss, and consequently higher range, when operating at lower frequencies, and the speed available on 5.8 GHz is not necessary. Additionally, while satellite communications is an easy solution when it comes to ensuring reliability and effectively infinite range, the limited speeds and exorbitant costs eliminate this as an option. Thus, a RF system operating in the 2.45 GHz band is to be used.

Investigating Unmanned Systems Technologies offering of communication systems for Beyond Visual Line-of-Sight (BV-LOS) operations, a plethora of options were found. However, due to the essence of radio-frequency design and the general uncertainty present in predicting communications system performance, selection of a radio-system was done using a combination of rapid preliminary sizing and trial and error.

The first system identified which promises sufficient range and bit-rate is Doodlelabs Mesh Rider series of radios operating at 2.45 GHz. The RF range and throughput estimation tool provided by Doodlelabs² is used for range estimation. The highest gain omni-directional antennas found that can reasonably be used on the UAV and ground station, with gains of 5.2dBi and 8.5dBi respectively are utilized. A conservative link margin of 15dB and minimum channel bandwidth of 3 MHz is used, with power limited by regulation to 30dBm. This grants a maximum range of 12.6 km and a bitrate of 0.8 Mbps. As this range is insufficient, this system is not further investigated.

The next system identified is the pMDDLRadio Data Link System by UAVOS [89]. This system includes support for an automatic tracking system which can enable the use of directional antennas with higher gains than those provided using an omni-directional antenna [89], [90]. Additionally, this system supports up to 1.51Mbps with a sensitivity of -102.5dBm on a 4 MHz channel using multiple-input multiple-output (MIMO) [89]. Using the tracking system [90], a 16dBi [91] antenna is usable at the ground station and preliminary calculations show that at 30km and with a 5.2dBi [92] antenna on the UAV, a link margin of up to 23.9dB is achievable. This is tested using immersionRCs RF Calculator³. Thus, the pMDDLRadio system is used with an automatic tracking station with a 16dBi antenna and a 5.2dBi antenna on the UAV

²<https://doodlelabs.bitbucket.io/radio-tech/throughput/>

³<https://www.immersionrc.com/rf-calculators/>

for telemetry and control. As the price of the pMDDLRadio system is not publicly available, and no other similar radio system shows publicly available pricing, the cost of the radio is not currently estimated or included in the cost of avionics.

While this link-budget is higher than generally necessary, the fact that the UAV will be flying rather low and thus close to the horizon means there is a decent chance of obstruction in the Fresnel zone [94]. The Fresnel zone indicates the zone outside through which radio-waves propagate which should ideally be free of obstacles, shown in Figure 9.3 [94]. In order to assume normal free-space losses, the general rule requires 60% of the zone to be free of obstacles [94]. Calculating the Fresnel zone for 2.45 GHz at 30 km a radius of 30.3 m is found. Thus, while the link budget is likely to allow communications at ranges of 30 km and beyond, it is very much a possibility that this signal will be degraded by the existence of obstacles within the Fresnel zone. In this case, it is fortunate that a very permissive link-budget is given, such that minor obstructions do not adversely affect the communication quality.

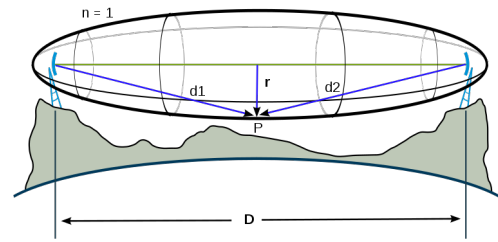


Figure 9.3: Fresnel Zone [93]

Starting in the year 2024, remote identification (RID) of drones is mandatory according to civil aviation authorities, including EASA and FAA [95], [96]. UAV weighing more than 249 g need to be equipped with an RID module to broadcast information about them, including location, altitude and velocity [97], [98]. To comply with these regulations, a certified RID module needs to be included in the UAV. The Holybro RemoteID Module is chosen as it is affordable, lightweight, and FCC and CE-approved [99]. It comes equipped with an antenna capable of transmitting RID data on both Bluetooth and WiFi with a range up to 5 km under ideal conditions.

While ADS-B (automatic dependent surveillance-broadcast) technology is mostly intended to monitor manned aviation, and the corresponding technology necessary for UAV based on regulations is RID, it is decided to include an ADS-B transceiver on the UAV. This is to satisfy the customer requirement STK-0.4.2, with the purpose of integrating the UAV into manned airspace for added safety. ADS-B generally has a much higher range than RID and most manned aircraft are required to have an ADS-B transponder. Aircraft equipped with ADS-B transponders transmit their position and other related data periodically, providing ATC with more accurate position data, and enabling aircraft equipped with ADS-B receivers to keep track of other aircraft in order to avoid in-air collisions [100]. There are some ADS-B modules designed specifically with UAV in mind. The uAvionix ping2020i, lightweight at 26 g and with an average power consumption of 500 mW [101], is a suitable module that is chosen to be used on the UAV.

9.7. Ground Control Station

In addition to the systems mounted on the UAV, some systems must also be placed at the ground control station. These systems are not restricted by the weight of the UAV, but are included in the transportation of the system.

The communication system described in section 9.6 requires the use of a radio, two antennas, and the relevant tracking system. As with on the UAV, the radio is another UAVOS pMDDLRadio. Attached to this system is the UAVOS ARM Antenna Tracking System [90], shown in Figure 9.4, which enables the use of highly directional antennas to communicate with the craft. Lastly, two rugged high-gain ANT-24G-YAG16 antennae are attached to the antenna tracking system. In sum, the ground radio system weighs 15.5 kg and draws up to 160 W of power. This places the antennae 5.3 m above the ground, and it is advised to place this ground station at the highest elevation possible within reason to maximize possible range.



Figure 9.4: UAVOS Automatic Tracking System [90]

Using an Ethernet cable, a computer can be connected to the radio to access devices on the UAV. This computer should run Windows in order to be able to fully interact with the HD25-LV using the control software. Control and command of the UAV is done using QGroundControl, which can run on Windows, MacOS, linux, or Android. This communicates with the UAV through the on-board computer and radio in order to execute commands and to keep the pilot in the loop.

9.8. Layout and Electrical Design

Once all components are chosen for the avionics system, their physical layout and electrical interfaces can be designed. An overview of all components chosen in this chapter is given in Table 9.5.

In addition to the components selected in this chapter, other components which interact with the electrical systems and their power requirements are given in Table 9.6. Interfaces with these components and their placements must also be

Table 9.5: Overview of Chosen Avionics Components

Component	Chosen product	Mass	Peak/Avg Power	Dimensions [mm]	Cost
Autopilot	CubeOrange+	73 g	15 W	38.3 × 38.3 × 22.3	€400
GNSS receiver	VectorNav VN-200CR	16 g	0.5 W	33.9 × 35.9 × 9.5	€840
GNSS antenna	Tallysman HC771	24 g	N/A	33.3 × 33.3 × 54.2	€130
Radar altimeter	Nanoradar NRA24	95 g	1.8 W/1.5 W	133 × 71 × 16.5	€300
LiDAR	Livox Avia	586 g	31 W/9 W	75.6 × 64.8 × 91	€1400
Companion computer	Raspberry Pi 5	67 g	25 W	85 × 56 × 20	€90
Camera	Trillium HD25-LV	375 g	75 W/10 W	71 × 71 × 109	~€10000
Radio	UAVOS pMDDLRadio	23 g	12 W	90.5 × 70.7 × 18.2	N/A
Antenna	ICEFIN24NMOHF	130 g	N/A	38 × 38 × 66.7	€40
Pitot-static tube	LUN 1154	30 g	6 W	12 × 12 × 150	N/A
Pressure sensor	MS4525DO	2 g	2.5 mW	12.4 × 17.4 × 7.2	€70
RID	Holybro RemoteID	16.5 g	0.1 W	35.3 × 23.5 (w/o antenna)	€30
ADS-B	uAvionix ping2020i	26 g	30 W/0.5 W	25 × 40 × 16	€2050
Total		1463.5 g	196.4 W/109.1 W	1.6 × 10 ⁶ mm ³	~€15350

considered at this phase.

Table 9.6: Power Requirements of Other Components

Component	Chosen Product	Peak/Average Power
Engine	Genpod 120 LRU	12 W/6 W
Servos	5x Volz DA 15-N-HT-30	5x8.4 W/4.2 W
Brakes	Electron-Retract E-Brake	27 W

9.8.1. Physical Layout

To start planning the physical layouts, first the components that need holes in the body of the UAV to monitor the external environment are identified. The pitot-static tube is positioned near the frontmost point of the nose, and extended out in the forwards direction a sufficient amount so that its measurements are of a relatively undisturbed airflow. To find the exact optimal position requires aerodynamic analysis of the body of the UAV that is beyond the scope of this design phase. However, for the low subsonic speeds the UAV is designed to operate in, a first approximation is that it is sufficient to have the holes measuring static pressure a few centimeters away from the body of the UAV to achieve clean measurements. The pressure sensor connected to the pitot-static tube is mounted on the inside of the nose near the pitot-static tube, to minimize the length of the tubing required to connect the instruments.

Besides the pitot-static tube, the placement of the camera, LiDAR, and radar altimeter are important to ensure that they have an unobstructed view in the forwards direction. The camera is mounted on a gimbal system under the nose of the UAV, while the LiDAR is mounted on the nose. The radar altimeter should be placed underneath the UAV, so that it points straight downwards. It is chosen to be placed on the underside of the nose behind the camera, as keeping the various components of the avionics system close together simplifies wiring. In the mounting of these components, care has to be taken that the geometry of the nose is not obstructing their view.

Next, the placement of the various antennae are considered. The GNSS antenna should be placed on top of the body of the UAV pointing upwards, as its intended purpose is to receive signals from satellites. The GNSS receiver should be placed inside the body of the UAV. As the GNSS receiver also contains an IMU and its output is a fusion of the GNSS and IMU data, it should be placed as close to the center of mass as possible to minimize the effect on the measurements of the UAV rotating about its center of mass. The RID and ADS-B modules depend on their own GNSS antennae for tracking, so they should be placed on top of the body to optimize the GNSS signal. They can be placed on the top side of the nose, to keep them close to the rest of the avionics systems.

The radio system chosen is a 2x2 MIMO (multiple-input and multiple-output), meaning that it combines two separate antennae to increase the bandwidth of the radio, and to improve the directionality of the radio system. The ICEFIN24NMOHF has optimal gain on a shallow, almost disk-shaped cone around and slightly upwards from it. The two antennae should be placed in different orientations as shown in Figure 9.5, so the sectors where they have maximum gain are oriented differently. One antenna should be placed on the bottom of the UAV pointing downwards, so its main lobe or the sector with maximum gain extends around and slightly below the UAV. The other should point sideways, perpendicular to the wing, so its main lobe extends behind, below and in front of it. This antenna should be placed on the side of the body. The radio system itself can be connected inside the nose of the UAV, near the other components.

Finally, the autopilot and companion computer are placed inside the nose of the UAV, where most of the avionics is located.

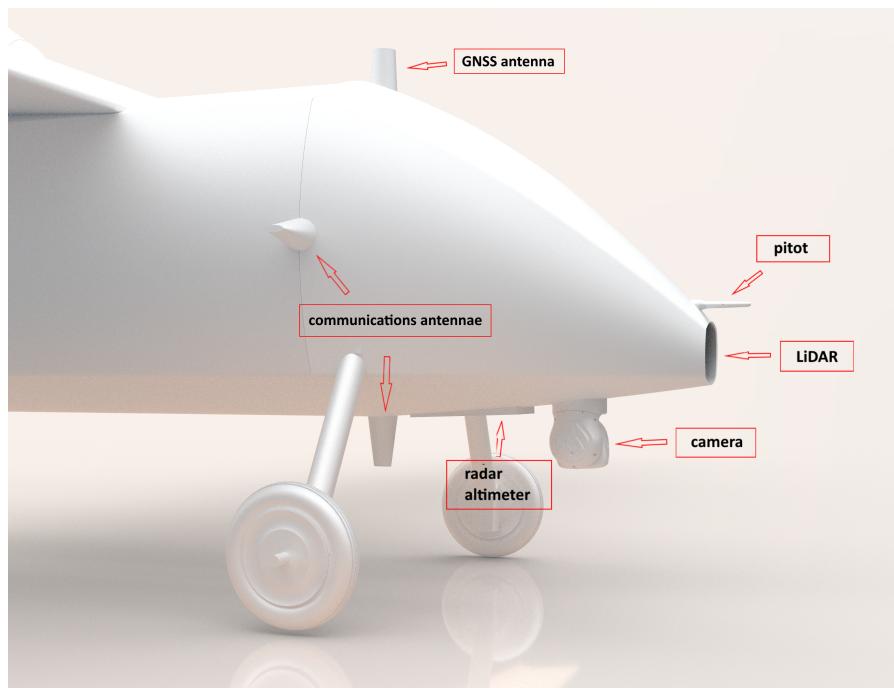


Figure 9.5: Placement of external avionics.

For their placement, the main consideration is the ease of assembling the entire avionics system: they should be placed so that wires can be easily attached and removed.

9.8.2. Electrical and Software Interface

The electrical interface of the entire avionics system is shown in a hardware block diagram in Figure 9.6. In the diagram, the communication links and directions of communication between the various components are shown. Additionally, the flow of power from the power subsystem is shown, and in particular, the voltages provided to the various components are presented. The communication interfaces shown in Figure 9.6 and their explanations are shown below:

- **Transistor-Transistor Logic Universal Asynchronous Receive Transmit (TTL UART)** is a method serial communications using a one- or two-wire transmit-receive interface. Data is sent by alternating voltages between logical high – 3.3 V or 5 V – and logical low – 0 V. Sending and receiving are asynchronous and if flow control/dedicated hardware is not used, messages may be lost if not read in time.
- **Inter-Integrated Circuit (I2C)** is a method of serial communications using a master-slave architecture. The master device controls communications and controls the clock signal for communications. Connections may be done using either two wires. In I2C, one master device may control multiple slaves using only a single bus through addressing.
- **Control Area Network (CAN)** is a complex method of communications using a multi-master serial bus. Any device on the bus may communicate with any other and messages are prioritized and sent first based upon the message ID. In this way, higher priority messages always arrive first on a CAN bus, while many devices can nevertheless communicate over the bus.
- **Pulse Width Modulation (PWM)** is a method of sending analog-like signals using digital signaling. By rapidly switching voltage levels based on a duty cycle, a long term average voltage can be used to approximate analog signal levels.
- **Ethernet** is another communication protocol for wired connections between devices. Standardized under IEEE 802.3, Ethernet allows extremely rapid communications between devices.

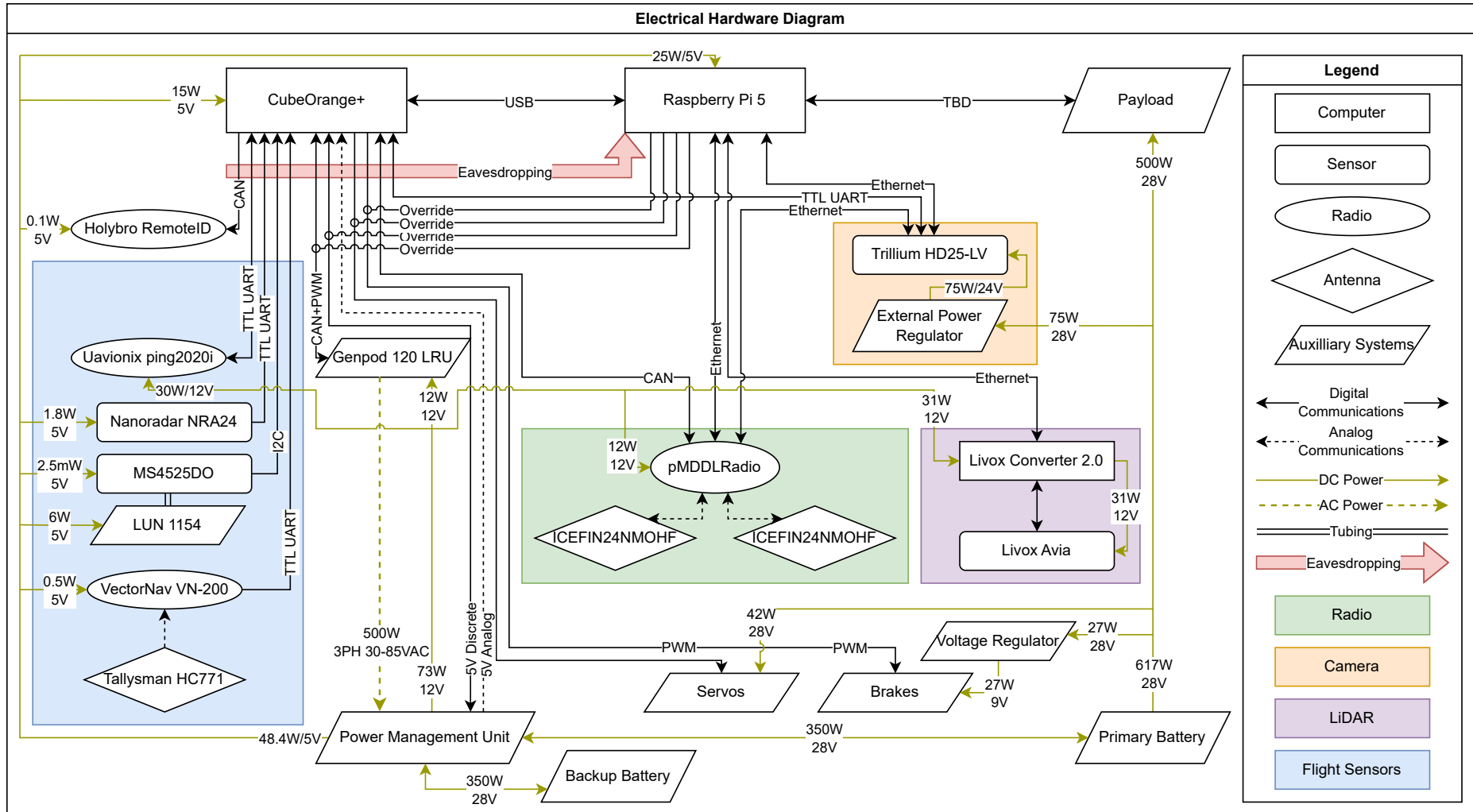


Figure 9.6: Electrical Hardware Diagram

Figure 9.7 describes the data sent on each bus, with rates given where available. Serial communication is defined in Hz, or the amount of messages sent per second. Signals such as PWM or analog are seen as continuous, as even if not actively being adjusted, they are being continuously sent and received. Ethernet communications are defined by the data-rate in Kbps.

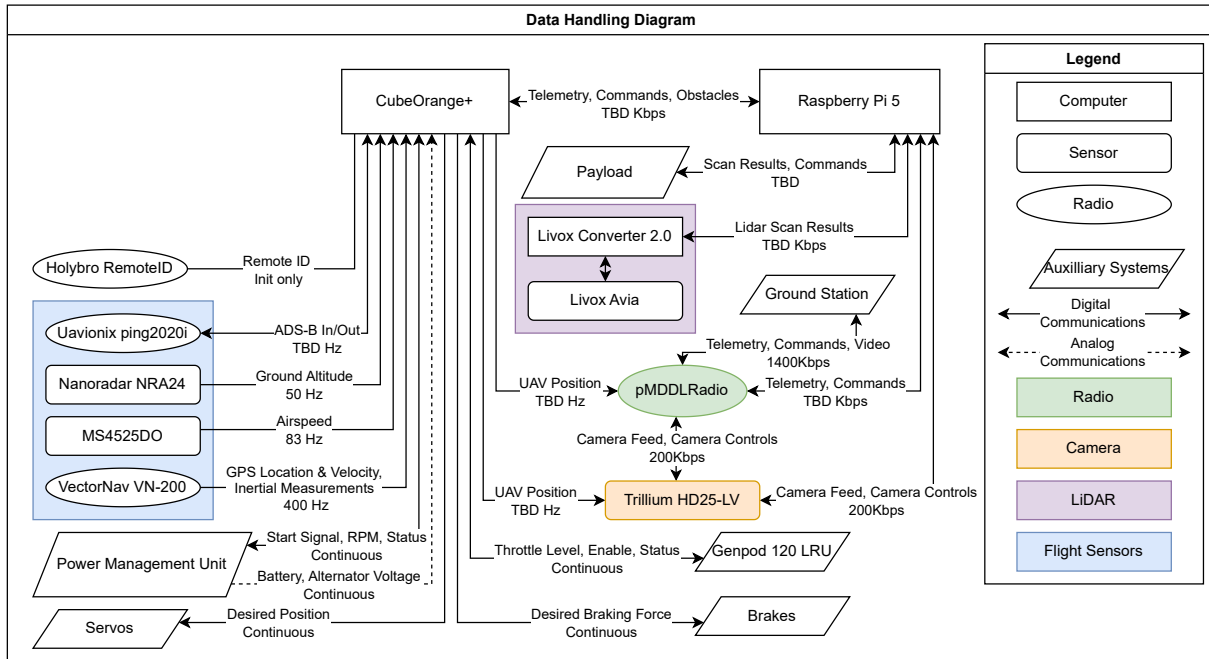


Figure 9.7: Data Handling Diagram

From Figure 9.6 it can be observed that power is distributed over 5 V, 12 V, and 28 V rails. The combined peak power requirement of all devices on the 5 V rail is 48.4 W. Another 73 W is required on the 12 V rail and finally 144 W is required on the 28 V rail. Finally, the payload draws 500 W. As the voltage required by the payload is not specified, this is placed on the 28 V rail as this is also the battery voltage. Given that the brakes and payload are not used at the same time, the maximum power draw on the 28 V rail is thus 617 W.

In order to distribute power over the three voltage levels, a power management unit is required. The Genpod 120 LRU engine selected in chapter 5 comes with a power management unit which can take the 3-phase 30 to 85 V alternating current (AC) provided by the starter-generator, and provide sufficient output for each of the three voltage levels. However, the weight and dimensions of this unit can not be found and there is a lack of information on the system available. While the specs do not match exactly however, the Sullivan SSRC-500C-10 [102] power management unit is likely the basis for the power management unit given the similarity of the datasheets and the starter-generator also being a Sullivan component. Thus, it is assumed the PMU weighs the same as this unit at, 1180 g and has dimensions of 232 × 103 × 68mm [102].

As the power required by the payload is equivalent to that which is provided by the engine, battery sizing only needs to handle the average loads from other flight components. Sizing for average power, the sum of all avionics components is 109.1 W. In addition, the engine draws 6 W. For the servo power, it is also assumed that during active flight the average power consumption is at most the rated power of 4.2 W per servo. This is seen as a conservative estimate granting a total average power draw of 136.1 W.

9.8.3. Battery Sizing

For battery sizing, it is assumed that the battery must be able to power these systems for the entire duration that the UAV is powered on, including the cruise phase. However, during the cruise phase power is generated such that batteries may recharge between take-off and landing. As such, the longest phase for which the batteries need to be sized is from the beginning of search to landing, as a critical power generation failure may occur at the end of search such that batteries can not be charged on the return cruise. According to the mission profile, as presented in section 11.4, the total mission time is estimated at 5 hours and 37 minutes, and the time after first cruise is 4 hours and 57 minutes.

Based upon the mission profile and the average power requirements during the flight, a total power draw of 673.7 W h is found. Brakes are not considered in this calculation as they are only applied for a very short time during landing and their power draw is thus seen as negligible. As it is the highest-voltage DC rail and it is easier to step-down than up, the battery is connected to the 28 V rail. This is also beneficial as the power management unit used contains the necessary hardware

to facilitate the charging of a battery on the 28 V rail from an external power source. As such, 8S lithium-polymer batteries operating at 29.6 V are used due to their good power densities. In order to provide 673.7 W h at this voltage, the total capacity must be at least 22.76 A h. For this purpose, the Maxamps LiPo 23000 8S 29.6v Battery Pack is selected as it can provide up to 680.8 W h of energy, at a weight of 3212 g [103].

While this does not provide a large margin of extra power draw relative to the calculated average power, the conservative assumptions made about power consumption of components such as actuators and computers, means there are additional safety margins available in the design. In addition, a Maxamps Graphene LiPo 670 8S 29.6v Battery Pack providing 19.8 W h backup battery is added, to ensure temporary smooth power if the main battery fails [104]. This assumes that a failure does not occur in both the power-generation and main battery at the same time, as this failure is seen as unlikely to occur without the existence of conditions that will lead to loss of vehicle. This battery also ensures that there is excess available energy in an emergency.

Following the design of a first prototype, more accurate estimates are likely to be available, as many components only provide knowledge of the maximum power consumption and not the average. Thus, in future iterations it is likely that the battery sizing is reduced, but the extent of this is as of yet unknown.

9.8.4. Wiring and Circuitry

Lastly, the weight of the electronics must consider the necessary wiring and circuitry to allow smooth power delivery and communications between devices. As this generally requires a greater degree of knowledge about the placement and interactions between components than is currently available, only a first estimation is used. Based upon the Class-II weight estimation performed in section 3.1, the electrical system mass is estimated at 1760 g. Given this also includes power conversion and the power management unit, the 1180 g power management unit is included in this weight. This leaves approximately 580 g of wiring and circuitry, which is seen as a reasonable weight. Further, the battery is included in the electronics weight, but this is not considered in section 3.1, and thus the total electronics weight is increased to 5122 g.

As such, the weight of electronics are distributed as given in Table 9.7. In total, the avionics and electrical system weight of 6585.5 g is 1505.5 g overweight relative to the Class-II estimation of 5080 g. As such, it may be desirable to increase the size of the engine-generator in a future iteration in order to cut the required battery mass.

Table 9.7: Weight and Cost Distribution of Electronic Components

Component	Weight	Cost
Battery	3212 g	\$1089
Backup Battery	150 g	\$84
Power Management Unit	1180 g	N/A
Wiring and Circuitry	580 g	N/A
Avionics	1463.5 g	€15350
Total	6585.5 g	€16446

9.9. Flight Software

At the current stage of design, it is not possible to create the software for the autopilot, companion computer, or ground control station. Nevertheless, the functionality required by the software can be defined and an overarching overview of the architecture is provided for the autopilot and companion computer.

First, the autopilot software is given in Figure 9.8. This defines the software functionality required by the autopilot and the order of operations for major phases. Additionally, this diagram provides the methods for handling errors and the backup routine in place on the autopilot side of the UAV. As shown in Figure 9.8 the autopilot is responsible for flying the UAV and keeping track of the UAV state and position.

Next, the companion computer software is given in Figure 9.9. The primary jobs of the companion computer are to process the LiDAR scans, logging and saving video, and communication with the ground station. In addition, the flight computer commands the autopilot and translates more advanced commands from the ground station into autopilot commands.

In order to satisfy SYS-AVN-07, the companion computer also implements a backup autopilot in case of failure of the primary autopilot. The software for this is implemented using PilotPi for PX4 [73], allowing the companion computer to act as an autopilot for sufficiently long enough to make a safe landing. In addition, this system is consistently eavesdropping on the communications between the autopilot and its peripherals as shown in Figure 9.6 in order to detect errors and failures.

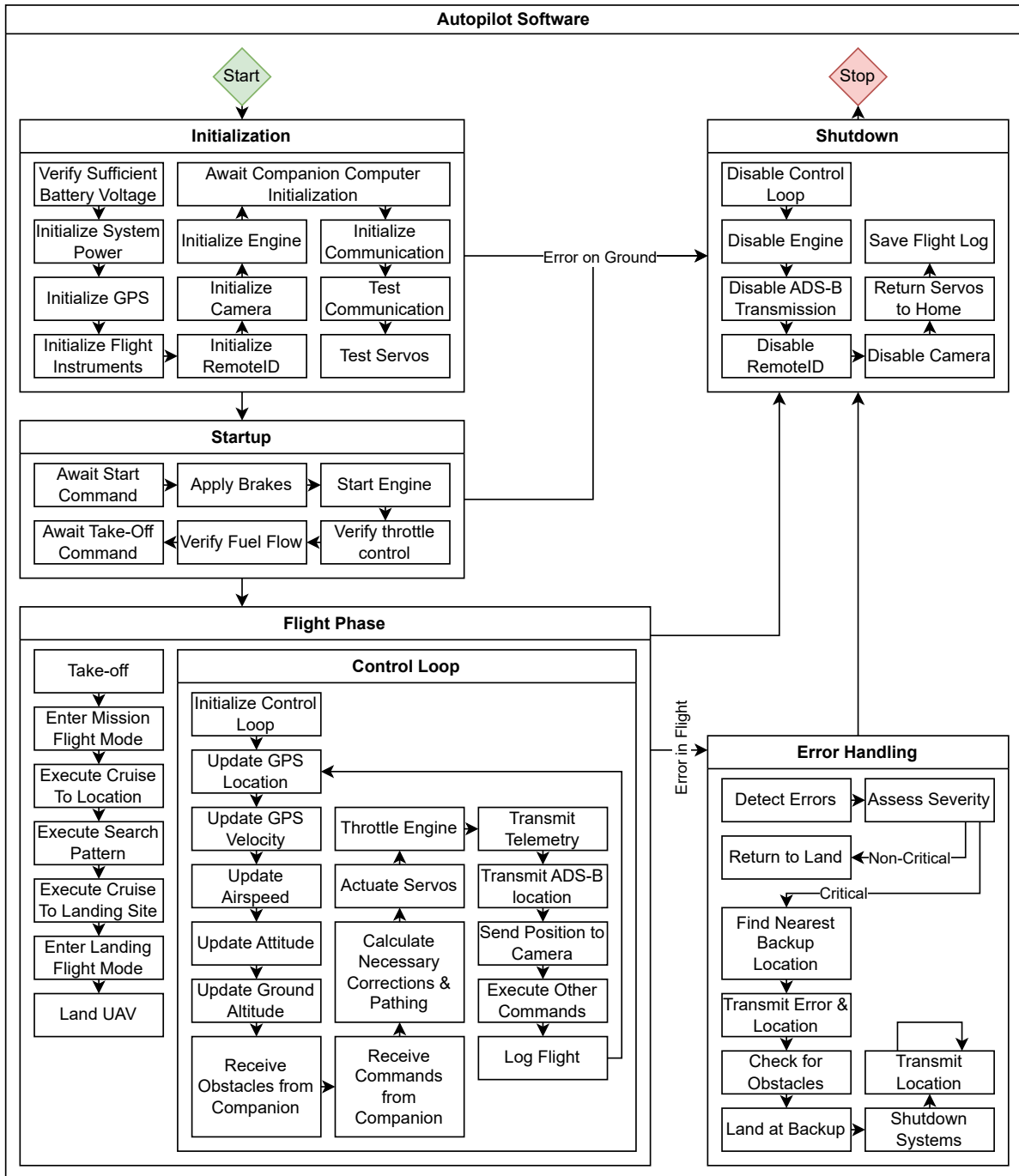


Figure 9.8: Autopilot Software Diagram

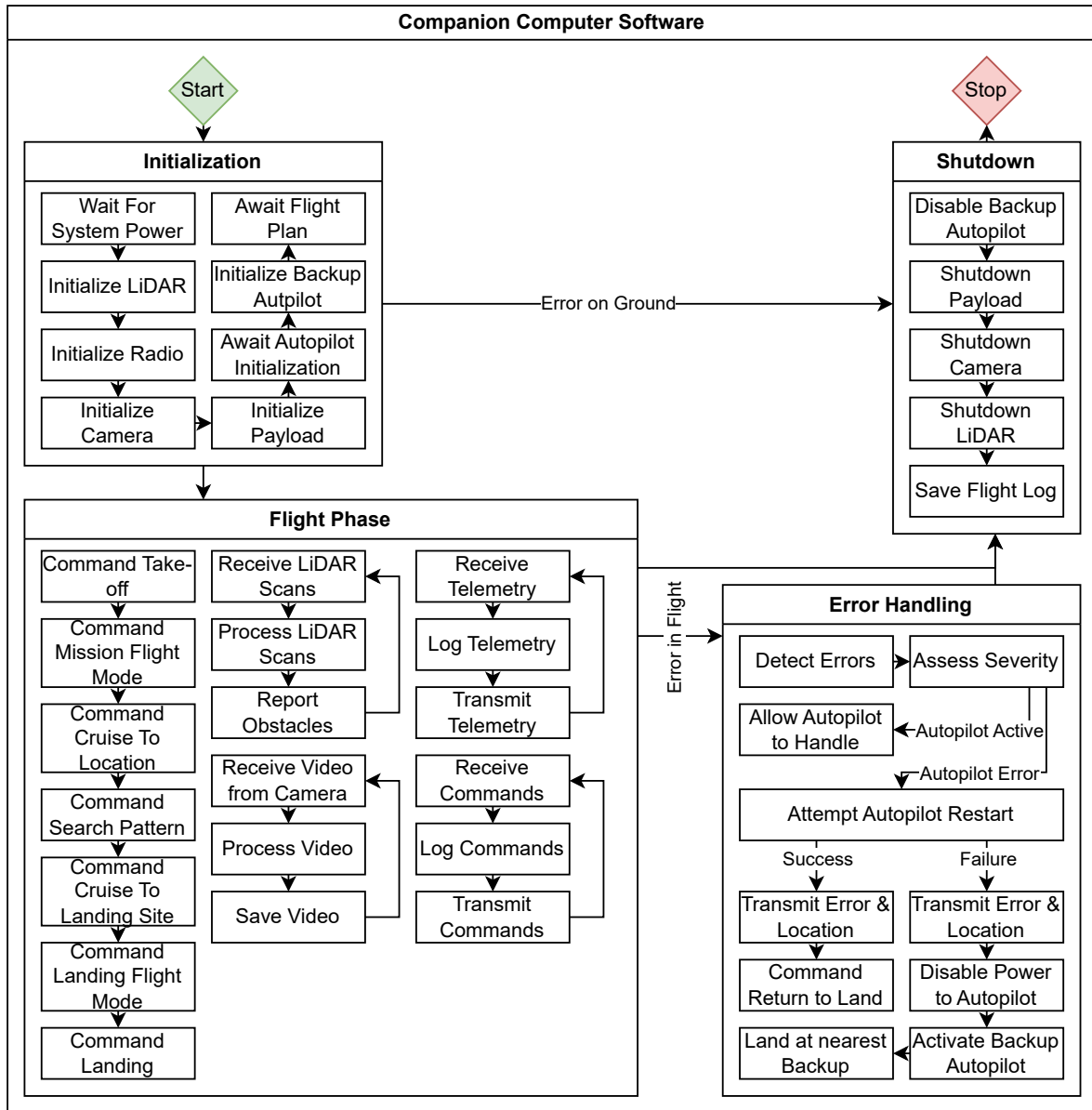


Figure 9.9: Companion Computer Software Diagram

9.10. Verification and Validation

Following the design of the avionics suite, verification is done to ensure that the avionics comply with the requirements. Using a compliance matrix, the avionics are checked against the requirements provided in Table 9.1. The compliance matrix is given in Table 9.8. Requirements marked with ITC are ones that are Intended To Comply, but that are not verifiable at this stage without implementing the software and testing with hardware.

Requirement SYS-AVN-NAV-04 is failed due to insufficient accuracy of the barometric sensors. It may be prudent to re-evaluate this requirement and its parent in the next iteration considering the relatively low importance of exact pressure altitudes. At sea-level, the difference in density, and consequently dynamic pressure, based on 25 m difference in altitude is from 1.225 kg m^{-3} to 1.222 kg m^{-3} , a change of less than 1%. Thus, this failure is seen as acceptable, and the requirement should be adjusted in future iterations of the design.

Table 9.8: Verification of Requirements for Avionics

ID	Check	Reasoning	Requirement
SYS-AVN-01	✓	Inspection: All components of avionics draw a total peak power of 196.4 W according to Table 9.5.	Avionics system shall draw no more than 200 W of power.
SYS-AVN-02	✓	Inspection: All components of avionics weigh a total of 1463.5 g according to Table 9.5.	Avionics system shall weigh no more than 2 kg.
SYS-AVN-03	✓	Inspection: All components of avionics cost a total of €15350 according to Table 9.5.	Avionics system shall cost no more than €20 000.
SYS-AVN-04	✓	Inspection: All components of avionics are placed within the required space, and total volume given in Table 9.5 is less than required.	Total volume of avionics, excluding communications, shall be no larger than $0.4 \times 0.3 \times 0.4$ m.
SYS-AVN-05	✓	Inspection: The two active sensors, the LiDAR and radar, are both models that are eye & human-safe.	Active sensors shall be eye & human safe.
SYS-AVN-06	✓	Inspection: All sensors affected by rain are sufficiently resistant to rain and pitot-static tube includes heating for rain.	Avionics shall be operable in 4 mm h^{-1} rain.
SYS-AVN-07	✓	Inspection: Critical flight sensors and controls have backups in other sensors.	Avionics shall implement redundancy on critical components.
SYS-AVN-08	✓	Inspection: PX4 is used for software development and is open-source [73].	Avionics shall use open-source software.
SYS-AVN-AUT-01	ITC	Inspection: PX4 implements self-takeoff and landing native [73].	Autopilot shall have self-takeoff & landing capabilities.
SYS-AVN-AUT-02	ITC	Inspection: LiDAR is capable of detecting markers to delineate runway [84].	Autopilot shall detect runway markers.
SYS-AVN-AUT-03	ITC	Inspection: PX4 is capable of accepting new landing locations in flight [73].	Autopilot shall support backup landing locations.
SYS-AVN-AUT-04	✓	Inspection: PX4 accepts new way-points in flight [73].	Autopilot shall support in-flight way-point updates.
SYS-AVN-AUT-05	✓	Inspection: X4 accepts manual operator override [73].	Autopilot shall support manual operator override.
SYS-AVN-AUT-06	✓	Inspection: CubeOrange+ supports up to 14 actuators through PWM [61].	Autopilot shall support at least 6 actuators.
SYS-AVN-AUT-07	ITC	Inspection: PX4 is capable of obstacle avoidance based on sensor data [73].	Autopilot shall avoid detected obstacles.
SYS-AVN-NAV-01	✓	Inspection: The VN-200CR GNSS receiver has a specified velocity accuracy of 0.05 m s^{-1} [68].	Navigation subsystem shall determine velocity with accuracy of at least 0.1 m s^{-1} .
SYS-AVN-NAV-02	✓	Inspection: The VN-200CR GNSS receiver's integrated IMU has an angular resolution of 0.001° [68].	Navigation subsystem shall determine attitude with accuracy of at least 0.1° .
SYS-AVN-NAV-03	✓	Inspection: The VN-200CR GNSS receiver's integrated gyroscope has a resolution of $0.02^\circ \text{ s}^{-1}$ [68].	Navigation subsystem shall determine attitude rates with accuracy of at least 0.1° s^{-1} .
SYS-AVN-NAV-04	Failed	Analysis: The integrated MS5611 barometer in the CubeOrange+ has accuracy of ± 1.5 mbar, translating to ± 12.5 m at 0 m density altitude [105].	Navigation subsystem shall determine density altitude with accuracy of at least 10 m.
SYS-AVN-NAV-05	✓	Inspection: NRA24 radar altimeter has accuracy of 0.02 m [72].	Navigation subsystem shall determine ground altitude up to 160 m with an accuracy of 0.05 m.
SYS-AVN-NAV-06	✓	Inspection: The VN-200CR GNSS receiver has a horizontal positional accuracy of 1 m [68].	Navigation subsystem shall determine position with accuracy of at least 1 m.
SYS-AVN-NAV-07	✓	Inspection: The VN-200CR GNSS receiver is included in the avionics subsystem	Navigation subsystem shall integrate GPS.
SYS-AVN-OBS-01	✓	Inspection: LiDAR has a maximum range of 450 m [83].	Obstacles shall be detected at ranges of at least 200 m.
SYS-AVN-OBS-02	✓	Inspection: LiDAR has maximum vertical sector $+28.6^\circ/-48.6^\circ$ and horizontal $\pm 35.2^\circ$ [83].	Obstacles shall be detected in vertical sector $+20^\circ/-40^\circ$ and horizontally $\pm 35^\circ$.
SYS-AVN-OBS-03	✓	Inspection: LiDAR can detect 20% reflectivity target at 230 m [83].	Obstacles larger than 0.25 m^2 shall be detected at a range of 200 m.
SYS-AVN-AUX-01	✓	Inspection: Raspberry Pi 5 is included as companion computer.	Avionics shall include a companion computer.
SYS-AVN-AUX-02	✓	Inspection: Trillium HD25-LV is available and controllable over radio [86].	There shall be a camera available to the operator.
SYS-AVN-COM-01	✓	Inspection: Ping2020i implements ADS-B functionality [101].	An ADS-B transponder shall be integrated.
SYS-AVN-COM-02	✓	Analysis: Link budget of 23.9 dB is available at 30 km range.	Communication range shall be at least 30 km line-of-sight.
SYS-AVN-COM-03	✓	Inspection: Communication occurs on 2.45 GHz worldwide ISM band [88].	Communication shall occur on worldwide license-free bands.

Aerodynamic Performance

10.1. XFLR5 modeling

10.1.1. Advantages and disadvantages of XFLR5

In order to access the aerodynamic performance of the aircraft XFLR5 software was used and verified with calculations made by hand using conventional methods. XFLR5 is an accredited software in the field of aerospace and is one of the primary tools used for the preliminary estimation of aerodynamic performance. [106] It uses XFOIL to analyze the aerodynamic behavior of the airfoil and then applies it to the 3D model of the airplane. The XFLR5 has a lot of advantages, which come at the cost of its limitations, which will be discussed further.

One of the main advantages of XFLR5 is its ease of use. Unlike advanced software such as Ansys, XFLR5 is a free open-source software that can be used by anyone and it does not require a special course to learn how to use it. It also has a visual display of the input geometry that allows visual inspections of the entire geometry. The software is designed specifically to deal with aircraft, which means that it is easy to iterate the aircraft geometry. For instance, changing the incidence angle of the tail comes down to just typing a different number and saving the change. It is a lot faster to create the 3D model of an aircraft in XFLR5, when compared to conventional 3D modeling software, such as 3DEXPERIENCE. Another advantage of the software is that it does not require the use of external software to create a 3D geometry. [106]

Another advantage of XFLR5 for this project specifically is that it is designed to analyze the performance of RC aircraft. This means that it is optimized for low-speed, light aircraft, and it is therefore well suited for UAVs. The results it provides are of reasonable accuracy for low-speed aircraft, as it deals with incompressible flow only. And the accuracy of the results improves with an increased number of panels, and results tend to converge, the verification of the results will be performed to evaluate performance.

The last advantage of XFLR5 is the amount of data that it can provide. XFLR5 can be used to obtain aerodynamic loading of the wing, obtain control derivatives, and optimal cruise conditions. In the future development of the project it can also be used to simulate the effect of control surfaces, this however was not done at this phase of the design, due to time limitations.

10.1.2. Disadvantages of XFLR5

Just like any software, XFLR5 has its limitations and disadvantages. The majority of the disadvantages and limitations of the XFLR5 arise from its advantages.

The autonomy of the software unfortunately means that it is only possible to simulate basic aircraft. It is not possible to import geometry from other 3D modeling software. And although that is not a big issue for the wing, for the fuselage it is. Fuselage modeling in XFLR5 is done by eye, and is therefore only an approximation of the actual fuselage of the UAV. Another disadvantage is that it can not model the landing gear or the engine nacelle. These limitations are addressed by the possibility of adding extra drag, which will be evaluated in section 10.5

Another disadvantage is the general underestimation of drag by the software, this is based on laminar flow assumptions and the modeling method used. For instance pressure drag is not considered, only viscous and induced drag are evaluated. This further limits the accuracy of predictions made for the fuselage.

10.1.3. Modeling method chosen

It was decided to use Fixed-Lift Ring Vortex Lattice Method (VLM2) analysis in XFLR5 for the aircraft. The fixed lift means that the software will balance the weight of the aircraft to the lift it generates, this analysis will be capable of providing stall speed and optimal cruise speed. The Ring Vortex Lattice Method (VLM2) allows for the sideslip to be accounted for, although, taking into consideration that primarily pitch stability is analyzed and the sideslip is set to 0° Horseshoe Vortex Method (VLM1) would have also been sufficient.

It was also decided to conduct analysis at ISA 0m altitude conditions. This means that the speed data obtained will be equivalent to airspeed and can be used in further development. The option to ignore body panels was chosen, as recommended by the software developer, and viscous flow was selected, and the wing planform option was selected, rather than its projection, for a better simulation of real-world conditions. By default, the weight of the aircraft of 55.3kg as predicted by chapter 3 is used, and the center of mass is positioned at 0.35 MAC and no extra drag is modeled unless stated otherwise in the section.

It is important to note that the amount of panels and their type of distribution in the model has a significant impact on the accuracy of the result. However, the computational time increases significantly when the number of panels is increased, which then limits the ability to easily iterate the design. There is a fine balance between the computational time and

Component	X-panels	Y-panels
Wing root section	30	30
Wing tip section	30	60
Horizontal tail	20	20
Vertical tail	20	10
Fuselage	151	50 (hoop)

Table 10.1: Panel distribution

the accuracy of the results. By means of trial and error, it was decided to use the following number of panels shown in Table 10.1

The last important note is that XLR5 works with $\sqrt{C_L^3/C_D^2}$ rather than with C_L^3/C_D^2 . Since the rest of the chapter will deal with maximizing C_L^3/C_D^2 it is important to note that the plots will be provided for the $\sqrt{C_L^3/C_D^2}$, and mathematically speaking by maximizing a square root of the number is the same as maximizing the number. Therefore the point where maximum $\sqrt{C_L^3/C_D^2}$ is obtained is also the point where maximum C_L^3/C_D^2 is obtained.

10.2. Stall angle determination

The initial results of the stability analysis have been providing unreliable incidence angles of the wing and the tail. The estimate for the incidence angle of the wing was 7° , which is not only unusual for high lift airfoils but would in practice mean that in cruise the fuselage would have a negative angle of attack with respect to the airflow, which generates drag and is likely to create a downwards force, instead of providing additional lift, as it would be for the positive angle of incidence. Therefore, it was decided to evaluate the incidence angle based on take-off performance.

For the design of the landing gear, the take-off angle was chosen to be 7.5° in section 8.4, it was then decided that the wing should stall at least at 7.5° , and preferably it should stall at 9° , to have the margin for gusts. To calculate the incidence angle, at first, the airfoil at different sections of the wing was considered. To estimate the stall angle of attack of the wing a total of 3 sections were considered: the root and tip chords of the wing and the position where the wing starts to taper at 0.7m. For all sections, Reynold's number was calculated assuming a cruise condition of 26 m/s at ISA 0m altitude, and the corresponding stall angle of the airfoil obtained from XFLR5 was recorded. From the result of the airfoil stall angle, it is evident that the root would stall first even without the negative twist angle of the wing. Next, the incidence angle of the wing with respect to the fuselage should be computed. The stall angle is evaluated as an angle of incoming flow with respect to the fuselage. Therefore, knowing that the stall angle of the airfoil at the root is 11° in order for the aircraft to stall at 9 degrees, the wing should have an incidence angle to the fuselage at 2° . This means that when the aircraft's body experiences a 9° angle of attack, the wing experiences 11° angle of attack and stalls. The rest of the sections are then evaluated to ensure that the wing starts stalling from the root. The fuselage-airfoil angle is defined as the 'twist' angle between the fuselage and the respective section of the wing. The stall angle of the section of the wing is then computed by subtracting the fuselage-airfoil angle from the stall angle of the airfoil. The results of this evaluation can be seen in Table 10.2

Section	Airfoil stall angle	Fuselage-airfoil angle	Stall angle
Root of the wing	11	2	9
0.7m of the wing	11.5	2	9.5
Tip of the wing	12.5	0	12.5

Table 10.2: Stall angle determination

10.3. Results of stability modeling

When computing the initial parameters for stability and control, i_h was thought to be the incidence angle of the tail and it was computed to be -11° based on the incidence angle of the wing of 2° as presented in Table 6.3. Such results have prompted the use of XFLR5 to optimize the performance of the aircraft. Fortunately, at a later design phase, a mistake in definition was spotted, as Torenbeek [28] uses i_{h_f} to define the incidence angle of the wing with respect to the fuselage, as illustrated in Figure 10.1. However, when this mistake was spotted the aerodynamic analysis had already been performed to optimize the design and achieve the final values. It was decided to not iterate the optimization process at the current phase of design. Instead, the newly obtained value for the tail incidence angle will be used to verify the XFLR5 model.

In section 6.2 i_h was computed to be -11 degrees, based on the wing incidence angle of 2° , as presented in Table 6.3. This result does not appear to be reasonable, considering that the airfoil stalls at -14° . The XFLR5 VLM2 analysis was performed to verify the result. The results are shown on Figure 10.2.

As can be seen from the top right plot of Figure 10.2, the moment coefficient C_m of 0 can not be obtained at any angle of attack, this means that the aircraft is always pitching up, meaning that the aircraft can not be trimmed based on the results

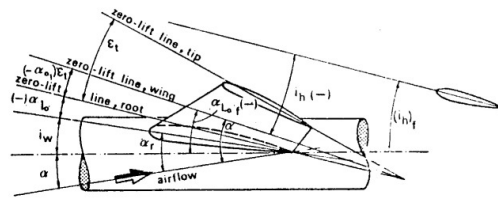


Figure 10.1: Tail incidence angle

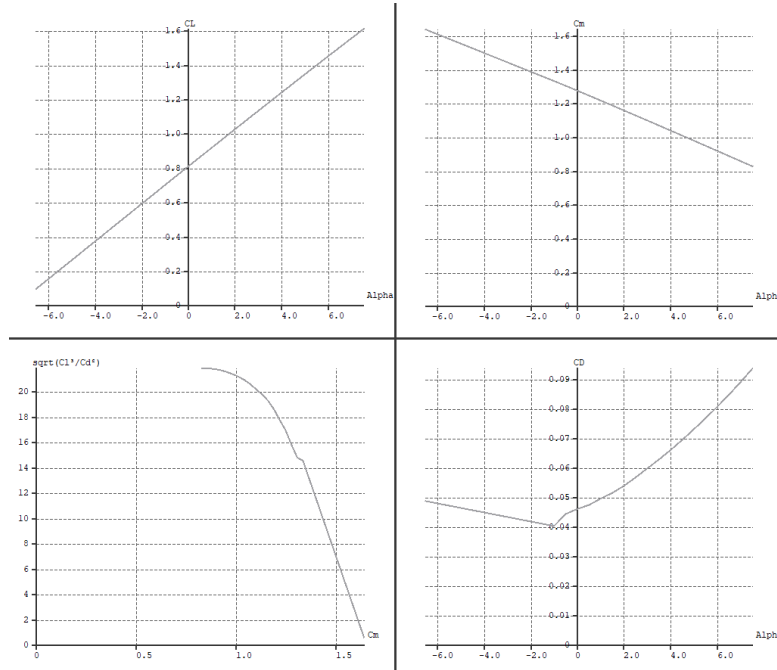


Figure 10.2: Aerodynamic performance of the aircraft for tail at an incidence angle of -11°

of analysis. Shift in c.g. can help to solve this problem, it was attempted to adjust the position of the c.g. from most after to most forward position assumed for ??, and in all cases C_m was always positive.

From the top left plot of Figure 10.2 it can be seen that the stall angle of the aircraft is 7.5° , which is below the predicted 9° by the procedure in section 10.2. The analysis has shown that the wing directly above the fuselage stalls first and the stall propagates from the root to the tip, as designed. This is a desired stall behavior, as the control surfaces (ailerons) located towards the tip of the aircraft remain available to control the aircraft in critical condition when the stall starts to occur, which is particularly handy for stall-spin situations. As the wing-fuselage interaction was ignored for preliminary stall angle estimation, it is considered better to use XFLR5 stall angle and C_{Lmax} estimate in further calculations, as it is more conservative and to a limited degree of accuracy accounts for wing-fuselage interactions. Even though XFLR5 does not accurately account for the wing-fuselage interaction, at the current phase of design this is the most accurate data available, and it is more conservative than not accounting for the wing-fuselage interaction at all. [107]

In conclusion, the result obtained with the conventional method for the incidence angle is not considered to be reasonable. This is probably because the method used by Torenbeek is designed for manned aircraft flying at substantially higher speeds. It is also not fully applicable to the high-lift airfoil selected, as XFLR5 is not capable of computing the zero-lift angle of the airfoil used for the wing, and the zero-lift angle is used to calculate the incidence angle.

10.4. Optimisation for cruise

Taking into consideration that the incidence angle obtained using Torenbeek has proven to be unreliable, it was decided to obtain the tail incidence angle using XFLR5, this will be done by optimizing the aircraft for the cruise. In order to optimize the aircraft for the cruise it was observed that the $\frac{C_L^3}{C_D^2}$, the closer to 0° is the optimum condition for flight, namely $\frac{C_L^3}{C_D^2}$, at 0° the fuselage drag would be minimal. This also means that with the current design, the engine would be producing only forward thrust at 0° , and last but not least, the closer to 0° the optimum cruise angle is, the more margin there is to stall angle, this means a larger safety margin for gusts and maneuvers. The tuning of the tail allows bringing optimum condition for cruise to a lower angle of attack of the aircraft, providing the margin to 7.5° , the margin is gained by the optimum cruise condition occurring at a lower angle, rather than by changing the stall angle, so the stall angle remains 7.5°

°. It is also important to note that the stall angle of the aircraft is not the same as the stall angle of the wing. The stall angle of the aircraft is evaluated with respect to the fuselage, just like the angle of attack of the aircraft. Due to the incidence angle of the wing experiences a different angle of attack than the fuselage and different sections of the wing experience a different angle of attack because of the twist of the wing.

Therefore, taking into consideration that the landing gear design accommodates the position of c.g. from 0 MAC to 0.35MAC, it was decided to use this as the most rear position of c.g. for cruise - 0.35 MAC. The tuning process in this case involves finding the incidence angle of the tail for which the optimum flight condition, maximum $\frac{C_L^3}{C_D}$ would occur at $C_m = 0$. Such an angle was found to be at 2.0 degrees. This yields the following results Figure 10.3

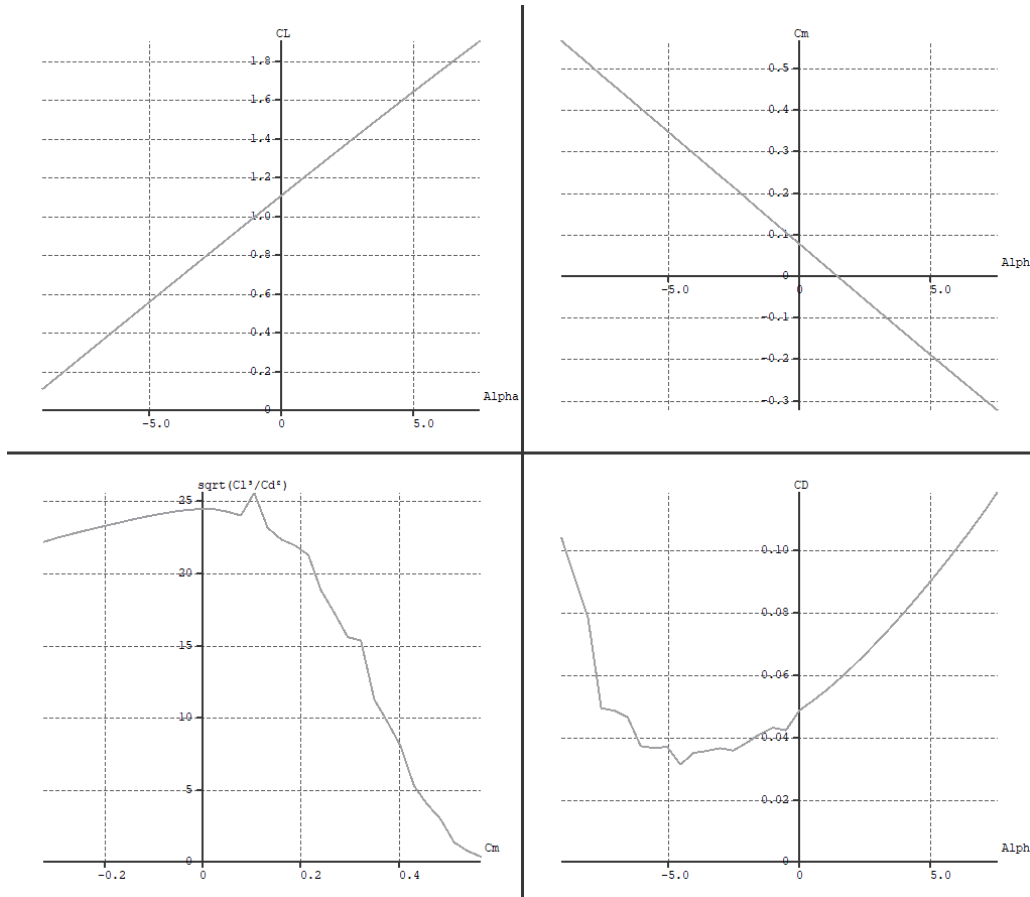


Figure 10.3: Performance of the aircraft

As can be seen the aircraft still stalls at 7.5 °, but the $C_{L_{max}}$ is now larger and has a value of 1.90. The zero moment coefficient $C_m = 0$ occurs at 1.5 degrees, and at the same angle, the maximum $\frac{C_L^3}{C_D}$ is reached, meaning that this is the optimum flight condition. All important data for this configuration is documented in Table 10.3

$\alpha_{C_m=0}$	1.5 °	α_{cruise}	1.5 °
C_{m_α}	0.0536	$C_{L_{cruise}}$	1.27
C_{m_0}	0.078	V_{cruise}	21.6 m/s
α_{stall}	7.5 °	$C_L^3/C_{D_{max}}^2$	595.36
$C_{L_{stall}}$	1.90	$C_L/C_{D_{max}}$	23.2
V_{stall}	17.6 m/s	$\alpha_{C_L/C_{D_{max}}}$	-1

Table 10.3: Main aerodynamic characteristics of the aircraft

10.5. Verification Validation of XFLR5

10.5.1. Lift and Drag

XFLR5 has predicted the $C_{L_{max}}$ to be 1.90. which closely aligns with the predictions made in ?? with conventional methods of 1.8, this is based on the selected airfoil having a $C_{L_{max}}$ of 2.1 and the aircraft typically having about 90% of that value. Moreover, the lift slope C_{L_α} was computed to be 0.108, which is close to the 0.11 gradient, that is predicted by the thin airfoil theory [28] and the value of 0.1106 is used in subsection 6.2.1, which was predicted using Torenebeek [28].

The XFLR5 simulation was originally performed with only the wing, fuselage, tail boom, and tail. This means that the contribution to the drag of the landing gear and engine mount was neglected. To assess the validity of the results, VL2 analysis was repeated this time with the addition of landing gear and engine mount drag. The drag of these components was taken from section 3.2. As can be seen from the Figure 10.4 the extra drag reduces the maximum $\frac{C_L^3}{C_D^2}$ reached as expected, and increases C_{D_0} . However, the contribution was not sufficient to change the cruise angle. The C_{D_0} of the original model is 0.035, and 0.037 was predicted for the analysis with landing gear and engine mount drag. These values have been compared with literature [8], for similar aircraft different aerodynamic software was used to access their drag coefficients which all fell in a range from 0.03 to 0.04. The predictions from XFLR5 align with those results much closer than section 3.2, which predicted C_{D_0} of 0.057. This means that the result for drag can be considered reasonable and can therefore be used for further design.

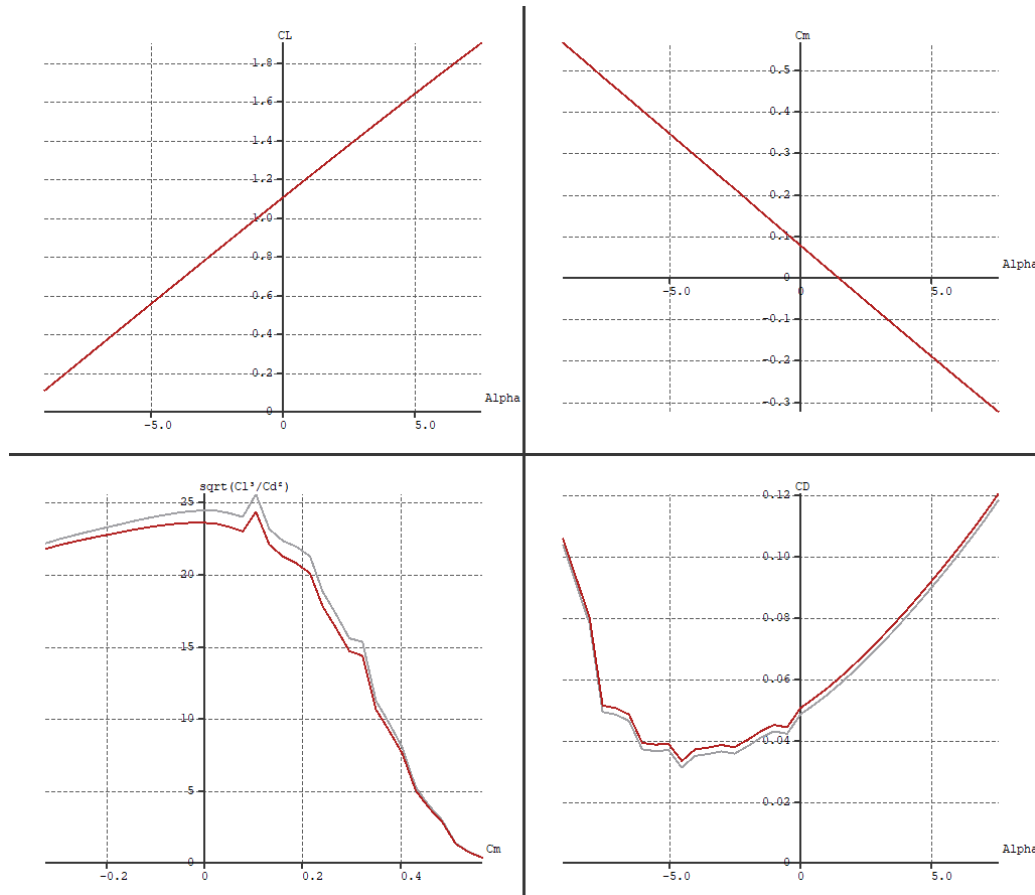


Figure 10.4: Comparison of the original model to 'extra drag' model, highlighted in red

10.5.2. Moment

The moment obtained with XFLR5 can be verified with Stability analysis. Figure 6.2 portrays the moment-lift curve of the aircraft, the moment coefficient than achieves a value of 0 at C_L of approximately 1.2 the XFLR5 predicts that its value is closer to 1.26, which is substantially close. The XFLR5 plot is pictured on Figure 10.5. The slope of the moment-lift curve also has a small variety, the value predicted by stability analysis is approximately -0.54, while the XFLR5 predicts -0.49. The values are substantially close together.

10.5.3. Tail incidence angle

The revised stability and control analysis detailed in section 6.2 has deduced that the tail angle of incidence should be 1° , for the incidence angle of the wing of 2° and the c.g. located at 0.35 MAC. This value appears to be far more reasonable and is substantially close to the 2° value obtained with XFLR5 optimization. This acts as an extra sanity check of the results.

10.6. Ultimate load

It is also possible to extract force distribution for XFLR5. This is particularly useful for further development of wing structure. In order to model the ultimate load case of 3.8g, the mass of the aircraft was increased to 315,2 kg, and the $C_m = 0$ condition was analyzed. With these settings, the equivalent airspeed of 51.6 m/s was recorded which is close to the previously established dive speed of 50 m/s. The data was extracted and plotted resulting in the plots displayed

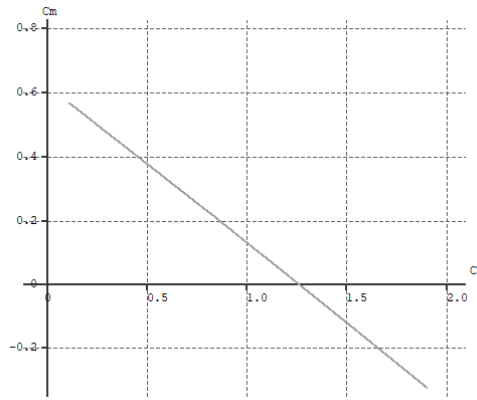
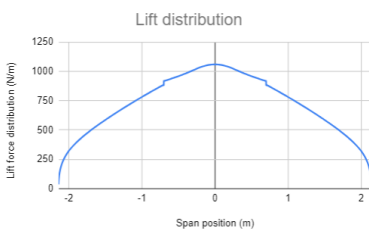
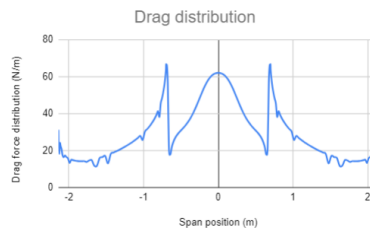


Figure 10.5: XFLR5 lift-moment plot

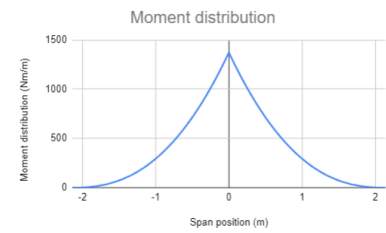
in Figure 10.6. As can be seen on Figure 10.6a, the maximum value of lift distribution was found to be 1058 N/m. The total lift generated by the wing is 3111 N, the total drag force was recorded at 131N, and from Figure 10.6c the maximum bending moment at the root was found to be 1371 Nm. It is worth noting that the drag of the wing has strange behavior around 0.7m point along the span, this is where the wing starts to taper and twist. As cosine distribution of panels was used for tapered and non-tapered sections of the wing, this is also the point where the mesh is interrupted, as can be seen on Figure 10.7. The discontinuity can also be observed on the lift distribution plot. It is therefore expected to be a mathematical model uncertainty. Which should be further evaluated in the future stages of the design. The advised mitigation method is to apply different meshes - cosine, sine, uniform, and based on that deduce the reliable result. The overall loads are considered sensible, as the lift of the wing fully balances out the weight of the aircraft, and the lift to drag ratio is 24, which is on the high end, but as described in subsection 10.5.1 the drag result obtained was substantially lower than class 2 drag estimation, and is of a reasonable order of magnitude.



(a) Lift distribution



(b) Drag distribution



(c) $y = 5/x$

Figure 10.6: Moment distribution

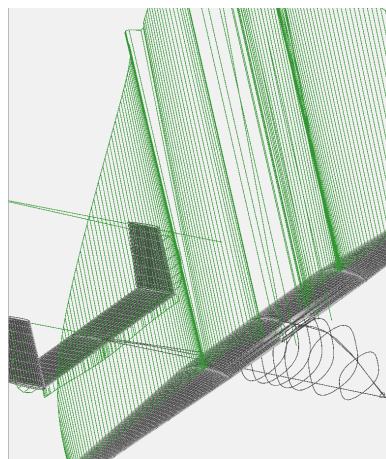


Figure 10.7: The model discontinuity

Flight performance

In this chapter, an overview of the primary flight characteristics is presented. The subjects of airfield performance, climb, the mission profile, fuel fractions, payload-range diagrams and noise are all discussed.

11.1. Flight performance requirements

For the flight performance, all requirements are system requirements, since the flight performance of the aircraft as a whole is evaluated. Thus, all relevant requirements can be shown in Table 11.1.

Table 11.1: Requirements for flight performance

ID	Requirement
SYS-FP-01	The UAV shall be able to take-off at 4000m density altitude.
SYS-FP-02	The UAV shall be able to safely abort a take-off at rotation velocity at 4000m density altitude.
SYS-FP-03	The UAV shall be able to safely land at 4000m density altitude
SYS-FP-04	The UAV shall be able to safely abort a take-off at rotation velocity at 4000m density altitude
STK-9.1-MIS-LGL-5	The UAV shall have a minimum rate of climb of at least 100feet/min
STK-1.2-MIS-RNG-1	The UAV shall have a 30km cruise range to search area.
STK-0.3.1-MIS-ENV-1	The UAV shall have an endurance of at least 4 hours for a temperature range between 5°C and 35°C and an altitude up to 2000 meters above mean sea level (MSL).
STK-0.3.8-MIS-ENV-3	The UAV shall have an endurance of at least 2 hours at a minimum temperature of -5°C and 35°C and an altitude up to 2000 meters above mean sea level (MSL).

11.2. Take-off and landing

The power and wing loading diagram produced in the midterm report [4], was developed with the understanding that a ground run of 500m was available for the take-off distance, namely the rolling distance. However, this is not the case. As the 500m road used as runway should be the balanced field length, so for this single-engine UAV, equal to the sum of the ground run distance and the distance required for the aircraft to come to a complete stop if the engine fails right at take-off speed. Hence, the power requirement is considerably different to what is shown in the wing loading diagram, as the rolling distance should be significantly shorter. This meant that the power requirement had to be investigated once more, before engine sizing and selection could take place.

In order to investigate the acceleration rate on the runway the following dependencies were found: Considering that the runway distance is fixed at 500m, and the UAV must be able to take-off from 4000m altitude. This means that the UAV must be able to accelerate to rotation velocity and be able to come to a complete stop after rotation velocity is reached, in the case of an aborted take-off. From this, the deceleration requirements of the UAV can be found, and the total distance that is required for the UAV to do this. This provides the total distance left over from the 500m runway in which the UAV must be able to take-off from. This take-off distance provides the minimum acceleration rate with which the aircraft must accelerate. The acceleration rate provides the thrust requirement, which is subsequently used to find the UAV's power requirement. In order to investigate the power requirement for the UAV when it is flying at the required climb rate of 100 ft/s at 4000m altitude, the rate of climb is multiplied by the weight and added to the product of the drag force and velocity. Which of these two cases provides the largest power requirement is going to determine the size of the propeller and engine.

For airfield performance, the distance of 500 m needs to be the balanced field length. As the aircraft has only one engine, in case of an engine failure the aircraft needs to be able to come to a complete stop. This places requirements on the brakes and the UAV.

For taking off, the following equations of motion apply:

$$\sum F = m \cdot a = T - D = T - D_{aero} - D_{fric} \quad (11.1)$$

and for landing

$$\sum F = m \cdot a = -D = -D_{aero} - D_{brake} \quad (11.2)$$

with

$$D_{aero} = \frac{1}{2} \cdot \rho \cdot V^2 \cdot S \cdot C_D \quad (11.3)$$

and

$$D_{fric} = \mu_{fric} \cdot (W - L) \quad (11.4)$$

Input				Output				
Name	Symbol	Number	Unit	Source	Name	Symbol	Number	Unit
mass	m	50	{\{}kg{\}}	Preliminary estimate	Take-off distance	$x_{\{TO\}}$	338	{\{}m{\}}
Power at sealevel	$P_{sealevel}$		{\{}W{\}}		Emergency stop distance	$x_{\{stop\}}$	147	{\{}m{\}}
Take-off thrust correction factor	k	0.5	{\{}-{\}}	Sadraey	Landing distance	$x_{\{land\}}$	312	{\{}m{\}}
Zero-lift drag	C_{D_0}	0.05	{\{}-{\}}	Aerodynamic estimate	Minimum runway length for full abort	$x_{\{abort\}}$	485	{\{}m{\}}
Lift coefficient	C_L	1.8	{\{}-{\}}	Aerodynamic estimate				
Aspect ratio	AR	12	{\{}-{\}}	Aerodynamic estimate				
Air density	ρ	0.8191	{\{}kg/m^3{\}}	[53]				
Wing loading	W/S	360	{\{}N/m^2{\}}					
Friction coefficient	μ_{fric}	0.06	{\{}-{\}}					
Brake coefficient	μ_{brake}	0.16	{\{}-{\}}	[111]				
Tailwind	V_{wind}	2	{\{}m/s{\}}					

and

$$D_{brake} = \mu_{brake} \cdot (W - L). \quad (11.5)$$

Thus, an essential first step is finding the thrust of the stationary propeller.

For landing, it is useful to see if it is possible to do only passive braking. Rough terrain has a coefficient of rolling resistance of roughly 0.04-0.08 [108], so 0.06 will be used. For the braking performance, a landing gear brake friction coefficient of 0.35 can be found, using the friction coefficient of car wheels on a surface [109]. For this source, the friction coefficient for asphalt closely matches aviation data collected by NASA [110], which makes it reasonable to use the provided values for aircraft too. However, active brakes can only reach around 90% of this value [53, p. 317], so 0.315 is used. As drag, brake force and rolling force are all dependent upon the lift, which is dependent upon the dynamic pressure, the deceleration changes throughout the entire time the UAV is coming to a stop.

Thus, the method required to find the stopping distance is numerical integration. The velocity was changed iterably, as a function of the accelerations caused by the forces retarding the UAV, with a reducing velocity decreasing aerodynamic forces, reducing aerodynamic drag. On the other hand, the reduced velocity increases ground frictional forces, by reducing the lift that the aerodynamic surfaces produce — as seen in equations 11.4 and 11.5.

The distance for accelerating was found to be the difference between the stopping distance and the length of the runway. From this, the minimum acceleration for take-off was found. This was also done using numerical integration, in a similar manner, by integrating the velocity of the UAV as it accelerated, to determine the frictional forces acting upon the aircraft during take-off. However, a lift coefficient of 1.8 is used, which is the lift coefficient at zero angle-of-attack. This produces the power requirement for the UAV to be 4.2 kW (at a pressure altitude of 4000 m), for a possible rejected take-off at an altitude of 4000 m, coming to a full stop within 500 m, based on a mass of 55 kg.

11.3. Climb

After take-off, the aircraft needs to be able to climb. For climbing, it is useful to fly at maximum excess power [53]. This gives a rate of climb of [53]:

$$RoC = \frac{P_a - D \cdot V}{W} \quad (11.6)$$

which can be rewritten to

$$P_a = RoC \cdot W + D \cdot V \quad (11.7)$$

with

$$D = \frac{C_D}{C_L} \cdot W. \quad (11.8)$$

For this drone, a minimum rate of climb of 30.48 m min^{-1} (requirement STK-9.1-MIS-LGL-5) is legally required. As the aircraft flies at an altitude of only 80 m above the ground (requirement STK-0.3.6), it is not necessary to allow for a faster rate of climb. With a climb speed of 30 m s^{-1} , the aircraft reaches the target altitude in under 3 minutes. However, this rate of climb is required to be reached at a pressure altitude of 4000 m. Using a mass of 55.3 kg, a rate of climb of 30.48 m min^{-1} , a lift-to-drag ratio of 10 and a velocity of 21.6 m s^{-1} , the required power for climb comes out to be 1447.4 W. Given the available engine power at sea level of 7 kW (4.2 at altitude) [24], the climb requirement is met easily.

11.4. Mission profile

As stated in the requirements, the aircraft is required to have a minimum loiter time-over-target of 4 hours. Thus, it is necessary to allot fuel for both legs of the cruise flight, as the 4 hours cannot be used to cruise to the target in the first place. As stated in the requirements, the aircraft is expected to fly a distance of at most 30 km. In addition, fuel needs to be allotted for take-off and landing, as well as for climb. So, it is useful to make an overview of the mission, which is provided in Figure 11.1. First, the aircraft takes off. Then, it climbs to an altitude of 80 m, before cruising to the target area. After having completed its mission, it can cruise back and finally descend and land.

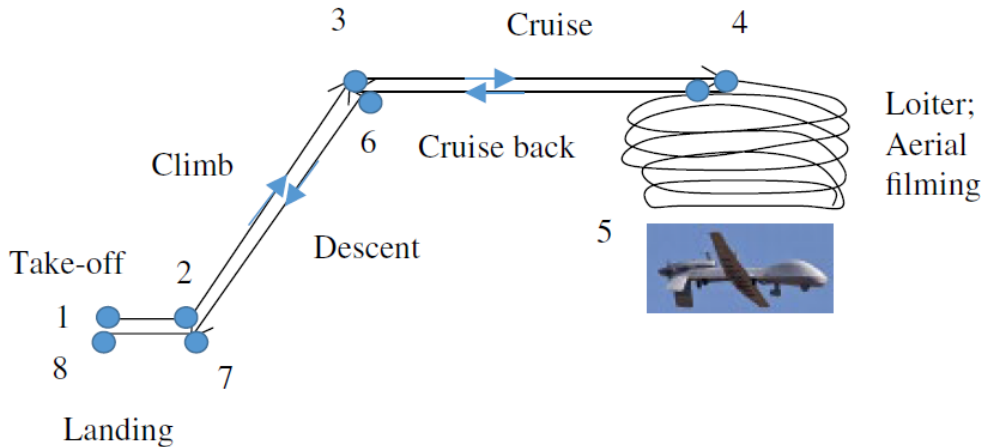


Figure 11.1: Mission profile of the minesweeper [65, Fig 2.2]

11.5. Fuel fractions

Now that an aircraft design is present, it is possible to evaluate the fuel fractions. This can be done using the method elaborated on in the book "Design of Unmanned Aerial systems" [65, Ch. 2].

The fuel fraction captures what percentage of the take-off weight is taken up by fuel weight. This can be determined by analyzing the fuel weight fractions of established mission segments which can be visualized in Figure 11.1 [65, Ch. 2]. This can be further used to determine the mission fuel fraction as can be seen in Table 11.4.

The fuel weight fractions for mission segments that are not fuel intensive can be approximated from statistics of existing UAVs, because they are relatively independent of the mission a UAV is performing. These mission segments include take-off, climb, descent and landing and their fuel weight fraction values can be seen in Table 11.2.

Table 11.2: Fuel weight fractions for typical mission segments [65, Table 2.4]

#	Mission segment	W_{i+1}/W_i
1	Take-off	0.98
2	Climb	0.97
6	Descent	0.99
7	Landing	0.997

For the cruise phases, which bring the UAV to and from the location at which the task is performed, and the loiter phase in which the mission is performed, the fuel fractions are more fuel intensive and can be calculated using Breguet's equations for maximum range and endurance, namely Equation 11.9 and Equation 11.10 [65, Ch. 2].

Therefore, the weight fractions $\frac{W_4}{W_3}$ and $\frac{W_6}{W_5}$, corresponding to cruise phases of the mission are approximated using the maximum range, namely Equation 11.9 [65, Ch. 2]. For this an estimation of the propeller efficiency η_p , the specific fuel consumption c_{sp} and the maximum lift-to-drag ratio $(\frac{L}{D})_{max}$ are necessary. The propeller efficiency and maximum lift-to-drag ratio have been estimated using typical values of these variables found in literature for similar fixed-wing UAVs [65, Table 2.6], while the specific fuel consumption has been determined from the BSFC of the chosen engine [24].

The maximum endurance (Equation 11.10) has been used to determine the fuel weight fraction $\frac{W_5}{W_4}$ which represents the loiter phase [65, Ch. 2]. For this the same values for propeller efficiency $\eta_p = 0.8$ is used as before. The specific fuel consumption is given by converting the BSFC (in g/kWh) to c_{sp} (in N W^{-1}). This gives $c_{sp} = 1.61 \cdot 10^{-6}$. Additionally, the velocity $V_{E_{max}} = 21.6$ and lift-to-drag ratio $(\frac{L}{D})_{E_{max}} = 10$ are used that were determined before.

To model the influence on the generator, it needs to be noted that the generator increases the required power by roughly 50% (chapter 5), from 1172 W to 1672 W. So, as a first rough approximation of the extra energy expended, this extra power can be modelled as some sort of drag. Modelling the expended energy allows for burning fuel to make the aircraft lighter, thus making the assumptions not needlessly conservative. Thus, the drag is multiplied by 1.5 to account for this extra energy. This is equivalent to multiplying the lift-to-drag ratio by 0.667. So, the effect of the generator is modelled by giving the aircraft a lift-to-drag ratio of only 6.67, rather than 10.

All values of the variables used can be found in Table 11.3. The equations for mass ratios are given as [53]

$$R_{max} = \frac{\eta_p}{c_{sp}} \left(\frac{L}{D} \right)_{max} \log \left(\frac{W_i}{W_{i+1}} \right) \quad (11.9) \quad E_{max} = 2 \cdot \frac{\eta_p}{c_p} \cdot \frac{C_L}{C_D} \cdot \frac{1}{V_{loiter}} \cdot \left(\sqrt{\frac{W_i}{W_{i+1}}} - 1 \right) \quad (11.10)$$

From this, the fuel fractions $\frac{W_4}{W_3}$ and $\frac{W_6}{W_5}$ are found to be equal to 0.991 and the loiter fuel fraction $\frac{W_5}{W_4}$ equal to 0.912. The results of the calculations elaborated upon are summarized in Table 11.4 and combined with the statistical values. However, due to the low flight altitude of only 80 m, the climb and descend fuel fractions are neglected and assumed to be part of the cruise fuel fraction. The total fuel fraction of 0.875 then gives a fuel mass of 6.91 kg when using the estimated MTOW of 55.3 kg, which is somewhat smaller than the 7.4 kg calculated in chapter 5, verifying that the original assumption was conservative.

Table 11.3: Breguet's equations variables

Symbol	Name	Value	Unit
R	Range	30000	m
E	Endurance	4	$hours$
V_{loiter}	Loiter speed	21.6	$\frac{m}{s}$
η_p	Propeller Efficiency	0.8	-
c_{sp}	Specific fuel consumption	1.61e-06	$\frac{N}{J}$
$\left(\frac{L}{D} \right)_{max}$	Maximum lift-to-drag ratio	6.67	-

Table 11.4: Resulting fuel fractions and budget

Symbol	Name	Value	Fuel mass (kg)
W_2/W_1	Take-off	0.98	1.101
W_3/W_2	Climb	1	0
W_4/W_3	Cruise	0.991	0.48
W_5/W_4	Loiter	0.912	4.73
W_6/W_5	Cruise back	0.991	0.44
W_7/W_6	Descend	1	0
W_8/W_7	Landing	0.997	0.15
$\frac{W_8}{W_1}$	Total fuel fraction	0.875	6.91

11.6. Payload-range diagrams

In this section, the payload-range diagram is drafted. Generally, this mission is designed to carry a 10kg payload of sensor equipment. However, it is interesting to see what happens with the endurance, and thus the range, when some of the payload mass is replaced with extra fuel. By carrying more fuel on board, the endurance will increase, which is another important parameter in the design of the mission. It needs to be mentioned that for this part of the mission the endurance is increased, which is expressed in additional range or distance traveled during loiter by assuming the UAV consistently flies at the maximum endurance velocity $V_{E_{max}}$ of 21.6 m s^{-1} . This happens during the fourth phase of flight.

with F the fuel flow in N s^{-1} . Converting this to the brake specific fuel consumption of the engine (given in $\text{g kW}^{-1} \text{ h}^{-1}$) gives a c_p of $1.61 \cdot 10^{-6}$. In chapter 5 it is shown that the fuel volume at take-off is 9.9 L and the mass 7.4 kg. It is clear that there is practically no space left in the fuel tank. Thus, the only option to extend the range is removing payload. It can be seen that, with a maximum payload of 10 kg, a MTOW of 55.3 kg and a fuel mass of 7.4 kg the aircraft has a range of 713.83 km. After this, it is possible to extend the range only by removing payload, which yields a ferry range of 886.2 km. This can then be plotted in Figure 11.2.

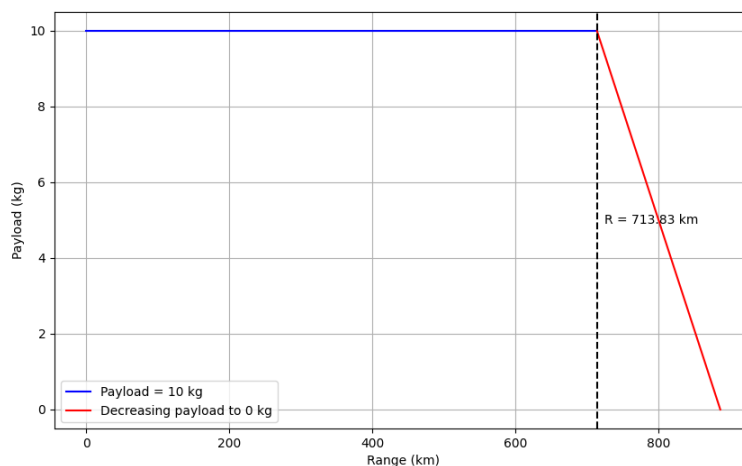


Figure 11.2: Payload-range diagram

11.7. Noise

An important aspect of aircraft performance is the noise characteristics, as it directly influences how much other people are affected by the vehicle. Thus, to investigate the noise characteristics, the field of aeroacoustics needs to be applied. However, this is a complex field, due to the non-linearity of the governing equations [112]. At the same time, noise

depends on several factors. The propeller and the engine are the most important contributors to noise [113]. Thus, an estimate for the propeller and engine noise needs to be found. Regrettably, the engine manufacturer neither specifies the noise of the engine nor the exact propeller. While a two-stroke is louder than a four-stroke engine in general [113], the exact noise characteristics of the chosen engine are not provided by the manufacturer. A muffler is present, so that reduces noise slightly [24]. The exact specification of the provided propeller is not provided either. Therefore, it is practically impossible to give an estimate of the noise at this stage.

Nevertheless, several mitigation strategies are available [113]:

- Use more blades
- Modify the blade shape
- Active noise control

At a later stage in the design, the noise characteristics can be investigated further and appropriate measures taken to reduce the noise.

11.8. Verification and validation

11.8.1. Unit tests

Unit tests for the different calculations made in this section are done using two methods, manually or by creating unit tests in the code. Functions that can be checked by hand are done so. Some examples of functions that are manually verified are: required power for rate of climb, calculating aerodynamic drag, brake force. For the functions that performed numerical integration, there are additional unit tests written into the code in order to verify them. This is done for the functions that calculate the take-off distance and the landing (stopping) distance. Considering that the previous (simpler) functions have been verified, they do not need to be verified in the unit test for the functions that use numerical integration. Both of these functions calculate the distance required, to take-off or stop. The unit test for this is integrating the accelerations twice to find the distance covered. Since the functions that these numerically integrating functions use have already been verified, their values can be set to zero, in order to simplify the manual calculation of the unit test. In order to know how long of a period the accelerations, caused by the various forces present in both situations, take place, the time taken to reach a certain velocity (take-off rotation velocity or zero velocity in case of landing) is required. This is found by integrating manually. This value is then checked in the code using the unit test module, and asserting the found value against the numerically integrated value. The range and endurance unit tests were performed by hand too, and compared to calculation method, namely, python code.

11.8.2. Subsystem verification

Having completed all the calculations for the performance of the aircraft, it is important to enquire whether all of the requirements that were set up in section 11.1, were indeed met. This is done by one of the four methods used to verify requirements (analysis, demonstration, inspection or testing), as elaborated upon in chapter 14 In Table 11.5, the compliance matrix of the structural requirements is visualised.

Table 11.5: Requirements for flight performance

ID	Check	Reasoning	Requirement
Fuselage (FUS)			
SYS-FP-01	✓	Analysis: Numerical integration simulation including all forces present.	The UAV shall be able to take-off at 4000m density altitude.
SYS-FP-02	✓	Analysis: Numerical integration simulation including all forces present.	The UAV shall be able to safely abort a take-off at rotation velocity at 4000m density altitude.
SYS-FP-03	✓	Analysis: Numerical integration simulation including all forces present.	The UAV shall be able to safely land at 4000m density altitude
SYS-FP-04	✓	Analysis: Simulation with summation of all power requirements throughout mission	Electrical power shall be available throughout a mission at altitude
STK-9.1-MIS-LGL-5	✓	Analysis: Simulation with all loads present.	The UAV shall have a minimum rate of climb of at least 100feet/min.
STK-1.2-MIS-RNG-1	✓	Analysis: Simulation all necessary loads and efficiencies.	The UAV shall have a 30km cruise range to search area.
STK-0.3.1-MIS-ENV-1	✓	Analysis: Simulation all necessary loads and efficiencies.	The UAV shall have an endurance of at least 4 hours for a temperature range between 4°C and 35°C and an altitude up to 2000 meters above mean sea level.
STK-0.3.8-MIS-ENV-3	✓	Analysis: Simulation all necessary loads and efficiencies.	The UAV shall have an endurance of at least 2 hours at a minimum temperature of -5°C and 35°C and an altitude up to 4500 meters above mean sea level (MSL).

Budgets

Part of any engineering project is calculating and breaking down the resources available. These are the power budget, presented in section 12.1, the drag budget in section 12.2, the data handling budget in section 12.3, and most importantly the mass budget in section 12.4. Another important, although less technical budget, is the cost budget presented in section 12.5. Afterwards, the market analysis is presented in section 12.6 to identify possible parties interested in the aircraft. Finally, based on the costs and market analysis a return on investment is presented in section 12.7.

12.1. Power budget

The power budget is mainly determined by the avionics, and further explanation of the numbers utilised can be found in chapter 9. The payload power draw is not included in the budget for clarity, as the payload power draw is twice that of the other components combined. Moreover, other than the camera system and payload all others are considered safety critical, and can be said to take up the auxiliary power budget.

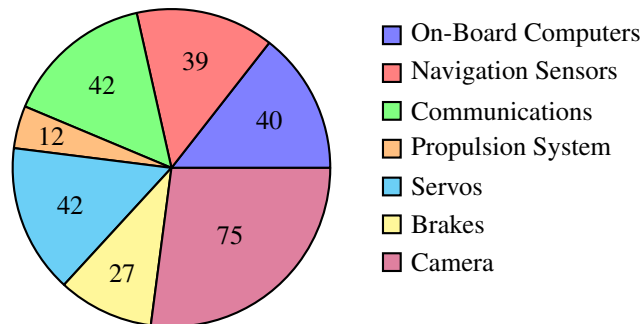


Figure 12.1: Power budget (peak, in W); N.B. 500W for payload not included

12.2. Drag budget

As a thorough aerodynamic analysis of the UAV is missing, the drag estimates have been developed according to [7, Sec.12.5]. The drag estimation process is performed in section 3.2.

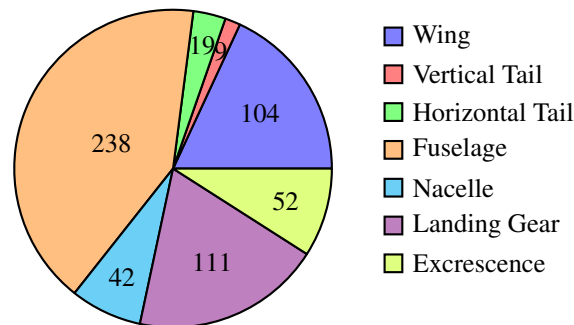


Figure 12.2: Zero lift drag sources (in drag counts)

12.3. Data handling budget

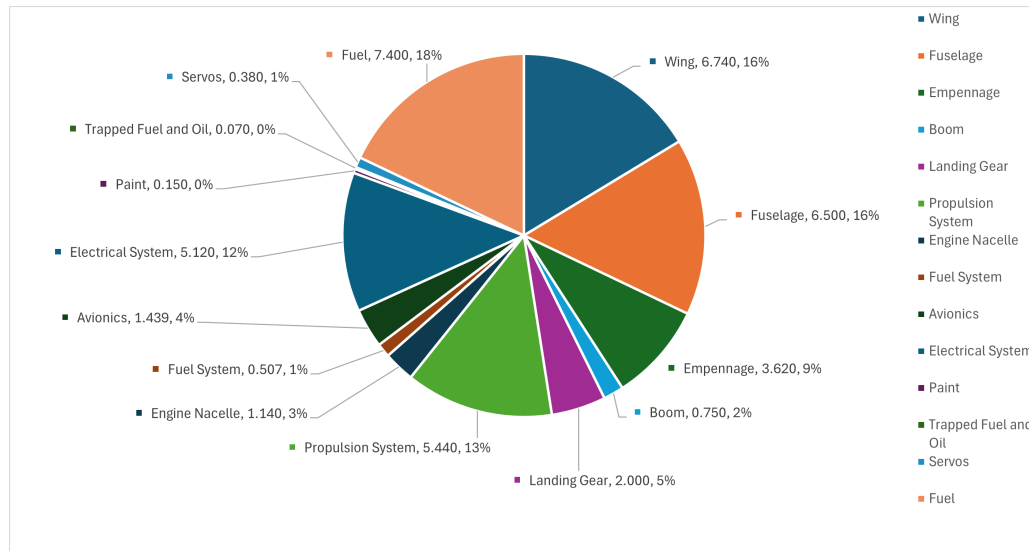
As in detailed in subsection 9.8.2, the data handling requirements are still to be determined. Nevertheless, it is expected that they are within magnitudes of kbps, and as such that no significant changes in architecture are to be caused by these.

12.4. Mass Budget

Starting from the class II weight estimation, with more definition produced by detailing the design, which can be found in chapter 7, the weight of the entire aircraft is calculated. Additionally, the components weights that have been selected are added to the breakdown in Table 12.1. Additionally, a mass budget pie chart can be found in Figure 12.3. The max take-off weight adds up to 50.86 kg, whereas the engine and wing sizing were performed for approximately 55 kg; This mass difference is used to account for all of the other components that have not been selected/ sized as of now.

Table 12.1: Outputs for Class II weight estimation

Name	Symbol	Value	Unit
Wing mass	W_{wing}	6.74	kg
Fuselage mass	W_{Fuse}	6.5	kg
Empenage mass	W_{EMP}	3.62	kg
Boom mass	W_{Booms}	0.75	kg
Landing gear mass	W_{LG}	3.2	kg
Installed engine mass	$W_{Eng,Installed}$	5.44	kg
Nacelle mass	W_{nac}	1.15	kg
Propeller mass	W_{Prop}	included in engine	kg
Fuel System mass	$W_{FuelSys}$	0.507	kg
Avionics mass	W_{Avion}	1.4385	kg
Electrical system mass	W_{Elec}	5.12	kg
Paint mass	W_{Paint}	0.15	kg
Trapped fuel and oil mass	W_{tfo}	0.07	kg
Servos	W_{Servo}	0.38	kg
Operational empty mass	OEW	35.07	kg
Fuel mass	W_{fuel}	7.4	kg
Payload mass	$W_{payload}$	10	kg
Maximum take-off weight	W_{TO}	52.47	kg

**Figure 12.3:** Mass budget (all weights in kg)

12.5. Cost budget

The cost of the manufactured components is calculated according to Equation 12.1. This takes into account the complexity and accuracy of the components, and the raw material cost. The price of aluminum to be used in Equation 12.1 is € 14.52 per kg¹. This could be further negotiated with the supplier to be lowered, but as it is expected to buy already manufactured components, that is out of scope for the current project. The precision is graded qualitatively on a scale of 1 to 4, where 1 is a component where little precision is required, while 4 is a component for which precision is critical.

$$\text{Components Price} = \text{Number of features}^{\text{precision}} \cdot \text{mass} \cdot \text{price/kg} \quad (12.1)$$

The full breakdown of the costs for the UAV can be found in Table 12.2. This characterizes costs based on whether they are fixed, i.e. independent of number of UAVs produced, sunk costs, i.e. only paid once (for tooling etc.), and variable costs, which vary with number of UAVs produced (components etc.). The rent is € 409, the location, 800 m² is large enough for all of the phases to happen at the same time, so rent is only paid once for all phases. The p

¹<https://onlinealuminium.nl/en-aw-7075-t651/>

Table 12.2: Cost budget estimation

Manufacturing costs				
Name	Cost type	Cost	Currency	Source
Engine	variable	25 870	\$	
Fuel tank	variable	590	\$	
Fuel lines	variable	54	\$	Estimated
Main wheels with brakes	variable	749	\$	
Braking controller	variable	54	\$	
Main gear strut	variable	387	€	calculated
Tail gear strut	variable	67	€	calculated
Autopilot	variable	400	€	
GNSS receiver	variable	840	€	
GNSS antenna	variable	130	€	
Radar altimeter	variable	300	€	
LiDAR	variable	1400	€	
Companion computer	variable	90	€	
Camera	variable	10 000	€	
Radio	variable	N/A	€	
Antenna	variable	40	€	
Pitot-static tube	variable	N/A	€	
Pressure sensor	variable	70	€	
RID	variable	30	€	
ADS-B	variable	2050	€	
Battery	variable	1089	€	
Backup battery	variable	84	€	
Wiring and circuitry	variable	250	€	estimated
Avionics	variable	15 350	€	
Fuselage:				
Bulkhead trusses	variable	2 655	€	calculated
Skin	variable	132	€	calculated
Horizontal trusses	variable	145	€	calculated
Wings:				
Panels	variable	3 267	€	calculated
Spars	variable	1 269	€	calculated
Empenage:				
Panels	variable	1 307	€	calculated
Spars	variable	508	€	calculated
Salaries	fixed, monthly	$6500 + 10 \cdot 2040$	[114]	
Rent	fixed, monthly	409	€	
Software licenses	fixed, yearly	43275	€	[115]
Tools and machinery	sunk	3322	€	
Packaging	variable	148	€	
Other and unforeseen	variable	5000	€	
Design costs				
Name	Cost type	Cost	Currency	Source
Salaries	fixed, monthly	$10 \cdot 6500 + 10 \cdot 2040$	€	[116]
Rent	fixed	409	€	
Software licenses	fixed, yearly	43275	€	[115]
Manufacturing tools	sunk	3322	€	
Office tools	sunk	28 525	€	[117] [118]
Office supplies	variable, monthly	262	€	
Maintenance and repair costs				
Name	Cost type and term	Cost	Currency	Source
Parts	variable, yearly	16,350	€	15% aircraft cost
Salaries	fixed, monthly	$6500 + 10x2040$	€	[114]
Rent	fixed, monthly	409	€	
Recycling and retirement costs				
Name	Cost type	Cost	Currency	source
Salaries	fixed, monthly	$6500 + 10 \cdot 2040$	€	[114]
Rent	fixed, monthly	409	€	https://en.realestates.bg/7320162
Tools	sunk	3322	€	

12.6. Market analysis

This section will define all parties that are in some way involved or have interest in the demining process in subsection 12.6.1 after which it will quantify the economic impact of mines in subsection 12.6.2, the cost of current demining operations in subsection 12.6.3, identify the most affected countries in subsection 12.6.4 and current organizations in subsection 12.6.5; Finally the current needs of customers are discussed in subsection 12.6.6.

12.6.1. Stakeholders

In 2016, an average of 23 people around the world lost their life or a limb to a landmine or another remnant of war, every day [119]. An encounter with a landmine is more than an incident, it's a life changing experience for a community, often troubled by their geographical location or economic status already. With the knowledge of this deep human impact, it is terrifying to realise that countries not party to the Ottawa treaty stockpile a collective total of 50 million landmines, with the largest stockpiles maintained by Russia, Pakistan, India, China and the USA [2]. By refusing to ratify the Ottawa treaty, these countries specifically threaten to further the usage of landmines, damaging lives and communities world wide and potentially growing the world-wide demining market, which currently sits at US\$913.5 million [2], even further.

In the beginning, it is useful to investigate which people and organizations have a vested interest in the success of this project. For this project, several stakeholders can be identified, which are presented with the reason of interest in 12.3.

Table 12.3: Table of stakeholders

Customer	The provider of the request for proposal. In the case of DSE, the customer is the group tutor.
Potential Customer	The potential costumers are the buyers of our product. The considered potential customers are demining NGOs, military and civilian Governments
Developers/Engineers	The team/organization working on developing the product, in case of DSE, that is the 09 team.
Investors	investors are organizations potentially interested in investing into the project: Banks (Banks may be interested in investing in this project, as it could generate some profit if enough aircraft can be sold), the military (Military has budget to invest, and the project may be of some interest to them) and the government if affected countries (The governments might be interested in investing into the drone that has potential to detect minefields and therefore provide knowledge of the safe area for rehabilitation and agriculture).
Deminers	Demining crews are affected by our project as it reduces the job market. It also provides a safer working environment for the workers.
Military in affected countries	The military in the affected countries may want the landmines to stay in place, for security reasons.
Military in other countries	The military in countries surrounding the affected countries may want the landmines removed for security reasons.
Affected government	The local governments of course have a reason to want the mines removed as soon as practical.
Civilian population	The civilian population can be further split into main clusters: private landowners (Farmers and other private landowners may be interested in paying for their land area to be checked for the presence of mines) and proximity inhabitants (Civilian populations living in proximity to minefields would be interested in their lives not being negatively affected by drone operations).
Air traffic control	Air traffic control would have to give flight permits for drone operation with a pilot or autonomously based on the predefined flight path.
Regulatory agencies such as EASA	Regulatory authorities such as legal entities of the countries the aircraft is operated in, such as Civil Aviation Authority are responsible for ensuring safe operation of the drone, and hence are stakeholders.
States not party to the Ottawa Treaty	The Ottawa Treaty bans use of mines in military conflicts due to high civilian casualties and prolonged effect. Many countries have not signed it and continue the use of mines for military purposes, producing minefields, these countries would most likely not appreciate a low flying aircraft with poor radar detection capabilities identifying exact location of the minefields. This has the potential to reduce effectiveness of minefields in armed conflicts, practically reducing return on investments for states that are not party to the Ottawa Treaty.

Based on this list, some stakeholders can significantly influence the project, while other stakeholders would like the project to succeed. Some stakeholders, such as regulation agencies, are not so much concerned with success of the aircraft as they are with public safety. For example, if the development is financed via stocks, one shareholder will not have much influence, but would want the product to turn a profit. Therefore, the stakeholders can be mapped in a stakeholder map as in Figure 12.4.

The potential customers are the buyers of our product. The considered potential customers are demining NGOs and civilian governments. Investors are organizations potentially interested in investing into the project. Banks may be interested in investing in this project, as it could generate some profit if enough aircraft can be sold. The military has a budget to invest, and the project may be of some interest to them. The governments might be interested in investing into the drone that has potential to make their country safer. The civilian population can be further split into private landowners, such as farmers, who may be interested in paying for their land area to be checked for the presence of mines, and proximity inhabitants, who would be interested in their lives not being negatively affected by drone operations. Non-signatories of anti-mine Ottawa treaty do not have much interest nor influence on the project.

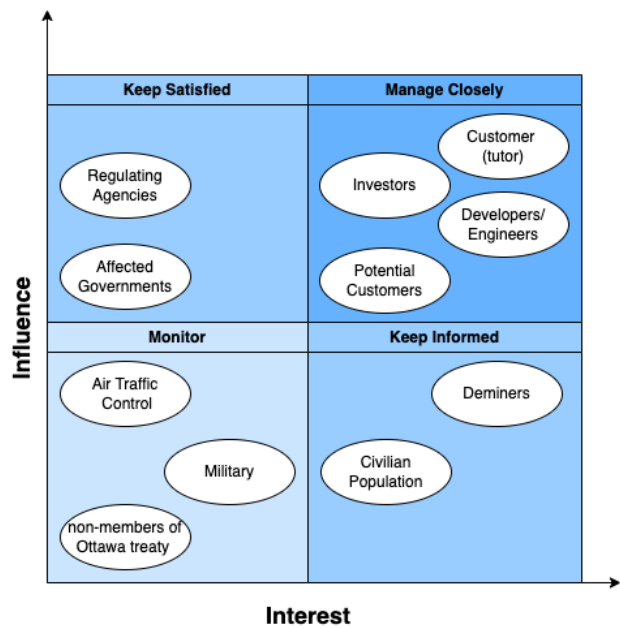


Figure 12.4: Analysis of the stakeholders

12.6.2. Economic Impact of Mines

An important economic consequence of minefields is the loss of arable land and productivity. For example, in 2019, up to 40 percent of arable land in Lebanon was considered contaminated with explosives [120]. In Libya, this number was 27 percent in 1995, with minefields often as old as World War II, so 60 years at that point in time [121]. Minefields still cause economic damage, long after the war is over.

The most important reason for this loss is the fact that agriculture is hazardous in a minefield, so people do not cultivate that land. Additionally, minefields lead to over-cultivation in other areas, loss of biodiversity (meaning less efficient agriculture), loss of cattle and the destruction of land due to mine removal [120]. A more recent example can be found in Ukraine where the Kyiv School of Economics estimates that the forgone revenue for every hectare of farmland contaminated with mines is US \$ 930 per year [122]. Especially for smaller farmers, this is a large economic challenge.

Finally, the most important reason for the loss of productivity is the loss of people. Every death and every limb maimed represents a loss of potential economic output. As the vast majority of casualties is male [2], landmines frequently cause the loss of a breadwinner. Naturally, such a death or crippling affects the entire family. While it is hard to quantify the loss, it is obvious that the 4710 world-wide confirmed casualties in 2022 represent a significant impact [2].

12.6.3. Cost of Demining

Demining a region brings significant costs. While the mines themselves often only cost between US \$3 and US \$75, clearing those is typically more expensive. The Geneva International Centre for Humanitarian Demining (GICHD) requires that all the mines in an area have been found, before an area can be declared safe [123]. According to an article of The international committee of the Red Cross, "the cost of clearance estimated by the United Nations, including support and logistic costs, is between US \$ 300 and US \$ 1,000 per mine" [121]. In addition to the monetary cost, the loss of human lives is an important cost as well, with the international committee of the Red Cross stating: "Mine disposal experts indicate that an average of one deminer is killed and two are injured for every 5,000 mines cleared" [121]. Given there are millions of mines dispersed all over the world, clearing them using traditional methods brings enormous costs, both monetary and human costs.

As the location and number of mines is often unknown, a useful metric is defining a cost per square meter of cleared land. According to a study by Geneva International Centre for Humanitarian Demining (GICHD) "various different costs for clearance were quoted by organisations giving figures from between US\$ 0.60 to US\$ 8.73 a square metre" [124], mostly varying by the cost of labour in the respective country. The GICHD also developed a model as a tool to study the costs of demining. This model gives costs of manual demining between US \$ 1.42 and US \$ 1.72 per square meter [124], based on a clearance rate of 1.5 hectare per platoon (around thirty people) per month. This further shows that demining large areas is not only expensive but also time consuming. Accelerating this process could certainly fill a market gap.

When looking at more recent examples it can be observed that costs have reduced slightly. According to the United

Nations Development Programme (UNDP), a full demining package for Ukraine costs an estimated US\$ 37 billion [125], [126], while, according to the Ukrainian government, an estimated area of 174,000 square kilometers requires demining [126], [127]. This results in a cost of US \$ 0.21 per square meter. This shows costs have decreased, however the amount of mines has increased as well. Thus total costs remain a major problem.

A study conducted by the Center for Food and Land Use Research at the Kyiv School of Economics[122] provides another more recent estimate for the cost of demining. According to them the price to demine a hectare of farmland is US \$ 1,781 or US \$ 0.178 per square meter[122]. This is in close agreement with the estimate by the UNDP and thus seems a more suitable estimation for current demining costs.

12.6.4. Countries Affected

The world is more heavily mined than one may think, with 61 countries known to be contaminated by minefields, and a further 11 countries suspected of having mines or other explosive residuals of war. The total area that each country suspects or is certain of contamination varies greatly. The countries with the largest areas known to be contaminated — in the range of 100 km² to 1,720 km² — are Afghanistan, Bosnia and Herzegovina, Cambodia, Croatia, Ethiopia, Iraq, Turkey, and Ukraine. In Iraq, almost 1,200km² (greater than Hong Kong) is contaminated by anti-personnel landmines and more than 500km² (greater than Andorra) by IEDs (improvised explosive devices). In Ukraine, 160,000km² (larger than Bangladesh) has been exposed to warfare and must be surveyed. A further five countries — Angola, Chad, Eritrea, Thailand, and Yemen, have a contamination between 20 km² and 99 km² (Approximately the areas of Delft and The Hague respectively). Thus, considering that the rate of world-wide demining was only 450 mines per day in 2023 [2], whilst the number of total laid landmines numbers 110 million [128], one can expect it to take 669 years to demine the world at current rates.

In this, a large distinction is made between confirmed and suspected hazardous areas. When an area has been confirmed by direct evidence to have a presence of mines or explosive remnants of war (ERW), it is labeled as a confirmed hazardous zone (CHA). When there is indirect evidence for contamination of mines or ERW and a reasonable suspicion, the area is labeled as a suspected hazardous area (SHA). For all countries with highly mined area listed above, both CHAs and SHAs are present. For example, Afghanistan has 119.94 km² of CHAs and 24.99km² of SHAs. Bosnia and Herzegovina on the other hand has 18.17km² compared to a 851.44km² of SHAs. For CHAs, the mines are known to be present hence, it is necessary to find individual mines. However, for SHAs, it must be determined whether there are mines at all, which is an entirely different mission. Thus, it will be paramount to clarify the mission statement before defining the UAV.

Based on the above mentioned market, it was decided to separate all researched countries zones denoting the expected performance in the region. The green zone countries are where full performance of the UAV is to be expected. The yellow zone countries are the countries where degraded operation is to be expected due to the high temperatures and altitudes that may be encountered during operations. Finally, the red zone countries are the countries which the UAV design does not consider, primarily due to heavy vegetation present being incompatible with minefield detection using currently known methods. These countries are shown in Table 12.4.

Table 12.4: Performance expected in each Country

Green zone	Bosnia and Herzegovina, Croatia, Ukraine, Zimbabwe
Yellow zone	Afghanistan, Iraq, Ethiopia, Angola, Turkey, Yemen, Chad, Eritrea
Red zone	Cambodia, Thailand

Lastly, when looking at national contributions to demining purposes, it is immediately apparent that the total national expenditure of most countries involved in demining operations in their own country is likely not enough in order to justify purchasing the product to be designed if the price requirement is only just met, namely that it shall not cost more than €500K per unit. Currently, Colombia spends the most on clearing landmines and cluster munitions (at 25.0 US\$ million yearly), with Turkey, Cambodia, Lebanon, Bosnia and Herzegovina, and Thailand being other significant spenders [2].

12.6.5. Organizations

Generally speaking, the governments in the affected countries do not have the funds necessary to remove all mines themselves. However, several international organizations are active in the field of demining. These range from large multifaceted organizations, such as the Red Cross and UNICEF, to smaller, more specialized organisations, such as the Fondation Suisse de Déminage. Additionally, various armed forces have combat engineers for removing landmines, although that is not the focus of this report. For the civilian market, the yearly total amount of money spent on demining is on the order of magnitude of \$1 billion, with most organizations having a budget of less than \$50 million [2]. Several organizations have already experimented with drones [129], [130], so there is potential to market this UAV and make the investment in this drone worth it.

12.6.6. Customer Needs

Before moving on to formulating the requirements for the vehicle, it is useful to directly state the needs of the customer. As mentioned before, this section mostly deals with the needs of international non-governmental organizations. For international organizations, a drone represents a significant portion of the budget. Therefore, not only the purchase, but also maintenance, fuel and operation need to be as cheap as possible per unit area cleared.

Additionally, the UAV needs to be safe, reliable and available. The drone should not endanger its users, neither via crashing nor via inadvertently triggering the mines. The point of reliability also ties into operating costs, as operating a drone that only functions half of the time is inefficient. Moreover, the drone should still be able to fly in adverse weather or different terrain conditions. It should also be a prerequisite to get the drone to the suspected minefield from its take off location.

Not only that, but some of the most important needs are specificity and sensitivity. In case of minefields, it is better to be safe than sorry, so false positives are preferred. Nevertheless, a false positive still represents a loss of time and money, so it should be avoided wherever possible.

Finally, the speed of detection is essential. While drones by their nature are faster than a person walking, it is still important to maximize the amount of area covered in a certain timeframe. Compromising too much on this aspect means that the design may be cheap to operate per flight hour, but perhaps not as useful as a slightly more expensive drone.

From this, it is obvious that several different aspects need to be weighed against one another. Thus, it is essential to evaluate the different needs and find a compromise that both satisfies the customer needs and is feasible and affordable to build.

12.7. Return on Investment

The UAV is designed for humanitarian reasons, and as such the organisation functions in a non-profit manner. The profit as such will be expected to be zero, although there will be a margin between cost to manufacture and purchase price to produce a "savings" budget to account for uncertainties, or to provide possible improvements for the UAV.

As calculated in section 12.5, the cost per aircraft is €107k. Putting a "profit" margin of 50% places the cost of the UAV at €160k. Considering a production rate of 10 aircraft per year, puts the yearly profit at €530k. The design costs for a year's worth of design, and sunk costs into tooling are €1073k. The return on investment as such will occur after more than 2 years' worth of production, after 22 aircraft; this takes into account that the first 2 UAVs produced will not be sold as they are expected to be used to solve teething issues.

Systems Analysis

In this section, an overview of the characteristics of the system as a whole is provided. It consists of a functional analysis, with relevant risk assessment, in section 13.1, which is followed by logistics and operations aspects in section 13.2. Finally, a reliability, availability, maintainability, and safety analysis is proposed in section 13.3.

13.1. Functional Analysis

A functional analysis of the aircraft, with functional risks and functional breakdown is performed, such that the scope of UAV's mission is certainly performed, and the

13.1.1. Functional Breakdown

Further developed from the functional breakdown previously developed, to include system level functions, the full functional breakdown diagram can be found in Figure 18.6. There are redundancies between the high-level aircraft functions and the system level functions, which is intentional. This is done such that there is no risk of omitting critical functionality.

13.1.2. Systems

Based on the design work performed, and the natural division re-identified during the process, the following systems have been re-identified:

- **Avionics:** This comprises all of the electronic components, including the on-board computer, the navigation sensors, and the power management system. The previously split systems have been coalesced into a single one due to their extremely close interactions.
- **Propulsion:** This represents the engine, propeller, fuel tank, and other related systems. These are coalesced into a single system again due to their close interaction, and the importance of interfacing between them.
- **Landing Gear:** As the name suggests, this system deals consists of the tyres and structure that supports the aircraft on the ground.
- **Wing:** This represents the main lift producing surface of the aircraft.
- **Control & Stability:** This represents mainly the empennage, as well as the control surfaces.
- **Payload:** For the purpose of the UAV, the payload is represented by a simple box, with a weight of 10kg. The development of the payload itself is considered out of scope.
- **Structure:** This represents the load bearing components of the structure, which will carry and transfer the load throughout the UAV.

13.1.3. System Functional Breakdown

The system level functions differ intentionally from the functions identified in the functional breakdown: aircraft level functions aim to serve the mission requirements, whereas system level functions aim to identify the requirements of each system, individually. This ensures that the functional identification is as complete as possible. This can be found together with the aircraft functional breakdown in ??.

The payload functions aren't developed, as these are out of scope for the current project.

13.1.4. Project Risk Assessment

Table 13.1: Risks identified pre-mitigation

Risk Identifier	Risk Description	Probability	Impact
1. RISK-TECH-PERF-01	One The engine becomes inoperative during flight.	Somewhat likely	Critical
2. RISK-TECH-PERF-02	The aircraft – after having performed detail design – is heavier than expected.	Somewhat likely	Moderate
3. RISK-TECH-PERF-03	The aircraft does not have enough endurance.	Somewhat likely	Critical
4. RISK-TECH-PERF-04	The aircraft does not have the expected manoeuvre performance.	Somewhat likely	Moderate
5. RISK-TECH-STAB-01	The aircraft is longitudinally less stable than expected.	Somewhat likely	Catastrophic
6. RISK-TECH-STAB-02	The aircraft is laterally less stable than expected.	Somewhat likely	Catastrophic
7. RISK-TECH-STAB-03	The aircraft fails to land in the area designated by the operator.	Somewhat likely	Moderate
8. RISK-TECH-STAB-04	CG shifts due to fuel consumption during flight.	Very Likely	Critical
9. RISK-TECH-STAB-05	Failure occurs in state estimation algorithms or sensors.	Very Likely	Critical
10. RISK-TECH-STRU-01	The main load-bearing elements are weaker than expected.	Somewhat likely	Catastrophic
11. RISK-TECH-STRU-02	Structural elements of the design are not in production anymore.	Somewhat likely	Slight
12. RISK-TECH-STRU-03	Structure degrades under harsh weather conditions.	Somewhat likely	Critical
13. RISK-TECH-STRU-04	Subsystems do not fit in the structural frame.	Likely	Critical
14. RISK-TECH-STRU-05	Structure is damaged due to take-off or landing on unmaintained road.	Likely	Critical
15. RISK-TECH-ELEC-01	The computing power is insufficient to control the drone.	Very unlikely	Catastrophic
16. RISK-TECH-ELEC-02	Electronic component fails.	Unlikely	Catastrophic
17. RISK-TECH-ELEC-03	UAV fails to upload path change.	Unlikely	Slight
18. RISK-TECH-ELEC-04	Short circuit occurs due to operation in rain.	Likely	Catastrophic
19. RISK-TECH-ELEC-05	The aircraft is jammed by a third party.	Somewhat likely	Catastrophic
20. RISK-TECH-PROP-01	Propulsion system fails.	Somewhat likely	Catastrophic
21. RISK-TECH-PROP-02	Insufficient thrust provided during take-off.	Somewhat likely	Catastrophic
22. RISK-TECH-AERO-01	The drag coefficient is higher than initially estimated.	Very likely	Moderate
23. RISK-TECH-AERO-02	The top-mounted engine leads to reduced aerodynamic performance.	Very likely	Moderate
24. RISK-TECH-SUST-01	Aircraft is not sustainable enough.	Very likely	Negligible
25. RISK-TECH-SUST-02	Aircraft produces too much noise.	Somewhat likely	Moderate
26. RISK-TECH-PAYL-01	Sensor fails.	Likely	Critical
27. RISK-TECH-PAYL-02	The required sensor is not available at the same time as the aircraft.	Very likely	Moderate
28. RISK-TECH-PAYL-03	Heavier payload needs to be mounted than initially estimated.	Very likely	Critical
29. RISK-TECH-PAYL-04	The number of false positive detections is high.	Likely	Slight
30. RISK-TECH-PAYL-05	The number of false negative detections is high.	Likely	Catastrophic
31. RISK-TECH-SAFE-01	Aircraft operator injured during take-off or landing.	Very Unlikely	Catastrophic
32. RISK-TECH-SAFE-02	Human is injured during drone operation.	Unlikely	Catastrophic
33. RISK-TECH-SAFE-03	Aircraft collides with a mine.	Somewhat likely	Catastrophic
34. RISK-TECH-SAFE-04	Aircraft is hit by a lightning strike.	Very Unlikely	Catastrophic
35. RISK-TECH-COST-01	Aircraft cost exceeding the budget.	Very likely	Moderate
36. RISK-TECH-GEN-01	A newer, much better component becomes available during development, making chosen components obsolete.	Very likely	Slight
37. RISK-TECH-GEN-02	Aircraft cannot be registered due to legal reasons.	Unlikely	Catastrophic

Table 13.2: Pre-mitigation risk map of high risks

Impact	Probability				
	Very unlikely	Unlikely	Somewhat likely	Likely	Very likely
Catastrophic			5, 6, 10, 19, 20, 21, 33	18, 30	
Critical			1, 3, 12	13, 14, 26	8, 9, 28
Moderate					22, 23, 27, 35
Slight					
Negligible					

Table 13.3: Posterior risk map of high risks

Impact	Probability				
	Very Unlikely	Unlikely	Somewhat Likely	Likely	Very Likely
Catastrophic					
Critical		5, 10, 18, 20, 21, 29, 32	6, 19		
Moderate		1, 3, 12	13, 14, 25, 27	8, 9, 22, 23	
Slight				26, 35	
Negligible					

Potential technical risks are combined in Table 13.1. High and high-medium risks (red, orange) were then analyzed in terms of preventative measures and desired contingency plan, explained in Table 13.4. To compare and contrast high risks pre- and post- mitigation, they were visualized in risk maps Table 13.2 and Table 13.3.

Special attention will be diverted to risk number 6, which describes lateral instability risk of the aircraft, the degree of which is uncertain at this stage of the project. The risk number 19, capturing third-party jamming is rather unavoidable and goes beyond the scope of the project, thus will be mostly accepted, and clearly communicated to the customers.

Table 13.4: Risks post-mitigation

Risk Identifier	Preventative measures	Contingency Plan	Probability	Impact
1. RISK-TECH-PERF-01	Implement a maintenance schedule for engines. Install engine health monitoring systems that analyze engine performance parameters in real time.	Establish procedures for operating the aircraft in one engine inoperative scenario without an engine. Define communication protocols between operator and ATC to coordinate emergency response.	Unlikely	Moderate
3. RISK-TECH-PERF-03	Explore fuel-efficient flight profiles, altitude optimization, and throttle control. Investigate more efficient engines, lighter structures and an aerodynamically more efficient design.	Implement emergency power management procedures to conserve energy and extend endurance. Use drop tanks.	Unlikely	Moderate
5. RISK-TECH-STAB-01	Ensure that the aerodynamic design of the wing and fuselage is optimized during the detailed design phase. Review the sizing of the horizontal stabiliser and control surfaces.	Provide operators with a flight envelope capturing aircraft stability and controllability limitations in target operation conditions. Notify about possible hazardous scenarios.	Unlikely	Critical
6. RISK-TECH-STAB-02	Ensure that all calculations for lateral stability derivatives are done throughout the design and thoroughly verified. Install yaw damper systems to mitigate yaw oscillations.	Adjust the dihedral and sweep to satisfy lateral stability conditions. Allow the operator to manually override flight control.	Likely	Critical
8. RISK-TECH-STAB-04	Calculate the expected CG position throughout the flight. Determine the optimal fuel placement within the aircraft. Monitor fuel consumption and distribution during flight.	Equip the aircraft with fuel dumping capabilities. Allow the operator to adjust CG manually in flight by transferring fuel between tanks.	Likely	Moderate
9. RISK-TECH-STAB-05	Implement redundant sensors. Calibrate and maintain sensors to ensure accuracy and reliability. Validate state estimation algorithms through simulation to identify weaknesses.	Develop procedures for activating the backup sensor system. Provide pilots with manual navigation procedures to navigate safely in the absence of reliable sensor data.	Likely	Moderate
10. RISK-TECH-STRU-01	Ensure load-bearing elements meet strength requirements. Incorporate structural reinforcements. Conduct a structural performance analysis under critical loading conditions.	Increase strength by accepting weight increase. Allow the operator to redistribute fuel in the event of element failure. Facilitate aircraft repair with easily dismountable structure.	Unlikely	Critical
12. RISK-TECH-STRU-03	Choose materials with high resistance to corrosion and fatigue. Apply weatherproof coatings and inspect for their quality. Monitor weather conditions to evade harsh weather.	Conduct emergency inspections following severe weather events. Provide recommendation on applicable temporary coatings for the aircraft.	Unlikely	Moderate
13. RISK-TECH-STRU-04	Consider subsystem placement early in the design process. Conduct detailed review in CATIA.	Explore alternative mounting solutions for subsystems that do not fit within the original structural frame.	Somewhat likely	Moderate
14. RISK-TECH-STRU-05	Assess the condition of the intended landing site. Configure the aircraft for operations on rough terrain by adjusting settings such as tire pressure, suspension stiffness, landing gear configuration.	Develop procedures for aborting takeoff due to detected damage. Dedicate part of the endurance budget to the go around phase of the flight. Design an easily replaceable landing gear in case of damage.	Somewhat likely	Moderate
18. RISK-TECH-ELEC-04	Ensure all electrical components are sealed. Route cables away from water accumulation areas. Design electrical compartments and enclosures with adequate drainage and ventilation.	Isolate affected electrical circuits to prevent the spread of short circuits. Install emergency power backup system.	Unlikely	Critical
19. RISK-TECH-ELEC-05	Accept the risk, designing against third-party misuse is beyond the scope of this project. Inform the operator about security threats and unauthorized access attempts.	Maintain clear communication channels between operator and ATC to report jamming incidents. Attempt to launch in the absence of third parties.	Somewhat likely	Catastrophic
20. RISK-TECH-PROP-01	Implement a rigorous maintenance schedule, and engine monitoring systems. Ensure that propulsion system components are manufactured and installed according to quality assurance standards.	Safely shut down the propulsion system and make use of an auxiliary power unit to maintain essential systems and functions.	Unlikely	Critical
21. RISK-TECH-PROP-02	Conduct performance analysis for target takeoff locations. Ensure the mass and drag estimates are as accurate as possible before selecting a propulsion system.	Consider limited sensor payload with lower weight. Consider flying at with limited endurance or with reduced sensor payload mass. Mount stronger engine.	Unlikely	Critical
22. RISK-TECH-AERO-01	Use the most recent estimates for drag and, check the estimates with an expert in the field, conduct computational fluid dynamics (CFD) simulations.	Adjust the flight profile, increase engine thrust or mount a different engine, clean the aerodynamic surfaces after each flight.	Likely	Moderate
23. RISK-TECH-AERO-02	Make extensive use of validated computational fluid dynamics.	Move the engine to the front of the aircraft.	Likely	Moderate
26. RISK-TECH-PAYL-01	Implement redundant sensors to provide backup measurements and ensure system reliability.	Implement alternate sensor fusion algorithms to compensate for the loss of the failed sensor.	Somewhat likely	Moderate
27. RISK-TECH-PAYL-02	Design the aircraft for sensors currently available, while keeping the possibility to upgrade the sensors later. Monitor the sensor market. Use reliable and future-proof sensors.	Stock spare sensors. Explore sensor fusion techniques to temporarily replace one sensor functionality with another.	Likely	Slight
28. RISK-TECH-PAYL-03	Incorporate a safety margin to the mass budget. Discuss with the customer the specifics of payload.	Adjust payload configurations and inform operators about payload capacities between target operation areas.	Somewhat likely	Moderate
30. RISK-TECH-PAYL-05	Ensure accurate calibration and fine-tune the sensitivity of detection sensors. Investigate noise filtering techniques.	Verify and validate sensor accuracy in a test environment. Assess the likelihood of false negatives based on mine pattern recognition. Explore Convolutional Neural Networks applications.	Unlikely	Critical
34. RISK-TECH-SAFE-03	Investigate the possibility of shielding critical and expensive systems from a blast. If possible, avoid making an emergency landing in a minefield.	Do not, under any circumstance, approach the crashed vehicle, without protective equipment. Instead, use a helicopter if possible or a mine-resistant vehicle to recover the aircraft.	Unlikely	Critical
35. RISK-TECH-COST-01	Pay special attention to cost at every point of development, taking a less than ideal component if costs savings are justified.	Revise the budget, use cheaper components, and ask for additional funding.	Likely	Slight

13.1.5. System Functional Hazard Assessment

A functional hazard assessment aims to identify the possible failures associated with aircraft functions, and sure mission critical failures are avoided. For this, [131], [132] were used; although these standards put forward safety assessment guidelines for civil aircraft, compliance with these standards more than ensures a safe design for a UAV.

In Table 13.6, the preliminary functional hazards assessment, for both aircraft as well as system functions can be found. It is created to ensure that system functions are easily identified, and critical functions can be determined based on the failure effects. The mitigation and contingency plans can be found in Table 13.7, which put forth the main methods to keep the risks in check. The criticality and likelihood the failures are determined according to Table 13.5.

Table 13.5: Explanation of criticality and likelihood for risks

5	Write-off	Very Likely	Near certain to happen during operation
4	A lot of damage, possible write-off	Likely	Expected to happen during operations for at least 1 UAV
3	Requires correction to prevent critical conditions	Somewhat Likely	May happen to at most 1 UAV during operations
2	Increased risk	Unlikely	Not expected to happen during operation
1	Inconvenience	Very Unlikely	May never happen

Table 13.6: Functional Hazards mitigation

Function	Subfunction	Failure ID	Failure Condition	Failure Classification	Indented Likelihood	Explanation
Avionics						
Provide Control Schema	Calculate Thrust Requirements	FC.FUN.AVN.01,i	Thrust required underestimated	3	3	Speed of the aircraft decreases, possibly drastically; thrust increases once speed loss is detected
		FC.FUN.AVN.01,ii	Thrust required overestimated	2	4	Speed of the aircraft increases, can be dangerous during landing approach; thrust decreases once speed gain is detected
	Calculate Control Requirements Transmit Commands	FC.FUN.AVN.01.1	False control requirements	4	2	Over correction of disturbances, failure to respond to disturbance
		FC.FUN.AVN.01.2	Commands not received by UAV components	5	1	No control over aircraft
Transmit Scan Results		FC.FUN.AVN.02	Scan results not received by ground control	2	4	Loss of time, no physical risk to aircraft
Provide Situational Awareness	Measure speed	FC.FUN.AVN.04.1,i	Speed overestimated	4	2	Aircraft is closer to stall speed than measured, can become dangerous
		FC.FUN.AVN.04.1,ii	Speed underestimated	3	3	Aircraft is faster than measured, can become dangerous during landing
	Measure altitude	FC.FUN.AVN.04.2	Wrong altitude measured	3	3	Performance differs from expectations, sensor behaviour differs from expectation
		FC.FUN.AVN.04.3	Wrong attitude measured	5	1	Can lead to total loss of aircraft
	Detect obstacles	FC.FUN.AVN.04.4,i	False positive	2	4	Can cause the UAV to waste energy avoiding obstacles that aren't there
		FC.FUN.AVN.04.4,ii	False negative	5	1	Can cause the UAV to crash
	Detect Landing Location	FC.FUN.AVN.04.5,i	False positive	5	1	Can lead the UAV to land in unsuitable location, crashing
		FC.FUN.AVN.04.5,ii	False negative	2	4	Can cause the UAV to waste energy searching for landing location
Distribute Power		FC.FUN.AVN.05,i	Insufficient power to control actuators	5	1	Can lead to loss of control and loss of aircraft
		FC.FUN.AVN.05,ii	Insufficient power to navigation sensors	5	1	Can lead to loss of aircraft
		FC.FUN.AVN.05	Insufficient power to other systems	2	4	Can lead to loss of scan data, or situational awareness for the operator
Propulsion						
Provide thrust	Control thrust	FC.FUN.PROP.01,i	Not enough thrust provided	3	3	Speed of the aircraft decreases, possibly drastically; thrust increases once speed loss is detected
		FC.FUN.PROP.01,ii	Too much thrust provided	2	4	Speed of the aircraft increases, can be dangerous during landing approach; thrust decreases once speed gain is detected
Provide power	Generate electrical power	FC.FUN.PROP.02,i	Not enough power provided to components	3	3	Some component functionality may be lost
Provide fuel	Transfer Fuel	FC.FUN.PROP.02,ii	Overpowering the system	4	2	Can lead to electrical system failure
		FC.FUN.PROP.03	Not enough fuel reaches the engine	3	3	Speed of the aircraft decreases, possibly drastically; thrust increases once speed loss is detected
Landing Gear						
Stabilize and Control UAV on the ground		FC.FUN.LG.01,i	Directional control of the aircraft is lost	5	1	Can lead to crashing off of the "runway"
Absorb Landing Shocks Deal with rough runway conditions		FC.FUN.LG.01,ii	Stability of the aircraft is lost	4	2	Can lead to aircraft falling on its side/ nose
		FC.FUN.LG.02	Structural failure at landing	5	1	Structural failure
		FC.FUN.LG.03		4	2	Can lead to aircraft crashing during take-off roll
Brake	Stop UAV Control direction through braking	FC.FUN.LG.04.1	Brakes fail	5	1	UAV fails to stop within intended distance, possibly leading it to crash
		FC.FUN.LG.04.2,i	One brake fails	3	3	UAV direction has to be maintained through rudder and tail wheel, can lead to getting off the road
		FC.FUN.LG.04.2,ii	Differential braking not usable	2	4	UAV direction has to be maintained through rudder and tail wheel
Structure						
Absorb wing loads	All	FC.FUN.STR.01	Structure fail	5	1	Wings fail, aircraft loss
Transfer fuselage loads		FC.FUN.STR.02	Structural fail	5	1	Can lead to aircraft loss
Absorb landing gear loads		FC.FUN.STR.03	Structural fail	5	1	Can lead to severe crash during landing
Provide avionics mountings		FC.FUN.STR.04	Avionics come loose in the nosecone	4	2	Components can be damaged, functionality can be lost in cruise
Absorb engine loads	All	FC.FUN.STR.05	Engine mounting fails	4	2	Can lead to loss of engine
Wing						
Provide lift		FC.FUN.WIN.01	Insufficient lift provided	4	2	Can lead to either reduced performance, or crashing

Table 13.6: Functional Hazards mitigation

Function	Subfunction	Failure ID	Failure Condition	Failure Classification	Indented Likelihood	Explanation
Mount control surfaces		FC.FUN.WIN.02	Control surfaces heavily disrupt airflow	3	3	Worse controllability
Control and Stability						
Ensure static stability		FC.FUN.CNS.01	Airplane is unstable to disturbances	3	3	Increased workload for the autopilot
Ensure stable eigenmotions		FC.FUN.CNS.02	Airplane is dynamically unstable	3	3	Increased workload for the autopilot
Provide attitude control		FC.FUN.CNS.03,i	Control is exaggerated	2	4	Increase workload for the autopilot due to oscillations
		FC.FUN.CNS.03,ii	Control is unresponsive	3	3	Increase workload for the autopilot, difficulties in pointing the UAV in the intended direction
Mount control surfaces		FC.FUN.CNS.04	Control surfaces heavily disrupt airflow	3	3	Worse controllability
Take Off						
Lift-off		FC.FUN.TOF.4.2.5	UAV cannot lift off from the ground during take-off procedure	5	1	Overshoot of take-off distance, can lead to catastrophic crash
Abort Take-off	Cut throttle	FC.FUN.TOF.4.2.4	Take-off roll cannot be aborted	5	1	Overshoot of take-off distance, can lead to catastrophic crash
		FC.FUN.TOF.4.2.4.a	Engine continues providing thrust	4	2	Brakes have to fight with engine to stop aircraft
Climb to altitude		FC.FUN.TOF.4.2.7	Aircraft cannot climb over obstacle	5	1	Obstacle in flight path not avoided, aircraft crashes
Communications						
Report Location		FC.FUN.COM.4.E.2.4,i	UAV does not communicate any location to ground control	2	4	Loss of situational awareness for the ground crew, little risk of damage to the aircraft
		FC.FUN.COM.4.E.2.4,ii	UAV communicates wrong position to ground control	2	4	Loss of situational awareness for the ground crew, little risk of damage to the aircraft
Communicate Findings		FC.FUN.COM.4.3.5,i	UAV does not communicate any scan results	1	5	Waste of time
		FC.FUN.COM.4.3.5,ii	UAV communicates corrupted scan results	1	5	Waste of time
Receive commands		FC.FUN.COM.4.3.6	UAV cannot be controlled from a distance	2	4	Can waste time scanning wrong location, or miss command to return to base if needed
Verify Landing permission		FC.FUN.COM.4.4.1.c	UAV lands without permission	4	2	Landing location can be discovered to be dangerous
Request take-off permission		FC.FUN.COM.4.2.2.c	UAV cannot take-off	1	5	Delay
Report status	All	FC.FUN.COM.4.N.7,i	UAV does not communicate any state to ground control	2	4	Loss of situational awareness for the ground crew, little risk of damage to the aircraft
		FC.FUN.COM.4.N.7,ii	UAV communicates wrong state to ground control	2	4	Loss of situational awareness for the ground crew, little risk of damage to the aircraft
Report Error and Position		FC.FUN.COM.4.E.1.c,i	UAV does not communicate any error to ground control	3	3	Loss of situational awareness for the ground crew, may be dangerous in case of critical error
		FC.FUN.COM.4.E.1.c,ii	UAV communicates wrong error to ground control	4	2	Loss of situational awareness for the ground crew, may be especially dangerous in case of critical error
		FC.FUN.COM.4.E.1.c,iii	UAV reports wrong position to ground control	4	2	Can be dangerous to ground crew coming to rescue/ delay rescue attempts
Sustainment						
Maintain Structural Integrity	Withstand Nominal Loads (and subsubfunctions)	FC.FUN.SUS.4.S.1.2,i	UAV fails due to fatigue earlier than expected	4	2	Can lead to earlier retirement of aircraft, or critical failure in flight
		FC.FUN.SUS.4.S.1.2,ii	UAV fails by yielding during nominal operation	4	2	Can lead to catastrophic failure if not properly dealt with
		FC.FUN.SUS.4.S.1.2,iii	UAV fails catastrophically during nominal operation	5	1	Unexpected catastrophic failure
	Withstand Ultimate Loads (and subsubfunctions) Periodically Check Components	FC.FUN.SUS.4.S.1.3	UAV fails catastrophically at ultimate load	4	2	Unexpected catastrophic failure
		FC.FUN.SUS.4.S.2.1,i	Components unable to be checked periodically	4	2	Not enough inspection architecture taken into account
		FC.FUN.SUS.4.S.2.1,ii	Components not checked periodically by user	5	1	Failures can be missed, leading to catastrophic failures in flight

Table 13.6: Functional Hazards mitigation

Function	Subfunction	Failure ID	Failure Condition	Failure Classification	Indented Likelihood	Explanation
	Identify Anomalous Performance of Components	FC.FUN.SUS.4.S.2.2	Component performance degradation not noticed	4	2	Can develop to critical conditions in flight
	Identify Possible Structural Failure	FC.FUN.SUS.4.S.1.4	Aircraft takes off with lower component strength	4	2	Can lead to catastrophic failure under high (but still nominal) loads
Perform Pre-Flight Operations						
Power Up Systems		FC.FUN.PRE.4.1.2	Systems cannot be powered up	2	4	Can lead to lost time, identifying and fixing the issue
Verify System Functionality	Verify Electrical Systems	FC.FUN.PRE.4.1.3.1,i	False negative of systems functionality	2	4	Leads to lost time, identifying and fixing the issue
		FC.FUN.PRE.4.1.3.1,ii	False positive of systems functionality	4	2	Can lead to critical failures at later stages
	Verify Communications Systems	FC.FUN.PRE.4.1.3.2,i	False negative of systems functionality	2	4	Leads to lost time, identifying and fixing the issue
		FC.FUN.PRE.4.1.3.2,ii	False positive of systems functionality	3	3	Leads to loss of situational awareness for user
	Verify Control Systems	FC.FUN.PRE.4.1.3.3,i	False negative of systems functionality	2	4	Leads to lost time, identifying and fixing the issue
		FC.FUN.PRE.4.1.3.3,ii	False positive of systems functionality	5	1	Can lead to catastrophic failure
Verify Propulsion System		FC.FUN.PRE.4.1.3.4,i	False negative of systems functionality	2	4	Leads to lost time, identifying and fixing the issue
		FC.FUN.PRE.4.1.3.4,ii	False positive of systems functionality	5	1	Can lead to catastrophic failure
Verify Payload		FC.FUN.PRE.4.1.3.5,i	False negative of systems functionality	2	4	Leads to lost time, identifying and fixing the issue
		FC.FUN.PRE.4.1.3.5,ii	False positive of systems functionality	3	3	Leads to lost time, useless mission
Perform Search Activities						
Travel to Search Area		FC.FUN.SRC.4.3.1	UAV unable to reach search area autonomously	3	3	Needs additional input from user
Determine Optimal Search Pattern		FC.FUN.SRC.4.3.2,i	Sub-optimal Pattern Determined	2	4	Loss of time
		FC.FUN.SRC.4.3.2,ii	Not all Area covered by search pattern	5	1	Could miss potential ERW
Conduct Search Pattern		FC.FUN.SRC.4.3.3	UAV unable to conduct search pattern	3	3	Needs identification of issues, and fixing can take time/ delay mission
Determine Bounds		FC.FUN.SRC.4.3.4	Bounds set outside legal/ mission limits	4	2	Could lead to UAV entering restricted airspace
Return to Base		FC.FUN.SRC.4.3.7	UAV not able to return on its own to base	4	2	Could need user input, or lead to crash landing
Land						
Approach Landing	Detect Landing Location	FC.FUN.LND.4.4.1.a	False positive	5	1	Can lead the UAV to land in unsuitable location, crashing
		FC.FUN.LND.4.4.1	False negative	2	4	Can cause the UAV to waste energy searching for landing location
	Align with Landing Area	FC.FUN.LND.4.4.1.b	UAV performs unaligned landing	4	2	Can lead to crashes on the landing field
Go-Around		FC.FUN.LND.4.4.3,i	Unable to detect need for go-around	4	2	Can lead to crashes or unfortunate situations on the ground
Land Aircraft	Reduce Throttle	FC.FUN.LND.4.4.3,ii	Unable to perform go-around	5	1	Can lead to crashes or unfortunate situations on the ground
		FC.FUN.LND.4.4.4.a	Engine throttle does not reduce	4	2	Brakes need to fight engine thrust to stop
Shut Down Systems	Enable Brakes	FC.FUN.LND.4.4.4.b	Brakes do not engage	4	2	Braking distance increases
		FC.FUN.LND.4.4.7	Systems shutdown does not initiate	3	3	Can cause danger to crew approaching UAV
Deal with Emergencies						
Determine Error	Determine Error Criticality	FC.FUN.EMG.4.E.1.a,i	Criticality overestimated	3	3	Can lead the UAV to return to base when not needed, or other unnecessary mitigation
		FC.FUN.EMG.4.E.1.a,ii	Criticality underestimated	5	1	Can lead to loss of UAV in case of critical failure

Table 13.6: Functional Hazards mitigation

Function	Subfunction	Failure ID	Failure Condition	Failure Classification	Indented Likelihood	Explanation
Emergency Land	Determine Position	FC.FUN.EMG.4.E.1.b	No/ wrong position determined	4	2	Can complicate recovery in case of failure/ crash landing
	Search for landing area	FC.FUN.EMG.4.E.2.1.a,i	False positive	5	1	Can lead the UAV to land in unsuitable location/ crashing
		FC.FUN.EMG.4.E.2.1.a,ii	False negative	4	2	Can delay the UAV in landing, increasing risks due to emergency
	Align with Landing Area	FC.FUN.EMG.4.E.2.1.b,i	UAV performs unaligned landing	4	2	Can lead to crashes on the landing field
		FC.FUN.EMG.4.E.2.1.b,ii	Unable to detect need for go-around	4	2	Can lead to crashes or unfortunate situations on the ground
Fill Energy Stores	Detect Potential obstacles	FC.FUN.EMG.4.E.2.1.c,i	False positive	5	1	Can lead the UAV to land in unsuitable location/ crashing
	Fill Fuel Tank	FC.FUN.EMG.4.E.2.1.c,ii	False negative	4	2	Can delay the UAV in landing, increasing risks due to emergency
		FC.FUN.GND.4.1.1.a	Fuel tank not filled	4	2	Can lead to loss of power, especially critical during take-off
	Fill Batteries	FC.FUN.GND.4.1.1.b,i	Batteries not filled	3	3	Can lead to lack of power to some components, but engine alternator should refill it
Apply Brakes		FC.FUN.GND.4.4.2.b,ii	Unable to apply brakes	4	2	Braking distance increases
Provide Energy						
Provide Electrical Power	Provide Power to Payload	FC.FUN.ENG.4.W.1.1	Insufficient power provided to payload	2	4	Lead to lost time, rescanning same area
	Provide Power to Communications Systems	FC.FUN.ENG.4.W.1.2	Insufficient power provided to communication systems	2	4	Leads to loss of situational awareness for ground crew
	Provide Power to Navigation Systems	FC.FUN.ENG.4.W.1.3	Insufficient power provided to navigation sensors	5	1	Leads to loss of state, can lead to catastrophic situation
	Provide Power to Propulsion Systems	FC.FUN.ENG.4.W.1.4	Insufficient power provided to propulsion systems	4	2	Can lead to loss of thrust/ developing into catastrophic situation
	Provide Power to Stability and Control Systems	FC.FUN.ENG.4.W.1.5	Insufficient power to actuators	5	1	Loss of control over aircraft, can lead to catastrophic situation
Generate Thrust		FC.FUN.ENG.4.W.2	No thrust is generated	4	2	Can lead to loss of thrust/ developing into catastrophic situation
Apply Throttle		FC.FUN.ENG.4.W.3	Throttle cannot be adjusted	4	2	Can lead to loss of thrust/ developing into catastrophic situation

Table 13.7: Functional Hazards mitigation

Failure ID	Mitigation Method	Contingency Plan
FC.FUN.AVN.01,i	Use of certified autopilot systems	Provide stall warnings to prevent significant speed decreases
FC.FUN.AVN.01,ii	Use of certified autopilot systems	Provide overspeed warnings
FC.FUN.AVN.01.1	Use of certified autopilot systems	Provide extreme attitude warnings
FC.FUN.AVN.01.2	Safe life electronics design	Ensure UAV static and dynamic stability
FC.FUN.AVN.02	Safe life electronics design	No need due to low failure impact
FC.FUN.AVN.04.1,i	Redundant sensor types	Provide overspeed warnings
FC.FUN.AVN.04.1,ii	Redundant sensor types	Provide extreme attitude warnings
FC.FUN.AVN.04.2	Redundant sensor types	Ensure sensor functionality at large range of altitudes
FC.FUN.AVN.04.3	Redundant sensor types	Validate attitude with visual sensors/ radar
FC.FUN.AVN.04.4,i	Verify and Validate sensors	No need due to low failure impact
FC.FUN.AVN.04.4,ii	Verify and Validate sensors	Catastrophic failure, no contingency possible
FC.FUN.AVN.04.5,i	Verify and Validate sensors	Catastrophic failure, no contingency possible
FC.FUN.AVN.04.5,ii	Verify and Validate sensors	No need due to low failure impact
FC.FUN.AVN.05,i	Safe life electronics design	Separate emergency electrical architecture
FC.FUN.AVN.05,ii	Safe life electronics design	Separate emergency electrical architecture
FC.FUN.AVN.05	Safe life electronics design	No need due to low failure impact
FC.FUN.PROP.01,i	Perform regular maintenance	Provide stall warnings which increase thrust
FC.FUN.PROP.01,ii	Perform regular maintenance	No need due to low failure impact
FC.FUN.PROP.02,i	Perform regular maintenance	Separate emergency electrical architecture for critical components
FC.FUN.PROP.02,ii	Use of regulated, certified power management systems; periodically check component functionality	Ensure circuit breakers are present in the system
FC.FUN.PROP.03	Use of regulated, certified fuel pumps; periodically check components	Measure fuel flow to engine and increase flow rate
FC.FUN.LG.01,i	Periodically check components	Catastrophic failure, no contingency possible

Table 13.7: Functional Hazards mitigation

Failure ID	Mitigation Method	Contingency Plan
FC.FUN.LG.01,ii	Ensure cg travel is within LG limits	Safety factors taken into account for structure to prevent significant damage
FC.FUN.LG.02	Landing flare to prevent overloading landing gear	Catastrophic failure, no contingency possible
FC.FUN.LG.03	Check take-off surface to be within acceptable limits	Abort take-off to ensure that minimal additional damage occurs
FC.FUN.LG.04.1	Check components before flight	Catastrophic failure, no contingency possible
FC.FUN.LG.04.2,i	Check components before flight	Brake while applying rudder and tail wheel steering
FC.FUN.LG.04.2,ii	Check components before flight	Use tail wheel for steering
FC.FUN.STR.01	Periodically check components	Catastrophic failure, no contingency possible
FC.FUN.STR.02	Periodically check components	Catastrophic failure, no contingency possible
FC.FUN.STR.03	Periodically check components	Catastrophic failure, no contingency possible
FC.FUN.STR.04	Check mountings before flight	Ensure wiring extra length so components don't disconnect
FC.FUN.STR.05	Periodically check components	Turn off engine and perform emergency landing
FC.FUN.WIN.01	Ensure weight is within calculated for wing sizing	Increase flight speed to ensure lift still occurs
FC.FUN.WIN.02	Perform aerodynamic analysis of aircraft with control surface	Consider redesigning control surfaces
FC.FUN.CNS.01	Ensure static and dynamic stability through calculating control derivative	Make sure autopilot can deal with unstable aircraft
FC.FUN.CNS.02	Ensure static and dynamic stability through calculating control derivative	Make sure autopilot can deal with unstable aircraft
FC.FUN.CNS.03,i	Ensure CG is within scissor plot limits	Make sure autopilot can deal with unstable aircraft
FC.FUN.CNS.03,ii	Ensure CG is within scissor plot limits	Make sure autopilot can deal with unstable aircraft
FC.FUN.CNS.04	Perform aerodynamic analysis of aircraft with control surface	Consider redesigning control surfaces
FC.FUN.TOF.4.2.5	Test engine performance prior to flight	Catastrophic failure, no contingency possible
FC.FUN.TOF.4.2.4	Test engine/ brakes prior to take-off	Catastrophic failure, no contingency possible
FC.FUN.TOF.4.2.4.a	Test engine performance prior to flight	Ensure measure to cut off fuel flow to engine
FC.FUN.TOF.4.2.7	Test engine performance prior to flight	Catastrophic failure, no contingency possible
FC.FUN.COM.4.E.2.4,i	Periodically check components	No need due to low failure impact
FC.FUN.COM.4.E.2.4,ii	Periodically check components	No need due to low failure impact
FC.FUN.COM.4.3.5,i	Periodically check components	No need due to low failure impact
FC.FUN.COM.4.3.5,ii	Periodically check components	No need due to low failure impact
FC.FUN.COM.4.3.6	Periodically check components	No need due to low failure impact
FC.FUN.COM.4.4.1.c	Add landing permission to operator checklist	Ensure landing location is safe
FC.FUN.COM.4.2.2.c	Request permission ahead of time	No need due to low failure impact
FC.FUN.COM.4.N.7,i	Periodically check components	No need due to low failure impact
FC.FUN.COM.4.N.7,ii	Periodically check components	No need due to low failure impact
FC.FUN.COM.4.E.1.c,i	Periodically check components	Ensure on board systems can deal with error autonomously
FC.FUN.COM.4.E.1.c,ii	Periodically check components	Ensure on board systems can deal with error autonomously
FC.FUN.COM.4.E.1.c,iii	Periodically check components	Consider adding redundant additional
FC.FUN.SUS.4.S.1.2,i	Periodically check components, take safety factors into account when designing structure	Replace cracked and damaged structural components
FC.FUN.SUS.4.S.1.2,ii	Periodically check components, take safety factors into account when designing structure	Replace cracked and damaged structural components
FC.FUN.SUS.4.S.1.2,iii	Periodically check components, take safety factors into account when designing structure	Catastrophic failure, no contingency possible
FC.FUN.SUS.4.S.1.3	Periodically check components, take safety factors into account when designing structure	Replace cracked and damaged structural components
FC.FUN.SUS.4.S.2.1,i	Periodically check components, take safety factors into account when designing structure	Replace cracked and damaged structural components
FC.FUN.SUS.4.S.2.1,ii	Periodically check components, take safety factors into account when designing structure	Catastrophic failure, no contingency possible
FC.FUN.SUS.4.S.2.2	Periodically check components, take safety factors into account when designing structure	Replace cracked and damaged structural components
FC.FUN.SUS.4.S.1.4	Periodically check components, take safety factors into account when designing structure	Replace cracked and damaged structural components
FC.FUN.PRE.4.1.2	Periodically check components and wiring	No need due to low failure impact
FC.FUN.PRE.4.1.3.1,i	Redundant sensors for system functionality	No need due to low failure impact
FC.FUN.PRE.4.1.3.1,ii	Redundant sensors for system functionality	Return and land
FC.FUN.PRE.4.1.3.2,i	Redundant sensors for system functionality	No need due to low failure impact
FC.FUN.PRE.4.1.3.2,ii	Redundant sensors for system functionality	Return and land

Table 13.7: Functional Hazards mitigation

Failure ID	Mitigation Method	Contingency Plan
FC.FUN.PRE.4.1.3.3,i	Redundant sensors for system functionality	No need due to low failure impact
FC.FUN.PRE.4.1.3.3,ii	Redundant sensors for system functionality	Catastrophic failure, no contingency possible
FC.FUN.PRE.4.1.3.4,i	Redundant sensors for system functionality	No need due to low failure impact
FC.FUN.PRE.4.1.3.4,ii	Redundant sensors for system functionality	Catastrophic failure, no contingency possible
FC.FUN.PRE.4.1.3.5,i	Redundant sensors for system functionality	No need due to low failure impact
FC.FUN.PRE.4.1.3.5,ii	Redundant sensors for system functionality	Return and land
FC.FUN.SRC.4.3.1	Ensure safety margins in communications architecture	Ensure control from ground possible
FC.FUN.SRC.4.3.2,i	Ensure ground mapping prior to search	No need due to low failure impact
FC.FUN.SRC.4.3.2,ii	Cover the search area multiple times	Reperform mission
FC.FUN.SRC.4.3.3	Ensure redundancy in autonomous control architecture	Manually control UAV to search
FC.FUN.SRC.4.3.4	Check limits before flight	Vacate restricted area and return to land
FC.FUN.SRC.4.3.7	Ensure safety margins in communications architecture	Ensure control from ground possible
FC.FUN.LND.4.4.1.a	Multiple redundant sensors check landing location suitability	Catastrophic failure, no contingency possible
FC.FUN.LND.4.4.1	Multiple redundant sensors check landing location suitability	No need due to low failure impact
FC.FUN.LND.4.4.1.b	Perform go-around in case UAV is unaligned	Ensure sufficient control on ground to realign with landing area
FC.FUN.LND.4.4.3,i	Take conservative requirements for go-around: if there is a possible need to abort landing, do not risk landing	Ensure that UAV can stop within determined landing area
FC.FUN.LND.4.4.3,ii	Ensure reserve fuel is sufficient to perform go-around and loiter	Catastrophic failure, no contingency possible
FC.FUN.LND.4.4.4.a	Periodically check components	Cut off fuel flow to engine
FC.FUN.LND.4.4.4.b	Periodically check components	Reduce landing distance with the use of opposite rudder inputs
FC.FUN.LND.4.4.7	Periodically check components	Disconnect electrical system
FC.FUN.EMG.4.E.1.a,i	Ensure multiple redundant sensors are present to detect emergency	No need due to low failure impact
FC.FUN.EMG.4.E.1.a,ii	Ensure multiple redundant sensors are present to detect emergency	Catastrophic failure, no contingency possible
FC.FUN.EMG.4.E.1.b	Periodically check components	Paint UAV with bright colors to be easily spotted visually
FC.FUN.EMG.4.E.2.1.a,i	Multiple redundant sensors check landing location suitability	Catastrophic failure, no contingency possible
FC.FUN.EMG.4.E.2.1.a,ii	Multiple redundant sensors check landing location suitability	Perform landing in any non-catastrophic area, i.e. not in a mine-field
FC.FUN.EMG.4.E.2.1.b,i	Perform go-around in case UAV is unaligned	Ensure sufficient control on the ground
FC.FUN.EMG.4.E.2.1.b,ii	Take conservative requirements for go-around: if there is a possible need to abort landing, do not risk landing	Ensure that UAV can stop within determined landing area
FC.FUN.EMG.4.E.2.1.c,i	Multiple redundant sensors check landing location suitability	Catastrophic failure, no contingency possible
FC.FUN.EMG.4.E.2.1.c,ii	Multiple redundant sensors check landing location suitability	Perform landing in any non-catastrophic area, i.e. not in a mine-field
FC.FUN.GND.4.1.1.a	Ensure refuelling is part of take-off checklist	Ensure fuel sensors are present that prevent take-off procedure
FC.FUN.GND.4.1.1.b,i	Check batteries prior to take-off	Ensure battery level sensors are present that prevent take-off procedure
FC.FUN.GND.4.4.2.b,ii	Periodically check components	Reduce landing distance with the use of opposite rudder inputs
FC.FUN.ENG.4.W.1.1	Take safety margins for power budget	No need due to low failure impact
FC.FUN.ENG.4.W.1.2	Take safety margins for power budget	No need due to low failure impact
FC.FUN.ENG.4.W.1.3	Redundant emergency battery for navigation sensors	Catastrophic failure, no contingency possible
FC.FUN.ENG.4.W.1.4	Make sure alternator first provides electricity to engine	Perform emergency landing
FC.FUN.ENG.4.W.1.5	Redundant emergency battery for control actuators	Catastrophic failure, no contingency possible
FC.FUN.ENG.4.W.2	Periodically check components	Perform emergency landing
FC.FUN.ENG.4.W.3	Periodically check components	Perform emergency landing

13.2. Logistics and Operations

Various aspects related to logistics have to be considered to ensure smooth operation of the UAV during minefield-mapping missions. The various stages of operations considered from a point-of-view focusing on logistics are detailed in Figure 13.1. The lifecycle of the UAV begins with manufacturing, testing and certification, which are detailed in Figure 15.1. At the same time, operators for the UAV can be trained so they can obtain the necessary certifications to operate such an aircraft in the target countries. Operators can be existing employees of the customer, or external personnel that can be employed by the customer at the same time as acquiring the UAV. In either case, there is the issue that ideally, the operator should be someone who is capable of controlling the UAV manually in case of emergency, while also having sufficient knowledge about minefields to be able to analyze the data produced by the payload of the UAV to locate possible minefields.

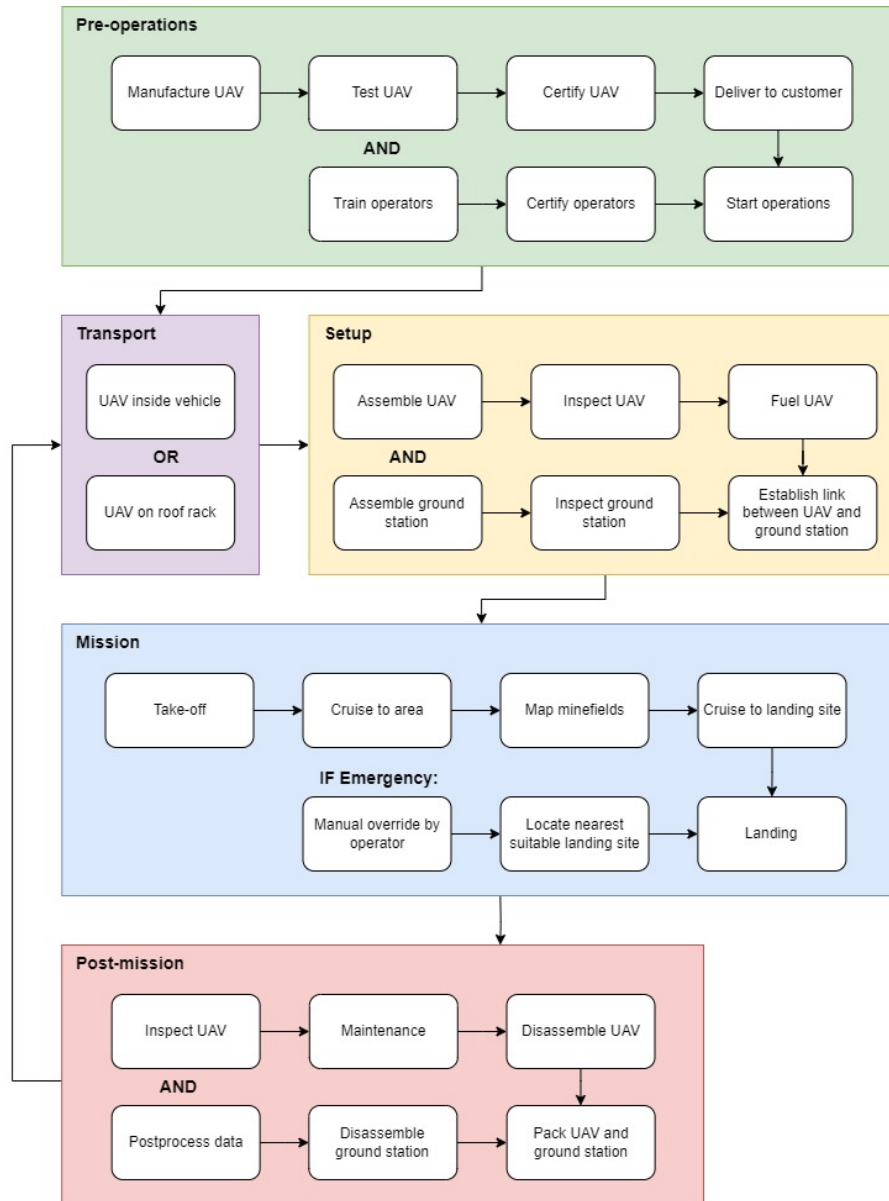


Figure 13.1: Operational flow diagram

Once the operator has been trained and certified and the completed UAV has been delivered to the customer, the actual operations begin with transporting the UAV to the site. Depending on the capacity of the vehicle used, the UAV can be transported either inside or on top of the vehicle. As the wingspan of 4.25 m is quite large, the wings are designed to be detachable near the root, so they can be transported separately, either in the back of a large car or attached to the roof rack.

Besides the UAV and ground station, fuel needs to be transported and thus makes an integral part of logistics. Standard gasoline is used to fuel the aircraft. Therefore fuel can be acquired locally as special fuels such as aviation gasoline don't need to be obtained. For safety reasons it is important that the UAV is emptied of fuel before transportation and fuel is only transported in containers meant for transportation of fuel, such as jerrycans. For this reason, the fuel tank of the UAV should have a drain valve or plug, and it should be emptied of fuel after every mission.

Once the area of operations has been reached, a suitable runway has to be located and prepared. An available straight 500 m stretch of road should have been identified from a map beforehand. It should be verified that its surface is suitably smooth for take-off and landing of the UAV, and it should be cleared of any possible debris. Additionally, traffic should be assessed, as traffic on the road needs to be stopped or redirected during take-off and landing of the UAV. Finally, beacons should be placed on the sides of the road to help the UAV align itself with the road during landing.

The main part of the setup before a mission is assembling the UAV to flight configuration. After assembly, it should be inspected thoroughly to make sure that there is no damage or signs of fatigue, and all components work as intended. At the same time, the ground station can be assembled and inspected, mainly by extending the antenna and setting it up at an elevated spot. Once the UAV and ground station have been set up and inspected, both can be turned off and communications between the two systems established and tested.

The mission itself is divided into five distinct phases: take-off, cruise to mission area, minefield mapping, cruise back to landing site, and landing. During nominal operations, all phases are carried out autonomously, with the operator merely monitoring the UAV. If there is an emergency during any of the phases, the operator is expected to assess the situation and, if communication is not lost, take over manual control. Depending on the emergency at hand, the UAV should either return directly to the original take-off site, or if engine power is lost and the distance is too large, the operator should locate the nearest suitable emergency landing site and guide the UAV to land there.

After a mission, whether successful or interrupted by a malfunction, inspection and maintenance of the UAV should be carried out. Inspection is done after every mission to assure that no damage has been sustained. Regular maintenance is carried out between a specified number of flight hours to ensure that the UAV stays operational for as long as possible. After inspection and possible maintenance, the wings of the UAV can be disassembled, the fuel tank emptied and the UAV converted into the transport configuration. At the same time, all data from the mission is analyzed and saved, and the ground station is disassembled and packed.

13.3. Reliability, Availability, Maintainability and Safety

In this section, the RAMS characteristics are discussed. This means specifically the concepts of reliability, availability, maintainability and safety. Reliability is a measure of how likely the system is to be able to perform its mission. Availability shows how often the system can be used. Maintainability is concerned with keeping the UAV operational. Finally, safety is mostly related to the aircraft being fail-safe. If something fails, loss of life and property must be avoided.

13.3.1. Reliability

In the previous report a preliminary reliability estimate has been developed according to statistical data based on similar UAVs. Chiesa et al. [133] presents both a small compilation of reliability and maintainability characteristics for (mainly military) UAVs, and a method for extrapolating these and estimating them for other designs. As such, a very rough estimate for a low altitude, short to medium endurance UAV puts the mission failure rate at $1.5 \times 10^{-3} \text{ h}^{-1}$ – one failure every 667 flight-hours – where mission failure constitutes solely critical failures that prohibit the completion of the mission [133]. This is an estimate that takes into account the added complexity inherent to military applications [133], while this complexity does not apply to the UAV presented in this report.

Following the selection of the most critical components of the UAV, it should be possible to make a more educated estimate of the vehicle's reliability. Inspecting the Mean Time Between Failures (MTBF) of components, a joint MTBF should be established for the aircraft as a whole.

The first component investigated is the engine. Unfortunately, the Genpod 120 LRU documentation does not provide information about the failure rate of the engine [24]. This is further exasperated by the fact that, as small two-stroke engines are very niche, there is insufficient information to calculate the specific MTBF of the engine based on known parameters. Thus, no reliability estimate can be made for the engine, and this is necessary to establish during testing instead.

For the electrical components, only the VN-200CR provides a MTBF of 150 000 h [68]. Additionally, the MS4525DO airspeed sensor provides a mean time to failure of more than 10 years, at least 87 660 h [77].

Given this general lack of information about the reliability of components, it is not possible to make an updated estimate for the aircraft reliability at this stage. Reliability of the airframe must instead be established either through thorough testing or with additional communication with manufacturers and requests for additional information. Hence, at this stage, the preliminary estimate of mission failure rate of $1.5 \times 10^{-3} \text{ h}^{-1}$ stands.

13.3.2. Availability

The availability of the system depends on the amount of maintenance work that is actually carried out, and on the "basic" failure rate. This includes all minor failures, which increase maintenance required, but do not cause the entire mission to fail. Based on Chiesa et al. [133], an estimate for the basic failure rate can be provided, similarly to that for mission

failure rate; this puts the basic failure rate at $15.1 \cdot 10^{-3}$ per flight-hour. More thorough availability estimates are even harder to provide at this stage of the design, especially since they depend heavily on the amount of maintenance work that is actually carried out.

However, for some components, the availability can be estimated. The engine maintenance schedule requires a full overhaul at the original manufacturer every 300 hours [24]. While the manufacturer recommends bringing a spare engine everywhere, as the engine can easily be replaced, this is an expensive and impractical option. Thus, it can be expected that the engine is removed for maintenance every 50-100 flights. For other components, maintenance requirements may be lower.

In addition to the total overhaul every 300 hours, there are also other jobs on the maintenance schedule. Spark plugs and air filters should be checked and adjusted every 50 hours and replaced every 100 hours [24]. In addition, the fuel filter requires checking every 50 hours [24]. These maintenance tasks are less extensive than the total overhaul and can be done by untrained personnel in the field. Thus, the effect of this maintenance on availability is limited.

13.3.3. Maintainability

The initial estimate for the maintenance requirements puts the maintenance man-hours per flight hour at 0.75 [133]. Again, this estimate is meant for complex military applications, where maintainability is not taken into account at an early stage of the design [133]. At a later stage, a full estimate for required maintenance can be performed.

Nonetheless, maintainability has been taken into account when designing the UAV. The engine is fully replaceable as a unit [24], making maintenance much simpler. In addition, the UAV does not have a retractable landing gear, flaps or airbrakes. This lack of moving parts on the aircraft (other than the control surfaces) further reduces required maintenance. Obviously, the most maintainable part is a part that does not exist in the first place. Accessibility has also been considered, as accessibility leads to easier maintenance [134, p. 97]. While also practical for other purposes, putting the avionics in the front makes it easier to access. In addition, all avionics are placed on a single plate, making maintenance less tedious. At a later stage, the inclusion of inspection holes can make maintenance and inspection of the airframe even easier.

The aircraft is expected to undergo regular, scheduled maintenance. While such maintenance is easy to schedule and plan for, it may be relatively wasteful. To avoid unnecessary maintenance, using artificial intelligence and data-driven techniques may be beneficial [135]. However, such techniques are far outside the scope of this project. Nevertheless, this is a side-track to further explore.

13.3.4. Safety

Reliability has already been extensively discussed. Therefore, this section mostly functions on the fail-safe principle, so how to avoid fatalities in case of a failure. Based on the fact that the most mined areas in the world are often sparsely populated, that minefields are generally not inhabited and the fact that the UAV carries no crew, it is expected that the risk posed to other persons is minimal. Nonetheless, a thorough safety analysis is required to determine the actual likelihood of an uncontrolled crash due to control failure, which is the scenario in which danger can be posed to other persons. This requires first an analysis of the probability of failure of each component. These probabilities lead to a likelihood of different failure scenarios. During the actual software design of the autopilot, these scenarios need to be taken into account when writing the software.

In case of a failure, under ideal circumstances the glide ratio is equal to the lift-to-drag ratio [53]. Given the lift-to-drag of roughly 10, this implies that the aircraft can find a landing spot within 800 m. However, this assumes that the aircraft does not need to turn, has full command and control, and is able to instantly recognize the need for an emergency landing. It need not be explained that these assumptions are not always valid. To improve safety and safe recovery of the aircraft it may be necessary to fly only over suspected hazardous areas smaller than 400 m in diameter. This makes the aircraft much more likely to find a safe (crash-)landing spot, outside a potential minefield.

Verification and Validation

In this chapter, the system as a whole will be verified and validated. In the previous chapters, the subsystems were treated individually which included code verification, unit tests, subsystem requirement verification and assumptions validations. Now, for the system as a whole, all system requirements are verified to check whether they are met in section 14.2. After this, the product will be validated to check whether it can actually perform its mission.

14.1. Model validation

During this project, the two main models that are used for validation are 3DExperience and XFOILR-5 which means that these models are to be validated as well. Since 3DExperience, the CATIA functions specifically, is used for relatively easy calculations, it does not need additional validation when the calculations it is used to validate match its outcomes. This was the case in chapter chapter 7 in which 3DExperience was used to calculate the weight of separate components. XFOILR-5 however, had to be validated as a model. This is because it is used to calculate aerodynamic characteristics which highly impact the stability and control characteristics as well. Out of the three model validation methods (experience, analysis and comparison) XFOILR-5 has been compared to test data at the Atmospheric Flight Mechanics Conference in 2016 [136]. It was stated that, through validation with a wind tunnel experiment that resembles the same conditions as the XFOILR-5 model, for low Reynolds numbers, XFOILR 5 is sufficiently accurate. Also, experience has shown that XFOILR 5 has been used as a source of validation for previous research. In 2022 it was used to validate results of a remotely controlled design-build-fly application [137]. Altogether, previous experience and comparison led to the conclusion that XFOILR 5 is a reasonable validation model to use in this project.

14.2. Product verification

To ensure the requirements that were set up in the baseline report are met, a series of compliance matrices are set up. In these matrice it is indicated whether the requirement is met and with what method and how that is verified. In this section, first the stakeholder requirements are analyzed. Then the mission requirements are looked at, after which the functional requirements of the UAV are checked. For each subsystem, there are also subsystem requirements to be verified. This is done in the chapter that entails the respective subsystem. When all lower-level flow-down requirements are met, the parent requirement shall also be met. For requirements that do not have specific flow-downs, the requirement is checked here.

14.2.1. Compliance Matrices

The compliance of the design to requirements are separated into levels of compliance. Requirements that are fully met are marked with a ✓ to indicate their completion. If necessary preconditions are provided for the completion of a requirement are done, but there is still major work required before the requirement can be seen as completed, requirements are marked ITC for Intended To Comply. Failed requirements are marked as Failed in the compliance matrix. Finally, requirements that are not in the current scope of the project and thus not evaluated are marked as OOS for Out Of Scope.

Requirements may also be stricken if they no longer apply, either due to in-applicability to current design or if the background is found to be incorrect.

The customer and stakeholder requirements compliance matrix is given in Table 14.1. Table 14.3 then provides the verification of the mission requirements. Finally, the functional requirements are checked in Table 14.3.

Table 14.1: Verification of customer and stakeholders requirements

Identifier	Check	Verification method	Requirement description
Mission			
STK-0.1.1	✓	Inspection: Fulfilled according to the functional requirements in Table 14.3	The minesweeper shall maintain a data link with the ground station over a range of at least 30 km.
STK-0.1.2	✓	Inspection: When customers are determined, the labour costs in respective regions are to be established	The minesweeper shall not cost more than €500k per aircraft.
STK-0.1.3	ITC		The operational costs, excluding ground personnel, shall be no more than €100 per hour.
Payload			
STK-0.2.1	✓	Inspection: Fulfilled according to the functional requirements in Table 14.3	The minesweeper shall be able to carry a payload of 10 kg.
STK-0.2.2	✓	Inspection: Fulfilled according to the functional requirements in Table 14.3	The minesweeper shall be able to carry a payload with dimensions 0.4m×0.5m×0.3m (width×length×height).
STK-0.2.3	ITC	Inspection: This shall be taken into consideration when choosing the sensors	Minefield detection sensor shall output the detection of a minefield, its size, bounds and probability of detection.
STK-0.2.4	✓	Inspection: Fulfilled according to the functional requirements in Table 14.3	Minefield detection shall be related to ground crews, along with the location, time, ground speed, and altitude of UAV, in real time.
STK-0.2.6	✓	Inspection: Fulfilled according to the functional requirements in FUN-ENG-4.W.1.1	The minesweeper shall provide at least 500 W of electrical power to the sensor payload.
Performance			
STK-0.3.1	✓	Analysis: Aircraft loading diagram, XFLR5	The minesweeper shall have an endurance of 4 hours.

STK-0.3.2-CND	✓	Analysis: Gear design	The minesweeper shall be able to take off and land vertically or from an unmaintained road of 500m long and 8m wide.
STK-0.3.3-CND	✓	Inspection: Fulfilled according to the chapter 11	The stall speed shall not be higher than 20 m/s.
STK-0.3.4	ITC	Demonstration: This will be done during flight tests	The minesweeper shall be able to perform pre-determined search patterns autonomously.
STK-0.3.5	ITC	Demonstration: This will be done during flight tests	The minesweeper shall be able to accept changes to the pre-determined mission while in flight.
STK-0.3.6	✓	Analysis - Aircraft loading diagram	Search patterns shall be executed at an altitude of 80 m above ground.
STK-0.3.7A	✓	Analysis - Aircraft loading diagram, XFLR5	Search patterns shall be executed at a ground speed of more than 15 m/s.
STK-0.3.7B	✓	Analysis - Aircraft loading diagram, XFLR5	Search patterns shall be executed at a ground speed of less than 40 m/s.
STK-0.3.8	Stricken	-	The minesweeper shall be able to fly in all climate conditions where mines are currently found.
STK-0.3.9	✓	Analysis: Control & Stability	The minesweeper shall be able to fly in adverse weather, not including storm conditions.
Safety and reliability			
STK-0.4.1	✓	Inspection: Explained in chapter 9	The minesweeper shall have autonomous obstacle avoidance system.
STK-0.4.2			The minesweeper shall have an ADS-B transceiver.
STK-0.4.3	ITC	Inspection: Required to meet flow down requirement	The minesweeper shall be able to fly in manned airspace.
STK-0.4.4	ITC	Inspection: This will be done during flight tests	The minesweeper shall remain in a pre-defined flight area.
STK-0.4.5	ITC	Test: This will be done during flight tests	The minesweeper shall have redundancy on critical flight control systems.
STK-0.4.6	ITC	Analysis: This will be done during flight simulation	The minesweeper shall be able to make a controlled crash-landing in a pilot chosen location in case of failure.
Sustainability			
STK-0.5.1-OPT	✓	Inspection: Fulfilled according to flow-down requirement FUN-PRO-2.3	Materials chosen shall be sustainable
STK-0.5.2-OPT	ITC	Inspection: This will taken into account during manufacturing	The minesweeper shall reuse military or civilian drone hardware.
Operator			
STK-1.1	ITC	Analysis: During flight simulation this can be tested	The health of the UAV operator shall not be endangered.
STK-1.2	✓	Inspection:	The UAV shall be able to takeoff within 30 km of the minefield.
STK-1.3	ITC	Analysis: During flight simulation this can be tested	The use of the UAV shall not endanger the operator during nominal operation.
STK-1.4	ITC	Inspection: This shall be determined after the sensors are chosen	The UAV shall report correctly whether a minefield is present.
STK-1.5	ITC	Inspection: This shall be determined after the UAV is developed	The UAV shall be available.
STK-1.6	✓	NO	The UAV shall have a long lifespan.
Developers/Engineers			
STK-2.1	✓	Inspection: See the report at hand	The detailed design of the UAV shall be completed by the end of DSE.
STK-2.3	✓	Inspection: One can see the fuselage has enough empty space	The UAV shall have space for stickers.
Investors			
STK-3.1	Stricken		The UAV shall be profitable for investors.
Deminers			
STK-4.2	ITC	inspection: Shall be proven to be safe	The operation of the UAV shall not endanger the demining crew, operator and operations.
Governments in Affected Countries			
STK-5.1	✓	Inspection:	The UAV shall be able to detect minefields cheaply.
Air Traffic Control			
STK-6.1	ITC	Inspection: Before operation this shall be ensured	The UAV shall not endanger other aircraft in the area during any part of operation.
STK-6.4			The UAV shall be able to communicate with air traffic control for the entire duration of the mission.
STK-6.5	ITC	Inspection:	The UAV shall be able to be uniquely identified from other aircraft operating in the area.
Civilian population			
STK-7.1	ITC	Test: When the UAV is tested, the sound waves shall be measured	The UAV shall not lead to hearing loss in the civilian population or hurt animals.
STK-7.2	ITC	Inspection: When the sensors for the UAV are chosen, this will be taken into account	The UAV shall not intervene with privacy of people living in proximity to minefields.
Regulating Agencies			
STK-9.1	✓	Inspection: Follows from research done in baseline report towards legal requirements	The UAV shall comply with all regulations.

Table 14.2: Verification of Mission Requirements

Identifier	Check	Verification method	Requirement description
STK-0.1.1-MIS-COM-1	✓	Inspection: Fulfilled by flow-down requirement SYS-AVN-COM-02	The UAV shall maintain a data link with the ground station over a range of at least 30 km.
STK-0.1.2-MIS-CST-1	✓	Inspection: Following from calculation in chapter 12	The UAV shall not cost more than €500k per unit.
STK-0.1.3-MIS-CST-2	✓	Inspection: Following from calculation in chapter 12	The operational costs, excluding ground personnel, shall be no more than €100 per hour.
STK-0.2.1-MIS-PLD-1	✓	Inspection: Following from flow down requirement SYS-FUS-02	The UAV shall be able to carry a payload of 10 kg.
STK-0.2.2-MIS-PLD-2	✓	Inspection: Following from flow down requirement SYS-FUS-03	The UAV shall be able to carry a payload with dimensions 0.4 m × 0.5 m × 0.3 m (width × length × height).
STK-0.2.3-MIS-PLD-3	OOS		Minefield detection sensor shall output the detection of a minefield, its size, bounds and probability of detection.
STK-0.2.4-MIS-PLD-4	OOS		Minefield detection shall be related to ground crews, along with the location, time, ground speed, and altitude of UAV, in real time.
STK-0.2.6-MIS-PLD-5	✓	Inspection: Fulfilled according to Figure 9.6.	The minesweeper shall provide at least 500 W of electrical power to the sensor payload.

STK-0.3.1-MIS-ENV-1	✓	Demonstration: Fulfilled according to flight performance	The UAV shall have an endurance of at least 4 hours for a temperature range between 5 °C and 35 °C and an altitude up to 2000 meters above mean sea level (MSL).
STK-0.3.8-MIS-ENV-3	ITC	Demonstration: Altitude analysis on endurance is done later	The UAV shall have an endurance of at least 2 hours at a minimum temperature of -5 °C and a maximum temperature of 45 °C and an altitude up to 4500 m above MSL.
STK-0.3.2-CND-MIS-TOF-1	✓	Fulfilled by flow-down requirement SYS-FP-02	The minesweeper shall be able to take off and land from an unmaintained road, at most 8 m wide and 500 m long for a density altitude of 5000 m.
STK-0.3.2-CND-MIS-TOF-2	ITC	Inspection: Further friction analysis is required.	The UAV shall be able to take off and land in vegetation of low intensity such as a grass field with a maximum height of 15 cm.
STK-0.3.2-CND-MIS-TOF-3	ITC	Demonstration: The correct obstacle height requires detailed analysis of the obstacles at the target area.	The UAV shall be able to clear an obstacle of TBDm height at TBDm distance after lift-off.
STK-0.3.2-CND-MIS-TOF-4- OPT	Stricken	Not relevant	The UAV shall be able to take off and land vertically.
STK-0.3.3-CND-MIS-ENV-2	✓	Inspection: Fulfilled by flow down requirement STK-0.3.3-CND	In case of a fixed wing UAV, the UAV shall have a speed of at most 20 m s ⁻¹ at an altitude of 2000 m above MSL.
STK-0.3.4-MIS-CTR-1	✓	Met according to chapter 9	The minesweeper shall be able to perform pre-determined search patterns autonomously.
STK-0.3.5-MIS-CTR-2	✓	Inspection: Fulfilled according to flow-down requirement SYS-AVN-AUT-04.	The minesweeper shall be able to accept changes to the pre-determined mission while in flight.
STK-0.3.6-MIS-SRC-1	✓	Met according to calculations in chapter 11	Search patterns shall be executed at an altitude of 80 m above ground.
STK-0.3.7A-MIS-SRC-2	✓	Met according to calculations in chapter 11	Search patterns shall be executed at a ground speed of more than 15 m s ⁻¹ .
STK-0.3.7B-MIS-SRC-3	✓	Met according to calculations in chapter 11	Search patterns shall be executed at a ground speed of less than 40 m s ⁻¹ .
STK-0.3.9-MIS-ENV-4	ITC		The UAV shall be able to take off and land with a cross wind of 9 m s ⁻¹ .
STK-0.3.9-MIS-ENV-5	✓	Analysis: Taken care of when doing flight performance analysis	The UAV shall be able to take off and land with a tail wind of 2 m s ⁻¹ .
STK-0.3.9-MIS-ENV-6- OPT	ITC	Analysis: As headwind is less limiting than tailwind, this requirement will be taken care of later.	The UAV shall be able to take off and land with a head wind of 15 m s ⁻¹ .
STK-0.3.9-MIS-ENV-7	✓	Inspection: Fulfilled according to flow-down requirement SYS-AVN-06.	The UAV shall be able to operate up until 4 mm of precipitation per hour.
STK-0.3.9-MIS-ENV-8	ITC		The UAV shall be able to operate up until TBDm s ⁻¹ gust speeds.
STK-0.4.1-MIS-CTR-3	ITC	Inspection: Intended to comply according to flow-down requirement SYS-AVN-AUT-07.	The UAV shall have autonomous obstacle avoidance system.
STK-0.4.2-MIS-CTR-4	✓	Inspection: Fulfilled according to flow-down requirement SYS-AVN-COM-01.	The UAV shall have an ADS-B transceiver.
STK-0.4.3-MIS-CTR-5	ITC	Inspection: Required to meet flow down requirement	The UAV shall be able to fly in manned airspace.
STK-0.4.4-MIS-CTR-6	ITC	Inspection: This will be done during flight tests	The UAV shall remain in a pre-defined flight area.
STK-0.4.5-MIS-CTR-7	✓	Inspection: Fulfilled according to flow-down requirement SYS-AVN-07.	The UAV shall have redundancy on critical flight control systems.
STK-0.4.6-MIS-CTR-8	ITC	Inspection: This will be done during flight tests	The UAV shall be able to make a controlled crash-landing in a pilot chosen location in case of failure.
STK-0.5.1- OPT -MIS-SUS-1	✓	Inspection: Fulfilled according to chapter 15	Materials chosen shall be sustainable.
STK-0.5.2- OPT -MIS-SUS-2	ITC	Inspection: This will taken into account during manufacturing	The UAV shall reuse military or civilian drone hardware.
STK-1.1-MIS-NSE-1- OPT	ITC	Analysis: Insufficient data available to do now	The operator of the UAV shall not be exposed to noise levels above 85dB, averaged over 8 hours.
STK-1.2-MIS-RNG-1	✓	Analysis: Included in fuel fractions of chapter 11.	The UAV shall have a 30km cruise range to search area.
STK-1.3-MIS-SAF-1	OOS		The UAV shall have a risk of injury of the operator of less than TBD per flight hour.
STK-1.4-MIS-SRC-4	OOS		The UAV shall not have a false negative rate larger than TBD.
STK-1.4-MIS-SRC-5	OOS		The UAV shall not have a false positive rate larger than TBD.
STK-1.5-MIS-REL-1	OOS		The UAV shall have a reliability of TBD per flight hour.
STK-1.5-MIS-REL-2	OOS		The UAV shall have an availability of TBD%.
STK-1.6-MIS-REL-3	OOS		The UAV shall have an operational lifespan of TBD.
STK-2.1-MIS-MNG-1	✓	Demonstration: The design has taken place.	The detailed design of the UAV shall be completed by June 28th 2024.
STK-2.3-MIS-VIS-2- OPT	✓	Inspection: Can be taken from chapter 7	The UAV shall have one or more dedicated surface(s), with a total area of at least 100 square centimetres, for sponsorship and stickers.
STK-3.1-MIS-CST-3	Stricken		The UAV shall achieve a return-on-investment of TBD percent after TBD years.
STK-3.1-MIS-CST-4	Stricken		The UAV shall achieve the break-even point after TBD years, counted from May 1st 2024.
STK-3.1-MIS-CST-5	✓	Inspection: Follows from chapter 12	The UAV shall not cost more than 500k to develop.
STK-4.2-MIS-SAF-3	ITC		All sharp edges of the UAV shall be clearly marked.
STK-5.1-MIS-CST-6	ITC		The UAV shall be able to detect minefields for a price lower than 1.5 US\$ per square meter.
STK-6.1-MIS-SAF-4	✓	Inspection: Fulfilled according to flow-down requirement SYS-AVN-COM-01.	The UAV shall have detect-and-avoid functionality.
STK-6.4-MIS-COM-2	✓	Inspection: Fulfilled according to Figure 9.8 and Figure 9.9.	The UAV shall be able to communicate its current position, speed, altitude, identification number, and heading
STK-6.4-MIS-COM-3	Stricken		The UAV shall be able to communicate with air traffic control for the entire duration of the mission.
STK-6.5-MIS-COM-4	✓	Inspection: Fulfilled according to flow-down requirement SYS-AVN-COM-01.	The UAV shall be able to be uniquely identified from other aircraft operating in the area.
STK-7.1-MIS-NSE-2	OOS		The UAV noise level shall be below TBD dB at TBD distance.
STK-7.1-MIS-NSE-3	OOS		The UAV shall not produce noise with a volume above 45 dB above 20 kHz and below 20 Hz.
STK-7.2-MIS-SAF-5	ITC		The UAV shall not intervene with privacy of people living in proximity to minefields.
STK-9.1-MIS-LGL-1	ITC		The UAV communications shall comply with the EU radio equipment directive 2014/53/EU.
STK-9.1-MIS-LGL-2	OO		The UAV design shall be registered with EASA.

STK-9.1-MIS-LGL-3	✓	Inspection: Avionics includes a remoteID system for identification.	The UAV shall be equipped with a remote identification system.
STK-9.1-MIS-LGL-4	ITC	Analysis: This extra fuel or battery power requires additional analysis.	The UAV shall have a minimum reserve fuel or electric power of 15% at the end of nominal operations.
STK-9.1-MIS-LGL-5	✓	Analysis: Shown to be fulfilled in chapter 11.	The UAV shall have a minimum rate of climb of at least 30.48 m min ⁻¹ .
STK-9.1-MIS-LGL-6	✓	Following from chapter 9	The UAV shall have an altimetry system to determine the altitude of the vehicle above ground level.

Table 14.3: Functional Requirements

ID	Check	Method & Reasoning	Requirement
Design (DES)			
FUN-DES-1	✓	Inspection: A report about the design is made	The minesweeper design shall take place.
FUN-DES-1.1	✓	Inspection: A Gantt chart is generated	The project Gantt chart shall define the timing and deadline management.
FUN-DES-1.2	✓	Inspection: A Work Breakdown Structure is provided.	The project work breakdown structure shall define the tasks to be worked on.
FUN-DES-1.3	✓	Inspection: A work flow diagram is provided.	The work flow diagram shall define the work process to be undertaken for design.
Transport (TRA)			
FUN-TRA-2.7	✓	Demonstration: Fitting the parts of the minesweeper in a car	All parts shall be transportable by road vehicles.
FUN-TRA-2.11	✓	Demonstration: Fitting the parts of the minesweeper in a car	All sub-assemblies shall be transportable by road vehicles.
FUN-TRA-3.4.1.i	ITC	Inspection: Disassembling the UAV	The UAV shall be able to be disassembled within two hours into multiple smaller parts.
FUN-TRA-3.4.1.ii	ITC	Demonstration: Transport the UAV in such trailer	The UAV with all operating equipment shall be transportable by road on a single 750kg limit trailer.
FUN-TRA-3.4.1.iii	ITC	Inspection: Put the UAV in such container	The UAV with all operating equipment shall be able to fit in an ISO standard 40ft shipping container.
FUN-TRA-5.0.4.2	ITC	Inspection: Put the UAV in such container	Once determined that the retired UAV will be given to a new owner, the UAV shall be transportable on a 750kg limit trailer, to the retirement location.
Produce (PRO)			
FUN-PRO-2.i	ITC	Inspection: Look at manufacturing location	All manufacturing and assembly shall be done in an enclosed environment.
FUN-PRO-2.ii	ITC	Inspection: Check the laws	All manufacturing and assembly shall be done following the local work environment laws.
FUN-PRO-2.1	✓	Demonstration: Following from decisions made in chapter 15	In case of different manufacturing methods are identified, a trade-off shall be made.
FUN-PRO-2.2	OOS		Final assembly shall be done in the European Union.
FUN-PRO-2.3	✓	Inspection: See that research is done in chapter 15	New manufacturing techniques shall be considered if they can be deemed as beneficial for the development of new components, sub assemblies or assemblies.
FUN-PRO-2.4	ITC	Inspection: When additional technology is made and manufacturers have been chosen	The UAV shall be able to be produced by technologies with a technology readiness level of 7 or higher.
FUN-PRO-2.13	ITC	Inspection: Fly the plane	The final assembly shall be flown at least once before release to the customer.
Retire (RET)			
FUN-RET-5.1	ITC	Inspection: When product is developed, regulations shall be written about this	The operator shall leave identification of when the UAV will need to be retired due to performance losses, to the manufacturer.
FUN-RET-5.1.1	ITC	Inspection: When product is developed, training shall be given to respective party	The manufacturer shall be able to identify performance losses.
FUN-RET-5.1.2	ITC	Inspection: When product is developed, training shall be given to respective party	The manufacturer shall be able to perform a trade off for retirement.
FUN-RET-5.3.a	ITC	Inspection: When retirement arises, this can be checked	NGOs shall be asked if they wish to obtain the retired drone.
FUN-RET-5.3.b	ITC	Inspection: When retirement arises, this can be checked	Research centres shall be asked if they wish to obtain the retired drone.
FUN-RET-5.3.c	ITC	Inspection: When retirement arises, this can be checked	Military users shall be asked if they wish to obtain the retired drone.
FUN-RET-5.3.d	ITC	Inspection: When retirement arises, this can be checked	General users shall be asked if they wish to obtain the retired drone.
FUN-RET-5.4.1	✓	Demonstration: Taking it apart according to chapter 15	The drone shall be able to be fully disassembled.
FUN-RET-5.5.1	ITC	Inspection: Statistics after decades of operation.	At least 5% of the UAV subassemblies shall be reusable after retirement.
FUN-RET-5.5.2	✓	Demonstration: Recycling plan in section 16.2	At least 80% of the entire UAV system shall be recyclable after retirement.
FUN-RET-5.6.1	ITC	Inspection: Statics after prolonged use	At least 20% of the UAV's components shall be reusable after retirement.
FUN-RET-5.6.2	✓	Demonstration: Statics after decades of use.	The metal components from the UAV system shall be recyclable.
FUN-RET-5.6.3	ITC	Inspection: Statics after decades of use.	10% of the electrical components from the UAV system shall be recyclable.
FUN-RET-5.6.4	✓	Demonstration: Minimal use of plastic in UAV, PVC film recyclable, see section 16.2.	40% of the plastic components from the UAV system shall be recyclable.
Communicate with external parties (EXT)			
FUN-EXT-3.1.1	✓	Inspection: The market analysis can be seen in chapter 12	Potential buyers shall be identified following a market analysis.
FUN-EXT-3.3	ITC	Inspection: When the distribution process is on the planning, this can be ensured	A distribution method shall be determined in agreement with the user.
FUN-EXT-3.2	ITC	Inspection: When the selling process is on the planning, this can be ensured	The price shall be decided in agreement with the user.
FUN-EXT-3.4.2.i	ITC	Inspection: This will be taken into account when a manufacturer is chosen.	The UAV shall be able to be picked up directly from production facility.
FUN-EXT-3.4.2.ii	✓	Inspection: Assembly happens at the manufacturing location according to chapter 15	The UAV shall be fully assembled at the production facility, with no assembly required by the customer, except for ease of transport.

FUN-EXT-3.1.2	ITC	Inspection: This will be done when the individual customers are determined	The willingness of the customer to collaborate with the producers shall be investigated.
FUN-EXT-2.6	ITC	Inspection: When the UAVs design is detailed enough, application for certification will be ensured	The parts shall be certified by competent authorities.
FUN-EXT-2.10	ITC	Inspection: When the UAVs design is detailed enough, application for certification will be ensured	The assemblies shall be certified by competent authorities.
FUN-EXT-2.14	ITC	Inspection: When the UAV's design is detailed enough, application for certification will be ensured	The final assembly shall be certified by competent authorities.
Takeoff (TOF)			
FUN-TOF-4.2.2.a FUN-TOF-4.2.2.b FUN-TOF-4.2.4	Stricken Stricken ✓	Inspection: Fulfilled by flow-down requirement SYS-FP-02	The UAV shall be able to undergo transition to take-off mode. The UAV shall be able to extend HLD. The UAV shall be able to abort takeoff and come to a complete stop within a runway of a length of 500 meters at any point during take-off in case of failure.
FUN-TOF-4.4.2.a FUN-TOF-4.2.5 FUN-TOF-4.2.5.i	OOS ✓ Stricken	Analysis: A python model is used in chapter 11	The UAV shall be able to cut thrust within 10 seconds of requirement. The UAV shall reach take-off speed within 350 metres. The UAV shall be able to perform 15 deg rotation without a tailstrike if a tricycle landing gear is used.
FUN-TOF-4.2.5.ii	✓	Inspection: Accounted for indirectly in landing gear positioning	No part of the drone (either wings, tail or otherwise) other than the landing gear shall touch the ground during a nominal take-off.
FUN-TOF-4.2.6.a FUN-TOF-4.2.6.b FUN-TOF-4.2.6.c	Stricken Stricken Stricken		The UAV shall be able to transition into flight mode. The UAV shall be able to retract HLD. The UAV shall have provision to store and retract landing gear.
Communicate (COM)			
FUN-COM-4.3.5	OOS	Out of scope as payload and consequently scan time is not in scope.	The UAV shall be able to communicate search results within 10 minutes.
FUN-COM-4.3.6	✓	Inspection: Fulfilled by flow-down requirement SYS-AVN-COM-02	The UAV shall be able to receive commands from ground control at a distance of 30 km.
FUN-COM-4.4.1.e FUN-COM-4.E.2.4 FUN-COM-4.N.7	Stricken OOS ITC	Inspection: Intended to comply according to Figure 9.8 and Figure 9.9.	The UAV shall be able to communicate with ATC when prompted. The UAV shall advertise crash landing locations for 5 minutes. The UAV shall be able to report current status to ground control.
FUN-COM-4.N.7.a	ITC	Inspection: Intended to comply according to Figure 9.8 and Figure 9.9.	The UAV shall be able to report remaining endurance with accuracy.
FUN-COM-4.N.7.b	✓	Inspection: Fulfilled according to flow-down requirement SYS-AVN-NAV-06.	The UAV shall be able to report current location with 1 m accuracy.
FUN-COM-4.N.7.c	ITC	Inspection: Intended to comply according to Figure 9.8 and Figure 9.9.	The UAV shall be able to report current state.
FUN-COM-4.G.1	ITC	Inspection: Intended to comply according to Figure 9.8 and Figure 9.9.	The ground control shall be able to receive the status of the UAV.
FUN-COM-4.G.2	ITC	Inspection: Intended to comply according to Figure 9.8 and Figure 9.9.	The ground control shall clearly report the current status to the user.
FUN-COM-4.G.2.a	ITC	Inspection: Intended to comply according to Figure 9.8 and Figure 9.9.	The ground control shall clearly report remaining endurance to the user with TBD accuracy.
FUN-COM-4.G.2.b	ITC	Inspection: Intended to comply according to Figure 9.8 and Figure 9.9.	The ground control shall clearly report current location of the UAV to the user.
FUN-COM-4.G.2.c	ITC	Inspection: Intended to comply according to Figure 9.8 and Figure 9.9.	The ground control shall clearly report current state of the UAV to the user.
FUN-COM-4.G.2.d	ITC	Inspection: Intended to comply according to Figure 9.9.	The ground control shall clearly report findings of the UAV to the user.
FUN-COM-4.G.3	ITC	Inspection: Intended to comply according to Figure 9.9.	The user shall be able to input commands to the ground control.
FUN-COM-4.G.4	OOS	Testing: To be tested with complete system.	The ground control shall transmit commands to the UAV with an packet loss of 1%.
Provide Sustainment (SUS)			
FUN-SUS-4.S.1.1	✓	Inspection: Fulfilled according to flow-down requirement SYS-STR-FUS-01	The UAV shall maintain structural rigidity.
FUN-SUS-4.S.1.2	✓	Inspection: Fulfilled according to flow-down requirements SYS-STR-FUS-(02-09)	The UAV shall withstand all nominal loads during operation.
FUN-SUS-4.S.1.2.a	✓	Inspection: Fulfilled according to flow-down requirements SYS-STR-FUS-(02-09)	The UAV shall withstand nominal operating loads.
FUN-SUS-4.S.1.2.b	ITC	Analysis: When further design is done and vibrational loads are considered, they will be simulated	The UAV shall withstand vibrational loads determined to occur.
FUN-SUS-4.S.1.2.c FUN-SUS-4.S.1.3	OOS ✓	Inspection: Fulfilled according to flow-down requirements SYS-STR-FUS-03 and SYS-STR-WIN-05	The UAV shall withstand fatigue loads of up to 100000 cycles. The UAV shall withstand ultimate loads of up to 3.8 g.
FUN-SUS-4.S.1.3.a	✓	Inspection: Fulfilled according to flow-down requirements SYS-STR-FUS-03 and SYS-STR-WIN-05	The UAV shall withstand maximum G-loading of up to 3.8 g.
FUN-SUS-4.S.1.3.b	✓	Inspection: Fulfilled according to flow-down requirement SYS-STR-FUS-06	The UAV shall withstand maximum landing loads of up to 2.5 g.
FUN-SUS-4.S.2.1	Stricken		The entire UAV shall be required to be fully checked every TBD flights.
FUN-SUS-4.S.2.2	OOS	-	The UAV shall self-identify structural issues.
Perform pre-flight checks (PRE)			
FUN-PRE-4.1.2	ITC	Inspection: All subsystems identified in chapter 9 have boot-up times of less than 2 minutes.	Pre-flight, all systems shall be able to be powered on within a booting time of 2 minutes.
FUN-PRE-4.1.3.1.a	✓	Inspection: Fulfilled according to Figure 9.8 and Figure 9.9.	Ground crew shall be able to verify that all systems are receiving nominal power before take-off.
FUN-PRE-4.1.3.1.b FUN-PRE-4.1.3.2.a	✓ Stricken	Inspection: Fulfilled according to Figure 9.8.	Ground crew shall be able to verify battery voltages prior to take-off. Prior to take-off the UAV shall establish communication with ATC, if taking off from an airport runway.
FUN-PRE-4.1.3.2.b	✓	Inspection: Fulfilled according to Figure 9.8 and Figure 9.9.	Prior to take-off the UAV shall establish communication with ground crew.
FUN-PRE-4.1.3.3.a	OOS	Inspection: To be written in the operations manual.	Ground crew shall verify that all control surfaces are functioning nominally, prior to take-off.
FUN-PRE-4.1.3.3.b	ITC	Inspection: Intended to comply according to Figure 9.8.	Prior to take-off, the UAV shall transmit it's attitude states.
FUN-PRE-4.1.3.3.c- OPT	Stricken		Ground crew shall verify that thrust vectoring is functioning nominally, prior to take-off.
FUN-PRE-4.1.3.4.a.i	ITC	Inspection: Intended to comply according to Figure 9.8.	Prior to take-off the UAV shall transmit the fuel flow sensor's data.

FUN-PRE-4.1.3.4.a.ii	ITC	Inspection: Intended to comply according to Figure 9.8.	Prior to take-off the UAV shall not prepare for take-off if the fuel flow sensor picks up anomalies.
FUN-PRE-4.1.3.4.b	OOS		Prior to take-off the ground crew shall temporarily spool up the engines to TBD% for TBD seconds.
FUN-PRE-4.1.3.4.c	ITC	Inspection: Intended to comply according to Figure 9.8. To be written in operations manual.	Prior to take-off the ground crew shall verify the functioning of the UAV's throttle to be working nominally.
FUN-PRE-4.1.3.5	ITC	Inspection: Intended to comply according to Figure 9.9. To be written in operations manual.	Prior to take-off the ground crew shall verify that all payload systems are running and no errors are present.
FUN-PRE-4.1.4	OOS	Inspection: To be written in operations manual.	Prior to take-off the ground crew shall verify that all ground systems are active and working nominally.
Perform search activities (SRC)			
FUN-SRC-4.3.1	ITC	Analysis: This will be tested in a flight simulation	The UAV shall be able to cruise to destination.
FUN-SRC-4.3.3.i	ITC	Analysis: This will be tested in a flight simulation	The UAV shall be able to determine a scanning pattern.
FUN-SRC-4.3.3.ii	ITC	Analysis: This will be tested in a flight simulation	The UAV shall be able to follow a pre-determined scanning pattern.
FUN-SRC-4.3.4	ITC	Analysis: This will be tested in a flight simulation	The UAV shall be able to determine minefield bounds with an accuracy of TBD metres.
FUN-SRC-4.3.7			The UAV shall be able to return autonomously to base (where it took off from).
Navigate (NAV)			
FUN-NAV-4.N.1	✓	Inspection: Fulfilled according to flow-down requirement SYS-AVN-NAV-06.	The UAV shall be able to identify its grid reference as a 10 grid reference at all times with at least 1 meter accuracy.
FUN-NAV-4.N.2.i	ITC	Inspection: Intended to comply according to flow-down requirements SYS-AVN-OBS-01, -03.	The UAV shall be able to identify all objects larger than 0.025 m ² in its current flight path.
FUN-NAV-4.N.2.ii			The UAV shall be able to identify chainlink fences in its current flight path.
FUN-NAV-4.N.3.a	✓	Inspection: Fulfilled according to flow-down requirement SYS-AVN-NAV-01.	The UAV shall be able identify its velocity within 0.1m/s accuracy.
FUN-NAV-4.N.3.b.i	Failed	Inspection: Failed according to flow-down requirement SYS-AVN-NAV-04	The UAV shall be able to determine its density altitude at all times within an accuracy of 10m.
FUN-NAV-4.N.3.b.ii	✓	Inspection: Fulfilled according to flow-down requirement SYS-AVN-NAV-05.	The UAV shall be able to determine its absolute altitude within an accuracy of 0.05m.
FUN-NAV-4.N.3.c	✓	Inspection: Fulfilled according to flow-down requirements SYS-AVN-NAV-02, -03.	The UAV shall be able to determine its attitude during operation within a tenth degree accuracy in the vehicle carried normal earth reference frame.
FUN-NAV-4.N.5	✓	Inspection: Fulfilled according to Figure 9.6.	The UAV will autonomously control its throttle.
FUN-NAV-4.N.6.a.i	✓	Inspection: Fulfilled according to Figure 9.6.	The UAV will have autonomous control in its pitch.
FUN-NAV-4.N.6.b.i	✓	Inspection: Fulfilled according to Figure 9.6.	The UAV will have autonomous control in its yaw.
FUN-NAV-4.N.6.c.i	✓	Inspection: Fulfilled according to Figure 9.6.	The UAV will have autonomous control in its roll.
FUN-NAV-4.N.6.a.ii	✓	Inspection: Following from chapter 6	The UAV shall be able to pitch TBD deg/s.
FUN-NAV-4.N.6.b.ii	✓	Inspection: Following from chapter 6	The UAV shall be able to yaw TBD deg/s.
FUN-NAV-4.N.6.c.ii	✓	Inspection: Following from chapter 6	The UAV shall be able to roll TBD deg/s.
FUN-NAV-4.N.5	OOS		The UAV shall maintain within 1 m/s of desired speed.
FUN-NAV-4.N.i	✓	Inspection: Avionics implement navigation.	The UAV shall have means of navigation.
FUN-NAV-4.N.6	OOS	-	The UAV shall be able to maintain desired altitude above ground level within 4 m.
FUN-NAV-4.N.2	✓	Inspection: Fulfilled according to flow-down requirement SYS-AVN-OBS-01	The UAV shall be able identify terrain.
FUN-NAV-4.N.ii	OOS		The UAV shall be able to adjust flight path and heading within TBD seconds.
FUN-NAV-4.N.iii	ITC	Inspection: Intended to comply according to Figure 9.8.	The UAV shall be able to determine required flightpath.
FUN-NAV-4.N.4	ITC	Inspection: Intended to comply according to flow-down requirement SYS-AVN-AUT-07.	The UAV shall undertake required actions to avoid obstacles.
FUN-NAV-4.N.iv	✓	Inspection: Following from chapter 6	The UAV shall be laterally stable.
FUN-NAV-4.N.v	✓	Inspection: Following from chapter 6	The UAV shall be longitudinally stable.
FUN-NAV-4.N.vi	✓	Inspection: Following from chapter 6	The UAV shall be directionally stable.
Land (LND)			
FUN-LND-4.4.1	ITC	Inspection: This will be taken into account when the software is developed	The UAV shall be able to autonomously perform the landing approach.
FUN-LND-4.4.1.a	Stricken		The UAV shall be able to autonomously determine the desired landing area.
FUN-LND-4.4.1.b	ITC	Inspection: This will be taken into account when the software is developed	The UAV shall be able to autonomously align with the landing area, with a ground track distance of 500 meters.
FUN-LND-4.4.2	Stricken		The UAV shall be able to prepare for landing within TBD seconds.
FUN-LND-4.4.2.a	Stricken		The UAV shall be able to transition to landing configuration within TBD seconds.
FUN-LND-4.4.2.b	Stricken		The UAV shall be able to extend HLD within TBD seconds.
FUN-LND-4.4.2.e	Stricken		The UAV shall be able to extend landing gear within TBD seconds.
FUN-LND-4.4.3.i	Stricken	-	The UAV shall be able to determine requirement for go-around.
FUN-LND-4.4.3.ii	✓	Inspection:	The UAV shall be able to perform go-around if requested.
FUN-LND-4.4.4	✓		The UAV shall be able to land on an unprepared runway with a length of at most 500 meters.
FUN-LND-4.4.4.a	OOS		The UAV shall stop providing thrust 60 seconds after touchdown.
FUN-LND-4.4.4.b	✓	Demonstration: It has a required stopping distance of 312 m	The UAV shall be able to come to a complete stop within 500 meters distance.
FUN-LND-4.4.7	OOS	-	The UAV shall be able to shut down systems within 180 seconds of touch down.
Deal with emergencies (EMG)			
FUN-EMG-4.E.i	ITC	Inspection: Intended to comply according to Figure 9.8 and Figure 9.9.	The UAV shall be able to deal with emergencies.
FUN-EMG-4.E.ii	OOS		The UAV shall be able to deal with loss of communication.
FUN-EMG-4.E.iii	ITC	Inspection: Intended to comply according to Figure 9.8 and Figure 9.9.	The UAV shall be able to crash land in case of engine failure.
FUN-EMG-4.E.1	ITC	Inspection: Intended to comply according to Figure 9.8 and Figure 9.9.	The UAV shall be able to self-determine errors.
FUN-EMG-4.E.1.a	OOS		The UAV shall not under-estimate error criticality.
FUN-EMG-4.E.1.b	✓	Inspection: Fulfilled according to flow-down requirement SYS-AVN-NAV-06.	The UAV shall determine current position with 1 m accuracy.
FUN-EMG-4.E.2.1.i	OOS		The UAV shall be able to crash land without more than TBD euro of damage suffered.

FUN-EMG-4.E.2.1.ii	ITC	Inspection: Intended to comply according to Figure 9.8 and Figure 9.9.	The UAV shall be able to identify safe crash landing locations.	
FUN-EMG-4.E.2.1.a	OOS		The UAV shall be able to identify landing location within TBD second after critical failure.	
FUN-EMG-4.E.2.1.b	OOS		The UAV shall align with identified landing area with a ground track of 500 metres.	
FUN-EMG-4.E.2.1.c	ITC		Inspection: Intended to comply according to Figure 9.8 and Figure 9.9. The UAV shall detect obstacle in identified landing area with a size of 5 cm from a distance of at least 0.5 km.	
Perform Ground Operations (GND)				
FUN-GND-4.2.1.i	✓	Analysis: The python model used in chapter 7 takes taxi conditions into account	The UAV shall be able to taxi under its own power.	
FUN-GND-4.2.1.ii	ITC		The UAV shall have a turn speed on the ground of at least TBD deg/s.	
FUN-GND-4.4.5.a	Stricken		The UAV shall be able to transition from flight mode to ground mode.	
FUN-GND-4.4.5.b	Stricken		The HLD of the UAV shall be able to be fully retracted while the UAV is on the ground.	
FUN-GND-4.1.1.a	✓		The UAV shall be able to be fully refueled (if chemical storage is used) within 5 minutes.	
FUN-GND-4.1.1.b	✓		The UAV shall be able to be fully recharged within 60 minutes.	
FUN-GND-4.2.2	✓		The UAV shall be able to perform all identified ground operations.	
FUN-GND-4.4.2.b	ITC		The UAV shall be able to come to a complete stop within 5 m when taxiing.	
Provide Energy (ENG)				
FUN-ENG-4.W.1	Stricken	Inspection: Fulfilled according to Figure 9.6.	The UAV shall provide TBD W of electrical power.	
FUN-ENG-4.W.1.1	✓		The UAV shall provide 500 W of power to payload.	
FUN-ENG-4.W.1.2	✓		Inspection: Fulfilled according to Figure 9.6.	The UAV shall provide TBD W of power to communications systems.
FUN-ENG-4.W.1.3	✓		Inspection: Fulfilled according to Figure 9.6.	The UAV shall provide TBD W of power to navigation systems.
FUN-ENG-4.W.1.4	✓		Inspection: Fulfilled according to Figure 9.6.	The UAV shall provide TBD W of power to propulsion systems.
FUN-ENG-4.W.1.5	✓		Inspection: Fulfilled according to Figure 9.6.	The UAV shall provide TBD W of power to stability and control systems.
FUN-ENG-4.W.2	ITC		The UAV shall provide 90 N of thrust.	
FUN-ENG-4.2.3			The UAV shall respond to throttle inputs within TBD seconds.	

14.2.2. Stricken Requirements

- **STK-0.3.2-CND-MIS-TOF-4-OPT:** Stricken as it is optional and was deemed not necessary.
- **STK-6.4-MIS-COM-3, FUN-COM-4.4.1.c, FUN-PRE-4.1.3.2.a:** Stricken as UAV should not be in direct contact with ATC based on weight class. Any contact to be had with ATC is to be done by operator.
- **FUN-SUS-4.S.2.1:**
- **FUN-PRE-4.1.3.3.c-OPT:** Stricken as UAV does incorporate thrust vectoring.
- **FUN-TOF-4.2.2.c, FUN-TOF-4.2.6.c** Stricken as UAV does not have retractable landing gear.
- **FUN-TOF-4.2.2.(a,b), FUN-TOF-4.2.6.(a,b), FUN-LND-4.4.2.(a,b), FUN-GND-4.4.5:** Stricken as UAV does not transition modes or use HLDs.
- **FUN-TOF-4.2.5.i** A tail gear is not used.
- **FUN-COM-4.N.7.a:** The accuracy component of this requirement is stricken as endurance accuracy is not well defined.
- **FUN-ENG-4.W.1:** This requirement is stricken as the amount of power required depends upon the design, and this should thus not be a requirement at this level.
- **FUN-ENG-4.W.1.(2-5):** The specific wattage of these requirements is removed, as the value in these depend on the design. Thus, these requirements are adjusted and this part is stricken from each requirement.

14.2.3. Requirements not met

- **STK-0.3.2-CND-MIS-TOF-1:** This requirement is the requirement stating that the UAV shall be able to take off and land from an unmaintained road, at most 8 m wide and 500 m long for a density altitude of 5000 m. This requirement was adjusted during the current design phase to a density altitude of 4000 m. It is found that the density altitude aspect of the requirement is killer for the operation of UAV. Simply put, a 500 m unprepared runway is not long enough to ensure that a failed take-off, due to for example an engine failure, at rotation velocity could not safely be aborted. Hence it is investigated whether a 4000 m density altitude could sufficiently be reached, this reduces the required engine power by 1.2 kW, to a more achievable power requirement of 4.8 kW, allowing for a smaller engine to be used, which impacts the weight of the aircraft significantly less. However, a justification that a smaller engine is easier to implement into the design is not acceptable. Hence it is necessary to investigate the importance of the 5000 m density altitude in comparison to a 4000 m. By researching the areas in Afghanistan, the only country with (suspected) minefields at these altitudes, which are affected or suspected to contain minefields, it is quickly found that 97% of the (suspected) minefields in Afghanistan are not in the high mountainous provinces, and that the majority of the (suspected) minefields are in the lower altitude provinces [138]. This is deemed as sufficient reasoning to reduce the density altitude part of requirement STK-0.3.2-CND-MIS-TOF-1 to 4000 m.
- **FUN-NAV-4.N.3.b.i:** The requirement for a 10 m accuracy of the density altitude is not met by the navigations system. However, as explained in section 9.10, the previous requirement is likely too stringent as the ± 12.5 m

ID	Requirement summary	Parameter to vary	Subsystems to consider
STK-0.2.1-MIS-PLD-1	Payload mass	Required payload mass	Wing weight, propulsion weight, fuselage weight
STK-0.3.1-MIS-ENV-1	Endurance	Required endurance	Wing weight, fuel weight
FUN-SUS-4.S.1.3.a	Maximum loading	Required load factor	Wing weight, landing gear weight, fuselage weight
STK-0.3.2-CND-MIS-TOF-1	Take-off limit	Pressure altitude of take-off	Wing size and weight, propulsion weight
STK-0.2.6-MIS-PLD-5	Payload power	Required payload power	Wing weight, propulsion weight, battery weight
STK-1.2-MIS-RNG-1	Distance to suspected minefield	Required cruise range	Required fuel

accuracy provided by the utilized sensor provides less than 1% error in pressure altitude at sea level. Thus, this requirement should be relaxed in future iterations.

14.3. Product Validation

Product verification focuses on seeing if the requirements are met which is done in the previous section. After this is done, it is to be checked that with a product that meets all these requirements, can actually perform the mission it is supposed to. This is the product validation and it can be done using several methods namely, end-to-end information system testing, mission scenario tests, operational readiness testing and stress testing and simulation. As the final product is not yet developed, this section recommends possible methods for product validation.

Before the aerodynamic design is finalized, a series of wind tunnel test shall be conducted to validate the aerodynamic simulations and to ensure the correctness of the results.

Next, a complete integration test of the electronic systems shall be conducted to see if systems operate together. By checking the compatibility of systems in testing, conflicts of compatibility can be discovered and rectified, and the electrical design can be validated.

Finally, several mission scenario tests can be conducted by feeding certain flight conditions to the system, and seeing of the subsystems generate a correct response to this information. For example, putting the aircraft in an upwards gust of wind, a pitch down moment shall be generated. An operational readiness test is to be done by all ground segments of the mission to see if they can perform the mission. For example, the communication line between ground station and the aircraft can be tested by a ground distance of 30 km between the two systems. By methods like these the ground department can be set operational ready. Lastly, stress testing could show the UAV can withstand some requirement exceeding conditions. Because of some conventional designing in certain departments, this may be valuable to look at.

14.4. Sensitivity Analysis

A sensitivity analysis is performed, in order to test the influence of parameters on the design. Doing so reveals the "weak spots" in the design. These weak spots will show in the ability of the design to conform to and meet a change in a requirement, by finding how much the different (sub)systems are changed when a requirement is adjusted. It is necessary to have an awareness of these effects for the following situations: When future developments take place and there is a want to update a subsystem or when an estimate of a subsystem's weight cannot be met. It is important to know how much of a margin is available in both situations.

In order to limit the scope of this investigation, the list of requirements is shortened to only the requirements that are key to or driving the design. From this shortened list, there are further requirements that are not investigated, due to their reduced importance in this stage of the design. For example, requirement FUN-EMG-4.E.ii (The UAV shall be able to deal with loss of communication), has not been included, even though it is driving. This is because this requirement is not influencing the major aspects of the design in the current design phase. For example, the weight is not heavily influenced by this requirement, as autonomously dealing with a communication loss is resolved by the flight computer. This computer must be present whether the requirement is fulfilled or not.

The sensitivity analysis is performed in the following manner: The most influential parameter of a key or driving requirement is identified. Then, the subsystems that are influenced by said parameter are identified. The effects of the change in the parameter are then analyzed for the subsystems identified and a correlation is made between the adjustment to the parameter and the change in the weight of the subsystem. The relationship will show just how sensitive each subsystem is to an adjustment of the most influential requirements. This method is performed for all of the driving requirements that are identified to significantly impact this stage of the design:

14.4.1. STK-0.2.1-MIS-PLD-1: Payload mass

One of the most important requirements is STK-0.2.1-MIS-PLD-1, which states that the UAV shall be able to carry a payload of 10 kg. Therefore, to perform the sensitivity analysis, the payload mass is first reduced to 5 kg and then increased to 15 kg. The new required size and weight are then determined for the wing and propulsion system separately.

Wing

For the load-carrying structure in the wing, an increase in total mass means an increase in the loads it should carry. Thus when the total mass changes the wing box and its parameters should also change to still meet the requirements. Changes to the wing box structure also mean the mass of the wing changes how much this changes can be assessed by sizing the wing box for a total mass of 5 kg less and 5 kg more than the take-off mass determined in section 3.1. The results of this are visualized in Figure 14.1a, where the relative change of the maximum take-off mass is plotted against the wing mass estimate. It can be seen that decreasing the take-off weight decreases the required mass of the wing box while increasing the take-off weight increases the required mass of the wing box as well. This is as expected and it can be seen in Figure 14.1a that the wing box mass is about 200 g lighter when the take-off mass is reduced by 5 kg and about 300 g heavier when the take-off mass is increased by 5 kg. This shows that a change in the take-off mass has significant effect on the structure of the wing and thus should be taken into account especially since this analysis does not include the weight increase of other subsystems, such as the propulsion, due to this increased take-off mass. It should be noted that the curve in Figure 14.1a is oscillating slightly. This can be explained by the nature of the genetic algorithm employed. It attempts to find an optimal solution that minimizes the mass however, it may not reach the same optimum every time. Instead, the algorithm may converge to another local optimum which is slightly worse than the global optimum which can introduce these oscillations in the graph. To minimize this the average mass of 10 separate iterations is plotted.

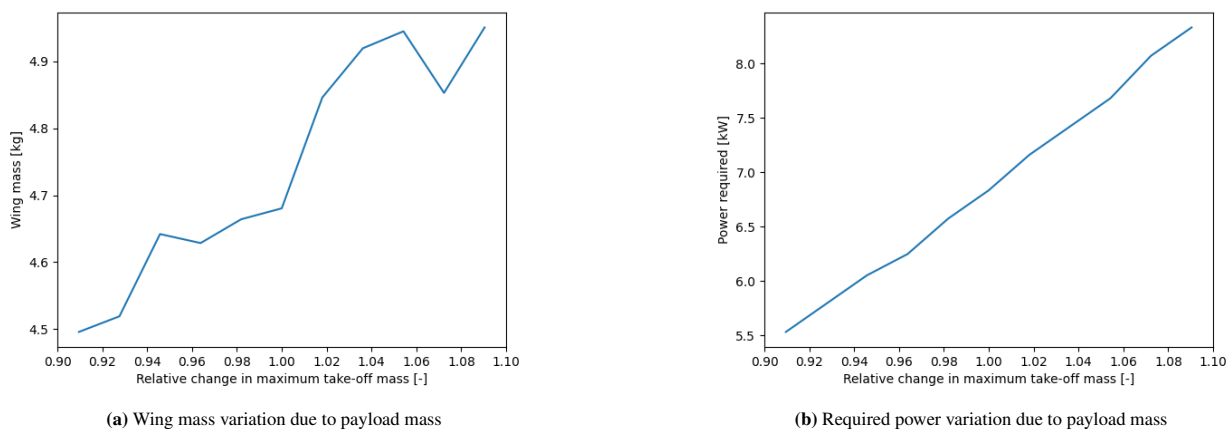


Figure 14.1: Sensitivity to weight increase

Propulsion

If the payload increases, the total mass increases. This leads to a larger required power to meet the 500 m runway requirement. To get the sensitivity of the engine mass to an increase in take-off mass, the numerical integrator of section 11.2 can be reused. After increasing the mass, the take-off power can be found using the new mass, via the method of bisection [139, p. 52]. This gives the graph shown in Figure 14.1b. From this graph, it is visible that the required power to take off increases by 281 W (at sea-level) for every extra 1 kg. Assuming a constant power-to-weight ratio of the engine package, this extra kilogram corresponds to an increase in engine mass of 0.22 kg. Not only that, but due to the fuel fraction of 12.5%, the take-off mass increases by a further 0.143 kg. This is absolutely not negligible, especially since snowball effects are not considered, so care must be taken to get an accurate estimate of the mass.

14.4.2. STK-0.3.1-MIS-ENV-1: Endurance

Another important requirement is STK-0.3.1-MIS-ENV-1, which requires that the UAV shall have an endurance of at least 4 hours for a temperature range between 5° C and 35° C and an altitude up to 2000 m above mean sea level (MSL). As endurance is a critical parameter for the fulfillment of the mission, it might be beneficial to increase the endurance at a later stage. For that reason, the required endurance is first reduced to 3 hours and then increased to 5 hours, still at an altitude of 2000 m.

Wing

In order to achieve an increased endurance it may be beneficial to increase the aspect ratio of the wing. This improves the efficiency of the UAV but has some consequences on the wing box and thus the weight of the wing. Increasing the aspect ratio means a larger wing span while keeping the surface area the same. Thus to see what effect this has on the wing box mass the procedure presented in subsection 7.3.4 is repeated but now with a larger wing span of 4.41 m and in turn a new root and tip chord of 0.427 m and 0.17 m respectively. Keeping all other parameters the same results in an aspect ratio of 13. Following the same procedure as presented in subsection 7.3.4 the mass of the wing box can be estimated. In order to get more accurate results this analysis was performed 10 times and resulted in an increased wing box weight of 4.87 kg. This is an increase of 370 g compared to the weight estimate from subsection 7.3.4. This indicates that an increased aspect ratio would likely result in a heavier wing and thus may not improve endurance much.

Fuel

For the required fuel mass due to an increase in required endurance, the fuel fraction can be recalculated for loiter. This fraction is given by [53, p. 288]

$$\frac{W_i}{W_i + 1} = \left(\frac{E \cdot V_1}{2} \cdot \frac{c_p}{\eta_j} \cdot \frac{C_D}{C_L} + 1 \right)^2 \quad (14.1)$$

and the full procedure for calculating the total fuel fraction is described in chapter 11. Increasing the endurance by 10% requires an increase in total fuel fraction from 12.5% to 13.2%. Given the originally estimated take-off mass of 55.3 kg, this corresponds to a fuel mass of 0.39 kg.

14.4.3. FUN-SUS-4.S.1.3.a: Maximum loading

For sustainment in flight, FUN-SUS-4.S.1.3.a states that the UAV shall withstand a maximum G-loading of up to 3.8g. However, it is possible that in the future this requirement is changed, such that a higher g-loading is wanted, for operations in stronger wind environments or if maneuver performance needs to be improved. It might be beneficial to do this in later stages, if operations in high-wind environments, such as the high-mountain regions of Afghanistan, are to take place.

Wing

An increase in G-loading means an increase in the loads the wing box should sustain in order to satisfy the requirements. To assess the effect of this increase, the wing box sizing procedure is repeated but now for a G-loading range from 2.8 to 4.8 g. The results of this can be seen in Figure 14.3. Here it can be seen that an increase in the load factor has a significant impact on the required wing box mass. An increase of 1 for the load factor increases the wing box mass by roughly 500 g. This is not insignificant at all as this does not yet include the effect of different subsystems. As such special care must be taken when the load factor is concerned and any increase of the sustained load factor should be limited.

14.4.4. STK-0.3.2-CND-MIS-TOF-1: Take-off limit

The requirement, STK-0.3.2-CND-MIS-TOF-1, states that the UAV shall be able to take off and land from an unmaintained road, which is 500 m long at a density altitude of 4000m. It is possible that for a certain mission, a shorter take-off is required or that take-off needs to be performed at a higher altitude, and hence adjustments need to be made to UAV. Hence, it is imperative to analyze the subsystems that are sensitive to this requirement.

Wing

In order to improve take-off performance the wing surface area may be increased. This in turn changes the wing box structure and thus may result in a new mass for the wing structure. To assess this change in wing mass the procedure presented in subsection 7.3.4 is followed again but now for a new wing span of 4.420 m, and root and tip chord of 0.455 m and 0.182 m respectively. This accounts for an increased wing surface area to 1.6 m². Following the wing box sizing procedure again results in a new mass estimate for the wing box of 4.93 kg. This is an increase of 430 g indicating that attempting to achieve better take-off performance adds a significant amount of weight. If this is combined with the weight increase of the propulsion system when take-off distance is attempted to be reduced one can see that this weight increase will quickly snowball out of control. Thus this indicates that the take-off performance is one of the most sensitive parts of the design.

Propulsion

Similar to increasing the OEW, decreasing the allowable take-off distance has serious implications for the engine sizing. Using numerical integration and the bisectional method, once again, the required engine power can be plotted as a function of the required take-off distance. This gives the curve in Figure 14.4a, where the required power is plotted against the relative change in take-off distance. From this, it can be seen that the take-off power decreases by 11.3 W for every 1 m

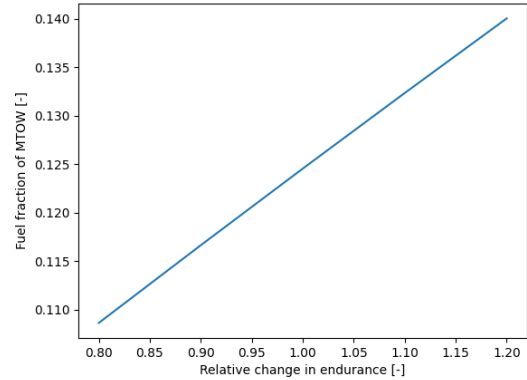


Figure 14.2: Total fuel fraction as a function of a change in endurance

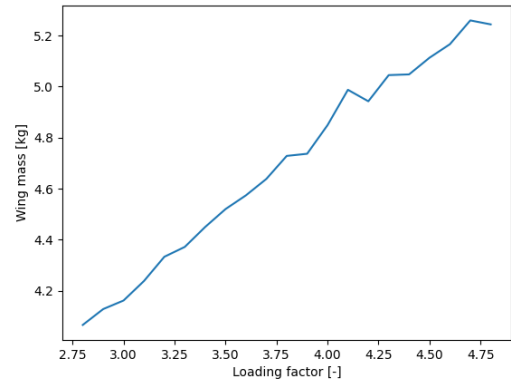


Figure 14.3: Wing mass due to load factor

of extra runway length. Thus, adding an extra 100 m to the runway can theoretically lead to a much smaller and lighter engine.

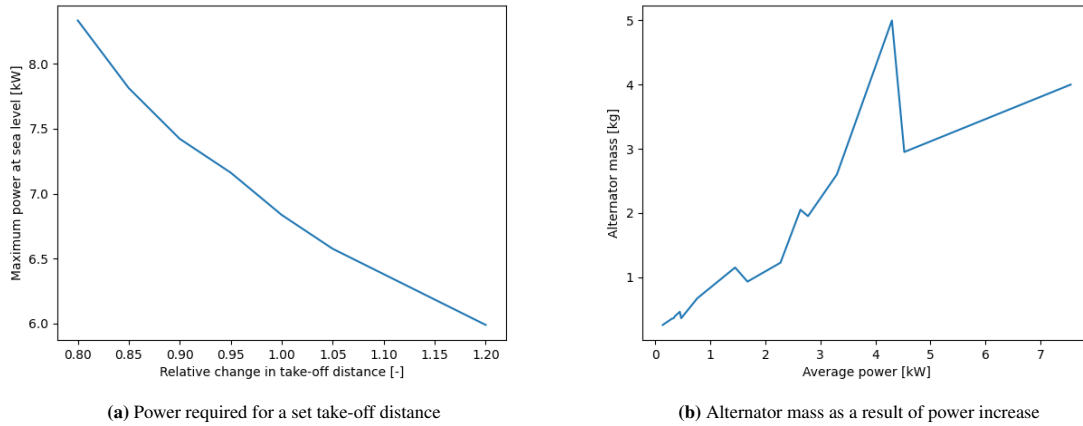


Figure 14.4: Sensitivity of the propulsion subsystem

14.4.5. STK-0.2.6-MIS-PLD-5: Payload power

STK-0.2.6-MIS-PLD-5 states that the minesweeper shall provide at least 500 W of electrical power to the sensor payload. However, if this increases, either the engine needs to provide excess power or additional batteries are required. Hence, the power is first reduced to 250 W, before increasing it to 750 W.

Propulsion

For the propulsion, the component most affected by the power is the alternator. Therefore, it is useful to look at the power-to-weight ratio of alternators. In the selected engine package, a 500 W Sullivan alternator is used [24]. While the exact alternator is not specified, the performance characteristics most match the S676-400U-01 model. This alternator has a mass of 670 g. Doing a regression of other alternators sold by the same company gives the graph shown in Figure 14.4b. From this, it can be seen that an increase of the required power by 1 W increases the mass by roughly 0.63 g. While not completely negligible, this mass is quite small compared to the mass of the engine.

Fuel

For the fuel, the BSFC of the engine of $590 \text{ g kW}^{-1} \text{ h}^{-1}$ can be used. Increasing or decreasing the payload power by 250 W leads to a mass added or removed of 590 g, respectively. This is a significant mass addition, especially since several small contributions can lead to even larger weight savings in the end.

Battery

If batteries are used to power the payload for 4 hours, a different story arises. The main battery used in the design has an energy density of $0.212 \text{ kW h kg}^{-1}$. As the loiter time is 4 hours, this implies that an addition of 250 W to the payload power increases the battery mass by 4.72 kg. This mass is so large that the usage of more fuel is strongly preferred.

14.4.6. STK-1.2-MIS-RNG-1: Distance to suspected minefield

According to STK-1.2-MIS-RNG-1, the UAV shall have a 30 km cruise range to search area. This requirement directly impacts operational range of the vehicle. For this reason, in this analysis the range is first decreased by 20% and then increased by 20%. For this requirement, the subsystems most impacted are the required fuel and the communications.

Fuel

For the fuel required due to an increase in range, it is necessary to look at the range equation. Due to the summation rules of exponentials, the fuel ratio due to a difference in range is given by modifying the Breguet range equation [53, p. 287]

$$\frac{W_i + 1}{W_i} = e^{-\frac{R \cdot c_p}{\eta_p} \frac{C_D}{C_L}} \quad (14.2)$$

with R in this case simply the difference in range. From this, it can be seen that even a 20% increase in range (from 30 km to 36 km) leads to a mass fraction for the extension of 0.998. This corresponds to less than 100 g extra of fuel, so can easily be neglected.

Communications

As the range increases, the antenna needs to be stronger for the same link budget. However, due to the low mass and power consumption of the radio, a reasonable increase in range does not significantly impact the other subsystems. Any

mass increase mostly comes from the additional power required. As mentioned before, more power implies either a larger generator or more fuel, hence increasing take-off mass.

14.4.7. Future possibilities

Currently, no weight relations are available for every subsystem. That is, at this moment, there are no clear formulae such as 'a 10% increase in required power adds 1 kg to the engine mass' or 'an increase of the load factor gives this much extra mass on the wing'. At a later stage it is useful to derive or determine such formulae. This allows for iteratively finding the weight, by summing the weight of all components in each step and using that new total weight as an input for all other components. Furthermore, it would then be possible to find the relationships to weight changes between subsystems, allowing for a determination of the sensitivity of all subsystems to a certain parameter originating from only one subsystem. After this, it is even possible to account for a change in requirements, such as an increase in range or endurance. However, at this stage of the design, not enough data is available to create these complex relations and interactions. What the sensitivity analysis at this stage does show is that take-off performance is one of the most limiting criteria for this design. It shows that changes to parameters regarding take-off have the greatest effect on the design and have the tendency to snowball the most.

Production Plan

In the midterm report of this project, a preliminary production plan for the UAV was given. Now that a lot more is known about the design and its parts, this plan is to be updated and reconsidered. In this chapter, the four previously determined phases of production, namely building structural parts, assembling those parts, installing subsystems and shipping the product, are elaborated upon. The materials of the UAV are known at this point of the design, thus manufacturing techniques for parts are discussed in section 15.1. When these parts are manufactured, they are to be assembled into the primary structure for which the suggested methods are presented in section 15.2. Consecutively, the off-the-shelf subsystems like the engine are to be installed for which the method is discussed in section 15.3 after which the last part of shipping the product to the client is discussed in section 15.4.

15.1. Manufacturing structural parts

The manufacturing of structural parts can be separated into two categories: manufacturing the aluminum, load carrying structural parts, and manufacturing the shaping structures. In this section, first the aluminum parts (including panels, stringers, spars and spar-caps) and their respective manufacturing techniques will be discussed. This includes the shaping of the thin plates in the wingbox, the spars, and the trusses of the fuselage structure. Besides the aluminum components, there are also shaping components for the airfoils and the fuselage that shall be produced.

15.1.1. Aluminum deformation

Making the choice to use Aluminium (7075-T6) as the material for the main load carrying structure, several manufacturing techniques were immediately ruled out. Additionally, because series length for production is reasonably small, it is the most cost beneficial to outsource manufacturing of parts to an external manufacturer. Because of the scope of this report, no manufacturers have been selected yet. However, for the selected production methods, it is made sure the production is not too specific, so that it could potentially happen close to target locations of the project.

For the manufacturing of the wingbox, the necessary parts can be seen in ???. Firstly, thin plates are required for the upper and lower panel, the stringers and the spars. These panels will be bought according to the required thickness as calculated in chapter 7. This thickness was not the same for all components but for manufacturing purposes were made more cohesive. The panels, trusses and spars each have one thickness. Several manufacturers deliver aluminum plates of differing thicknesses used for aerospace purposes, like for example [140]. It is ensured a suitable manufacturer of these thin plates will be found. This plates can then be sized to the required dimensions. The manufacturing technique that was chosen to do so, is laser beam cutting. This is a cutting method broadly used in the aerospace industry [141] and it can cut through metal sheets of up to 25 mm thick [142], which captures the thickness of all thin plates needed for the wingbox. The panels for the upper and lower load carrying parts of the wingbox are then finished. The stringers are still to be formed into the right shape. Since the three required stringers are all of the same thickness and need to be bent in a 90° angle, only one manufacturing technique is required. Bending, rubber deforming, stretching and deep drawing have been considered as deforming methods for the thin sheets. The book *Materials Processing: A Unified Approach to Processing of Metals, Ceramics and Polymers*, mentions the advantages and disadvantages of each method. Deep drawing is a suitable technique for the creation of stringers and can be used in the aerospace industry. However, since it requires a non-universal tool, it is not cheap. The best product series is 10000-100000 products, which is a lot more than necessary for this project. Bending operations, especially V-bending, are generally more suitable for smaller product series as they require more labour hours, but less extensive tools. Rubber deforming had the big advantage that one universal tool can be used for different stringer shapes. It requires a large pressing force but since the stringers are L-shaped, which is an easy shape, this should not be a problem. [143]. With all information about these metal sheet deforming techniques, it is suggested that either bending or rubber deforming are used to shape the L-stringers. Since manufacturing will be outsourced, the final decision is up to one of the many companies that provide these services. If it turns out that buying pre-shaped L-stringers, this can also be considered. In the choice of company, requirement FUN-PRO-2.3 will be taken into account, aiming for a company using refreshing manufacturing techniques taking sustainability into account. The spars are assumed to be manufactured by the same producer.

15.1.2. Shaping structure

Besides the aluminum load-carrying structure, there is also a Styrofoam shaping part of the wing that will support the shape of the airfoil. Assumed that Styrofoam can be bought in the entire dimension of one wing, it only requires shaping into the right airfoil before it can be used in assembly. When choosing a manufacturing technique for this, it is important to note the material is no longer a thin aluminum plate, but it is a bulk material. Different techniques are to be considered. In metal alloys, machining is often used to alter a bulk of material. This however, creates scrap material in the form of chips, no longer available for usage afterwards. Since this is not sustainable, other manufacturing techniques are explored. Companies that process bulks of Styrofoam often use (a combination of) hot wire-, cold wire- or laser beam cutting [144],

[145]. This is less wasteful as the remaining material can be used for other purposes since it is still in one piece. These methods are therefore worth considering

Wire electrical discharge machining is a non-contact subtractive manufacturing process that uses an electrically charged thin wire with a dielectric fluid to cut a metal part into different shapes. However, this can be used in metal materials mainly in which it has a broad variety of advantages like accuracy and speed. [146] Hot wire cutting uses a comparable technique, but without using electrons to cut. It has several advantages, including minimal waste and high efficiency which are both applicable for cold- and hot wire cutting.[147] The two biggest advantages for hot wire cutting specifically are that it can cut complex shapes in a consistent matter.[148] For the airfoil this means it can be cut into the same shape easily, along the length of the wing. Therefore the manufacturing technique advised to use is hot wire cutting. This can be adjusted in consultation with the chosen manufacturer.

15.2. Assembling primary structure

When all parts for the wing are manufactured, assembly shall be started. This process can be divided into the assembly of the wing structure and the attachment of the wing to the fuselage structure. Some of the subsystems (the avionics, power distribution subsystem etc.) will have to be integrated with the load carrying structure right away because of accessibility issues. An important consideration is that expensive, off-the-shelf subsystems, are to be integrated as late as possible to prevent any damage to the equipment being done during assembly.

Firstly, the assembly of the different parts of the wingbox shall happen. Different techniques can be used of which examples are bolting, riveting, adhesive bonding and welding. These assembly techniques have impact on the load carrying abilities of the parts. Because they have not been taken into account during the structural design, the choice of assembly method shall be left to a later stage of the design. For now, the assumption is made that the wing box is assembled without the assembly method interfering with the load carrying abilities. The same goes for the fuselage structure.

15.3. Installing subsystems

Integrating subsystems into a UAV from a structural perspective is a meticulous engineering process that ensures all components fit and function harmoniously within the aircraft's design. This involves creating a robust framework that accommodates the physical and electrical interfaces of avionics, propulsion, navigation, communication, and payload systems. Engineers must consider factors such as weight distribution, aerodynamics, vibration isolation, and thermal management to maintain the UAV's structural integrity and performance. The placement of each subsystem is strategically planned to optimize space and ensure easy access for maintenance and upgrades. This can also be seen in Figure 15.1.

15.4. Shipping

Lastly, the product can be prepared for transport. This includes steps such as taking off any removable components, such as wings. It also includes adding spare parts and the manual to the box and adding a shipping label. The size of the box shall fit in most long-range commercial transport aircraft or fit into a 10 foot shipping container and thus the UAV can be shipped using a simple truck, or ship, after which it can be handed over to the customer.

Based on all steps mentioned above, the vehicle can be manufactured and prepared for hand-over to the customer. After this, it can begin its operational mission to find landmines and help humanity. For further reference, in Figure 15.1, a flow diagram is shown of the full manufacturing plan.

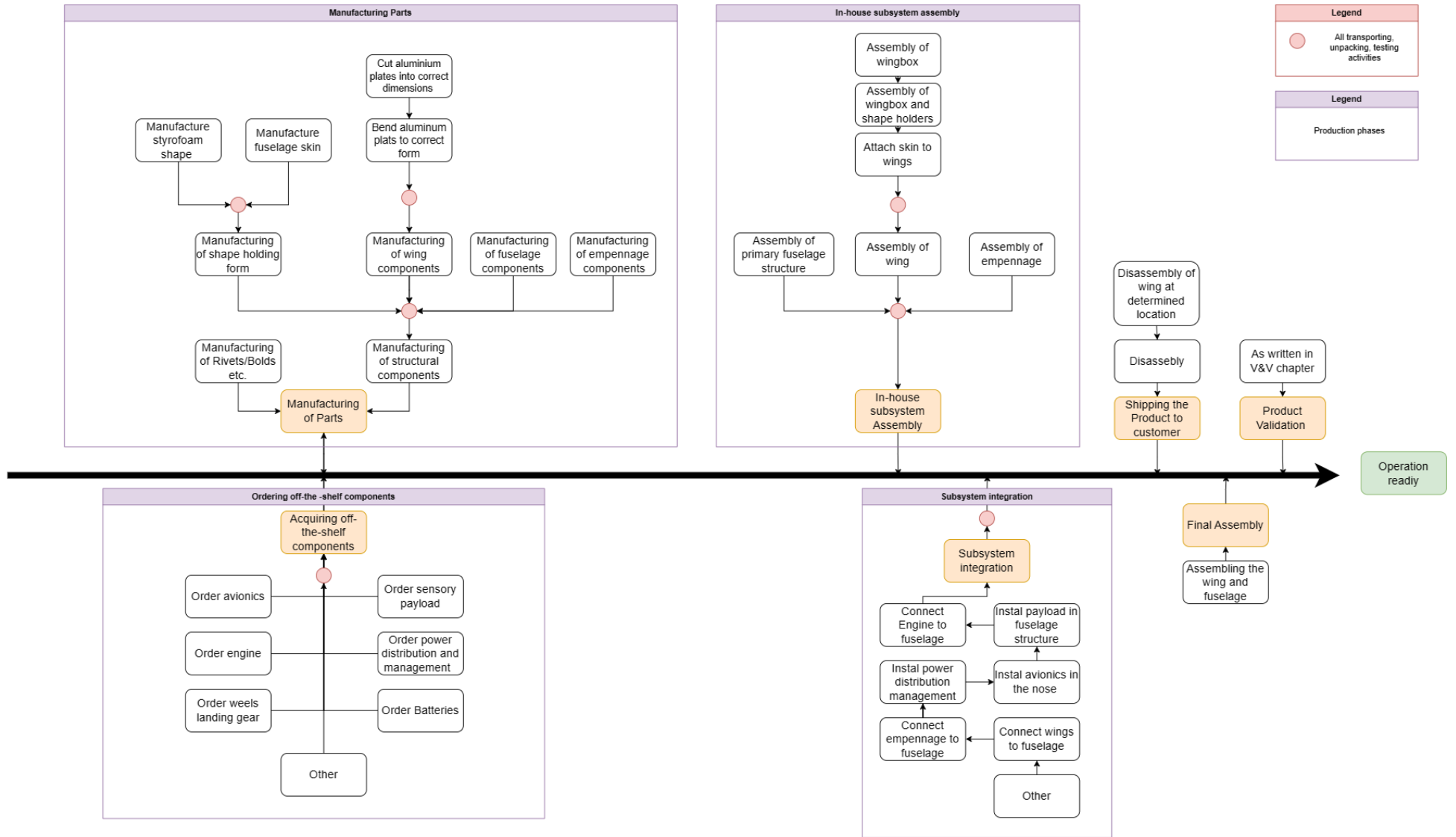


Figure 15.1: Production Flow Diagram

Sustainable Development Strategy

When one thinks about sustainability often what is first thought of is the impact on the environment and CO₂ emissions. However, the UAV designed to detect minefields is highly beneficial to social sustainability. This chapter concerns the sustainable development strategy employed. First, the main aspects of social sustainability the UAV is contributing to are mentioned in section 16.1. After this, the sustainability of the product is measured in two main ways. Firstly, the carbon footprint of the entire life cycle of the product should be assessed. Secondly, the recyclability of the product should be considered. Then, section 16.2 discusses the environmental impact of the UAV during the entire life-cycle and plans to reduce the negative externalities that are presented. Finally, in section 16.3, some strategies to further mitigate the environmental impact are discussed. In this section, also the recycling of the product is discussed.

16.1. Social Sustainability

To assess the social sustainability of the UAV, the UN sustainable development goals are considered [149]. Although the UAV can positively touch upon all sustainability goals through humanitarian demining, the ones that are considered to be of greatest impact are presented.

Zero Hunger

Arable land is frequently used for minefields during armed conflicts and landmines regularly injure and kill farmers, both of which negatively impact critical food production [2]. In the Democratic Republic of Congo, improvised mines intentionally prevent farming as they were emplaced in arable land [2, p. 43]. Even arable land that is not actually contaminated may be regarded as such due to suspicion or fear of mines. According to [122], explosive ordnance contamination affects nearly 19% of farms below 250 hectares in areas near the front line in Ukraine, with an annual economic loss of around \$930 ha⁻¹. Further, Vietnam experienced a 50% reduction in rice yield as a result of a fall in soil productivity from landmines [150].

Humanitarian demining makes a significant impact in the access to safe farmland, as the majority of land cleared by MAG is arable land. [151] In this way, improvements in the demining process have an impact on world hunger and food security, and the designed UAV can make an impact in this by decreasing the time required to identify minefields.

Good Health and Well-Being

By mapping and marking minefields that are to be cleared, a sizable impact is made in promoting the well-being of all populations living in the presence of minefields. Victims of mines are often not killed, but instead heavily injured, with immense detriment to their health [2]. This leaves many victims with life-long injuries and disabilities including the loss of limbs and a major reduction in function [2, pp. 75-81].

In addition to the physical injuries related to mines, there are also effects on mental health. According to [2, p. 80], most mine survivors in Sri Lanka were found to suffer from PTSD. Nations that experience a lot of mine-related accidents require considerable networks and systems to assist survivors and victims of mines with mental health [2, pp. 75-81]. Thus, through assisting the global demining process, the UAV can make a sizeable impact on the good health and well-being of those living in mine-affected areas.

Decent Work and Economic Growth

Mines affect the prospects of the population of a mined country, as mined land cannot be properly utilized. Simply freeing up a larger area improves the work opportunities of the population. In Ukraine, it is estimated that contamination costs \$930 ha⁻¹ in lost revenue annually for small-scale farmers [122]. With an estimated price of full farmland demining at \$1781 ha⁻¹, the complete payback period is in excess of 30 years, as not all revenue is profit [122]. This is a significant burden for small farmers [122]. Thus, a reduction in the price of non-technical and technical surveys helps to drive these costs down and foster economic growth and development in areas contaminated post-war. In addition to the cost of lost land, there are other economic hurdles related to contamination. Mines impose large costs on a country from the additional healthcare expenses for victims and survivors of mines [2]. If these resources are freed up, more economic resources are available for use in aiding growth and development. Hence, by reducing the cost of the survey stage and assisting in demining operations, the designed UAV can contribute to the proliferation of decent work and economic growth.

Clean Water and Sanitation

In addition to the direct effects of mines on populations, there are also indirect environmental effects. As mines and explosive remnants of war remain in the ground, deterioration occurs and the internal compounds may leak into the environment [150]. Explosives such as TNT or RDX are often used in mines, leaking into the surroundings and contaminating soil and groundwater [150]. These substances and their decompositions exhibit extremely dangerous properties as they are long-

lived, carcinogenic, and toxic [150]. Further, as these substances are generally water soluble, they easily travel and can be lethal to humans and wildlife alike [150]. With this in mind, the acceleration of the survey phase and demining operations through the use of the designed UAV can reduce the impact of pollution due to explosives through better surveys.

Ensure sustainable consumption and production patterns

The aircraft and the support infrastructure around it are designed with this sustainability goal in mind. The recycling of components is maximized and measures are taken to minimize the emissions and carbon footprint throughout the life cycle. All these measures are detailed in section 16.2

16.2. Life-Cycle Analysis

The environmental impact of the UAV consists of multiple contributions. For example, not only does the UAV impact the environment during its operations, but also during its development. This section aims to discuss the environmental impact of the UAV. To get a complete view of the environmental impact of the product, the entire life cycle is analyzed. This starts with the development of the product. Subsequently, the production is investigated after which the operational period is analyzed. Finally, the end of life is considered as well.

To limit the environmental impact of the UAV during its entire lifetime the production process also has to be assessed. Production can be a very wasteful process thus there is an aim to limit the waste during production. This starts already during the design process where choices on production techniques are made, but continues during the production phase as well.

One way to limit the environmental impact during the production process is through the concept of lean manufacturing. As stated by [152], lean manufacturing is the dynamic, knowledge driven, and customer-focused process through which all people in a defined enterprise continuously eliminate waste with the goal of creating value. This means that during production, activities that don't add value to the UAV are avoided as much as possible. This means activities such as unnecessary transport and wasteful use of materials should be avoided. Altogether, this limits the negative environmental impact.

Another way of limiting the environmental impact during production is by keeping the principle of a circular economy in mind. As stated by [153], The circular economy is a model of production and consumption, which involves sharing, leasing, reusing, repairing, refurbishing, and recycling existing materials and products as long as possible. In this way, the life cycle of products is extended. This means maximizing the use of materials by creating a closed-loop system where materials are reused and recycled. Applying this during the production process means enabling easy disassembly of the UAV. This facilitates not only re-usability at the end of life but also enables the replacement of damaged parts, thus extending the lifetime of the UAV.

This section will be addressed from the perspective of the life-cycle depicted on Figure 16.1. The life-cycle deals with the life of the product after the development is completed, it is crucial to separate the two stages. Development involves the design of the product from an engineering perspective, it involves making a list of all outsourced components, making 3D models and technical drawings of all parts that need to be manufactured, and essentially designing all individual parts of the aircraft as well as a manufacturing manual for them. The life-cycle however is the logistics of all the infrastructure around producing, operating, and retiring the aircraft after it leaves the design board. Figure 16.1 depicts the lifecycle of the product and its stages will be used for the rest of the section to navigate through the lifecycle of the product.

16.2.1. Development

The sustainability of the UAV already starts during its development. As UAV is designed, sustainability is considered during all design choices. During the development phase, it is important to consider the life cycle of the product, and design choices should be made taking into consideration emissions during all phases. In doing so the final design is ensured to be more sustainable. It has to be mentioned that the first priority of the UAV is functionality and mission performance, and efforts are made to reduce emissions and recycling of materials where possible. Therefore, the relative weight of this criteria did differ per situation, to ensure the mission goal is achieved, which, as mentioned previously in section 16.1, has a great impact upon social sustainability. Sometimes options that result in more emissions are chosen as the better option due to the improved performance.

For the concept trade-off, sustainability was considered as part of multiple criteria. Efficiency was an important trade-off criteria which also leads to a more sustainable UAV in terms of carbon emissions during use. Also, reliability was considered as a criterion, higher reliability leads to lower maintenance. Maintenance is part of the use stage from Figure 16.1. Maintenance requires the production of spare components (sourcing and manufacturing), transportation of parts and/or UAV to the repair site (distribution), and recovery of the failed components.

There were a lot of decisions made within different subsystems, which affected different phases of the life cycle. The decisions made throughout the design will be detailed within the most relevant part of the cycle, and the analysis will start with use.

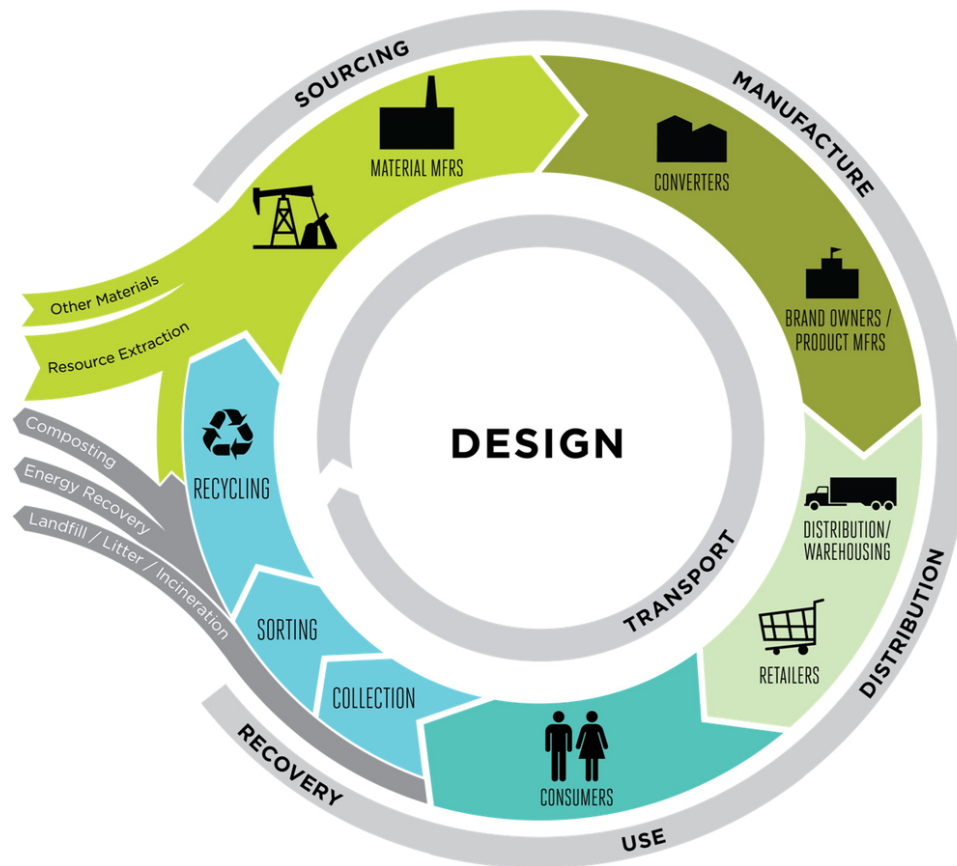


Figure 16.1: Life-cycle analysis of the product after design phase.

16.2.2. Use

During use the aircraft's propulsion system is responsible for the majority of emissions. There are two main factors that need to be considered for emissions: weight and efficiency. The heavier the aircraft the more energy it will require to operate, so more fuel and increased emissions. The more efficient the engine is the better it is in converting fuel to energy. In our case, the weight of the aircraft and the emissions of the engine will be primary ways of minimizing emissions in use.

For the lightweight design of the aircraft, for load-carrying components, it was decided to use aluminum 7075-T6 alloy, for its high performance and the weight savings it offers. Furthermore, styrofoam is used in the leading edge of the wing as it has a very low density, and is capable of providing the desired airfoil shape. The kevlar tank was also chosen for the purpose of saving weight. Lightweight was also the driving requirement when selecting avionics. To sum up, a lot of attention was paid to the weight minimization of all subsystems. This snowballs into a smaller lightweight aircraft that uses less material and fuel.

In the propulsion system trade-off in ??, emissions are one of the trade-off criteria. The use of clean energy for the propulsion system is investigated to further improve the sustainability of the UAV and align with the guidelines given by the UN [149]. It turned out that sustainable means of propulsion such as hydrogen- or battery-electric systems were not suitable for the desired application of the UAV. As the UAV is operated in remote areas post-conflict, sufficient infrastructure is not guaranteed. This means that hydrogen and electricity may not be readily available. Following the trade-off, it was concluded that gasoline-based engines were a better option for the propulsion system. With this engine choice, the efficiency of the engines becomes even more important to reduce emissions. Additionally, biofuels, or fuels containing a percentage of biofuel, are considered an important step to achieving sustainability goals, and therefore a bio-fuel compatible engine was chosen.

Another significant contributor to emissions is maintenance. Maintenance of aircraft requires the production of spare parts, their transportation to the repair site, or transportation of the aircraft to the repair site. There are two options considered for maintenance, both can be made scalable, but depending on the production numbers one may be preferred over the other. The first option is to bring the aircraft to the centralized maintenance hub, which is better suited for large production numbers. The second option is local repairs that the customer is directly responsible for.

In the first case, the manufacturer of the UAV would be directly responsible for the condition of the UAV. As the manufacturer would be overseeing the aircraft throughout its lifetime, the history of every component can be maintained for the

recovery phase from Figure 16.1. The availability of a full record would allow for more parts to be recycled and reused without quality compromises. The main source of emission in this case would be the transportation of the aircraft to and from the maintenance site. The emissions of transporting spare parts to the maintenance site can be avoided by locating the maintenance hub next to the production site. Transportation of the aircraft to the maintenance site is the 'consumer' responsibility and therefore will not be addressed. Transportation from the maintenance site, however, can be affected by the manufacturer, and in this case, the most sustainable option of transport available can be chosen (shipping or electric car). As the engine's time between overhauls is 300 hours [24], the majority of the minor repairs will be performed during overhaul maintenance.

In the second case the 'consumer' is fully responsible for the aircraft and its emissions during use. This means that the manufacturer is only responsible for manufacturing defects. When a certain component fails, the client can then order new components from the manufacturer. The manufacturer in this case should offer a free shipment to the customer for the broken component or even provide a discount on a new component if the old one is shipped back, this is a 'Collection' phase of the life-cycle from Figure 16.1. The manufacturer should then be responsible for diagnosing and recycling the broken component. The manufacturer in this case can also minimize the transportation emissions by choosing the most sustainable method of component delivery available.

An important step that was taken during the development phase was the minimization of required maintenance. Maintainability, complexity, and risk of failure were important criteria in many design choices. Minimization of critical failure points and unscheduled repairs would lead to more transportation emissions for maintenance purposes.

The last contributing factor is transportation emissions. The transportation of the product by car between different locations results in emissions, unfortunately not much can be done about it from the development perspective. It is left up to the operator to minimize carbon footprint by using sustainable means of transport for crew and UAVs.

16.2.3. Recovery

The recovery stage starts with the 'retired' aircraft being shipped back to the manufacturer in exchange for a discount on a new aircraft, and the shipment costs shall be covered by the manufacturer. Transportation emissions shall be minimized in the same way as maintenance. Upon arrival at the site, the aircraft is disassembled and individual components should be inspected for further use, in particular, the electronics are likely possible to be reused for new aircraft or as replacement components for maintenance of other aircraft. This of course should involve proper testing of the components to ensure that they still perform according to designed standards. After all individual components have been inspected and the ones that can be reused are filtered out, the stock for recycling is stored on-site until it builds up to a sufficient volume to be transported to external recycling facilities.

There are multiple materials that can be recycled. The primary structural material is a high-grade aluminum 7075-T6 alloy. According to some research, it can be recycled without degraded performance, and meet the requirements. [154]. However, it is not a common practice, in most cases, the alloy is recycled into lower-grade aluminum, meaning that most likely it will exit the life-cycle at this stage, going into other industries with lower performance requirements.

The styrofoam, that is used for the leading edge of the wing can be recycled back into styrofoam. [155] This would be done by an external company, from which the recycled styrofoam would be used again. The PVC plastic film used for coating the wing leading edge can also be recycled, just like aluminum however, it may have degraded performance, in which case it can be used in other industries for less demanding applications.

The electrical components and LiPo battery would be recycled to the best extent possible using the help of external organizations, sustainable recycling of electronics already exists, and considering an increase in electronic waste the growth of the electronics recycling industry is expected. [156] The kevlar tank, being an off-the-shelf component, can not be recycled into a new component by the manufacturer of the UAV, or subcontractor. Kevlar as a material is however recyclable, and therefore it will be recycled for further use elsewhere. Another off-the-shelf component is the engine, the engine is a complex component just like electronics. The possibility of engine disassembly and recycling of individual components will be investigated at a later stage of the project.

Unfortunately, it is likely that some of the off-the-shelf components can not be recycled. In this case, it will have to either go to combustible waste with energy generation or landfill, depending on the material.

It is important to note that transportation to the recycling site and the recycling itself results in carbon emissions during this phase of the life cycle. The emissions of the recycling industry are typically less than for creating a new raw material.[157], which makes it appealing from a sustainability point of view. Combustion of waste for energy production also results in CO₂ emissions, however considering the purification systems available at energy production sites, it is considered a more sustainable solution than landfills for the non-recyclable waste. Landfills are not considered sustainable as they release biogas, which is primarily composed of methane and carbon dioxide, they can cause fires and contaminate groundwater. [158]

16.2.4. Sourcing

During sourcing, all necessary components for new aircraft need to be produced. Since the majority of the aircraft components and subsystems will be manufactured externally and delivered to the final assembly site, in the development stage limited decisions can be made.

As explained in subsection 16.2.3, some of the aircraft components from the old aircraft may be reused, this prevents emissions of manufacturing and delivering new components, and minimizes the extraction of raw material. The modularity of the design makes this easier. Such components are directed straight into the manufacturing phase.

As described in chapter 15 manufacturing of the load-carrying components will be delegated to an external company, in this case, the best that can be done is choosing the most sustainable company. Ideally, the company would recycle the 7075-T6 alloy, but otherwise, metals for this alloy will have to be part of resource extraction from Figure 16.1. Production of the load-carrying structures will be a significant contributor to the carbon footprint of our product, therefore mitigation, such as carbon offset can be utilized, which will be looked at in section 16.3.

The styrofoam can be purchased from the recycling facility directly and used in manufacturing, and if possible the same should be done with the PVC film for wing coating.

Unfortunately, landing gear wheels, electronics, fuel tanks, and engines are off-the-shelf components. The sourcing of materials and sustainability of their manufacturing fall out of control of the UAV manufacturer, the best that can be done is choosing the most sustainably manufactured option from the market, in further development the selected options can be reevaluated for similar alternatives, and the possibility of requesting the manufacturer to use recycled material can be evaluated.

16.2.5. Manufacturing

Manufacturing will be done at the assembly site where all delivered components are assembled into an airplane. The majority of the carbon footprint of the site will result from typical operational consumption, namely the use of electricity, water, and transportation around the assembly site. In order to minimize the emissions at this phase, the production should be based in the country where most of the energy supply comes from 'green energy', and equipment with high efficiency should be chosen for on-site use.

Use of locally manufactured products can also aid in minimizing emissions. Producing most of the components of the UAV in the same region, thus minimizing transportation helps to reduce the environmental impact. Manufacturing parts locally reduces the distance components need to travel, thereby decreasing emissions associated with transportation. Local production of the components would also decrease the complexity of managing the logistics which leads to more efficient operations.

16.2.6. Distribution

The distribution of the product in the case of the UAV involves on-site storage and transportation to the customer. The emissions during transportation can be minimized by choosing sustainable means of transport for delivery. Unfortunately, as the customers operate in many countries around the world, it is not possible to minimize emissions by locating the manufacturing site in the country of use.

16.3. Environmental Impact Mitigation Strategies

Some environmental impacts caused by the UAV and its development can not be avoided. The magnitude of this impact can be decreased by employing carbon offset as a mitigation strategies which are discussed in this section.

One of the ways that the environmental impact can be mitigated is through carbon offset. This means for example that any greenhouse gas emission can be mitigated by investing in projects that reduce or remove these emissions elsewhere. Depending on the magnitude of the emissions generated by the UAV and/or its development process this is a viable option. If the cost of reducing emissions of the UAV outpace the cost of equivalent carbon offsets, it may be prudent to focus on maximizing performance and instead use offsetting strategies. Part of the revenue generated could be invested in green energy projects to offset the emissions generated by the UAV. This serves the additional benefit of generating more green energy and subsequently aligning with the UN sustainable development goals [149].

Future Design and Development

After the conclusion of the DSE project, the design and development of the Airborne Minesweeper enters a new phase, marked by future development. The phases of development after DSE completion are divided into a few categories, which are executed at various stages of the product release. An overview of these phases is in Figure 17.2, and the phases identified are described below:

- X.2.1: The first step is to finalise the design. In X.2, the design is further refined. It starts by refining the design for every subsystem. While an exhaustive list is not provided here, this stage encompasses tasks such as the full design of control surfaces and interfaces between parts.
- X.2.2: Running somewhat concurrent, but also somewhat behind designing the UAV, is the verification and validation of every subsystem. This includes both non-destructive and destructive testing of components. Some fatigue testing is also performed here.
- X.2.3 Once all subsystems are developed, the final check shows whether the proposed system will theoretically meet all requirements. If this is not the case, iteration is necessary.
- X.2.4 In the likely case that not all requirements are immediately satisfied, it is necessary to iterate on the design. In this task, the system-level characteristics are iterated upon.
- X.2.5 Likewise, if iteration is necessary on the subsystem level, that can happen too. While the subsystems are already fully refined, they may still be improved. For example, optimization of the fuel budget may lead to a lower required fuel mass, making the fuel tank lighter.
- X.3.1 If the vehicle meets all requirements on paper, it is necessary to build and assemble a prototype. This is done in this task.
- X.3.2 Verification and validation of the system is arguably one of the most important tasks. In this task, the system is shown to have the same characteristics as expected from the design. This is also the first time the UAV actually flies and is therefore a major milestone.
- X.3.3 The second major milestone is the compliance check with all requirements, hence certification. By showing him or her that the system meets every requirement, the customer can be confident that the system will fulfil its purpose. If the aircraft does not meet all requirements, further iteration is necessary, which induces costs.
- X.3.4 Finally, once a sufficient number of customers has been found, the aircraft can enter mass production. The production is extensively documented in chapter 15, so that is not repeated here.
- X.4.1 While design is still taking place, the marketing department gets to work. By contacting future operators early on, the design can be adapted to the needs of the customers and the customers can reserve the budget for this large an investment.
- X.4.2 Once the aircraft is operational and entering production, personnel are trained on the operation and maintenance of the vehicle.
- X.4.3 The start of operation is the final milestone. If this milestone is reached, the project can rightfully be called a success.
- X.4.4 While the aircraft is operational, the operators send flight data to the manufacturer, to help with development. If there is a critical error affecting multiple operators, there may be a flaw in the design. The data allows the manufacturer or design company to remedy this flaw.
- X.4.5 Likewise, collecting feedback from customers is also important. By collecting this feedback, an overview can be gained of the efficacy of the product.
- X.4.6 At the same time, while the aircraft is in operation, the marketing department works on selling more aircraft. By expanding the customer market, demining can be sped up significantly.
- X.5 Finally, if major flaws are detected during operation or customers have points to improve the vehicle, these points may be considered. If the initial vehicle is successful, a revised version may be developed. However, this is currently still speculation and something to be considered in the future.

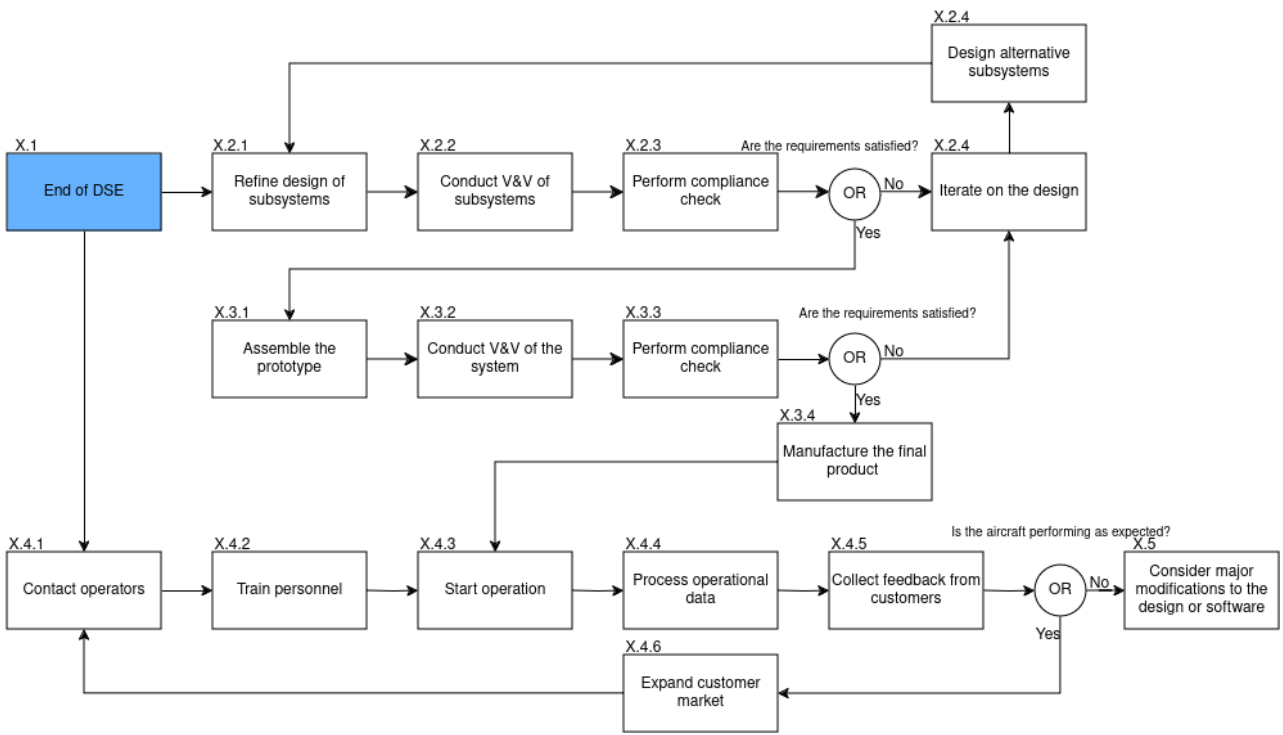


Figure 17.1: Future design and development roadmap

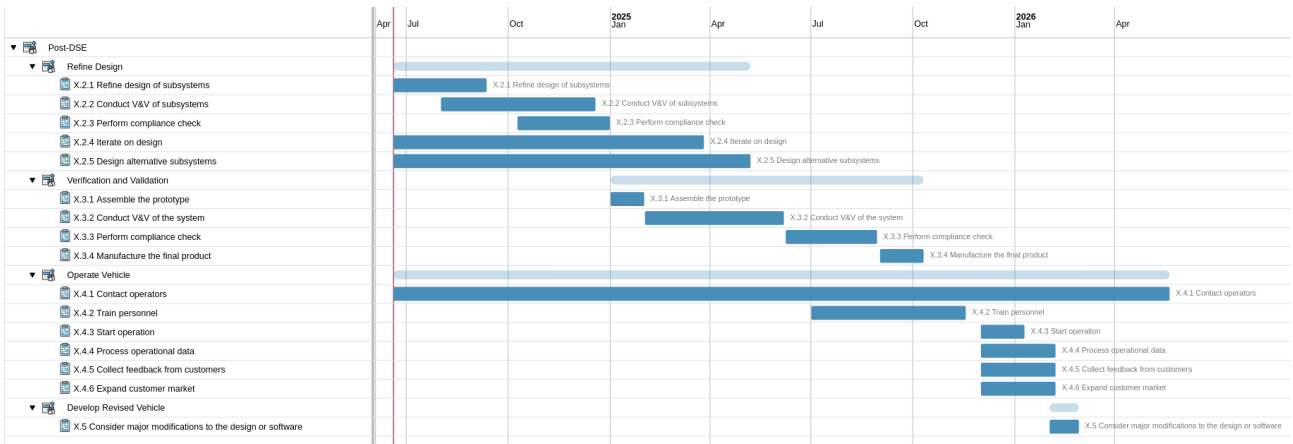


Figure 17.2: Gantt chart for phases after DSE

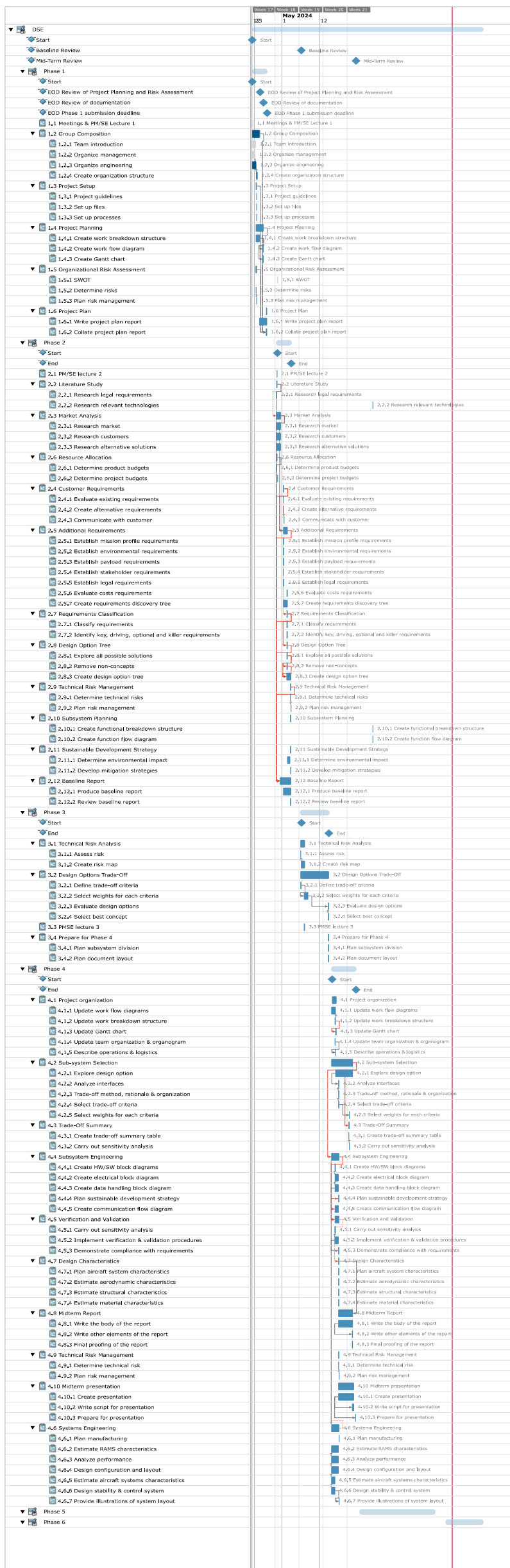


Figure 18.2: Gantt chart

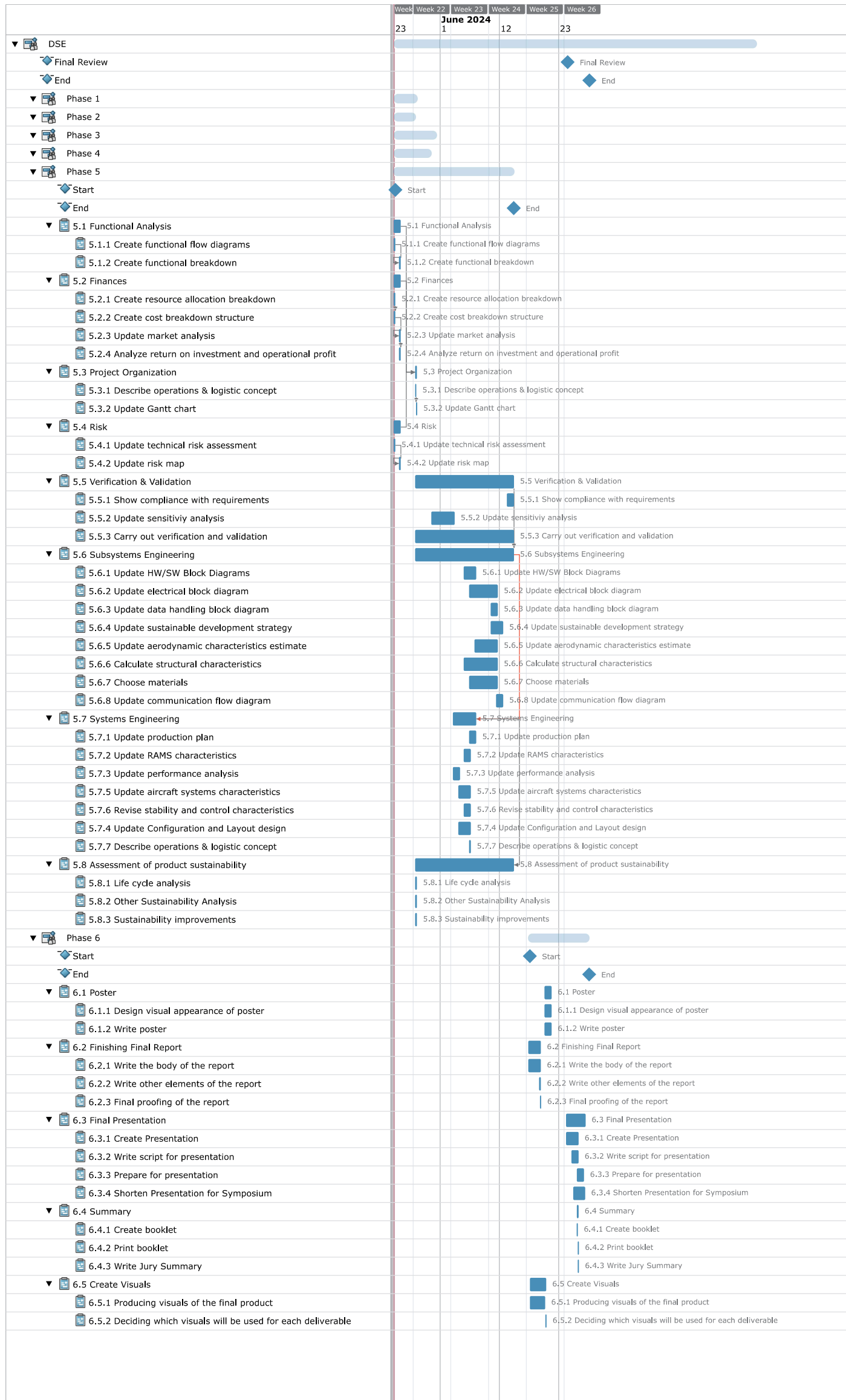


Figure 18.3: Gantt chart

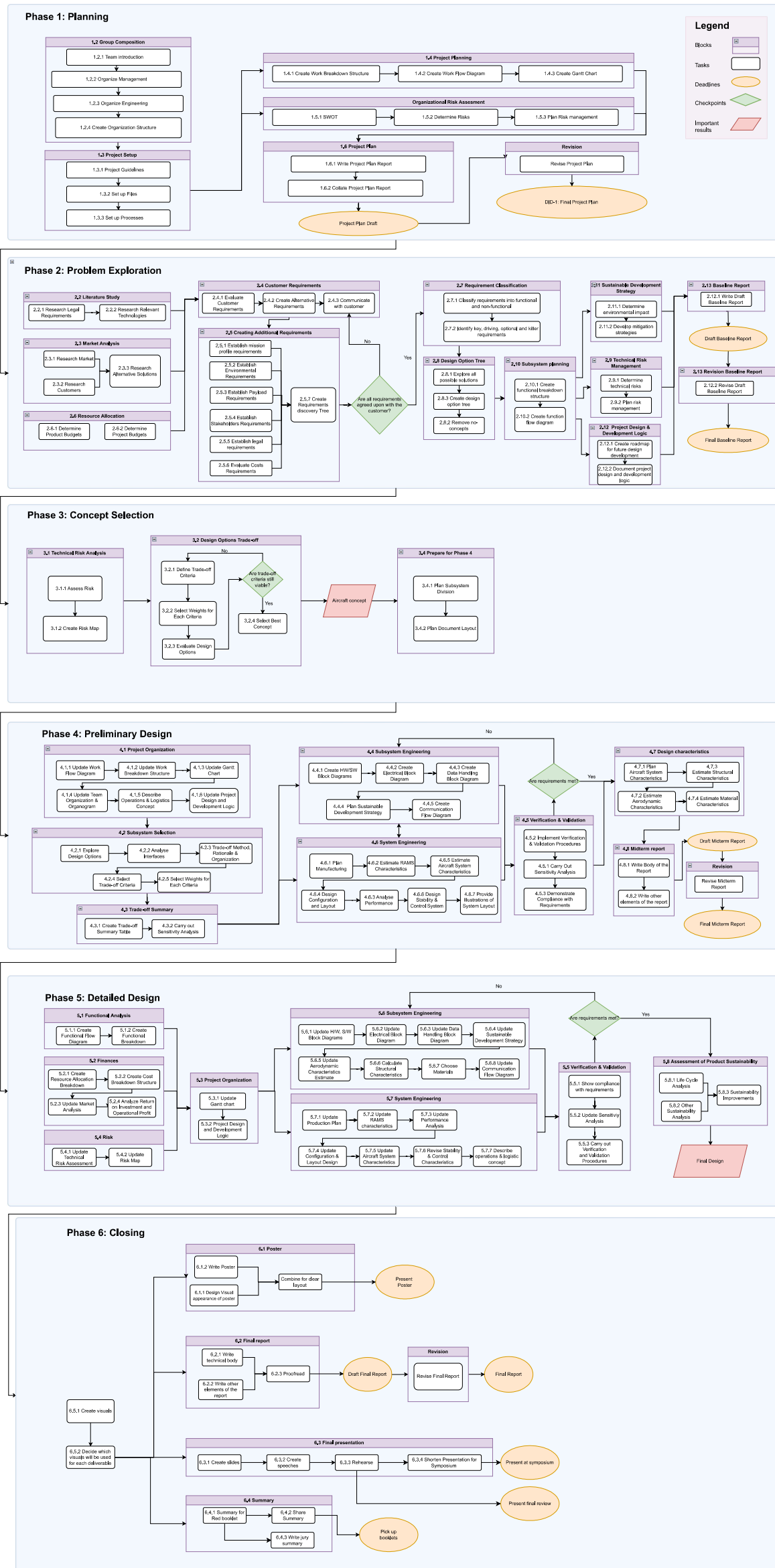


Figure 18.4: Work flow diagram

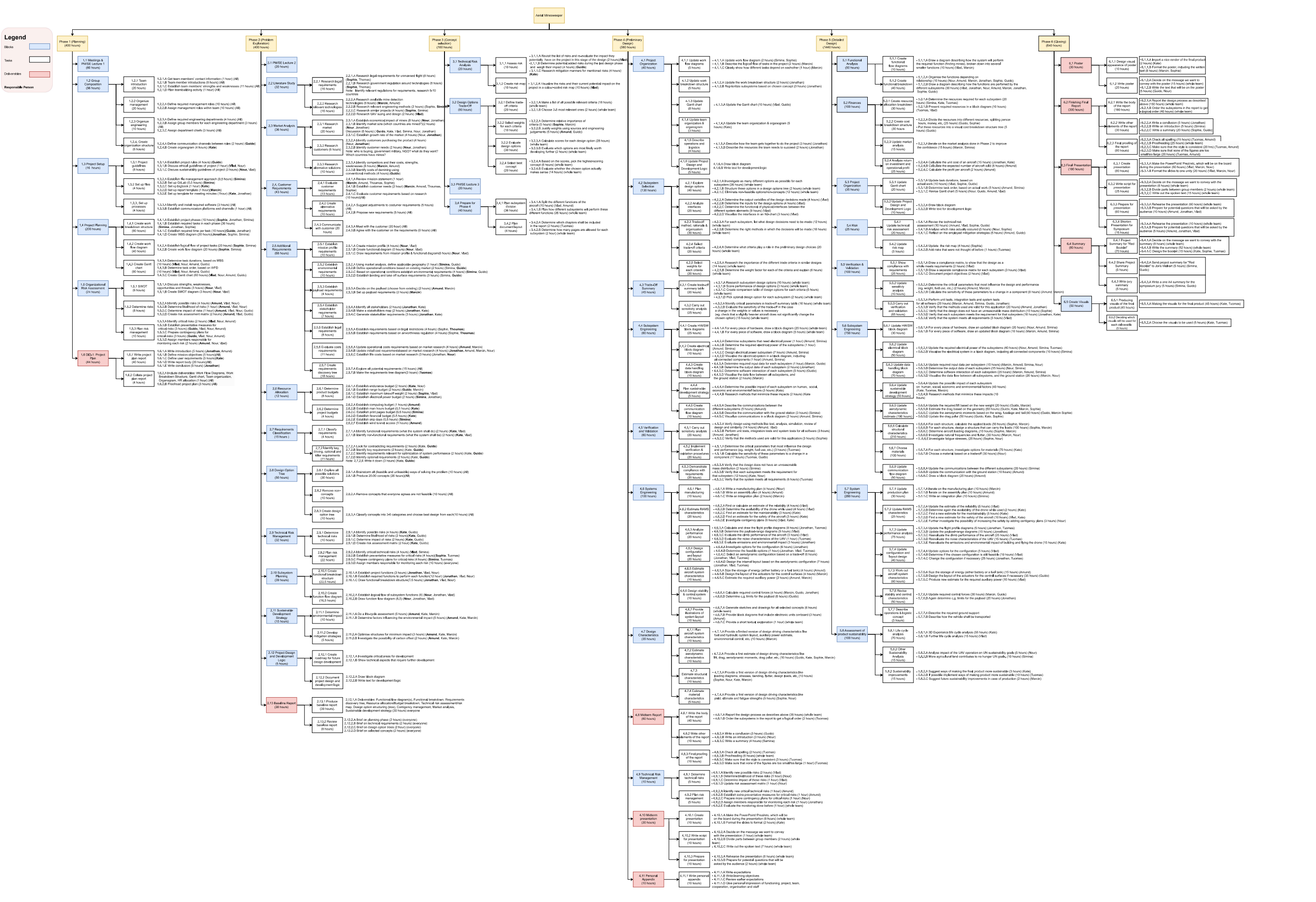


Figure 18.5: Work breakdown diagram

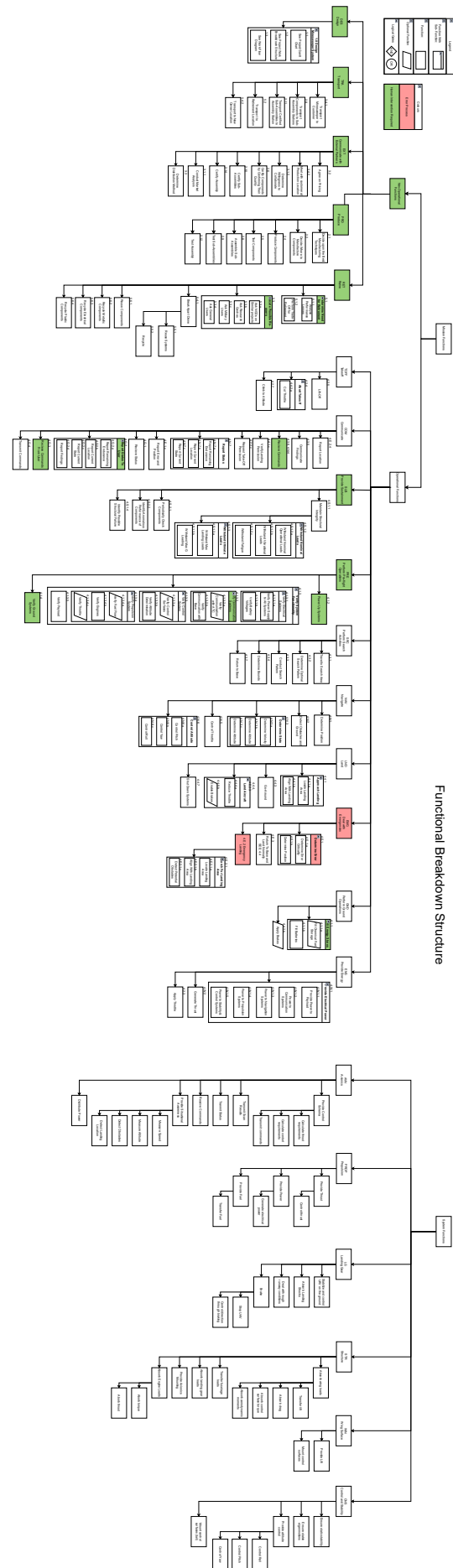


Figure 18.6: Functional Breakdown Diagram, with System Functions

Conclusion

The aim of this report is to present the design process of a UAV to perform humanitarian mine-sweeping operations. In previous reports, as reiterated in this report, the mission and project objectives have been established, and requirements were designed. Preliminary design and configurations trade-offs were also previously performed, and are thus reiterated. In this report, the detailed design of the UAV is presented, including the majority of systems and subsystems.

Class II estimations provides the background for sizing of essential UAV systems, providing bounds for system mass and drag. With this in mind, a wing planform is selected and the loading conditions of the UAV are established. Utilizing this power loading, an engine is sized and selected. Next, the empennage and control surfaces are integrated in the design and sized as appropriate to achieve stability and control requirements. Structural design and sizing is then performed for the wing and fuselage. This leads into the landing gear design, placing the gear and sizing the wheels and brakes. Finally, the avionics are designed and the electrical architecture and software design is laid out in detail.

Following the design stages, the aerodynamic and flight performance is analysed and critical diagrams are provided. This then leads into the estimation of current budgets including mass, cost, power, drag, and data handling. System analysis is then performed, providing functional analysis of the UAV and its system. In addition, the logistics and operations of the UAV is explored and the current best estimates of RAMS is provided. The requirements and design methods are then checked using verification and validation methods to ensure the quality of the design.

A production plan is then presented, providing the foundations of how the UAV may be produced. In order to ensure the sustainability of the project, a sustainable development strategy is then presented and a life-cycle analysis is performed. Planning for the future, the future design and development logic then provides the post-DSE plan. Finally, the organization and planning of the project as a whole is elaborated upon.

As a result of the design process, the UAV shown in Figure 19.1 was designed. Utilizing a conventional fixed wing configuration with tail-dragger landing gear, the UAV is designed to perform in rough environments and to search for minefields in hard-to-reach areas. The easily-replacable two-stroke piston engine is placed on top of the fuselage for protection against foreign object debris and to improve ground clearance, while the H-tail guarantees stability independent of engine throttle. In the fuselage, a large 10 kg sensor package is placed which – combined with a 4 hour endurance – provides ample ability to assist humanitarian demining efforts through assistance in the non-technical survey.



Figure 19.1: Final UAV Design

In the continuation of this detail design, most systems require future effort concerning their integration. Fuel lines and a filling system must be designed for the propulsion system, control surfaces hinges must be designed, circuitry and wiring for the electronics must be placed, and much more is still not complete. These tasks are left as future work that should be continued in order to make the UAV a viable design.

At this stage, the detail design meets most requirements, but there are still some requirements that are not met. As such, there is also a necessity for critical evaluation of the requirements but also the design, in order to ensure that there is a conformity between requirements and design.

Lastly, the payload to be placed in the UAV must be designed. As this has been designated out of scope, it is left as a future exercise that should be completed for this UAV to be able to perform its mission.

References

- [1] United Nations. "The deadly legacy of landmines | un news." (Apr. 2023), [Online]. Available: <https://news.un.org/en/story/2023/04/1135252> (visited on 04/24/2024).
- [2] International Campaign to Ban Landmines, "Landmine monitor 2023," Geneva: IBL-CMC, Nov. 2023. [Online]. Available: https://www.the-monitor.org/media/3389440/landmine-monitor-2023_web.pdf (visited on 04/24/2024).
- [3] Geneva International Centre for Humanitarian Demining. "Survey." (2024), [Online]. Available: <https://www.gichd.org/our-response/operations-management/survey/> (visited on 05/29/2024).
- [4] A. Kiste, E. Skorobogatova, G. van der Veen, et al., "Airborne minesweeper: Midterm report," 2024, unpublished.
- [5] J. Gundlach and J. A. Schetz, *Designing Unmanned Aircraft Systems: A Comprehensive Approach AIAA EDUCATION SERIES*. American Institute of Aeronautics and Astronautics, 2012.
- [6] J. Roskam, *Airplane Design*, 6th ed. Lawrence, Kansas, USA: DAR Corporation, 2018.
- [7] D. P. Raymer, *Aircraft Design-A Conceptual Approach*, second. American Institute of Aeronautics and Astronautics, 1992, pp. 77–100.
- [8] F. Götten, M. Havermann, C. Braun, F. Gómez, and C. Bil, "On the applicability of empirical drag estimation methods for unmanned air vehicle design," in *2018 Aviation Technology, Integration, and Operations Conference*, 2018, p. 3192.
- [9] J. Anderson, "Fundamentals of aerodynamics," in New York: McGraw-Hill Education, 2017, pp. 38–73.
- [10] J. Mueller, M. Paluszek, and Y. Zhao, "Development of an aerodynamic model and control law design for a high altitude airship," in *AIAA 3rd "Unmanned Unlimited" Technical Conference, Workshop and Exhibit*, Sep. 2024. DOI: 10.2514/6.2004-6479. [Online]. Available: <https://arc.aiaa.org/doi/abs/10.2514/6.2004-6479>.
- [11] D. Dulin and T. Takahashi, "Design implications of elliptical planform wings," Jan. 2015. DOI: 10.2514/6.2015-0397.
- [12] "Jump 20 group 3 vtol medium uas | defense vtol drone | airoverenvironment, inc." (), [Online]. Available: <https://www.avinc.com/uas/jump-20>.
- [13] "Mini mugin 2600mm carbon fiber h-tail/v-tail uav platform mugin uav." (), [Online]. Available: <https://www.muginuav.com/product/mini-mugin-2-6m-uav-t-tail-v-tail-platform/> (visited on 05/17/2024).
- [14] M. Hussain, "Detailed design of 120 seater passenger aircraft aircraft design project-ii," Ph.D. dissertation, Nov. 2019. DOI: 10.13140/RG.2.2.15108.48009.
- [15] B. CASTANIE, C. BOUVET, and M. Ginot, "Review of composite sandwich structure in aeronautic applications," *Composites Part C: Open Access*, vol. 1, p. 100004, 2020, ISSN: 2666-6820. DOI: <https://doi.org/10.1016/j.jcomc.2020.100004>. [Online]. Available: <https://www.sciencedirect.com/science/article/pii/S2666682020300049>.
- [16] A. A. van Heusden, "Recycling of composite materials," pp. 1–68, 2017.
- [17] S. Hilton, "Top techniques for composite production for uavs." (2022), [Online]. Available: <https://blog.polymeranocentrum.cz/top-techniques-for-composite-production-for-uavs/> (visited on 06/03/2024).
- [18] R. Vos, M. Hoogreef, and B. Zandbergen, "Aerospace design and systems engineering elements ae1222-ii." (2022), [Online]. Available: <https://brightspace.tudelft.nl/d21/le/content/407821/Home> (visited on 05/22/2024).
- [19] F. Oliviero, *Formula sheet aircraft*, 2022.
- [20] C. A. A. of Zimbabwe, *Civil aviation (remotely piloted aircraft) regulations (si 271/2018)*, 2018.
- [21] Eezi-Awn, "ADVANCE 1 plettenberg," Wild Access. (2021), [Online]. Available: <https://www.wildaccess.co.za/products/k9-roof-rack-for-toyota-100-series-land-cruiser-by-eezi-awn> (visited on 05/14/2024).
- [22] Skybrary. "Mean aerodynamic chord (mac)." (2024), [Online]. Available: <https://skybrary.aero/articles/mean-aerodynamic-chord-mac> (visited on 06/11/2024).
- [23] M. H. Sadraey, *Aircraft Design: A Systems Engineering Approach*. Chichester, UK: John Wiley & Sons, Ltd, 2012, ch. 9, pp. 479–545, ISBN: 978-1-11-835270-0. DOI: <https://doi.org/10.1002/9781118352700>. [Online]. Available: <https://onlinelibrary.wiley.com/doi/abs/10.1002/9781118352700> (visited on 05/16/2024).
- [24] HFE International. "Genpod 120: Owner's manual." (), [Online]. Available: <https://hfe.aero/wp-content/uploads/2024/01/HFEDCN660-REV-A.pdf> (visited on 06/13/2024).
- [25] Massachusetts Institute of Technology. "11.7 performance of propellers." (), (visited on 05/16/2024).
- [26] The Engineering Toolbox. "Fuels - densities and specific volumes." (2024), [Online]. Available: https://www.engineeringtoolbox.com/fuels-densities-specific-volumes-d_166.html (visited on 05/29/2024).
- [27] Mugin UAV. "Mugin 10l kevlar fuel tank." (), [Online]. Available: <https://www.muginuav.com/product/mugin-10l-kevlar-fuel-tank/> (visited on 06/15/2024).
- [28] E. Torenbeek, *Synthesis of subsonic airplane design: an introduction to the preliminary design of subsonic general aviation and transport aircraft, with emphasis on layout, aerodynamic design, propulsion and performance*. Springer Science & Business Media, 2013.
- [29] D. F. Oliviero. (2024), [Online]. Available: <https://brightspace.tudelft.nl/d21/le/content/407821/Home> (visited on 05/29/2024).
- [30] J. M. et al., "Flight dynamics," Lecture Notes, Mar. 2013.
- [31] Volz Servos. "DA 15-N-HT Volz servos - actuators manufactured in Germany," volz-servos.com. (2024), [Online]. Available: <https://www.volz-servos.com/actuators/detail/da-15-n-ht/> (visited on 06/18/2024).
- [32] Quorneng. "Control horn positions? - rc groups," rcgroups.com. (2024), [Online]. Available: <https://www.rcgroups.com/forums/showthread.php?3327171-Control-Horn-Positions> (visited on 06/25/2024).
- [33] Hobby King. "Blog - how to setup servos and control horns," hobbyking.com. (2024), [Online]. Available: <https://hobbyking.com/en-us/blog/servos-control-horns/> (visited on 06/25/2024).
- [34] J. E. Williams and S. R. Vukelich, "The usaf stability and control digital datcom. volume i. users manual," *McDonnell Douglas Astronautics co St Louis mo*, 1979.
- [35] G. I. R. A. Elham M. van Tooren, "An advanced quasi-analytical weight estimation method for airplane lifting surfaces," *Society of Allied Weight Engineers*, 2012.
- [36] T. Megson, *Aircraft Structures for Engineering*. Oxford, UK: Elsevier, 2008, ISBN: 978-0-7506-6739-5.
- [37] D. Howe, *Aircraft Loading and Structural Layout*. AIAA, 2004. DOI: <https://doi.org/10.1002/9781118352700>. (visited on 06/06/2024).
- [38] R. Sedaghati, "Multidisciplinary optimization standardization approach for integration and configurability," *Department of Mechanical and Industrial Engineering Concordia University*, 2006.
- [39] Abbott Aerospace Uk. "Web shear buckling." (2019), [Online]. Available: <https://www.abbottaerospace.com/aa-sb-001/15-local-stability-isotropic-materials/15-2-general-buckling-expression/15-2-3-web-shear-buckling-rectangular/> (visited on 06/07/2024).
- [40] R. C. Hibbeler, "Engineering mechanics," Pearson Education, Inc., 2016.
- [41] Abbott Aerospace UK Ltd. "6.1.2 first moment of area." (), [Online]. Available: <https://www.abbottaerospace.com/aa-sb-001/6-section-properties/6-1-introduction/6-1-2-first-moment-of-area-q/>.
- [42] "Aluminum 7075-t6; 7075-t651." (), [Online]. Available: <https://www.matweb.com/search/DataSheet.aspx?MatGUID=4f19a42be94546b686bbf43f79c51b7d&ckck=1>.
- [43] J. Melkert and C. Rans, "Structural analysis & design." (2023), [Online]. Available: <https://brightspace.tudelft.nl/d21/le/content/512864/viewContent/3071111/View> (visited on 06/17/2024).
- [44] R. Alderliesten. "Assumptions in truss analysis." (), [Online]. Available: [https://eng.libretexts.org/Bookshelves/Mechanical_Engineering/Introduction_to_Aerospace_Structures_and_Materials_\(Alderliesten\)/02%3A_Analysis_of_Statically_Determinate_Structures/05%3A_Internal_Forces_in_Plane_Trusses/5.04%3A_Assumptions_in_Truss_Analysis](https://eng.libretexts.org/Bookshelves/Mechanical_Engineering/Introduction_to_Aerospace_Structures_and_Materials_(Alderliesten)/02%3A_Analysis_of_Statically_Determinate_Structures/05%3A_Internal_Forces_in_Plane_Trusses/5.04%3A_Assumptions_in_Truss_Analysis) (visited on 06/13/2024).
- [45] S. V. B. P. Shwetha K, "Comparison between thin plate and thick plate from navier solution using Matlab software," *International Research Journal of Engineering and Technology*, vol. 5, pp. 2675–2680, 6 Jun. 2018. [Online]. Available: <https://www.irjet.net/archives/V5/i6/IRJET-V5I6500.pdf>.
- [46] T. Wierzbicki. "9.2: Deflection behavior for beam with compressive axial loads and transverse loads," Massachusetts Institute of Technology. (2024), [Online]. Available: [https://eng.libretexts.org/Bookshelves/Mechanical_Engineering/Structural_Mechanics_\(Wierzbicki\)/09%3A_Advanced_Topic_in_Column_Buckling/9.02%3A_Deflection_Behavior_for_Beam_with_Compressive_Axial_Loads_and_Transverse_Loads](https://eng.libretexts.org/Bookshelves/Mechanical_Engineering/Structural_Mechanics_(Wierzbicki)/09%3A_Advanced_Topic_in_Column_Buckling/9.02%3A_Deflection_Behavior_for_Beam_with_Compressive_Axial_Loads_and_Transverse_Loads) (visited on 06/17/2024).

- [47] N. S. Currey, *Aircraft Landing Gear Design: Principles and Practices*, 4th ed. Washington D.C., USA: American Institute of Aeronautics and Astronautics, Inc., 1988.
- [48] Federal Aviation Administration, *Airplane Flying Handbook (FAA-H-8083-3C)*. Oklahoma City, USA: United States Department of Transportation, Federal Aviation Administration, 2021, ISBN: 9781510771949.
- [49] Tost. "Technical specification landing wheel mini 150 v modified valve hole." (Aug. 2017), [Online]. Available: https://wingsandwheels.com/media/wysiwyg/PDF/Tost/031513_Mini_150_V_Specification.pdf.
- [50] Tost. "Tost flugzeuggeratebau: Product catalog." (Aug. 2017), [Online]. Available: https://www.tost.de/tost-cms/wp-content/uploads/katalog/Tost_Catalogue_engl_2021.pdf.
- [51] E. Retracts. "Set wheels & brakes ø150 mm (pair)." (2024), [Online]. Available: <https://www.electron-retracts.com/product/150-wheelbrake/> (visited on 06/18/2024).
- [52] Revtec. "Revtec - airplane wheels - rubber w/ nylon rim - 50mm - shaft dia. 3mm - 2 pcs." (), [Online]. Available: <https://revtec.be/en/product/GF-3165-003/revtec-airplane-wheels-rubber-w-nylon-rim-50mm-shaft-dia-3mm-2-pcs> (visited on 06/11/2024).
- [53] G. Ruijgrok, *Elements of airplane performance*, 2nd ed. Leeghwaterstraat 42, Delft: Delft Academic Press, 2013.
- [54] S. Gudmundsson, "The anatomy of the landing gear," in *General Aviation Aircraft Design*, S. Gudmundsson, Ed. Boston: Butterworth-Heinemann, 2014, ch. 13, pp. 547-580, ISBN: 978-0-12-397308-5. DOI: <https://doi.org/10.1016/B978-0-12-397308-5.00013-1>. [Online]. Available: <https://www.sciencedirect.com/science/article/pii/B9780123973085000131> (visited on 05/16/2024).
- [55] S. Gudmundsson, Ed., *General Aviation Aircraft Design*. Boston: Butterworth-Heinemann, 2014, p. ii, ISBN: 978-0-12-397308-5. DOI: <https://doi.org/10.1016/B978-0-12-397308-5.03001-4>. [Online]. Available: <https://www.sciencedirect.com/science/article/pii/B9780123973085030014>.
- [56] E. C. Courses. "Secant formula." (2016), [Online]. Available: <http://www.engineeringcorecourses.com/solidmechanics2/C5-buckling/C5.2-secant-formula/theory/> (visited on 06/06/2024).
- [57] D. Riehle, "The economic motivation of open source software: Stakeholder perspectives," *Computer*, vol. 40, no. 4, pp. 25-32, 2007. DOI: 10.1109/MC.2007.147.
- [58] Unmanned Systems Technology. "Uav autopilot | autopilots for drones & uas | autopilot manufacturers," unmannedsystemstechnology.com. (2024), [Online]. Available: <https://www.unmannedsystemstechnology.com/expo/uav-autopilot-systems/> (visited on 06/04/2024).
- [59] UAVOS Inc. "Ap 10.2 uav autopilot system - uavos," uavos.com. (2024), [Online]. Available: <https://www.uavos.com/products/autopilots/ap10-2-automatic-control-system-for-uav-mini/> (visited on 06/04/2024).
- [60] uAvionix. "George - uavionix," uavionix.com. (2023), [Online]. Available: <https://uavionix.com/products/george/> (visited on 06/04/2024).
- [61] CubePilot. "The cube orange+ standard set," cubepilot.org. (2024), [Online]. Available: <https://cubepilot.org/#/cube/features> (visited on 06/04/2024).
- [62] Embention. "Autopilot 1x for drone (uav) & evtol | veronte ecosystem," embention.org. (2024), [Online]. Available: <https://www.embention.com/en/product/1x/> (visited on 06/04/2024).
- [63] MicroPilot. "Mp2128g2 advanced uav autopilot," micropilot.com. (2024), [Online]. Available: <https://store.micropilot.com/product-p/a-2128-g2.htm> (visited on 06/04/2024).
- [64] Auterion. "Skynode x - the best autopilot for autonomous robots," auterion.com. (2023), [Online]. Available: <https://auterion.com/product/skynode-x/> (visited on 06/04/2024).
- [65] M. H. Sadraey, *Design of Unmanned Aerial Systems*. Chichester, UK: John Wiley & Sons, Ltd, 2020, ISBN: 9781119508618. DOI: <https://doi.org/10.1002/9781119508618>.
- [66] u-blox. "Real-time kinematic (rtk)." (2022), [Online]. Available: <https://www.u-blox.com/en/technologies/rtk-real-time-kinematic> (visited on 06/06/2024).
- [67] W. Stempfhuber, "3d-rtk capability of single gnss receivers," *International Archives of the Photogrammetry, Remote Sensing and Spatial Information Sciences*, 2013.
- [68] VectorNav, *Vn-200 smd gnss/ins*, 2023.
- [69] L. Wanninger, M. Thiemi, and V. Frevert, "Multi-frequency quadrifilar helix antennas for cm-accurate gnss positioning," *Journal of Applied Geodesy*, 2022.
- [70] Tallysman, *Hc771 single-band helical antenna*, 2019, [Online]. Available: <https://www.tallysman.com/app/uploads/2020/02/Tallysman%20%AE-HC771-Datasheet.pdf>.
- [71] Nanoradar. "24ghz alimeter radar nra24." (2019), [Online]. Available: <http://en.nanoradar.cn/Article/detail/id/372.html> (visited on 06/06/2024).
- [72] Nanoradar, *White paper on nra24 millimeter wave radar*, 2017.
- [73] PX4, *PX4 autopilot user guide | PX4 guide (main)*, docs.px4.io, 2024, [Online]. Available: <https://docs.px4.io/main/en/> (visited on 06/18/2024).
- [74] J. Tilmans, S. Jackisch, and D. Moormann, "Investigation of the influence of rain on pitot-static measuring systems of unmanned aerial vehicles," 2024.
- [75] M. P. a.s. "Pitot-static systems." (2024), [Online]. Available: <https://www.mikrotechna.cz/index.php/en/aerospace-manufacturing/pitot-static-systems> (visited on 06/06/2024).
- [76] Hwurzburg. "Pitot tube considerations," ArduPilot. (2024), [Online]. Available: <https://ardupilot.org/plane/docs/common-pitot-considerations.html> (visited on 06/06/2024).
- [77] TE Connectivity, *MS4525DO*, te.com, 2024, [Online]. Available: https://www.te.com/commerce/DocumentDelivery/DDEController?Action=showdoc&DocId=Data+Sheet%7FMS4525DO%7FB10%7Fpdf%7FEnglish%7FENG_DS_MS4525DO_B10.pdf%7FCAT-BLPS0002 (visited on 06/19/2024).
- [78] J. Anderson, *Introduction to Flight*. McGraw-Hill Education, 2016.
- [79] Digital Dutch. "1976 standard atmosphere calculator." (), [Online]. Available: <https://www.digitaldutch.com/atmoscalc/> (visited on 06/07/2024).
- [80] J. N. Yasin, S. A. S. Mohamed, M.-H. Haghbayan, J. Heikkonen, H. Tenhunen, and J. Plosila, "Unmanned aerial vehicles (uavs): Collision avoidance systems and approaches," *IEEE Access*, vol. 8, pp. 105 139-105 155, 2020. DOI: 10.1109/ACCESS.2020.3000064.
- [81] N. Aswini, E. Krishna Kumar, and S. Uma, "Uav and obstacle sensing techniques—a perspective," *International Journal of Intelligent Unmanned Systems*, vol. 6, no. 1, pp. 32-46, 2018. DOI: <https://doi.org/10.1108/IJIUS-11-2017-0013>.
- [82] J. Kim, B.-j. Park, and J. Kim, "Empirical analysis of autonomous vehicles lidar detection performance degradation for actual road driving in rain and fog," *Sensors*, vol. 23, no. 6, 2023, ISSN: 1424-8220. DOI: 10.3390/s23062972. [Online]. Available: <https://www.mdpi.com/1424-8220/23/6/2972>.
- [83] LIVOX. "Avia lidar sensor - livox," livotech.com. (2024), [Online]. Available: <https://www.livotech.com/avia> (visited on 07/04/2024).
- [84] B. Wilkinson, H. Lassiter, A. Abd-Elrahman, et al., "Geometric targets for uas lidar," *Remote Sensing*, vol. 11, p. 3019, Dec. 2019. DOI: 10.3390/rs11243019. [Online]. Available: https://www.researchgate.net/publication/337958175_Geometric_Targets_for_UAS_Lidar#fullTextFileContent (visited on 06/17/2024).
- [85] Botland. "Raspberry pi 5 8GB botland - robotic shop," botland.store. (2024), [Online]. Available: <https://botland.store/raspberry-pi-5-modules-and-kits/23905-raspberry-pi-5-8gb-5056561803326.html> (visited on 06/17/2024).
- [86] Trillium. "Trillium | HD25," trilliumeng.com. (2024), [Online]. Available: <https://www.trilliumeng.com/gimbals/hd25> (visited on 06/17/2024).
- [87] Gremesy. "Vio g1 - gremesy," gremesy.com. (2022), [Online]. Available: <https://gremesy.com/vio-g1-store> (visited on 06/13/2024).
- [88] ITU, "Articles," in *Radio Regulations*, vol. 1, 2020, pp. 35-186.
- [89] UAVOS Inc. "pMDDL Radio data link system - UAVOS," uavos.com. (2024), [Online]. Available: <https://www.uavos.com/products/communication-systems/pmddlradio-data-link-system/> (visited on 06/17/2024).
- [90] UAVOS Inc. "Automatic tracking system - UAVOS," uavos.com. (2024), [Online]. Available: <https://www.uavos.com/products/communication-systems/automatic-tracking-system/> (visited on 06/17/2024).
- [91] RF Solutions. "A rugged high gain antenna for 2.4ghz & WLAN," rfsolutions.co.uk. (2024), [Online]. Available: <https://www.rfsolutions.co.uk/antennas-c8/a-rugged-high-gain-antenna-for-2-4ghz-wlan-p174> (visited on 06/17/2024).
- [92] Mouser Electronics. "ICEFIN24NMOHF Pulse electronics | Mouser Netherlands," mouser.com. (2024), [Online]. Available: <https://nl.mouser.com/ProductDetail/Pulse-Electronics/ICEFIN24NMOHF?qs=50X2FYPcxemzSedcODkTHQ%3D%3D> (visited on 06/17/2024).
- [93] Averse. "Fresnel diagram," wikimedia.org. (2007), [Online]. Available: <https://commons.wikimedia.org/wiki/File:FresnelSVG.svg> (visited on 06/17/2024).

- [94] J. D. Parsons and P. J. D. Parsons, *The mobile radio propagation channel*. Chichester, UK: John Wiley & Sons, Ltd, 2000, vol. 2, ISBN: 0-470-84152-4.
- [95] EASA. “Remote identification will become mandatory for drones across europe.” (2023), [Online]. Available: <https://www.easa.europa.eu/en/document-library/general-publications/remote-identification-will-become-mandatory-for-drones-across> (visited on 06/06/2024).
- [96] FAA. “Remote identification of drones.” (2024), [Online]. Available: https://www.faa.gov/uas/getting_started/remote_id (visited on 06/06/2024).
- [97] Dronetag. “What is remote id?” (2024), [Online]. Available: <https://drone-remote-id.com/> (visited on 06/06/2024).
- [98] FAA. *Remote identification (remote id) is here. are you ready?* 2023. [Online]. Available: https://www.faa.gov/uas/getting_started/remote_id/3-RID-Remote_ID_Main (visited on 06/06/2024).
- [99] Holybro. “Remote id.” (2024), [Online]. Available: <https://holybro.com/products/remote-id?variant=43034167312573> (visited on 06/06/2024).
- [100] RTCA, Inc. *Minimum aviation system performance standards for automatic dependent surveillance broadcast (ads-b)*, 2002.
- [101] uAvionix. “The world’s smallest and lightest ads-b solution for suvs.” (2024), [Online]. Available: <https://uavionix.com/products/ping2020/> (visited on 06/07/2024).
- [102] Sullivan. “Ssrc-500c-10 | sullivan,” [sullivanuv.com](https://www.sullivanuv.com/product-item/ssrc-500c-10/). (2024), [Online]. Available: <https://www.sullivanuv.com/product-item/ssrc-500c-10/> (visited on 06/17/2024).
- [103] Maxamps Lithium Batteries. “LiPo 23000 8S 29.6v battery pack,” [maxamps.com](https://maxamps.com/products/lipo-23000-8s-29-6v-battery-pack). (2024), [Online]. Available: <https://maxamps.com/products/lipo-23000-8s-29-6v-battery-pack> (visited on 06/17/2024).
- [104] Maxamps. “Graphene LiPo 670 8S 29.6v battery pack,” [maxamps.com](https://maxamps.com/collections/8s-lipo-battery-29-6v/products/graphene-lipo-670-8s-battery). (2024), [Online]. Available: <https://maxamps.com/collections/8s-lipo-battery-29-6v/products/graphene-lipo-670-8s-battery> (visited on 06/17/2024).
- [105] TE Connectivity, *MS5611-01BA03 barometric pressure sensor, with stainless steel cap*, te.com, 2024. [Online]. Available: https://www.te.com/commerce/DocumentDelivery/DDEController?Action=showdoc&DocId=Data+Sheet%7FMS5611-01BA03%7FB3%7Fpdf%7FEnglish%7FENG_DS_MS5611-01BA03_B3.pdf%7FCAT-BLPS0036 (visited on 06/18/2024).
- [106] F. Oliviero. “Aerospace design and systems engineering elements ii ae2111-ii aircraft part.” (2022), (visited on 05/31/2024).
- [107] A. Deperrois, *Theoretical limitations and shortcomings of xflr5*, XFLR5, 2019.
- [108] Engineering Toolbox. “Rolling resistance.” (2024), [Online]. Available: https://www.engineeringtoolbox.com/rolling-friction-resistance-d_1303.html (visited on 06/03/2024).
- [109] P. Cenek, N. Jamieson, and M. McLarin, “Frictional characteristics of road-side grass types,” Jan. 2000.
- [110] T. Yager, *Friction Characteristics of Three 30 by 11.5-14.5, Type 8, Aircraft Tires with Various Tread Groove Patterns and Rubber Compounds*, 1977. [Online]. Available: <https://books.google.nl/books?id=zesQAQAIAAJ>.
- [111] ICAO. “Aircraft braking performance standards.” (2023), [Online]. Available: <https://www.icao.int/Meetings/grf2019/Documents/Presentations/GRF2019%20S8%20John%20Gadzinski%20-%20Four%20Winds%20Aerospace.pdf> (visited on 06/05/2024).
- [112] A. Hirschberg and S. Rienstra, “An introduction to aeroacoustics,” vol. 1823, pp. 18–7, Aug. 2004.
- [113] D. Miljkovi, “Methods for attenuation of unmanned aerial vehicle noise,” in *2018 41st International Convention on Information and Communication Technology, Electronics and Microelectronics (MIPRO)*, 2018, pp. 0914–0919. DOI: 10.23919/MIPRO.2018.8400169.
- [114] M. V. Farré. “Average salary in bulgaria.” (2024), [Online]. Available: [https://talentup.io/blog/average-salary-in-bulgaria/#:~:text=5%20Conclusion-,Average%20salary%20overview,2%2000%20\(about%20E2%82%AC1%2020\)](https://talentup.io/blog/average-salary-in-bulgaria/#:~:text=5%20Conclusion-,Average%20salary%20overview,2%2000%20(about%20E2%82%AC1%2020)) (visited on 06/19/2024).
- [115] Dassault Systemes. “Create and manage sophisticated mechanical projects.” (2024), [Online]. Available: <https://www.3ds.com/store/catia-mechanical-designer> (visited on 06/19/2024).
- [116] Glassdoor. “Engineering salaries in amsterdam, netherlands.” (2024), [Online]. Available: https://www.glassdoor.sg/Salaries/amsterdam-engineering-salary-SRCH_IL.0,9_IM1112_KO10,21.htm (visited on 06/19/2024).
- [117] Signa. “Signa expert cad manufacturing workstation - autocad, revit, solidworks certified - amd, intel cpus.” (2024), [Online]. Available: <https://www.signa.com/products/signa-expert-cad-workstation> (visited on 06/19/2024).
- [118] Dell. “Cad workstations.” (2024), [Online]. Available: <https://www.dell.com/en-us/lp/cad-workstations> (visited on 06/19/2024).
- [119] I. C. to Ban Landmines. “Why landmines are still a problem.” (2024), [Online]. Available: <https://www.icbl.org/en-gb/problem/why-landmines-are-still-a-problem.aspx#:~:text=The%20biggest%20stockpiles%20of%20antipersonnel,China%2C%20and%20the%20United%20States> (visited on 04/29/2024).
- [120] H. Garbino, “The impact of landmines and explosive remnants of war on food security: The lebanese case,” *THE JOURNAL OF CONVENTIONAL WEAPONS DESTRUCTION*, vol. 23, no. 2, pp. 21–26, 2000.
- [121] L. Doswald-Beck, P. Herby, and J. Dorais-Slakmon. “Basic facts: The human cost of landmines - icrc.” (Jan. 1995), [Online]. Available: <https://www.icrc.org/en/doc/resources/documents/misc/57jmcj.htm> (visited on 04/29/2024).
- [122] I. Piddubnyi, “Russia’s war in ukraine: Price and opportunity cost of demining land of small-scale agricultural producers general context and objective,” Kyiv School of Economics, Aug. 2023. [Online]. Available: https://kse.ua/wp-content/uploads/2023/09/Mining-brief_Final-1.pdf (visited on 05/30/2024).
- [123] G. I. C. for Humanitarian Demining, *A Guide to mine Action*, 5th ed. 2014.
- [124] G. I. C. for Humanitarian Demining, *A study of manual mine clearance*. Geneva International Centre for Humanitarian Demining, 2005, ISBN: 2884870407.
- [125] “Demining ukraine: Bringing lifesaving expertise back home | un news.” (2023), [Online]. Available: <https://news.un.org/en/story/2023/07/1138477> (visited on 04/29/2024).
- [126] I. Osmolovska, “Walking on fire: Demining in ukraine,” *Globsec*, 2023. [Online]. Available: www.globsec.org.
- [127] K. Nieczypor. “Ukraine: The worlds biggest minefield | osw centre for eastern studies.” (Nov. 2023), [Online]. Available: <https://www.osw.waw.pl/en/publikacje/osw-commentary/2023-11-22/ukraine-worlds-biggest-minefield> (visited on 04/29/2024).
- [128] Minesweepers. “Facts about landmines.” (2013), [Online]. Available: <https://landminefree.org/contact/> (visited on 04/29/2024).
- [129] M. Baji, “Testing of remotely piloted aircraft systems with a thermal infrared camera to detect explosive devices at contaminated areas and validation of developed standard operational procedures,” 2021.
- [130] H. International, “2021 hi network annual report,” 2021.
- [131] “Guidelines for Development of Civil Aircraft and Systems,” SAE Aerospace, Standard, Dec. 2012.
- [132] “Guidelines and methods for conducting the safety assessment process on civil airborne systems and equipment,” SAE International, Standard, Dec. 1996.
- [133] S. Chiesa, S. C. Aleina, M. Fioriti, and R. Fusaro, “Contribution to rams estimation in early design phases of unmanned aerial vehicles-uavs,” Working paper proposed for publication in *Journal of Mechanics and Control*, Tech. Rep., 2014.
- [134] B. S. Blanchard, D. Verma, and E. L. Peterson, *Maintainability: A Key to Effective Servicability and Maintenance Management*. John Wiley & Sons, Inc., 1995, ISBN: 0-471-59132-7.
- [135] M. Baptista, S. Sankararaman, I. de Medeiros, C. Nascimento Jr, H. Prendering, and E. Henriques, “Forecasting fault events for predictive maintenance using data-driven techniques and arma modeling,” *Computers & Industrial Engineering*, vol. 115, Nov. 2017. DOI: 10.1016/j.cie.2017.10.033.
- [136] D. Communier, M. F. Salinas, O. C. Moyao, and R. M. Botez, “Aero structural modeling of a wing using CATIA V5 and XFLR5 software and experimental validation using the Price-Paidoussis wing tunnel,” Jun. 2015. [Online]. Available: <https://arc.aiaa.org/doi/pdf/10.2514/6.2015-2558>.
- [137] D. S. Hayashibara, “XFLR5 as a design tool in remotely controlled design-build-fly applications,” 2022. [Online]. Available: <https://arc.aiaa.org/doi/epdf/10.2514/6.2022-0003>.
- [138] S. Hall, “30 years of impact: An evaluation of the mine action programme of afghanistan,” *Tech. Rep.*, 2021. [Online]. Available: https://www.unmas.org/sites/default/files/evaluation_report_of_mine_action_programme_of_afghanistan.pdf.
- [139] K. E. Katkinson, *Aircraft Landing Gear Design: Principles and Practices*, 4th ed. Washington D.C., USA: American Institute of Aeronautics and Astronautics, Inc., 1988.

- [140] GORE and SKYFLEX6. "Gore6 skyflex6 aerospace materials for civil & military applications reliable aircraft sealing and aircraft surface protection." (2023), [Online]. Available: https://www.gore.com/SKYFLEX-Aerospace-Materials?xcmp=skyflex_aero_ppc_skyflex_google_NA%7C%7Cother-materials&s_kwcid=AL!13180!3!310997011193!p!g!aircraft%20materials&gad_source=1&gclid=Cj0KQjw4MSzBhC8ARIsAPFOuyWeCvqAxiJkUM6j2T7N_luULfeHRBrpPPpb9y4wqOGXQCmBu-AKovEaAiIrEALw_wcB (visited on 06/18/2024).
- [141] Hygrade laser profiling. "Which industries typically use a laser cutter?" Hygrade laser profiling. (), [Online]. Available: <https://www.hygradelaser.com.au/top-7-industries-that-use-laser-cutting-technology#:~:text=Known%20for%20its%20extensive%20utilisation,airplane%20parts%2C%20and%20spacecraft%20components.> (visited on 06/18/2024).
- [142] 3DEXperience. "Laser cutting: Advantages & inconvenients," 3DEXperience. (), [Online]. Available: <https://www.3ds.com/make/solutions/blog/laser-cutting-advantages-inconvenients> (visited on 06/18/2024).
- [143] L. F. Francis, *Materials Processing, A Unified Approach to Processing of Metals, Ceramics and Polymers*. Academic press, 2016, ISBN: 978-0-12-385132-1. DOI: <https://doi.org/10.1016/C2009-0-64287-2>.
- [144] CNC Multitool. "High-precision cold wire cutting," CNC Multitool. (2024), [Online]. Available: <https://www.cnc-multitool.com/> (visited on 06/19/2024).
- [145] De Laser Frezer. "Pe-foam lasersnijden," De Laser Frezer. (2024), [Online]. Available: https://www.delaserfrezer.com/kunststof/pe-foam-inlays-laten-lasersnijden/?gad_source=1&gclid=CjwKCAjwg8qzBhAoEiwAWagLrHE8h26TTmpQPvtS19dgJETdvmFuAA0m10TrTgPK4qKJOrPALOaGPBoCWkwQAvD_BwE (visited on 06/19/2024).
- [146] Wayken. "Wire edm cutting: How it works & applications," Wayken. (Oct. 21, 2022), [Online]. Available: <https://waykenrm.com/blogs/wire-edm-process/> (visited on 06/19/2024).
- [147] J. Schlick. "What is cold cutting: Definition, types, machines & cost," Techni WaterJet. (Nov. 7, 2023), [Online]. Available: <https://www.techniwaterjet.com/cold-cutting/> (visited on 06/19/2024).
- [148] Foam Order. "Foam cutting tools: Hot knife, hot wire & more," Foam Order. (2024), [Online]. Available: <https://www.foamorder.com/learning-center/diy/foam-cutting-tools> (visited on 06/19/2024).
- [149] United Nations. "Take action for the sustainable development goals." (), [Online]. Available: <https://www.un.org/sustainabledevelopment/sustainable-development-goals/> (visited on 04/24/2024).
- [150] A. Gangwar, "Impact of war and landmines on environment," in *Forum Proceedings: Landmines-Challenges to Humanity and Environment*, vol. 20, Srinigar, India, Apr. 2003. [Online]. Available: <https://lib.icimod.org/api/files/50677757-0b2b-435d-87fc-3ec39f3b4f2a/1409.pdf> (visited on 05/30/2024).
- [151] S. Goring. "The transformative impact of mine action on agriculture and food security," MAG. (Mar. 2024), [Online]. Available: <https://www.maginternational.org/whats-happening/the-impact-of-mine-action-on-agriculture-and-food/> (visited on 05/30/2024).
- [152] T. Sijpkes, "Challenge the future AE3211-II production of aerospace systems lecture 9b: Lean manufacturing," TU Delft. [Online]. Available: <https://brightspace.tudelft.nl/d21/le/content/615479/viewContent/3628226/View> (visited on 05/01/2024).
- [153] "Circular economy: Definition, importance and benefits | topics | european parliament." (May 2023), [Online]. Available: <https://www.europarl.europa.eu/topics/en/article/20151201STO05603/circular-economy-definition-importance-and-benefits> (visited on 05/13/2024).
- [154] J. Z. Rui Lin Bo Liu and S. Zhang., "Microstructure evolution and properties of 7075 aluminum alloy recycled from scrap aircraft aluminum alloys," *Journal of Materials Research and Technology*, vol. 19, p. 3171, 2022. DOI: <https://doi.org/10.1016/j.jmrt.2022.05.011>.
- [155] The Engineering Toolbox. "The ultimate guide to styrofoam recycling: From waste to sustainable solutions," greentheory.com. (2023-08-16), [Online]. Available: <https://www.greentheory.me/post/the-ultimate-guide-to-styrofoam-recycling-from-waste-to-sustainable-solutions> (visited on 06/18/2024).
- [156] Recycle. "How are electrical items recycled?" recycelenow.com. (2021), [Online]. Available: <https://www.recycelenow.com/how-to-recycle/electrical-item-recycling> (visited on 06/18/2024).
- [157] C. Robinson and K. Huun. "The impact of recycling on climate change," University of Colorado Boulder. (2023-01-15), [Online]. Available: <https://www.colorado.edu/center/2023/12/15/impact-recycling-climate-change> (visited on 06/18/2024).
- [158] "Landfills: A serious problem for the environment," Sustainability for all. (N.D.), [Online]. Available: https://www.activesustainability.com/environment/landfills-serious-problem-environment/?_adin=01670309623 (visited on 06/18/2024).

Drawings and Layout

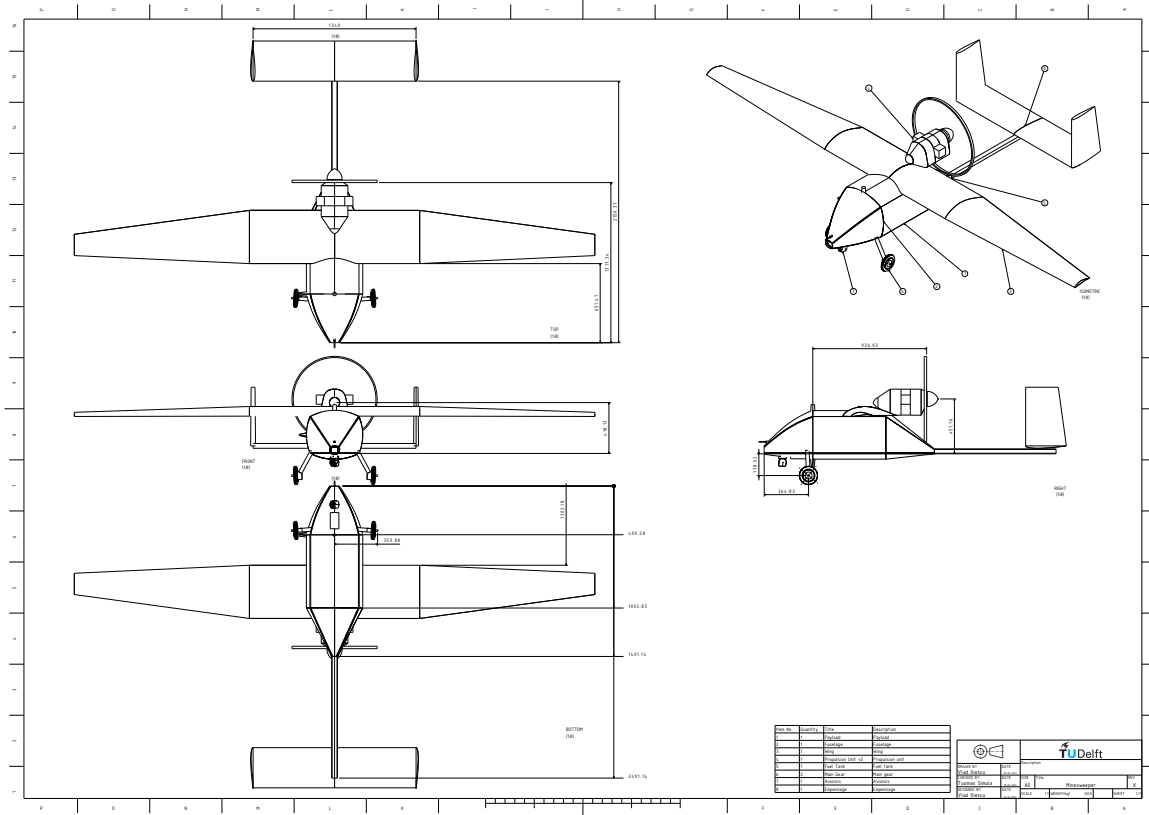


Figure A.1: Entire UAV Assembly Drawing

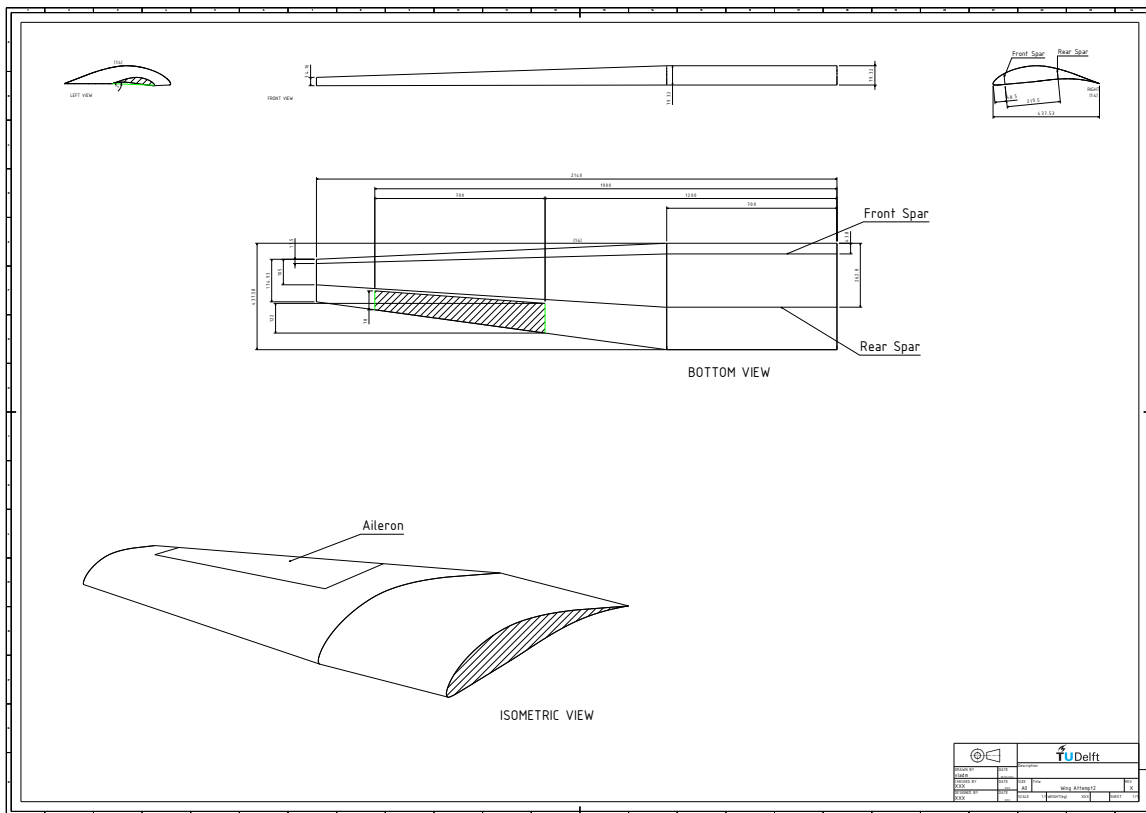


Figure A.2: Wing Surface Drawing (right)

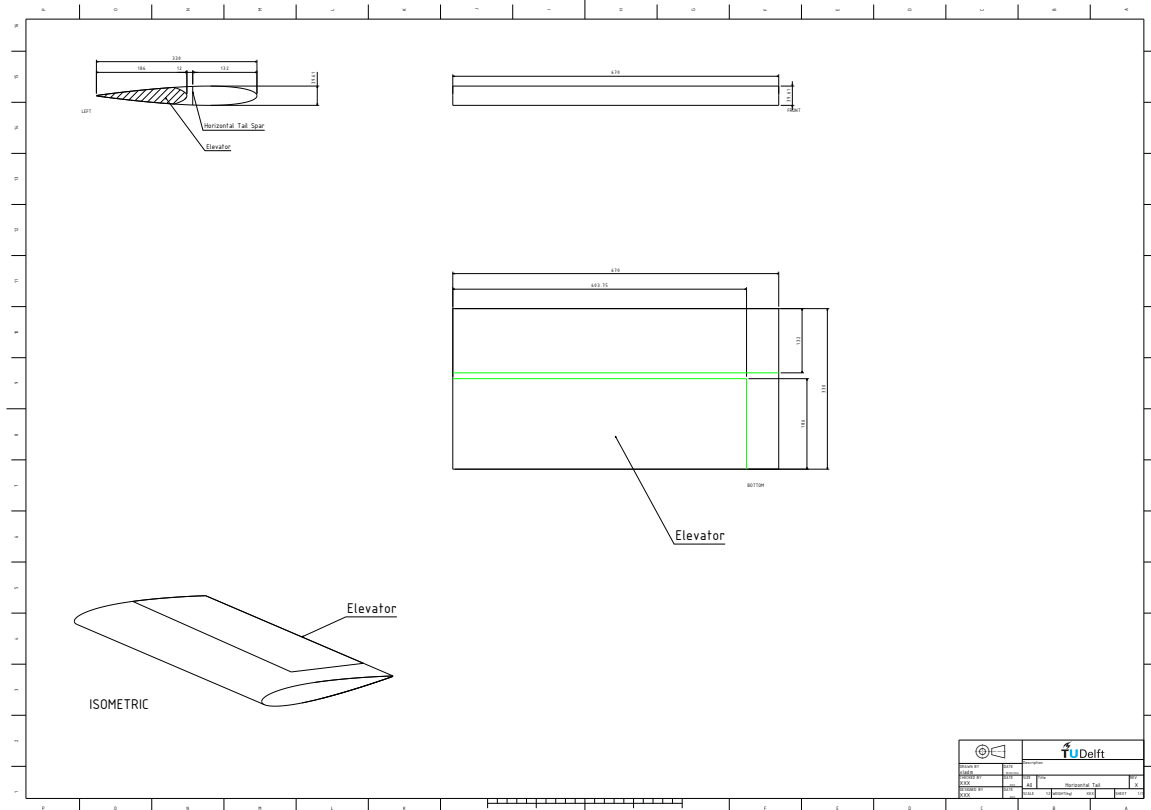


Figure A.3: Horizontal Tail Surface Drawing (right)

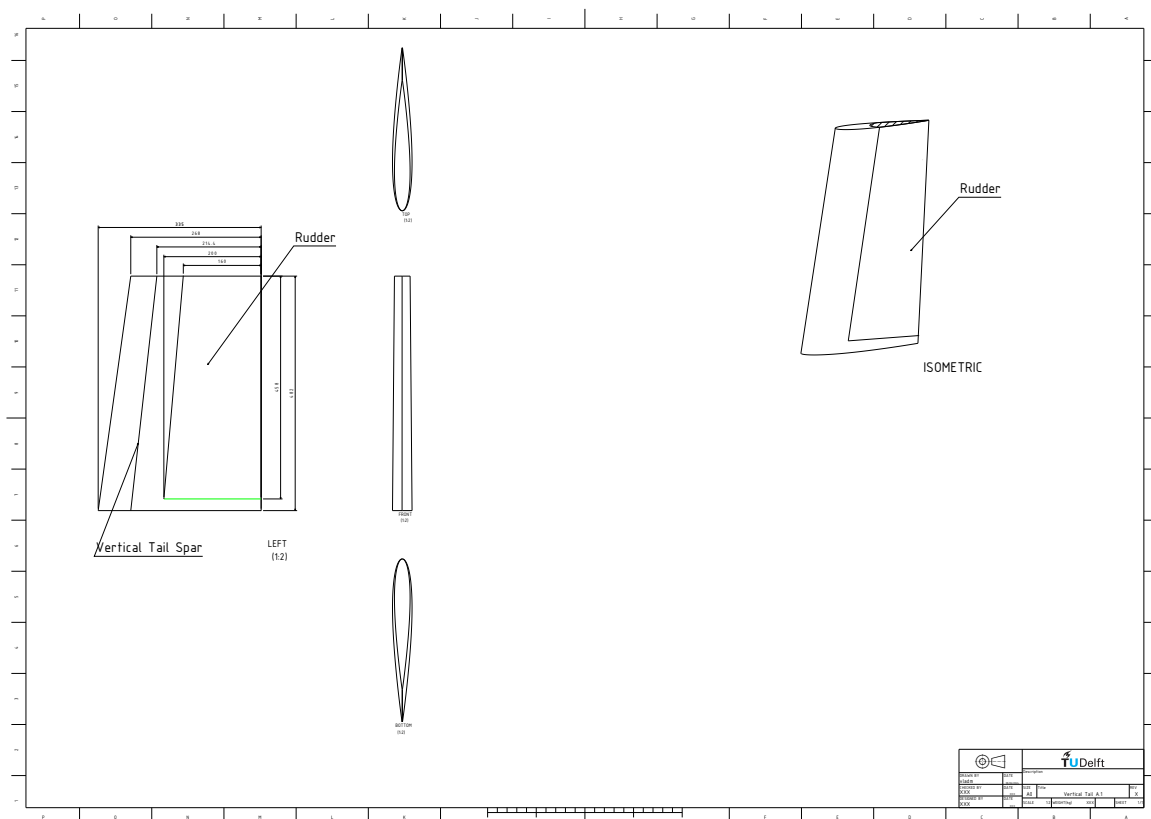


Figure A.4: Vertical Tail Surface Drawing

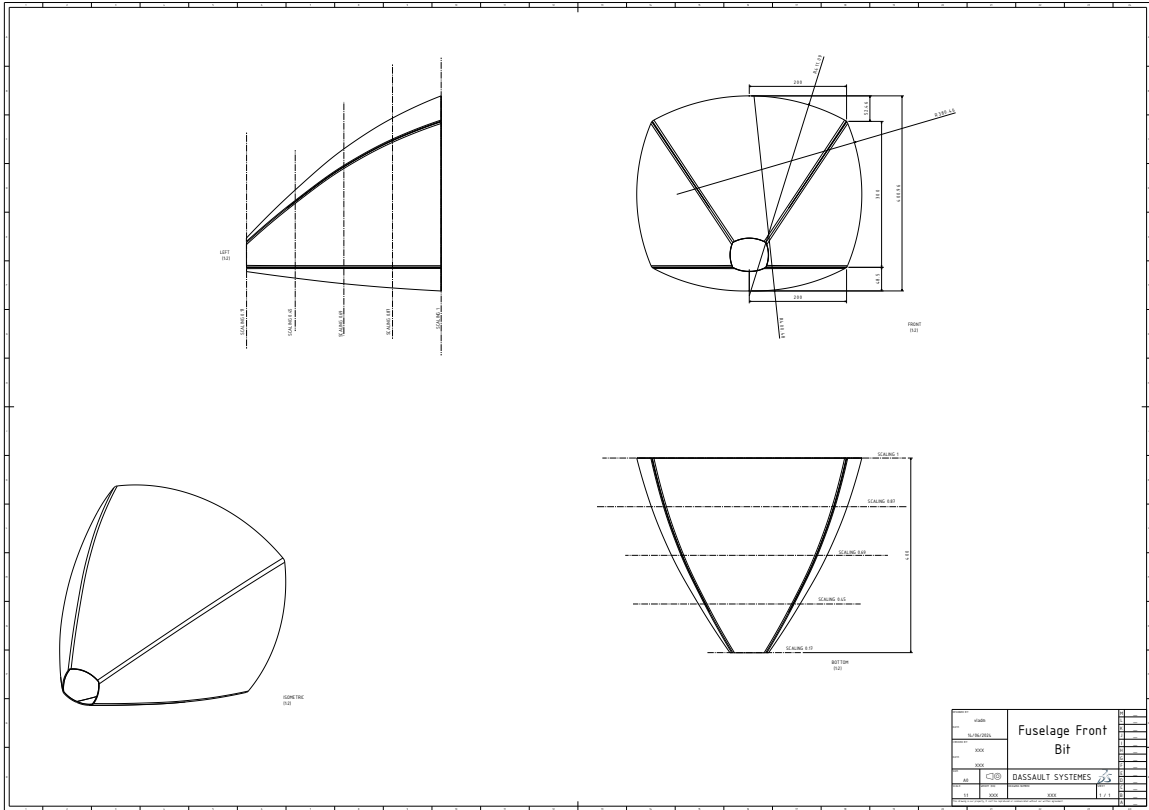


Figure A.5: Fuselage Fore Part Drawing

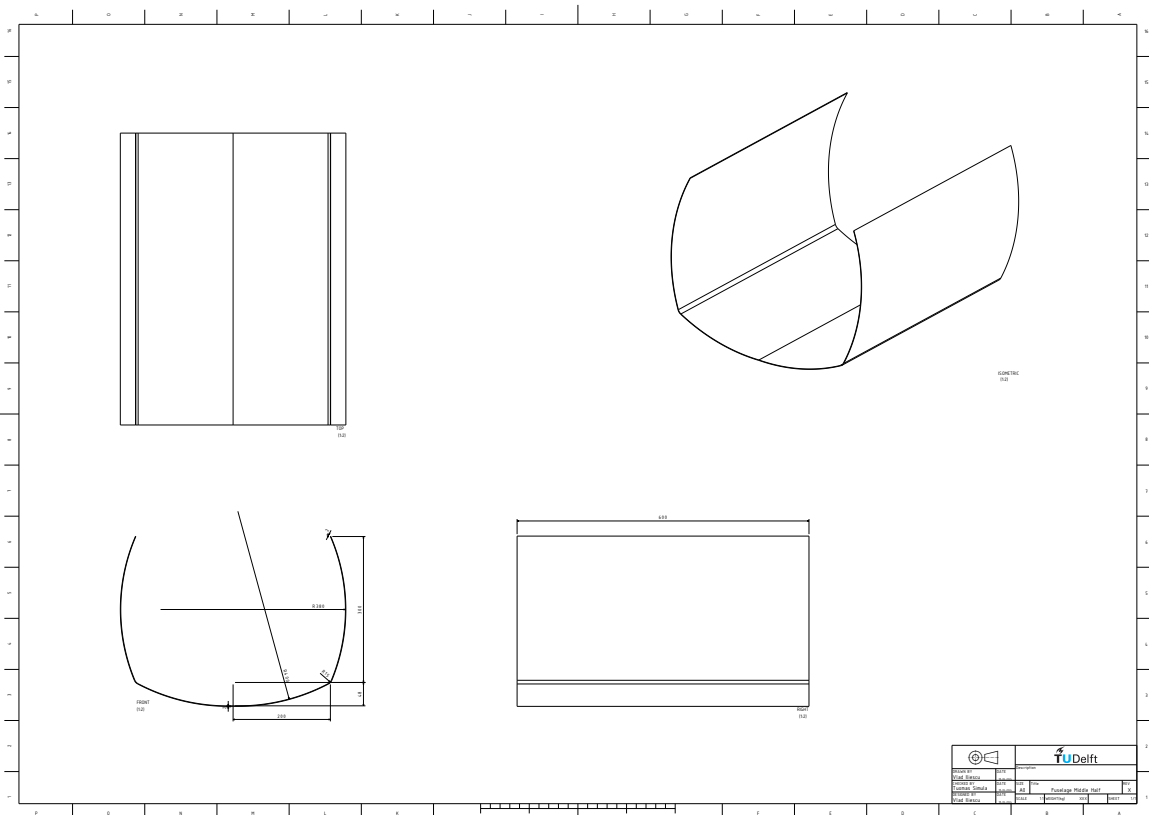


Figure A.6: Fuselage Middle Bottom Half Drawing

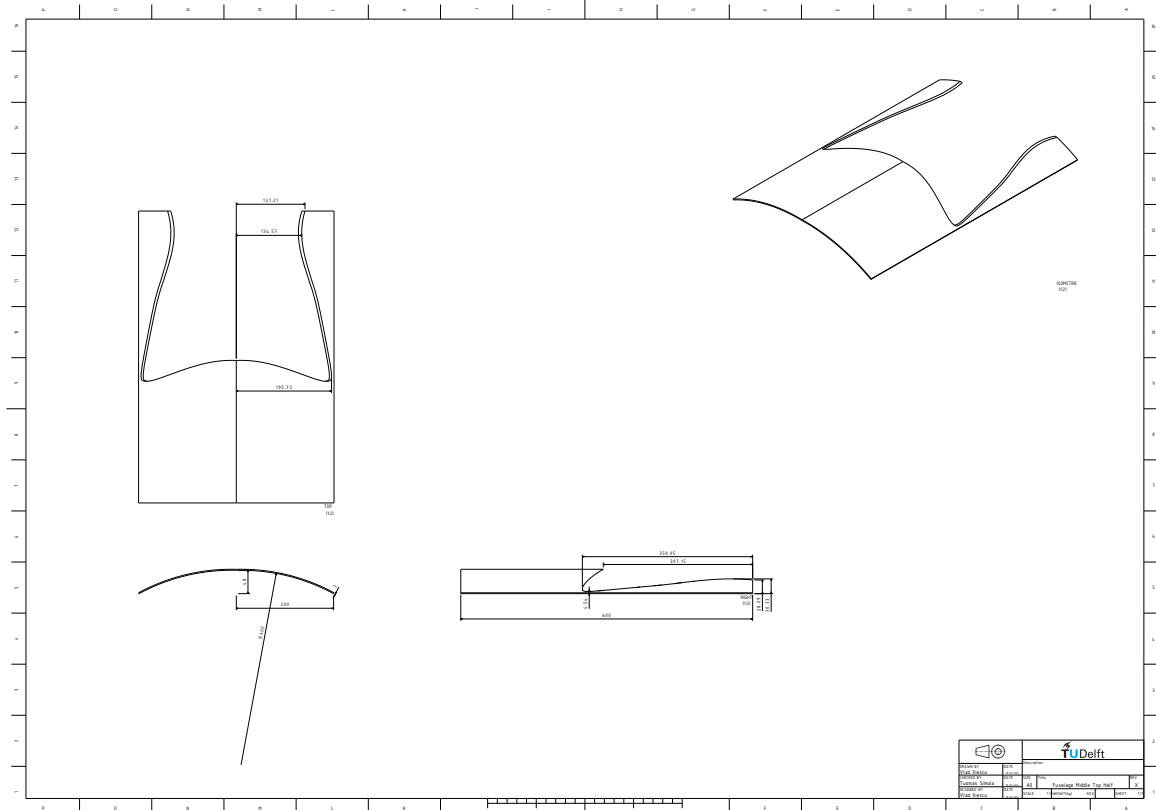


Figure A.7: Fuselage Middle Top Middle Half Drawing

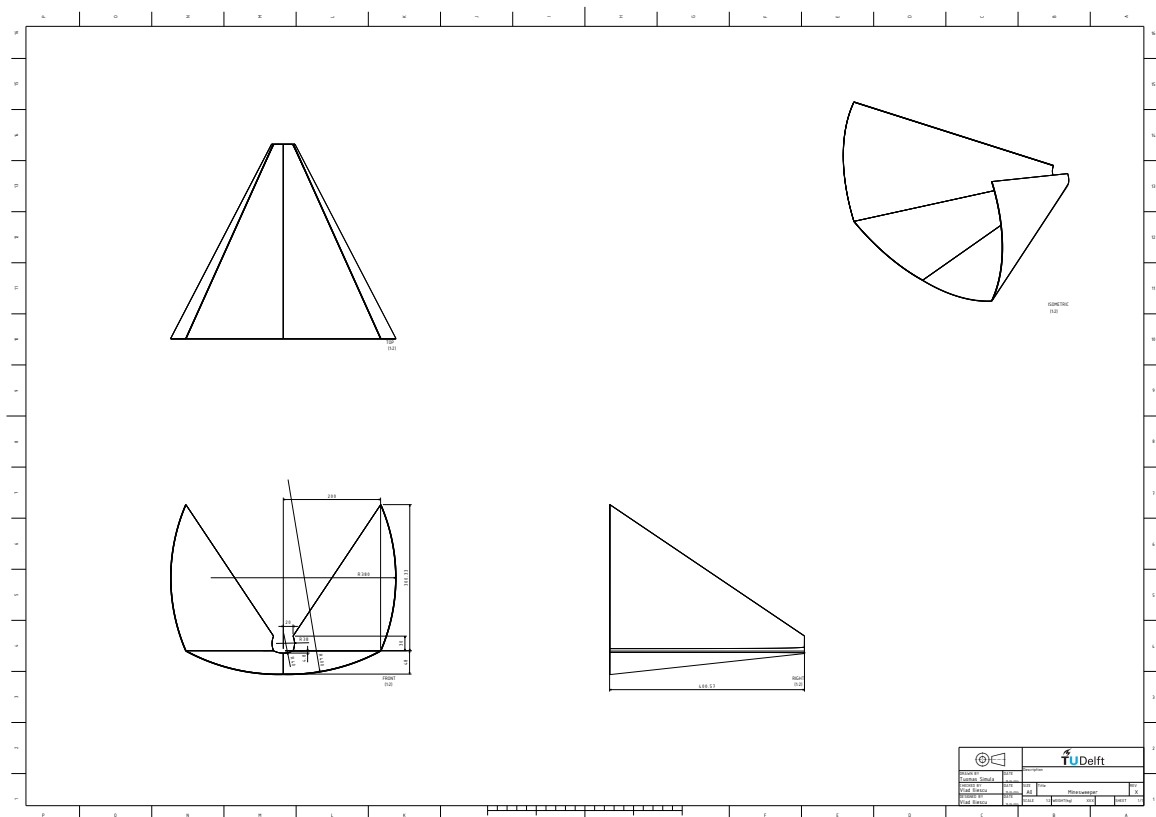


Figure A.8: Fuselage Aft Bottom Part Drawing

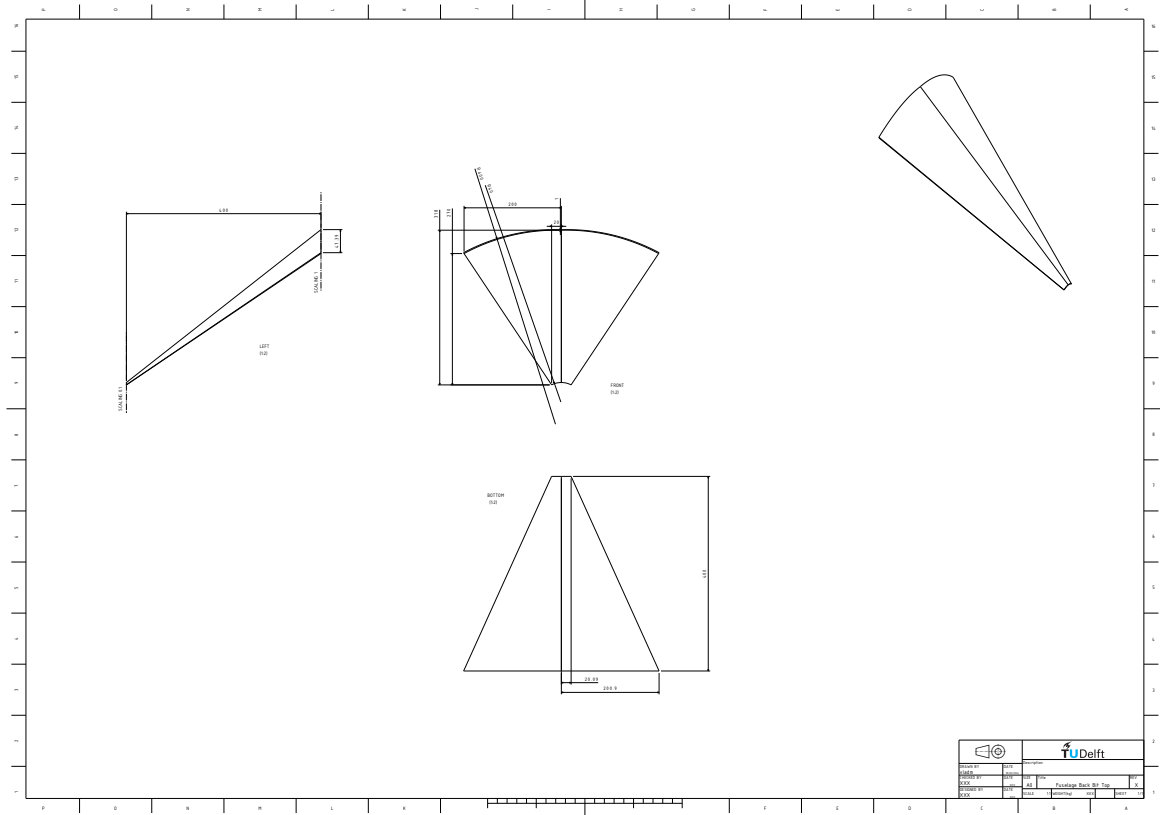


Figure A.9: Fuselage Aft Top Part Drawing

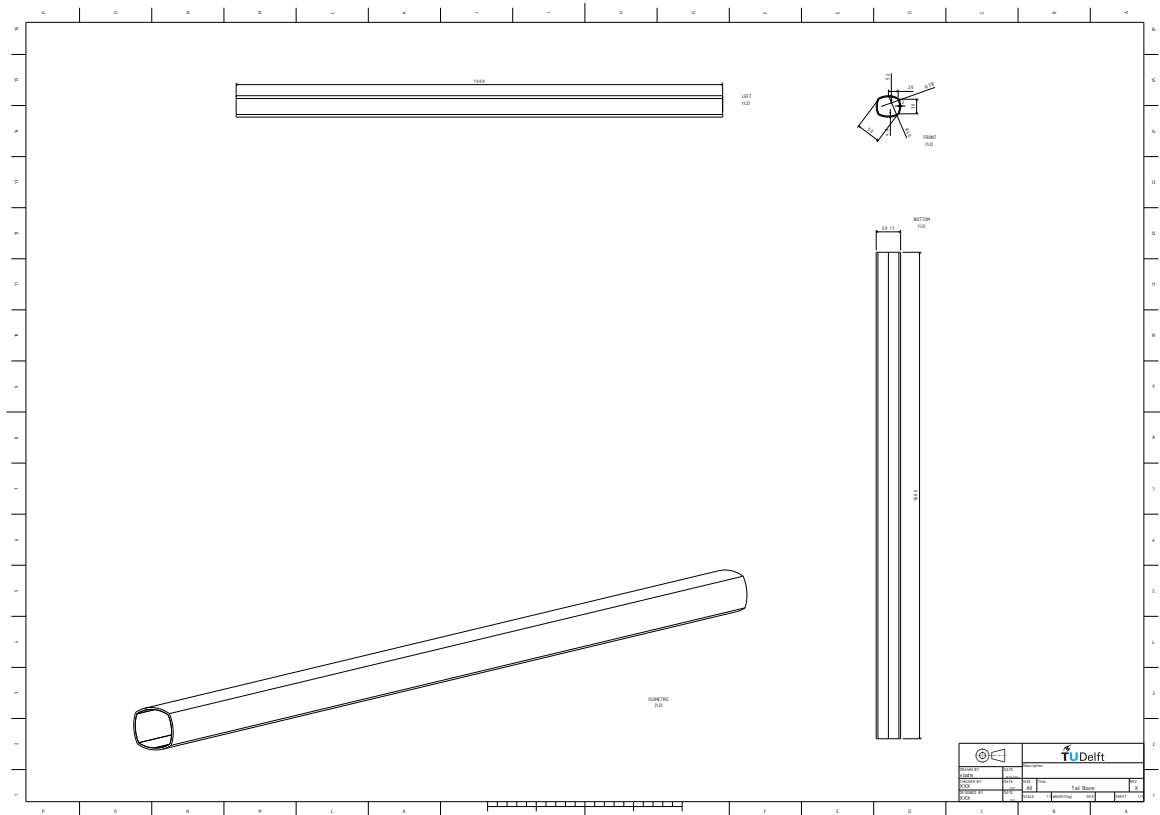


Figure A.10: Tail Boom Drawing

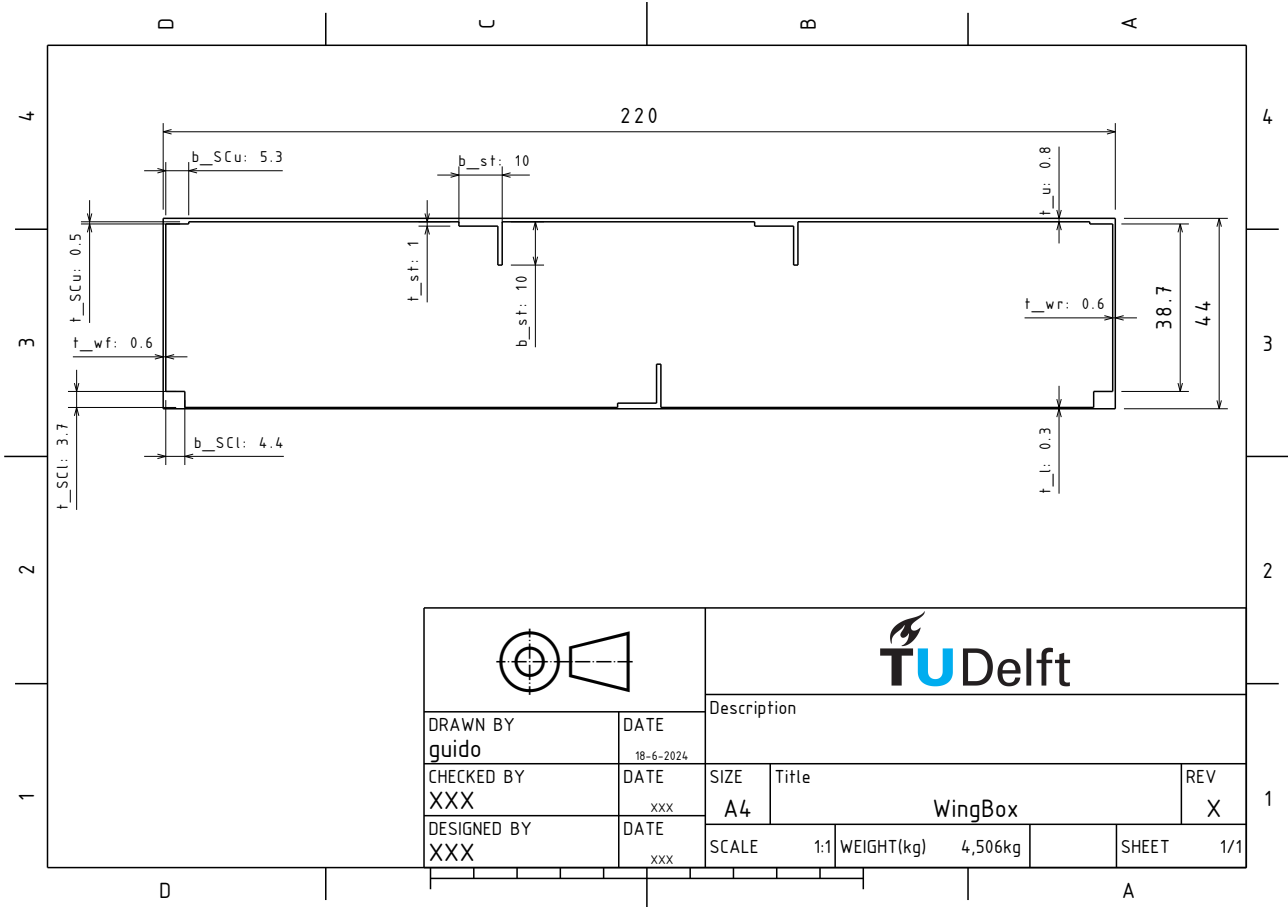


Figure A.11: Wing Box Drawing

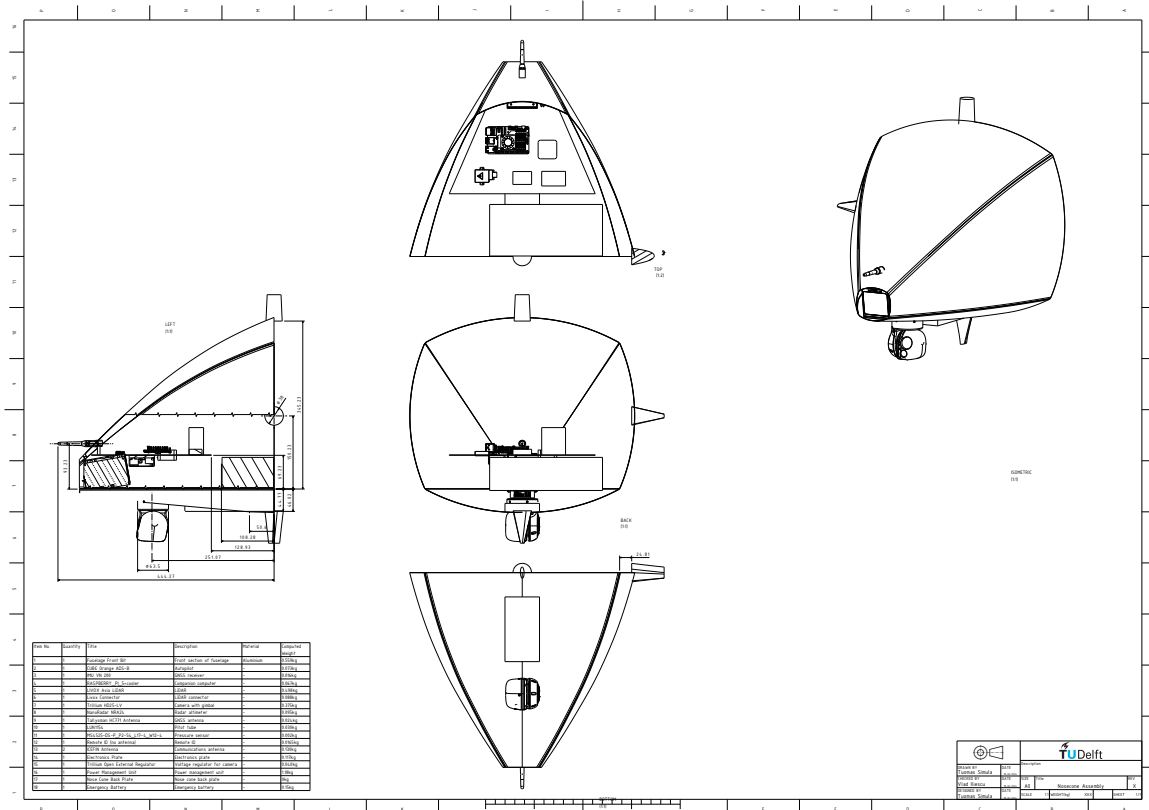


Figure A.12: Nose Assembly Drawing